AD

USAAVLABS TECHNICAL REPORT 68-60

STUDIES OF HELICOPTER ROTOR NOISE

By

M. V. Lowson
J. B. Ollerhead

January 1969

U. S. ARMY AVIATION MATERIEL LABORATORIES
FORT EUSTIS, VIRGINIA

CONTRACT DAAJ02-67-C-0023
WYLE LABORATORIES
HUNTSVILLE, ALABAMA

Disclaimers

The findings in this report are not to be construed as an official Department of the Army position unless so designated by other authorized documents.

When Government drawings, specifications, or other data are used for any purpose other than in connection with a definitely related Government procurement operation, the United States Government thereby incurs no responsibility nor any obligation whatsoever; and the fact that the Government may have formulated, furnished, or in any way supplied the said drawings, specifications, or other data is not to be regarded by implication or otherwise as in any manner licensing the holder or any other person or corporation, or conveying any rights or permission, to manufacture, use, or sell any patented invention that may in any way be related thereto.

Disposition Instructions

Destroy this report when no longer needed. Do not return it to the originator.

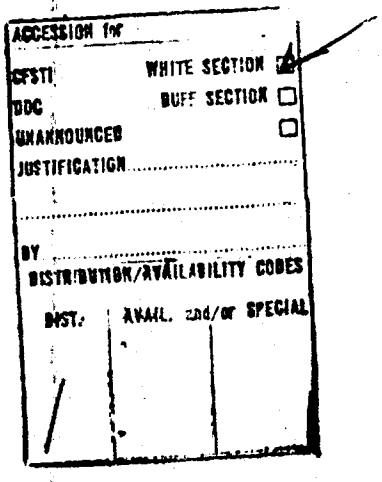

DEPARTMENT OF THE ARMY
U. S. ARMY AVIATION MATERIEL LABORATORIES
FORT EUSTIS, VIRGINIA 23604

This report has been reviewed by the U. S. Army Aviation Materiel Laboratories and is considered to be technically sound. The scientific opinions expressed in the report are those of the authors and do not necessarily reflect the position of the U. S. Army Aviation Materiel Laboratories. The report is published for the dissemination of information and the stimulation of thought.

Task 1F121401A14801
Contract DAAJ02-67-C-0023
USAAVLABS Technical Report 68-60
January 1969

STUDIES OF HELICOPTER ROTOR NOISE

Final Report

Wyle Research Staff Report WR 68-9

By

M.V. Lowson and J.B. Ollerhead

Prepared by

Wyle Laboratories
Huntsville, Alabama

for

U.S. ARMY AVIATION MATERIEL LABORATORIES
FORT EUSTIS, VIRGINIA

ABSTRACT

A comprehensive study of the problem of helicopter noise radiation is presented. After a review of the basic features of the noise, the limited experimental data are reviewed in some detail, and empirical laws are proposed. An exact theoretical expression for the noise radiation is derived. This expression has been used as the basis for the development of a comprehensive computer program to calculate helicopter noise at any field point, including all effects of fluctuating airloads and rigid and flexible blade motions. Details of this program are presented in a companion report. Under very reasonable approximations, an analytic expression has been found for the sound field far from the helicopter. Computations based on this expression have been made. The results show that it is the very high harmonics of the loading which contribute to the important harmonics of the sound field. For instance, calculation of the tenth harmonic of a four-blade rotor requires a knowledge of loading harmonics up to the sixtieth. Details of such loadings are not available from theory or experiment. Therefore, rotor aerodynamic loadings have been reviewed in detail, and empirical harmonic decay laws have been derived. Loading phases appear to be best described as random, and this introduces simplification in the theory, together with the necessity for definition of a correlation length. Results of a parameter study show trends basically in agreement with experiment, with sound at the higher harmonics basically proportional to thrust times disc loading times tip velocity squared. For the lower harmonics, the dependence on tip velocity is to the 2B power where B is the number of blades. The effect of forward speed is to increase the sound radiated forward and to decrease that radiated aft, causing a difference between fore and aft radiation of as much as 20 dB for the second and third harmonics at a forward Mach number of 0.25. An effective rotational Mach number concept is introduced which enables the effects of forward speed to be calculated, to good accuracy, directly from results for the hover case. The overall sound directionality pattern is found to have a minimum slightly above the plane of the disc and a broad maximum about 20 degrees below. The effects of both the near field and the blade motion are found to be small. Appendices present analyses of the blade motion effects and of the noise radiation by random blade loadings. Appendix III presents design charts for the noise radiation based on the theory that reduces the calculation of noise to a simple algebraic procedure. The theory generally shows fair agreement with experiment for overall levels and good agreement for trends. The charts presented should therefore be of direct use for design trade-off studies.

FOREWORD

The work reported herein was performed by Wyle Laboratories Research Staff, under Contract DAAJO2-67-C-0023, for U.S. Army Aviation Materiel Laboratories, Fort Eustis, Virginia. The work was carried out under the technical cognizance of Mr. William E. Nettles of the USAAVLABS staff. A companion report, USAAVLABS TR 68-61, gives details of the computer program specially developed for helicopter noise calculations under this contract.

Wyle Laboratories personnel directly associated with the project included Dr. M.V. Lowson, Mr. J.B. Ollerhead, Mrs. M. Setter, and Mr. R.B. Taylor.

TABLE OF CONTENTS

TABLE OF CONTENTS (Continued)

TABLE OF CONTENTS (Continued)

LIST OF ILLUSTRATIONS

LIST OF ILLUSTRATIONS (Continued)

LIST OF ILLUSTRATIONS (Continued)

LIST OF ILLUSTRATIONS (Continued)

LIST OF SYMBOLS

Note: Symbols throughout the report generally correspond to conventional acoustic usage. In Section 4, conventional aerodynamic symbols are used, and a list of differences is given at the beginning of Section 4.

a_0	speed of sound in free air, ft/sec
a_n, b_n	Fourier coefficients of nth harmonic sound radiation (Equation (8)), lb/ft^2
c	blade chord, ft
dB	decibels. 20 $\log_{10}$ (pressure ratio). Pressure ratio is re: .0002 $dyne/cm^2$ unless stated. Note: 1 $dyne/cm^2$ = 1 μbar.
g	general expression for source strength
i	$\sqrt{-1}$
i,j	tensor suffixes (i, j = 1, 2, 3)
k	loading power law exponent
m	sound harmonic number
n	sound harmonic number (n = mB)
p	fluctuating pressure, lb/ft^2
r	distance from source to observer, ft
r_1	distance from rotor hub to observer, ft
s	nondimensional blade radius
t	time at observer, sec
t'	retarded time, sec
v_i	(i = 1, 2, 3) velocity components, ft/sec
w	circular frequency

LIST OF SYMBOLS (Continued)

x_i	(i = 1, 2, 3) observer position
y_i	(i = 1, 2, 3) source position
x, y, z	Cartesian coordinates set in rotor, x along rotor axis, ft
A	disc area, ft^2
A_λ	complex Fourier coefficient of source input (Equation (20))
B	number of blades
C_L	blade lift coefficient
C	outboard (radial) component of force, lb
C_n	complex Fourier coefficient of sound (Equation (27))
D	drag-force component in circumferential direction, lb
C_{T_b}	blade thrust coefficient = $T/B \frac{1}{2} \rho \overline{\Omega R^2}\, c\, R$
F_i	(i = 1, 2, 3) components of force per unit volume
F_λ	harmonic amplitude of total blade force, lb
F_{E_λ}	harmonic amplitude of effective blade force, lb
HP	installed horsepower
Hz	Hertz - International unit for cycles per second
J_n	Bessel functions of the first kind, order n
K	Glauert downwash coefficient
L	blade lift, cosine loading harmonic, lb
M	source Mach number
M	rotational Mach number of rotor = $\Omega R/a_0$

LIST OF SYMBOLS (Continued)

M_F	hub forward Mach number
M_r	component of convection Mach number in direction of observer
M_0	hub convection Mach number
M_{0r}	hub convection Mach number in direction of observer
Q	mass source strength per unit volume
R	radius of source on rotor, ft
R	rotor radius, ft
S	blade plan area, ft^2
SPL	Sound pressure level, dB re: .0002 dyne/cm^2 unless otherwise stated
T	rotor thrust (component parallel to axis), lb
T_{ij}	(i, j = 1, 2, 3) acoustic stress tensor
U_P	velocity component normal to plane of rotation, ft/sec
U_T	velocity component in plane of rotation, ft/sec
V_T	rotor tip speed, ft/sec
W	weight of helicopter, lb
Y	distance of observer from rotor axis, ft
$\alpha_\lambda, \beta_\lambda$	Fourier coefficients of source input (Equation (23))
η	coordinates moving with the source
θ	angle around disc ($\theta = 0$ on y-axis)
λ	loading harmonic number
μ	advance ratio

LIST OF SYMBOLS (Continued)

π	3.14159 ...
ρ	density, slugs/ft^3
τ	retarded source time $\tau = t - r/a_0$, sec
ϕ	angular position of observer from y-axis, rads
ψ	rotor azimuth angle, rads
Σ	summation
ω	frequency, rads/sec
Ω	rotor rotational speed, rads/sec
Suffices	
λ	indicates effect due to λth loading harmonic only
n	indicates sound at nth harmonic only
T, D, C	effects due to thrust, drag, and outward components of force, respectively
$(\sim)$	vector or tensor quantity
[ ]	retarded time operator
$\lvert\ \rvert$	modulus
R	real part
I	imaginary part

1.0 INTRODUCTION

The present work is a further step in the U.S. Army Aviation Materiel Laboratories-sponsored research into the causes of, and means for controlling, helicopter noise. This overall research program has now been in progress for several years, since it first became apparent that noise radiation was an important factor in helicopter operations, both military and civil. Several studies of helicopter noise have now been performed both from the experimental [1-7] and the theoretical [8-12] points of view. However, it is unfortunately still true that the basic noise problem is far from being solved, or even understood.

This report concentrates on the problems caused by the far-field noise radiation of the helicopter. Aural detection of a helicopter is a significant factor in the success of tactical missions.[13] The unique characteristics of helicopter noise not only cause the noise to propagate for exceptionally great distances but also probably enable an experienced listener to distinguish the type of aircraft, its range, and its direction of flight. In the commercial sphere, high noise levels threaten the success of the very operations which a helicopter is uniquely able to perform; that is, operations out of terminals in built-up and often heavily populated areas which are inaccessible to conventional aircraft. There are already many instances where the disadvantages of noise have been found to outweigh other advantages of helicopter travel. However, it should be pointed out that internal noise problems are also severe. In addition to the obvious problem of interference with communications, noise levels inside the crew compartment are sufficiently high to constitute a very definite health hazard to helicopter aircrews. Figure 1 is a 1/3-octave band analysis of the noise in the cockpit of a CH-47 B in cruising flight.[7] Superimposed on this spectrum are hazardous noise exposure curves[7] and the amount of sound attenuation which can be expected from well-designed and well-fitting helmet/earmuff combinations. It is obvious that the noise level is dangerously high. Nevertheless, internal noise problems will not be specifically studied in this report, although many of the methods developed and the results obtained are relevant to both the internal and the external noise field.

Helicopter noise can be divided into two basic groups: that arising aerodynamically and that arising mechanically. However, with the exception of piston engine exhaust noise, the "mechanical" sound sources, including those due to the gearbox, transmission, and the various vibrating components, are important to the internal and near-external fields only. In the far-external field, the aerodynamically generated sound is dominant. The latter is associated with the rotor airloads and includes various types of noise which are commonly known as rotational noise, vortex noise, and "blade slap". Which of these is most significant depends on a number of factors, the most important of which are the location of the observer and the flight and configuration of the helicopter. At moderate distances from the helicopter, the various sources, listed in their order of importance to the subjectively judged magnitude of the sound, or loudness, are:[3]

- Blade slap (when it occurs)
- Piston engine exhaust noise
- Tail rotor rotational noise
- Main rotor vortex noise
- Main rotor rotational noise
- Gearbox noise
- Turbine engine noise
- Other sources

At very short distances inside the helicopter, gearbox noise becomes more important, as noted previously. At extreme distances, approaching the range at which the sound is barely audible, blade slap and main rotor rotational noise may be the only components which are heard, because atmospheric and other sound absorption effects remove the high-frequency energy from the spectrum. Main rotor rotational noise contains the major part of its energy at low and subaudible frequencies.

1.1 DEFINITION OF ROTOR NOISE SOURCES

The basic subject of the present study is therefore the noise radiated by the rotor. This consists of three of the sources mentioned above: blade slap, rotational noise, and vortex noise. A brief review of the characteristics of each is given below. However, the underlying source of the noise radiated by a helicopter rotor is the fluctuating forces upon it, and the basic cause of these forces may be found by examination of the rotor aerodynamics. Thus, in order to understand the noise, it is important first of all to understand the rotor aerodynamics.

The main feature of rotor aerodynamics is the lack of symmetry. In forward flight the advancing blade encounters substantially higher air velocities than does the retreating blade, giving rise to cyclic variations in the resulting airloads. The equilibrium of the rotor is maintained by a combination of cyclic pitch control and the freedom of the rotor blades to flap.

However, the most important feature of the helicopter aerodynamics from the standpoint of noise and vibration is the rotor wake. Each blade acts in the same way as a wing in flight, and the lift on it generates a vortex wake behind it which has a strong tendency to roll up into a concentrated vortex core. Each blade must therefore pass over the concentrated vortex wake left by its predecessor. Depending on advance ratio, net lift force, and so on, this vortex may pass either extremely close

to, or far away from, the following blade. If the vortex passes close to the blade, then a substantial local increase in lift will occur temporarily. These comparatively rapid increments in lift, caused by vortex interaction, are very efficient noise radiators. It appears that a very large part of the observed noise from a helicopter can be attributed to these vortex effects.

Blade Slap

A particularly severe type of noise is well known in helicopter operation under the name "blade slap". It is found that under various conditions (for instance, during low power descent), the helicopter produces a particularly loud slapping or banging noise, which occurs at the blade passage frequency. This occurs at precisely those conditions where the vortex wake can be expected to pass very close to the rotor, and can be particularly severe on a tandem-rotor aircraft where the wake from the first rotor can pass through the second. Blade slap can also occur on high speed rotors and in this case is associated with transonic flow over the rotor blades. Thus there are two possible sources of blade slap, due to either vortex interaction or transonic flow. It may be noted that the description of the phenomenon is fairly straightforward acoustically, and both the effects mentioned above can be readily predicted from the theory. Cases corresponding to blade slap are discussed in Section 6.1 of this report. Reference should also be made to the studies by Leverton and Taylor.[6]

When it occurs, blade slap is by far the loudest source of noise observed on the helicopter. However, it seems inappropriate to consider blade slap as a separate phenomenon. The helicopter rotor is always undergoing some form of vortex interaction, and blade slap is simply a particularly severe form. Perhaps it is more realistic to suppose that, at least from the acoustic point of view, the helicopter is always flying under some degree of blade slap.

Rotational Noise

Rotational noise is usually regarded as that sound which is directly attributable to the steady and fluctuating lift and drag forces acting on the rotor. This is the major source of noise from propellers [15,16,17] and helicopter tail rotors, where the fundamental frequency is of the order of 100 Hz.* For the helicopter main rotor, the fundamental frequency is significantly lower, around 10 Hz, due to the lower rotational speed. Rotational noise has a spectrum consisting of a number of very narrow peaks occurring at integral multiples of the blade passage frequency. However, its importance is often underestimated because of its very low frequency and the fact that most of its energy is contained within "subaudible" frequencies. The quotation marks here are used because the subaudible frequency range is in fact difficult to define,

* Hertz (Hz) is the new international unit for frequency. 1 Hertz = 1 cycle per second.

since what cannot be heard can often be felt through other physiological sensations. The subjective character of rotational noise is highly dependent upon its harmonic content. The relative amplitudes of the higher harmonics vary from helicopter to helicopter and strongly depend upon the flight condition. If the harmonic amplitudes fall off rapidly (with harmonic number), the sound can best be described as a "thumping" which occurs at the blade passage frequency. As the harmonic decay becomes less, that is, as the higher harmonics increase in amplitude, the thumps sharpen into bangs and eventually into "blade slap". An example of this effect is the sound of a helicopter flying overhead at a fairly high speed and low altitude. As the machine approaches, the characteristic sound is a sharp popping which decays to a thumping sound as the aircraft flies overhead. Subsequently, the rotational content becomes barely perceptible as the aircraft recedes, with the tail rotor noise dominating the observed sound.

A sound component which is very similar in nature to rotational noise is termed "thickness noise".[17] This arises due to the displacement of air particles as a blade passes through their volume. Like rotational noise, thickness noise has a frequency spectrum consisting of a number of discrete harmonics of the fundamental blade passage frequency, which is the rotational frequency multiplied by the number of blades. However, this is rarely an important source of helicopter noise except at very high tip speeds. Thickness noise has not been considered in this report.

Vortex Noise

Vortex noise is the name given to the distinctive "swishing" sound which characterizes helicopter noise at short distances. It is sometimes thought to be caused by the turbulence associated with the blade boundary layers, but it is probably principally due to the interaction of the blades with wake turbulence. Vortex noise is random in nature and contains sound energy which is spread over a substantial portion of the audible frequency range. Rotor vortex noise differs from other, more familiar, forms of random noise, such as wind noise or jet noise, in that its amplitude and frequencies are modulated. This is due to the varying relative distance and velocity between the source and the observer because of blade rotation, which causes harmonic variations in both amplitude and frequency.

Experimental data presented in this report indicate that, contrary to previous opinions, rotational noise may continue to dominate the sound spectrum up to frequencies of 400 Hz and higher. The previous belief that vortex noise becomes more significant at frequencies greater than about 100 Hz may well be the result of two factors: (1) one-third-octave analysis of helicopter noise does not distinguish individual harmonics at the higher frequencies, and (2) previous theoretical results predicted that rotational noise decays more rapidly than it does in practice. It is likely that improved narrow band analysis of helicopter noise will show that rotational noise is significant through the major part of the audible frequency range and, thus, that previously identified "vortex" noise is really part of the rotational noise output of the helicopter.

It is clear from the preceding discussion that all significant forms of rotor noise are due to the fluctuations and motions of the pressures acting on the blades. For this reason, it is somewhat difficult, and indeed of doubtful justification, to separate rotational noise, vortex noise, and blade slap. It is shown in this report that observed rotational noise harmonics, even at relatively low frequencies, are most likely explained by random phase variations in the higher blade loading harmonics. Main rotor rotational noise harmonics as high as the thirty-fifth are discernable in experimental data for two-blade rotors. To obtain theoretical predictions of these harmonic amplitudes with any accuracy requires knowledge of at least 100 harmonics of the rotor airloads. Such fluctuations correspond to pressure variations occurring within the dimensions of a blade chord; a condition approaching the domain of "vortex" noise generation. Similarly, blade slap is said to occur when the observed sound becomes highly impulsive in nature, which in turn is the result of the blade loading harmonics' reaching some critical level. It could be argued that "blade slap" is always present in helicopter noise; it is merely a question of degree.

The fundamental object of the report is to predict all possible forms of the noise radiated by the helicopter main rotor. This is achieved by applying the basic acoustical equations which give the sound radiation from a known fluctuating force distribution. These basic equations were recently derived in a convenient form by Lowson.[8,9] Thus, the problem of predicting the noise radiation reduces to the problem of predicting the rotor dynamic loads. Unfortunately, the accurate calculation of the noise field requires an extremely detailed knowledge of the fluctuating loads. For instance, it will be shown that calculation of the tenth sound harmonic for a four-blade rotor (a case which is certainly of practical interest) requires a knowledge of the loadings up to about the sixtieth. This knowledge is not at present available, either from experiment or theory. Indeed, the only loading harmonics which can at present be specified will be shown to have a negligible sound output. Thus, in order to calculate the sound field, these high harmonic loadings must be predicted, and an important part of the present work has been to derive semiempirical predictions for these.

Because of the complexity of the acoustic problem, a complete solution is possible only via a digital computer. A key secondary objective is therefore to reduce computer time to a minimum. The previous theoretical studies [10-12] have been accomplished using this general approach, and reasonable, although far from complete, agreement with experiment was found. Computing time using these approaches was of the order of minutes per field point. The present work uses a different basic expression for the computer studies, which removes one of the principal problems that cause excessive computer time. Computer time for the present, more complete solution has been reduced to about 10 seconds per field point, and this solution includes all flapping and lagging effects as desired. In addition, under very reasonable approximations, an analytic solution has been obtained. The solution is a rather complex collection of Bessel functions and still requires computer calculation, but computer time for this case can be reduced to the order of a tenth of a second per field point. Furthermore, this basic analytic solution has revealed several

important features of the noise generation process which are of considerable help in understanding the problem.

Thus, two very different approaches, the exact numerical method and the approximate analytic solution, have been used in the work. The two approaches give identical answers if appropriate, identical input conditions are used. This self-checking feature of the present calculations is important in establishing confidence in the results. Fair agreement with experiment is also found, although experimental data are far from being either complete or trustworthy. Previous theoretical studies have shown that rotational noise can be predicted with reasonable accuracy at the lower frequencies. The present work illustrates some of the deficiencies of earlier knowledge and shows how theory and experiment complement each other to yield methods for the accurate estimation of rotational noise throughout its important frequency range.

2.0 REVIEW OF THE PROBLEM

2.1 REVIEW OF EXPERIMENTAL DATA

One of the major difficulties in establishing a proper understanding of helicopter noise is the lack of good experimental data. Several studies have been performed,[1-7] but all suffer from deficiencies. Few investigators have performed a sufficiently detailed study of the problem, and even the detailed studies have often given data which are of very limited application. Furthermore, comparison of results from different investigations on the same helicopter often reveals discrepancies of 10 dB or more. Nevertheless, in order to provide a basis for the report, it is felt that a review of the data is necessary. Attempts have been made in each case to determine the leading trends, and empirical formulas for noise characteristics are given. It should be noted that all the formulas given apply under restricted circumstances, and considerable care should be exercised in any attempt to apply the formulas to any real prediction case.

From many points of view, the first reported study, by Hubbard and Maglieri,[1] still gives the most useful information on the rotor noise problem. They measured noise from a helicopter rotor on a test tower. The tower was over a diameter high, so that ground interference should not be too severe. Noise was measured at only two locations: at the hub and on the ground at 1 diameter from the hub, but the rotor was run over a very wide range of disc loadings and tip speeds. Although these ranges are outside the useful practical limits, the results do show important trends, which would have been difficult to pinpoint with any confidence in a more restricted experiment. A plot of the overall levels, as measured on the ground 1 diameter away from the rotor, is given in Figure 2. The data should be fairly realistic, although there seems to be a possibility of downwash-induced noise at the microphone for the high disc loading cases. There are several features that can be observed on this graph. First it can be observed that noise levels rise rapidly with tip speed. However, for any specific tip velocity, the noise level reaches a minimum at an intermediate value of disc loading. The same effect is shown in the one-third octave band spectra in Figure 3, also taken from Hubbard and Maglieri's paper. At very high disc loadings the rotor stalls, and this causes major increments in noise. Points corresponding to stalled operation are marked on Figure 2. At very low disc loadings the noise also rises. This is due to the vortex wake interaction effects discussed in the Introduction. Indeed, Hubbard and Maglieri appear to have been the first to report the blade slap phenomenon. Note the increase in sound output at low disc loadings for the 900 ft/sec case. This corresponds to the blade slap condition.

The data shown in Figure 2 may be replotted in a form suitable for making predictions of overall noise level. It will be assumed that helicopters will not, in general, run in conditions close to stall or blade slap. When such extreme points are removed from Figure 2, the data may be replotted as shown in Figure 4. This figure probably applies for collective pitches of the order of 8 degrees. Variation of collective pitch is, of course,

reflected in the thrust term. It will be observed that fairly good collapse is obtained. The double logarithmic plot of Figure 4 is convenient for establishing power law trends. It will be observed that the sound level rises at a much faster rate with velocity at high tip speeds than at low. This is a further important feature of the noise. Most helicopters operate with tip speeds in the range of from 500 to 800 fps. Over this range the data collapse to a straight line fairly well. From this, an empirical prediction law for overall levels at a 500-ft sideline may be obtained as

$$dB_{500} = 60 \log_{10} V_T + 10 \log_{10} T - 127 \qquad (1)$$

where V_T = tip speed

T = rotor thrust (lift)

Correction of Equation (1) to other ranges r may be readily accomplished by

$$dB_r = dB_{500} + 20 \log_{10} (500/r) \qquad (2)$$

It should be pointed out that, in the derivation of Equation (1) from the data in Figure 4, two assumptions have been made. First, it was assumed that, for constant disc loading, the sound output was proportional to rotor diameter squared. This seems physically reasonable and was found to apply theoretically in the related case of compressor noise.[18] Second, it was assumed that Hubbard and Maglieri's results could be corrected to 500 ft, assuming spherical spreading, as in Equation (2). This assumption is probably accurate to within a dB or so, as will be shown later in the report. Furthermore, Hubbard and Maglieri do not give one-third octave plots below 100 Hz, and there is therefore some doubt as to the lower frequency limit in their overall response data. It might also be pointed out that there are some theoretical reasons that suggest a thrust-squared law in Equation (1), so that the thrust term would then be $20 \log_{10} T$. However, the thrust term shown here has a good empirical fit to the limited data available, as is shown by the collapse in Figure 4. It should be noted that configuration changes may well be important. Equation (2) applies essentially to a two-blade case. Data from Cox and Lynn[3] suggest that a three-blade rotor may be about 3 dB quieter than a two-blade rotor with the same thrust and tip speed.

Since thrust is proportional to tip velocity squared, Equation (1) implies a velocity to the eighth power law for the noise. Acousticians should note that this variation is not too surprising. The sixth power law for dipole noise applies only to isolated dipole

fluctuating forces. Distributions of force (for instance over the rotor disc) imply higher order multipoles and associated higher order velocity powers. Indeed, a simple propeller obeys a velocity to the tenth power law over most of its operating range of interest.

Stuckey and Goddard[5] recently presented new acoustic data on a rotor tower test. Their 50-ft-diameter rotor was only 20 feet from the ground, and vortex reingestion with consequent increases in noise level is to be expected. Their data are unlikely to be representative of hover out of ground effect, but the data may be applicable to lift-off maneuvers. They give fairly complete data, which justify analysis. No simple effect of noise harmonics is observed. The harmonic level varies almost randomly from harmonic to harmonic and from test to test. This effect is probably due, at least in part, to the vortex reingestion effects mentioned above. However, some trends can be seen. Figure 5 gives harmonic levels measured for a high and low collective pitch at high and low rotational speeds. Figure 5 shows a fairly constant 10-dB increase in going from the low to the high thrust condition. Note that spectral shapes in each case are changed little. However, there is a very definite change in spectral shape between the high and the low tip speed case. The lower harmonics are considerably increased. At low tip speeds, the sixth to thirteenth harmonics are almost 5 dB higher than the first; at high tip speeds, the effect is reversed, with the first harmonic about 7 dB higher.

As was mentioned above, considerable scatter is present in Stuckey and Goddard's results. However, in order to establish some general trends, the graphs shown in Figure 6 have been prepared. The highest harmonic given in the data of Stuckey and Goddard, the fifteenth, is taken for reference. It was found that the sound level obeyed a V^2T^2 law when V is tip velocity and T is rotor thrust. Figure 6a shows the sound level against thrust, corrected for velocity. It is clear that a T^2 law gives a good fit to the data. Figure 6b gives the sound level against velocity, corrected for thrust. Here, considerable scatter may be observed, and the V^2 law cannot be regarded as definitely established. It is of particular interest to note that several points at about 11 to 13 degrees collective pitch are about 5 to 10 dB low. This probably corresponds to a cleaner flow condition, as was observed in Hubbard and Maglieri's data, and offers some hope for a noise control method. If the V^2T^2 law is accepted, then, since $T \sim V^2$, an overall V^6 law can be inferred. The V^6 law is, of course, the classical dipole power dependency expected for a force.[4,9]

Figure 7 shows the equivalent graphs for the first harmonic. Far more scatter is apparent here. The velocity law is more like V^8 or greater, as opposed to the V^2 law for the fifteenth harmonic. Part of this is undoubtedly due to the increase in microphone response as the fundamental becomes of higher frequency with increase in tip speed. This accounts for a V^2 increase, so that the observed V^8 law implies an actual V^6 law. It may be noted that use of the assymptotic form of the Bessel functions suggests a V^{2B} law at the fundamental frequency where B is the number of blades.

Stuckey and Goddard's data were taken on a three-blade rotor, and a V^6 law is then suggested theoretically, in broad agreement with the experimental results. It might also be noted that the same arguments, including blade number and microphone response, applied to Hubbard and Maglieri's two-blade rotor would suggest a $V^6 T^2$ law for the fundamental frequency. A V^6 law is suggested in Equation (1), but probably little weight should be placed on this. The data plotted against thrust in Figure 7a again suggest a T^2 law. Considerable scatter occurs here, basically due to the scatter in the velocity case. For any fixed tip velocity, the data correspond quite closely to the T^2 law. No detailed prediction equations will be given based on these data, but the general trends should be noted, particularly the fact that the significance of the lower harmonics increases with tip speed.

For the complete helicopter, there is again little data. Sternfeld et al,[2] gave an extremely large amount of acoustic data on many different vehicles. However, their program was primarily aimed at internal noise levels, and most of their reported data are not in a convenient form for analysis in the present problem. The most useful study for the present work was that of Cox and Lynn.[3] They performed a detailed investigation of the noise from a UH-1A helicopter. Typical overall levels in their tests are also shown in Figure 4. The extremely good agreement between Hubbard and Maglieri's results for an isolated rotor and Cox and Lynn's results for the complete helicopter should be noted. This reinforces the contention that the main rotor is the principal source of sound and is support for the use of Equation (1) for prediction purposes. Unfortunately, no other data have been found in a convenient form for inclusion in Figure 4, so that the use of Equation (1) cannot be regarded as completely justified. However, it may be of some use in noise predictions where parameters do not vary too much from those of the source data.

Cox and Lynn also performed some narrow band spectral analyses of their acoustic signal. However, an error was apparently made in the identification of the fundamental frequency as 11 Hz in their original graph. Use of a 10-Hz fundamental as shown leads to much better agreement with observed frequency plots. Figure 8 is based on their results with this correction, and it suggests that the noise radiation from the complete helicopter can be divided into four parts:

- Main rotor rotational noise
- Tail rotor rotational noise
- Main rotor vortex noise
- Gearbox noise

Levels of these sources, broadly as suggested by Cox and Lynn, are shown in Figure 8.

The test vehicle was turbine powered, and this probably accounts for most of the radiation above 2000 Hz. Results for a reciprocating engine helicopter would show additional noise peaks at the engine firing frequency (about 100 Hz) and its harmonics at about the same level as the main and tail rotor harmonics shown. It can be seen that the harmonics associated with the main rotor rotational noise predominate at lower frequencies (< 100 Hz). At the midfrequency range (100 to 400 Hz), the tail rotor harmonics appear more significantly, and the main rotor "vortex" noise is important at around 500 Hz. It should be noted that this particular order of significance is not necessarily true for all helicopters. For instance, the UH-1A operates with a particularly high blade tip speed. As was shown by Stuckey and Goddard's data (Figure 5), reduction of tip speed will markedly reduce the levels of the first few main and tail rotor harmonics, but only reduce higher harmonics and vortex noise to a lesser degree.

This "vortex" noise justifies further study. It is generally considered to be defined by the background noise showing in the spectrum below the peaks due to the tail rotor harmonics, as is shown in Figure 8. Several attempts have been made to predict this vortex noise by empirical techniques based on the assumption that it is entirely random or broad band in nature (for example [4,5,12]). In fact, it seems very likely that the "vortex" noise component as generally defined really represents some of the higher harmonics of the main rotor rotational noise. Figure 9 gives a recent ultranarrow (2 Hz) spectral analysis of noise from a UH-1B helicopter under lift-off conditions recorded at Wyle Laboratories.[7] Considerable care was taken to ensure that the spectral analysis was as accurate as possible. To produce this one figure, approximately 2 hours of analysis time was required. Such detail has not previously been given in the reported data, and Figure 9 shows several new and interesting effects.

The most significant effect is that harmonics of the main rotor blade passage frequency are identifiable up to at least 400 Hz or about the 36th harmonic of the noise. In other words, the background noise level beneath the tail rotor harmonics is due to the higher harmonics of the main rotor, at least from 100 to 400 Hz. Figure 9 shows how the true broad-band background level is about 3 to 5 dB below what is usually described as "vortex" noise. The small subharmonic halfway between the principal blade passage harmonics is also of interest. The UH-1 has two blades, and this subharmonic is clearly due to incomplete cancellation of the noise radiated by each blade. Identical radiation from each blade is always assumed theoretically, and Figure 9 shows how this is not necessarily true.

Several authors have attempted to predict rotor noise levels above the tenth harmonic. As was shown above, sound at these frequencies contains contributions from both the rotor harmonics and the vortex noise. Both sources have been combined by previous investigators as "vortex" noise, and equations for its sound contribution given. Davidson and Hargest[4] quote results from Goddard and Stuckey to suggest

an approximate formula for the vortex noise, which can be written as

$$dB_{500} = 20 \log_{10} V_T + 20 \log_{10} T - 10 \log_{10} S - 25.5 \quad (3)$$

where S = total blade plan area

Schlegel et al,[12] also give a formula for vortex noise which can be rewritten as

$$dB_{500} = 20 \log_{10} V_T + 20 \log_{10} T - 10 \log_{10} S - 43 \quad (4)$$

The fact that the functional dependence of each empirical form is the same is encouraging, but it will be observed that Davidson and Hargest's equation (3) predicts 17.5 dB more noise than Schlegel's equation (4). Davidson and Hargest's result is intended to apply immediately underneath the rotor, and they suggest that much less vortex noise is radiated sideways. Their correction for this effect would reduce their prediction by about 10 dB for the position used by Schlegel et al, in their tests. The arguments, and data, put forward by Davidson and Hargest cannot be said to offer any real support for this correction, but the correction does appear to be included in their predictions, so that it must be removed for comparison with Schlegel. Several other effects suggested by Davidson and Hargest would tend to increase the predicted noise level still further. The divergence between the two equations is not readily explainable. Possibly, the increased number of blades (five and six) used by Schlegel et al, contributed to the reduced noise. Empirically, perhaps 5 dB should be added to Equation (4) for prediction purposes. Stuckey and Goddard[5] recently presented further data on a rotor tower test, some of which were discussed above. For the "vortex" noise effects, they find essentially the same velocity dependence as other investigators but suggest a 1.66 power law for the thrust variation. However, these data are thought to be rather limited in application because of the ground interference effects noted previously.

In order to interpret helicopter noise data, it is of extreme importance to consider the comparative significance of the various sound sources from the detectability point of view. The significance of helicopter noise lies in its effect on a human observer. It is well known that the ear does not respond to all sounds equally. Indeed, sounds which are very low (< 100 Hz) or very high (>10,000 Hz) in frequency are not heard well. Figure 10 gives a curve of equal loudness against frequency. In other words, sounds which seem to have the same loudness will actually have comparative measured intensities which lie on the curve shown in Figure 10.

The measured sound pressure levels of Figure 9 have been replotted in Figure 11a.

Using the weighting curve of Figure 10 on these data gives Figure 11b. This figure gives the apparent significance of the sound from the observer's point of view. Note that while Figure 11a suggests that the main rotor is the dominant source of noise, Figure 11b suggests that from the point of view of a human observer, the tail rotor can be important. Furthermore, the peak main rotor sound level occurs at the second harmonic in Figure 11a. The first harmonic was below the range of adequate microphone response for these data. Figure 11a therefore suggests that either the first or the second harmonic is the largest. However, reference to Figure 11b shows that the principal rotor harmonic, as far as the human observer is concerned, is the third. Application of the same correction to the Stuckey and Goddard results suggest that the tenth to fifteenth harmonics were the most important. In the remainder of the report, results will usually be given in terms of their absolute intensities; but it will be important to bear in mind the distorting effect of the human ear in evaluating these results from the point of view of detectability.

A further important effect is the attenuation of sound during its propagation over long distances. The subject is too complicated to be studied in detail here, since it depends on many parameters, such as the height of the helicopter above the ground, atmospheric humidity, type of ground cover, and so on. Discussions may be found in References 7, 13, 19, and 20. However, the key point is that all the high-frequency noise will be rapidly attenuated, typically at more than 30 dB/1000 ft for frequencies above 1000 Hz. Thus, from the detectability viewpoint, there is little significance in any noise above 1000 Hz. For instance, the gearbox is often the dominant source inside the helicopter[2] but will never be significant for detectability.

Finally, in any discussion of the significance of various sources of noise, it is important to bear in mind the limitations imposed by the method of presenting the data. It is usual to present helicopter noise data in the form of narrow band spectra, as was shown in Figures 5 and 6. This is reasonable because of the many discrete frequencies present, which can be identified only in such a plot. Consider the spectrum sketched below, which shows a discrete frequency spike at 100 Hz with a lower broad-band level extending between 95 and 105 Hz. It seems obvious that the discrete frequency peak is far more important. However, although the discrete frequency spike is 10 dB higher than the broad-band level, the broad-band level extends over a wider range, 10 times wider in fact. Thus, the discrete frequency spike and the broad-band level as shown actually have equal contributions to the overall power, and they could be regarded as having equal importance. Unfortunately, there is no automatic way of measuring the comparative

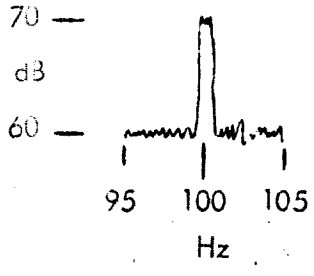

contributions of various sources on an overall power basis. Only the overall contribution from the combined sources can be measured. Comparative contributions can be calculated only by a tedious addition of the various terms observable in narrow-band data, such as in Figure 5. These calculations have been made for this spectrum and are shown in Figure 11c.

Note the very different appearance of Figure 11c compared to Figure 11a. Figure 11a suggests that tail rotor harmonics are predominant over the frequency range of from 100 to 400 Hz; but Figure 11c shows that both main rotor rotational noise and main rotor "vortex" noise are equally important. This again shows the significance of the main rotor as a noise producer. If the subjective correction curve of Figure 10 is now applied to Figure 11c, the result is Figure 11d. Figure 11d gives yet another order of magnitude for the noise field. It is thought that, of the many possible ways of considering the data, the one-third octave plot (subjectively corrected), as shown in Figure 11d, is probably the most meaningful from the detectability viewpoint. However, for the basic reporting of acoustic data, the narrow-band analysis (uncorrected for subjective effects) of Figures 8 and 9 is the most helpful.

In conclusion of this brief review of available data, it is worthwhile to give two further empirical equations which relate to engine noise. A result from Davidson and Hargest's paper[4] may be quoted to give the noise radiation of a piston engine as

$$dB_{500} = 37.5 + 17.7 \log_{10} HP \qquad (5)$$

where HP is the installed horsepower. For an axial flow jet engine compressor, a result from Reference 18 may be used.

$$dB = 50 \log_{10} V_T + 20 \log_{10} D - 86 \qquad (6)$$

where V_T = the compressor tip velocity and D = the duct diameter.

2.2 REVIEW OF THEORY

Initial attempts to predict helicopter rotor noise utilized the large body of analysis built up to describe the noise radiation from propellers, for example References 15 to 17. It was inevitably found that, although propeller noise theory was sometimes fairly accurate for the first harmonic of the helicopter rotational noise, it was grossly in error - by over 100 dB in many cases - for the higher harmonics. A typical example is shown in Figure 12a, which will be discussed in more detail below. In fact, propeller noise theory was found to be unacceptable for predicting the higher harmonic sound radiation even for propellers.

An obvious possible reason for the discrepancy between this theory and helicopter experiments was the existence of large fluctuating forces on the blades in the hel-

copter case, and this was suggested by many workers. As a result of two detailed theoretical studies, by Schlegel[12] and Loewy and Sutton,[10,11] the potential significance of the fluctuating forces is now clear. It is the opinion of the authors of this report that all the significant higher harmonic sound effects (except possibly at transonic or supersonic speeds) can be attributed to these unsteady loadings.

The two studies mentioned above justify further review. A comparison of the theoretical and experimental results from each report is given in Figures 12 and 13. Both investigations use substantially the same approach. The equations for sound generation from a point force are written, and expressions for the radiation from the complete rotor are found by integration over the rotor disc. A difference in form between the basic equations used results from the use of the Garrick and Watkins[16] moving-axis form by Loewy and Sutton[10] and the more usual fixed-axis form by Schlegel et al.[12] In each approach, the necessary integrals are evaluated on a computer. Both approaches retain the acoustic near-field terms in the point source radiation. (By way of explanation, a fluctuating point force produces an acoustic pressure field which contains two components, one of which falls off as r^2 and one as r, where r is distance. Clearly, sufficiently far away from the source, only the last (acoustic far-field) term is significant. For calculations near the source (say a wavelength or so), the first (acoustic near-field) term must be retained. Schlegel et al's approach does assume a second "geometric" far-field approximation, whose terms of order $(R/r)^2$ where R is rotor radius, can be neglected, thus simplifying the integration. All far-field approximations will be valid sufficiently far from the helicopter. Schlegel et al use a rectangular distribution approximation to the chordwise loading pattern, while Loewy and Sutton use an analytic approximation which leads to complex algebraic expressions. This difference is thought to be insignificant. The effect of chordwise loading is discussed in detail in Section 5.2.

Schlegel et al[12] give detailed comparisons of their theory and experiments only for the first four harmonics of the noise. Fair agreement is found for the first two, but it is clear that underestimation of the fourth, and presumably higher, harmonic occurs. However, it should be noted that they achieve a substantial improvement over the basic propeller noise calculations due to Gutin.[15] This can be seen in Figure 12a. Their report shows very clearly that the higher harmonics of the loading have important contributions to the higher harmonics of the noise. Loewy and Sutton[10,11] come to the same general conclusions, but their report appears to contain some errors. For instance, they show experimental data with peak frequencies which do not occur at the blade passage frequency and its harmonics. It is difficult to conceive of any mechanism by which this could occur. Certainly the explanation put forward by Loewy and Sutton of random variations due to downwash would not explain it. Such variations can cause only broadening of the observed peak and not a shift of its center frequency. It appears that at some point in the analysis between recording and final plot, a frequency reference was mislaid. The most likely source of error is that the frequencies shown as harmonic intervals in their original graph are actually 10-Hz

intervals. Using their observed fundamental frequency of 14.7 Hz, then, gives harmonics in good agreement with the experimental data. This corrected version of their results is shown in Figure 13. The accuracy of prediction of the amplitude of the harmonics is improved slightly over their original graph, but the levels are still too low.

Other problems also arise in the interpretation of Loewy and Sutton's results. The very substantial near-field effects found by Loewy and Sutton were not observed by Schlegel et al, nor are they found in the present work. It seems likely that an error occurred in Loewy and Sutton's computations, which led to underestimation of the far-field noise. This explains, to some extent, why predicted levels in Figure 13 are lower than measured data. A further problem arises in the definition of higher harmonic airloads by Loewy and Sutton. They use data from Scheiman[21] which gives up to 24 values per revolution. The basic Nyquist rule for frequency analysis states that only harmonics up to one-half the number of available points can be calculated.[22] Thus, in this case, only harmonics up to the twelfth can be calculated. Harmonics up to the tenth were given by Scheiman. However, Loewy and Sutton plot harmonics out to the twentieth. This procedure must be in error due to folding frequency (or "aliasing") effects, and explains the excessively high values of loading harmonics found by Loewy and Sutton, which undoubtedly went a considerable way toward offsetting the far-field radiation underestimate noted above. Further applicable theoretical work has been accomplished in References 18, 23, and 24, but numerical estimates of direct application to the helicopter problem are not given. Section 3.5 gives a brief comparison of these latter studies and the present work.

3.0 THEORETICAL ACOUSTICS

3.1 THE GENERAL EQUATIONS FOR SOUND GENERATION

In this section the general equations for sound generation will be derived from first principles. Throughout this section, Tensor notation with the summation convention will be used. This notation is particularly convenient for reducing the volume of mathematics. For example, the continuity equation may be written

$$\frac{\partial \rho}{\partial t} + \frac{\partial (\rho v_i)}{\partial x_i} = Q \qquad (7)$$

where ρ = the density

t = time

Q = the rate of introduction of mass per unit volume, which may vary in any desired way over space

x_i = a three-dimensional Cartesian coordinate representing x_1, x_2, x_3 as i takes on the values 1, 2, 3.

v_i = a velocity component representing v_1, v_2, v_3, as i takes on the values 1,2,3.

The Einstein summation convention used here requires that when the same index is repeated in any term, then the summation of that term over all values of the index is necessary. Thus, the second term in the above equation can be expanded as

$$\frac{\partial (\rho v_i)}{\partial x_i} = \frac{\partial (\rho v_1)}{\partial x_1} + \frac{\partial (\rho v_2)}{\partial x_2} + \frac{\partial (\rho v_3)}{\partial x_3}$$

The simplicity achieved by using this notation is apparent.

Similarly, the equation for the conservation of momentum can be written

$$\frac{\partial (\rho v_i)}{\partial t} + \frac{\partial (\rho v_i v_j)}{\partial x_j} + \frac{\partial p_{ij}}{\partial x_j} = F_i \qquad (8)$$

where F_i = (i = 1,2,3) the components of external force per unit volume acting over the fluid.

p_{ij} = the nine component stress tensor which includes the viscous and internal pressure forces on the fluid.

In Equation (8) the suffix i can again take on the values 1, 2, 3, but here each different value implies a separate equation. Equation (8) is a form of the compressible Navier-Stokes equations. Both the second and the third terms on the left-hand side of Equation (8) have a repeated index j and therefore require summing. Writing out Equation (8) in the long, conventional notation would require a total of three equations, each with eight terms. Again, the advantages of the present Tensor notation are clear.

Differentiating Equation (7) with respect to t and Equation (8) with respect to x_i and subtracting gives

$$\frac{\partial^2 \rho}{\partial t^2} = \frac{\partial Q}{\partial t} - \frac{\partial F_i}{\partial x_i} + \frac{\partial^2 (\rho v_i v_j + p_{ij})}{\partial x_i \partial x_j}$$

Again, differentiation of Equation (8) with respect to x_i introduces a double suffix i, which requires summing. Doing the same operation without Tensor notation would have required differentiation of three original equations by three different variables followed by summing, but in the present notation the result is obvious. In order to derive the equation for sound generation, the term

$$a_0^2 \, \partial^2 \rho / \partial x_i^2$$

is subtracted from each side, first done by Lighthill,[25] giving finally the general equation for sound generation as

$$\frac{\partial^2 \rho}{\partial t^2} - a_0^2 \frac{\partial^2 \rho}{\partial x_i^2} = \frac{\partial Q}{\partial t} - \frac{\partial F_i}{\partial x_i} + \frac{\partial^2 T_{ij}}{\partial x_i \partial x_j} \qquad (9)$$

where $T_{ij} = \rho v_i v_j + p_{ij} - a_0^2 \rho \delta_{ij}$

$\delta_{ij} = 1, \; i = j \; ; \; = 0, \; i \neq j$ (The Kronecker δ)

a_0 = the speed of sound in the undisturbed fluid.

The left-hand side of Equation (9) is the wave equation ($\partial^2/\partial x_i^2 \equiv \nabla^2$), and the right-hand side can be regarded as a collection of acoustic source terms. The wave equation is given in terms of a (fluctuating) density ρ but, if desired, can be easily

converted to pressure p by putting $p = a_0^2 \rho$, which will apply in most practical problems.

It may be observed that ρ (or equivalently p) occurs on both sides of Equation (9), so that in principle Equation (9) cannot be solved directly. In practice, the terms on the right-hand side may be regarded as known, and expressions for the sound field can be obtained using the well-known solutions to the Wave Equation.

Each term on the right hand of Equation (9) represents a different possible acoustic source mechanism. The first, $\partial Q/\partial t$, gives the effect of mass introduction. In a helicopter, an example could be the tip jet rotor. Mass sources are the most efficient radiators of sound at low speeds. The second term, $\partial F_i/\partial x_i$ (note the necessary summation), gives the effect of fluctuating forces acting on the air. Since the helicopter rotor exerts substantial fluctuating forces on the air, this is the term of prime interest in the present study. The third term, $\partial^2 T_{ij}/\partial x_i \partial x_j$, incorporates a rather large number of effects, the most important of which, in general, is that of turbulence. T_{ij} may be regarded as an acoustic stress tensor. Note that since i and j may independently take on three values, T_{ij} actually has nine components. Fortunately, this term is of little interest in the present work, and it is unlikely to be significant in the helicopter noise problem unless the rotor is driven by high-speed turbulent jets. It is possible to derive several quite interesting general features associated with each of these noise radiation mechanisms, such as velocity dependence and directionality. However, this will not be done here. A discussion is given in Reference 9.

3.2 SOLUTION OF THE GENERAL EQUATION

The solution to the wave equation is well known. If the right-hand side of Equation (9) is written as $g(\underset{\sim}{y})$, the solution to (9) is

$$\rho = \frac{1}{4\pi a_0^2} \int \left[\frac{g}{r}\right] d\underset{\sim}{y} \qquad (10)$$

where ρ = a fluctuating density

r = the distance from source to observer

$\underset{\sim}{y}$ = the coordinate of the source position

The symbol $\sim$ under y implies that y is a vector quantity. This symbol is used because it requires a printer to use heavy (Clarendon) type, as is usual for vectors. The brackets around the g/r term are of extreme importance, since they imply evaluation of their contents at "retarded" time $\tau = t - r/a_0$. Because sound travels at a finite speed through the air, sound heard at the same observer time from different parts of an

extended source must actually have been emitted at different source times. Thus, unless proper account is taken of these retarded time effects, the acoustic calculations are invalid.

Although Equation (10) does give the solution in principle, the actual source terms on the right-hand side of Equation (9) contain differentials, and Equation (10) thus requires some further manipulation before it can be used in any simple manner. Several methods of reducing Equation (10) to a more useful form are available (for example, References 8 and 18), but for the present problems it is most convenient to proceed along the following lines, which follow in part a method suggested by Lighthill.[25]

We need to solve the equation

$$W(\rho) = -\frac{\partial F_i}{\partial x_i} \tag{11}$$

where W represents the wave equation, and where the source terms on the right-hand side of Equation (9) have been specialized to include just the force terms, which are the only terms of interest in the present helicopter problem. Consider the equation

$$W(\rho_i) = -F_i \tag{12}$$

which, by Equation (10), has the solution

$$\rho_i = \frac{-1}{4\pi a_0^2} \int \left[\frac{F_i}{r}\right] d\underset{\sim}{y} \tag{13}$$

Differentiating (12) with respect to x_i gives

$$W\left(\frac{\partial \rho_i}{\partial x_i}\right) = -\frac{\partial F_i}{\partial x_i} \tag{14}$$

Comparison of Equations (11) and (14) gives the solution to (11) as

$$\rho = \frac{\partial \rho_i}{\partial x_i} = \frac{-1}{4\pi a_0^2} \frac{\partial}{\partial x_i} \int \left[\frac{F_i}{r}\right] d\underset{\sim}{y} \tag{15}$$

The above derivation shows how the solutions to the wave equation for the force terms may easily be generated from those for a simple source g, simply by differentiation. This method will be used in detail in Section 3.4 to derive expressions for the noise radiation from the fluctuating forces on the helicopter rotor. However, first of all, Equation 15 will be used directly to give a convenient computer formula for calculation of the noise from an arbitrarily moving fluctuating force distribution.

3.3 THE MOVING FLUCTUATING FORCE

If we now assume that the forces are in motion, it is convenient to specify the forces in a moving frame of reference, for example, on the helicopter rotor. Suppose that coordinates measured in this frame are defined by $\underset{\sim}{\eta}$ and that the origin of these coordinates is moving with velocity $a_0 \underset{\sim}{M}$. Then, at any instant, the $\underset{\sim}{\eta}$ and $\underset{\sim}{y}$ coordinate systems are connected via

$$\underset{\sim}{\eta} = \underset{\sim}{y} - \underset{\sim}{M} a_0 t$$

However, in Equation 15 we are not required to evaluate the integral at any instant t. Instead, the integral must be evaluated at the appropriate retarded time $\tau = t - r/a_0$; i.e., over

$$\underset{\sim}{\eta} = \underset{\sim}{y} + \underset{\sim}{M} r - \underset{\sim}{M} a_0 t$$

Thus, in the coordinate transformation from fixed to moving axes, it is appropriate to use, as first suggested by Lighthill,[25]

$$\underset{\sim}{\eta} = \underset{\sim}{y} + \underset{\sim}{M} r \tag{16}$$

This axis transformation also affects the volume element of the integration in (15), and the integral must be divided by the Jacobian of the transformation

$$J = \begin{vmatrix} \partial\eta_1/\partial y_1 & \partial\eta_2/\partial y_1 & \partial\eta_3/\partial y_1 \\ \partial\eta_1/\partial y_2 & \partial\eta_2/\partial y_2 & \partial\eta_3/\partial y_2 \\ \partial\eta_1/\partial y_3 & \partial\eta_2/\partial y_3 & \partial\eta_3/\partial y_3 \end{vmatrix} = 1 - M_r$$

where $M_r = M_i(x_i - y_i)/r = \left\{ M_1(x_1 - y_1) + M_2(x_2 - y_2) + M_3(x_3 - y_3) \right\} / r$

is the component of the convection Mach number in the direction of the observer.

Equation (15) thus becomes

$$\rho = \frac{1}{4\pi a_0^2} \frac{\partial}{\partial x_i} \int \left[\frac{F_i}{r(1 - M_r)} \right] d\eta \tag{17}$$

The derivative $\partial/\partial x_i$ is operating on both an integral over η and a retarded time operator, both of which are functions of x. For any function $f(t)$,

$$\left[f(t) \right] = \left[f(t - r/a_0) \right]$$

Thus, the partial derivative with respect to x_i, keeping η constant of f, is given by the chain rule as

$$\frac{\partial}{\partial x_{i(\eta)}} \left[f \right] = \left[\frac{\partial f}{\partial x_{i(\eta)}} - \frac{\partial r}{\partial x_{i(\eta)}} \frac{1}{a_0} \frac{\partial f}{\partial t} \right] \tag{18}$$

Now $$\frac{\partial}{\partial x_{i(\eta)}} = \frac{\partial}{\partial x_{i(\eta)}} \left| x_j - y_j \right|^2 = \frac{x_j - y_j}{r} \frac{\partial}{\partial x_{i(\eta)}} (x_j - y_j)$$

From Equation (16), $$\frac{\partial}{\partial x_{i(\eta)}} (x_j - y_j) = \delta_{ij} + M_j \frac{\partial r}{\partial x_{i(\eta)}}$$

Hence, $$\frac{\partial r}{\partial x_{i(\eta)}} = \frac{x_i - y_i}{r(1 - M_r)}$$

and when this is in Equation (18),

$$\frac{\partial}{\partial x_{i(\eta)}} \left[f \right] = \left[\frac{\partial f}{\partial x_{i(\eta)}} - \frac{x_i - y_i}{r(1 - M_r)} \frac{1}{a_0} \frac{\partial f}{\partial t} \right] \tag{19}$$

Now the order of magnitude of the first term on the right-hand side of Equation (19) is $1/r$ where r is a typical distance from the source, whereas the order of magnitude of the second term is $f/a_0 = 1/\lambda$ where f is a typical frequency and λ is a typical wavelength. Thus, when the observation point is many wavelengths from the source, the

first near-field term may be ignored. Hence, when (19) and (17) are used, the expression for the sound radiation in the far field due to an arbitrarily moving force distribution is

$$p = \frac{1}{4\pi a_0^2} \int \left[\frac{x_i - y_i}{a_0 r (1 - M_r)^2} \frac{\partial}{\partial t} \left(\frac{F_i}{r(1 - M_r)} \right) \right] d\underline{\eta} \qquad (20)$$

If desired, the time differentiation may be performed to give

$$p = \frac{1}{4\pi a_0^2} \int \left[\frac{x_i - y_i}{a_0 r (1 - M_r)^2} \left(\frac{\partial F_i}{\partial t} + \frac{F_i}{1 - M_r} \frac{\partial M_r}{\partial t} \right) \right] d\underline{\eta} \qquad (21)$$

where

$$\frac{\partial M_r}{\partial t} = \frac{x_i - y_i}{r} \frac{\partial M_i}{\partial t} \qquad (22)$$

is the component of the acceleration (divided by a_0) in the direction of the observer. Equation (21) was derived for the special case of a point source.[8] Note that both Equations (20) and (21) apply only if the force distribution is not changing in size. This will be the case for helicopter applications.

Further discussions on the utilization of Equation (21) for computer calculation of sound levels is given in Section 5.0. In the next section, analytic solutions for the noise radiation from a helicopter will be given using methods which are an extension of those presented in Section 3.2.

3.4 RADIATION FROM A HELICOPTER ROTOR

As shown in Section 3.2, the sound radiation from a fluctuating force can be found from the solution for a simple source by differentiation. In the helicopter, fluctuating axial, circumferential, and radial components of force occur. Rather than calculate the effects of each force component separately, it is convenient to solve the problem for the rotating simple source first and then just to differentiate in the appropriate direction to determine results for the various force components.

Suppose that the fluctuating source is defined by a Fourier series

$$g(\theta) = \alpha_0 + \sum_{\lambda=1}^{\infty} \alpha_\lambda \cos \lambda\theta + \beta_\lambda \sin \lambda\theta \qquad (23)$$

where θ is the angle around the rotor disc from the y-axis and is equal to Ωt, where Ω is the angular velocity of the rotor. It is convenient for the present problem to define also a complex Fourier series by

$$g_2(\theta) = \sum_{\lambda=-\infty}^{+\infty} A_\lambda \exp(-i\lambda\theta) \tag{24}$$

$$\left.\begin{aligned} \text{so that} \quad A_\lambda &= A_{\lambda R} + iA_{\lambda I} = (\alpha_\lambda + i\beta_\lambda)/2 \\ A_{-\lambda} &= A_{\lambda R} - iA_{\lambda I} = (\alpha_\lambda - i\beta_\lambda)/2 \\ A_0 &= \alpha_0 \end{aligned}\right\} \tag{25}$$

Since the source is defined in terms of moving source coordinates, it is necessary to transform Equation (15) from y to η coordinates using Equation (16). In a manner identical to that used to obtain Equation (17), we find that

$$p = \frac{1}{4\pi}\int \left[\frac{q}{r(1-M_r)}\right] d\eta \tag{26}$$

where the relation $p = a_0^2\rho$ has also been used.

Specializing to a point source causes the η integration to vanish. For any harmonic function the Fourier coefficients are given, in complex form, by

$$C_n = a_n + ib_n = \frac{\omega}{\pi}\int f \exp in\omega t \; dt$$

where the integral is over any period. Replacing f by the point source version of Equation (26) gives the complex magnitude of the n^{th} sound harmonic as

$$C_n = \frac{\Omega}{4\pi^2}\int \left[\frac{q}{r(1-M_r)}\right] \exp in\Omega t \; dt \tag{27}$$

Now change from observer's time t to source time τ by $\tau = t - r/a_0$, $dt = d\tau(1 - M_r)$, giving

$$C_n = \frac{1}{4\pi^2}\int_0^{2\pi}\left[\frac{g}{r}\right]\exp i\,n\,(\theta + \Omega r/a_0)\,d\theta \qquad (28)$$

where $\Omega\tau$ has been replaced by θ.

It can be seen from Figure 14 that

$$\lambda^2 = x^2 + Y^2 + R^2 - 2YR\cos(\theta - \phi) \qquad (29)$$

where x,y = Cartesian coordinates with x along the rotor axis

Y = the radial distance of the observer from the rotor axis

R = the effective radius of the point source

ϕ = a reference angle between the y-axis and the observer

If the observer is far from the rotor, so that $(x^2 + Y^2) >> R^2$, then Equation (29) may be approximated to give

$$r = r_1 - \frac{YR}{r_1}\cos(\theta - \phi) \qquad (30)$$

where $r_1 = (x^2 + Y^2)^{0.5}$ is the distance of the observer from the rotor hub.

Using the approximation of Equation (30) and the source terms defined by Equation (24) in Equation (28) gives

$$C_n = \frac{1}{4\pi^2}\int_0^{2\pi}\sum_{\lambda=-\infty}^{+\infty}\frac{A_\lambda}{r_1}\exp i\left\{(n-\lambda)\theta + \frac{n\Omega r_1}{a_0} - \frac{n\Omega YR}{a_0 r_1}\cos(\theta - \phi)\right\}d\theta$$

which can be written

$$C_n = \frac{1}{4\pi^2}\int_0^{2\pi}\sum_{\lambda=-\infty}^{+\infty}\frac{A_\lambda}{r_1}\exp i\left\{(n-\lambda)(\theta-\phi) - \frac{n\Omega YR}{a_0 r_1}\cos(\theta-\phi)\right\}d(\theta-\phi)$$

$$\times\ \exp i\left\{\frac{n\Omega r_1}{a_0} + (n-\lambda)\phi\right\} \qquad (31)$$

Since the integral applies over an interval 2π, it can be expressed in Bessel function form, using formula 42 in M[illegible]26

$$2\pi i^{-n} J_n(z) = \int_0^{2\pi} \exp i\,(n\theta - z\cos\theta)\, d\theta \qquad (32)$$

so that

$$C_n = \frac{1}{2\pi} \sum_{\lambda=-\infty}^{+\infty} i^{-(n-\lambda)} \frac{A_\lambda}{r_1} J_{n-\lambda}\left(\frac{n\Omega Y R}{a_0 r_1}\right) \exp i\left\{\frac{n\Omega r_1}{a_0} + (n-\lambda)\phi\right\} \qquad (33)$$

Equation (33) gives, in complex form, the sound harmonics from a point simple source describing a circular path. The equation could be applied directly to the calculation of rotating mass sources, provided that the time differential is observed (see Equation (9) and that proper account is taken of momentum output (see References 8 and 9). However, we are interested in deriving the results for the force cases, which are

$$\left.\begin{aligned}
\text{Axial} \qquad & \frac{-\partial C_n}{\partial x} = -\sum_{\lambda=-\infty}^{+\infty} i^{-(n-\lambda)} \frac{in\Omega x}{2\pi a_0 r_1^2} A_\lambda J_{n-\lambda}\left(\frac{nMy}{r_1}\right) \\
\text{Circumferential} \qquad & \frac{-1}{R}\frac{\partial C_n}{\partial \phi} = -\sum_{\lambda=-\infty}^{+\infty} i^{-(n-\lambda)} \frac{i(n-\lambda)}{2\pi r_1} \frac{A_\lambda}{R} J_{n-\lambda}\left(\frac{nMy}{r_1}\right) \\
\text{Radial} \qquad & +\frac{\partial C_n}{\partial R} = +\sum_{\lambda=-\infty}^{+\infty} i^{-(n-\lambda)} \frac{n\Omega Y}{2\pi a_0 r_1^2} A_\lambda J'_{n-\lambda}\left(\frac{nMy}{r_1}\right)
\end{aligned}\right\} \qquad (34)$$

Only the far-field terms have been retained in Equations (34).

The prime on the Bessel function in the radial expression denotes differentiation; $M = \Omega R/a_0$ is the rotational Mach number of the point force. Negative signs must be applied in the first two equations because differentials are based on observer coordinates, whereas the differential in the last equation is on a source coordinate.

Notation in Equations (34) must now be changed to specify the forces acting. The three components by simple Fourier series are defined as

$$\left.\begin{aligned}
&\text{Thrust} && T(\theta) = a_{0T} + \sum_{\lambda=1}^{\infty} a_{\lambda T}\cos\lambda\theta + b_{\lambda T}\sin\lambda\theta \\
&\text{Drag} && D(\theta) = a_{0D} + \sum_{\lambda=1}^{\infty} a_{\lambda D}\cos\lambda\theta + b_{\lambda D}\sin\lambda\theta \\
&\text{Outward Components} && C(\theta) = a_{0C} + \sum_{\lambda=1}^{\infty} a_{\lambda C}\cos\lambda\theta + b_{\lambda C}\sin\lambda\theta
\end{aligned}\right\} \quad (35)$$

The thrust, drag, and outward components of force are assumed to act in the axial, circumferential, and radial directions respectively. In conversion to thrust, a minus sign must be incorporated because the force on the air is in the negative x-direction.

Equations (34) are converted to the required form using Equations (25). Note that terms for both plus and minus λ in the summations in (34) contribute to the result for any given loading harmonic. Thus, the final result for the complex magnitude of the sound harmonic is

$$C_n = a_n + ib_n$$

$$= \sum_{\lambda=0}^{+\infty} \frac{i^{-(n-\lambda)}}{4\pi} \left\{ \frac{n\Omega x}{a_0 r_1^2} \left\{ +i a_{\lambda T}\left(J_{n-\lambda} + (-1)^{\lambda} J_{n+\lambda}\right) - b_{\lambda T}\left(J_{n-\lambda} - (-1)^{\lambda} J_{n+\lambda}\right) \right\} \right.$$

$$- \left\{ \frac{i a_{\lambda D}}{R r_1}\left((n-\lambda)J_{n-\lambda} + (-1)^{\lambda}(n+\lambda)\, J_{n+\lambda}\right) \right.$$

$$\left. - \frac{b_{\lambda D}}{R r_1}\left((n-\lambda)J_{n-\lambda} - (-1)^{\lambda}(n+\lambda)J_{n+\lambda}\right) \right\}$$

$$\left. + \frac{n\Omega Y}{a_0 r_1^2} \left\{ a_{\lambda C}\left(J'_{n-\lambda} + (-1)^{\lambda} J'_{n+\lambda}\right) + i b_{\lambda C}\left(J'_{n-\lambda} - (-1)^{\lambda} J'_{n+\lambda}\right) \right\} \right\} \quad (36)$$

The argument of all the Bessel functions is $n\Omega y/r_1$. Note also that

$$2J_n' = (J_{n-1} - J_{n+1}).$$

For computation the result of Equation (36) must be expanded into real and imaginary parts. The detailed results are

$$a_{n\lambda} = \frac{n\Omega}{4\pi a_0 r_1}\left\{\frac{x a_{\lambda T}}{r_1}\left(J_{n-\lambda} + (-1)^{\lambda} J_{n+\lambda}\right) - \frac{a_{\lambda D}}{nM}\left\{(n-\lambda)J_{n-\lambda} + (-1)^{\lambda}(n+\lambda)J_{n+\lambda}\right\}\right.$$

$$\left. - \frac{y b_{\lambda C}}{2r_1}\left\{J_{n-\lambda+1} - J_{n-\lambda-1} - (-1)^{\lambda}\left(J_{n+\lambda+1} - J_{n+\lambda-1}\right)\right\}\right\}(-1)^{\frac{n-\lambda-1}{2}}$$

$n-\lambda$ odd

$$a_{n\lambda} = \frac{n\Omega}{4\pi a_0 r_1}\left\{\frac{x b_{\lambda T}}{r_1}\left(J_{n-\lambda} - (-1)^{\lambda} J_{n+\lambda}\right) - \frac{b_{\lambda D}}{nM}\left\{(n-\lambda)J_{n-\lambda} - (-1)^{\lambda}(n+\lambda)J_{n+\lambda}\right\}\right.$$

$$\left. + \frac{y a_{\lambda C}}{2r_1}\left\{J_{n-\lambda+1} - J_{n-\lambda-1} + (-1)^{\lambda}\left(J_{n+\lambda+1} - J_{n+\lambda-1}\right)\right\}\right\}(-1)^{\frac{n-\lambda-2}{2}}$$

$n-\lambda$ even

$$b_{n\lambda} = \frac{n\Omega}{4\pi a_0 r_1}\left\{\frac{x a_{\lambda T}}{r_1}\left(J_{n-\lambda} + (-1)^{\lambda} J_{n+\lambda}\right) - \frac{a_{\lambda D}}{nM}\left\{(n-\lambda)J_{n-\lambda} + (-1)^{\lambda}(n+\lambda)J_{n+\lambda}\right\}\right.$$

$$\left. - \frac{y b_{\lambda C}}{2r_1}\left\{J_{n-\lambda+1} - J_{n-\lambda-1} - (-1)^{\lambda}\left(J_{n+\lambda+1} - J_{n+\lambda-1}\right)\right\}\right\}(-1)^{\frac{n-\lambda}{2}}$$

$n-\lambda$ even

$$b_{n\lambda} = \frac{n\Omega}{4\pi a_0 r_1}\left\{\frac{\cdots}{\cdots}\left(J_r \cdots -(-1)^{\lambda} J_{n+\lambda}\right) + \frac{\cdots}{n M}\left\{(n-\lambda)J_{n-\lambda} \cdots -(-1)^{\lambda}(n+\lambda)J_{n+\lambda}\right\}\right.$$

$$\left. + \frac{\gamma a_\lambda C}{2r_1}\left\{J_{n-\lambda+1} - J_{n-\lambda-1} - (-1)^{\lambda}\left(J_{n+\lambda+1} - J_{n+\lambda-1}\right)\right\}\right\} \cdots \quad (37)$$

where the additional subscript λ implies that only the one λ loading harmonic is considered. The complete sound field is given by the summation of sound radiated by all harmonics.

3.5 COMMENTS ON THE RESULTS

Equations (37) give the complete solution for the sound radiated by fluctuating airloads on a rotor. The results are limited in two ways. First, the equations do not apply close to the rotor, say, within a few wavelengths or rotor diameters. This is not important for most practical noise problems. Second, they do not include the effects of blade motion. This point has been studied using the general computer program based on Equation (21) and is also studied analytically in Appendix I. One extremely important effect not explicitly given in Equations (37) is the effect of blade number. If B blades are present, harmonics which are not integral multiples of B will cancel out. Those harmonics which are multiples of B will add. Thus, the effect of blade number may be included in Equations (36) and (37) by replacing n by mB. In this case, the coefficients of the force harmonics must be taken as the values for the complete rotor, which are B times the values for the individual blades.

It is of particular interest to consider the case $\lambda = 0$ in Equation (36). This corresponds to the case of steady loading only, as is assumed for a propeller. Using $\lambda = 0$ in Equation (36) gives substantial cancellation, with the final result

$$C_n = \frac{(i)^{-n+1}\, n\Omega}{2\pi a_0 r_1}\left\{\frac{xT_0}{r_1} - \frac{D_0}{M}\right\} J_n\left(\frac{nMy}{r_1}\right) - \frac{i^{-n}\, n\Omega}{2\pi a_0 r_1} \cdot \frac{YC_0}{2r_1}\left\{J_{n-1}\left(\frac{nMy}{r_1}\right) - J_{n+1}\left(\frac{nMy}{r_1}\right)\right\} \quad (38)$$

The first term in the above equation is identical with the classical propeller noise solution due to Gutin,[15] while the second, the radial component term, is the same as that derived in Reference 9. The reduction of the general solution to particular cases previously obtained is a helpful test of the mathematics.

The effect of forward velocity is also of considerable interest. In Reference 8 it was pointed out how the equations for constant velocity convection of the hub could be obtained from those for the stationary case by replacing the term r_1 in the stationary case by $r_1 (1 - M_{or})$, where M_{or} is the component of the hub convection Mach number in the direction of the observer. In utilizing this transformation, it is important to note that it applies to the retarded position of the helicopter. In other words, the dimension r_1 used must be taken as the distance from the observer to the position of the helicopter when it emitted the sound. Relation of the results to the instantaneous position of the helicopter requires another transformation. Details are given in Section 5.1 and in the companion report.[40] It may also be noted that virtually identical transformations were presented in Reference 18, where it was also shown that the above $(1 - M_{or})$ correction term gave the Garrick and Watkins,[16] moving propeller result directly from that of Gutin,[15] for the stationary case.

Perhaps it should also be noted that the results of Equation (36) are not entirely new. During the course of the current study, a major new book on acoustics by Morse and Ingard,[23] was published. Equation 11.3.20 of that book gives the sound radiation by a propeller in unsteady flow, which corresponds to the helicopter rotor case. Only thrust and drag terms are considered in that equation. The results are derived in a rather different manner, but they agree with those derived here. No numerical analysis of the results is given, but several additional points of interest are discussed. A report by Arnold et al,[24] also treats a similar case, the problem of the "singing" propeller in underwater acoustics. Here, frequencies other than the fundamental were allowed to occur, and it was found that multiple frequencies were produced by frequency modulation effects. Finally, a recent report by Lowson,[18] covers the related case of jet engine compressor noise. Again, only thrust and drag terms were considered, but results were obtained by a method different from that given here and are in agreement. Analytic expressions for overall acoustic power radiation were also given which can be of use to the present problem.

4.0 ROTOR AERODYNAMICS

It was noted in Section 2.1 that the basic source of helicopter noise is the main lifting rotor (or rotors), and a brief discussion of the general problem was presented to support this statement. In this section a closer look is taken at the fundamental aerodynamic phenomena which generate rotor noise, and suitable techniques for evaluating their magnitudes are examined. It is not intended to present a rigorous treatment of the subject of rotor aerodynamics; this is a complex subject in its own right, but the fundamentals are covered in sufficient detail to serve as an introduction to rotor noise generation and to postulate some realistic source terms for the noise theory. Emphasis is placed on the acoustic implications of each aspect of the problem.

The notation in this section is somewhat different from that in preceding sections, since an attempt has been made to use conventional helicopter aerodynamics symbols wherever possible (in particular, following References 27 and 28). Symbols used in this section that have different meanings elsewhere are listed below.

a	lift curve slope
a_o	coning angle, rads
c	blade chord, ft
c_o	effective root chord, ft
e	effective disc area correction $= s_2^2 - s_1^2$
k_i	blade twist integral[28] $= t_{i+1}\ \vartheta_T$
n	harmonic number
r	blade radial position, ft
s	nondimensional radial station $= r/R$
s_1	station defining inboard end of blade
s_2	station defining effective outboard end of blade
t_i	blade taper integral[28] $= 4 \int_{s_1}^{s_2} \frac{c}{c_o}\ s^{i-1}\, ds$
A	disc area $= \pi R^2$, ft^2
A_1	longitudinal cyclic pitch coefficient, rads

B_1 lateral cyclic pitch coefficient, rads

C_{T_b} blade thrust coefficient $T/\frac{1}{2}\rho(\Omega R)^2 R a B C_o c_o$

I blade moment of inertia about flapping hinge, slugs ft^2

R rotor radius, ft

γ blade inertia coefficient $I/\frac{1}{8}\rho R^4 a C_o$

ϑ blade pitch, rads

ϑ_c collective pitch (nominal), rads

ϑ_R collective pitch measured at blade root, rads

ϑ_T total blade twist root to tip (washout)

λ downwash coefficient

μ advance ratio = $V/\Omega R$

ϕ blade angle of attack, rads

ψ rotor azimuth angle, rads

4.1 NOISE GENERATION BY AERODYNAMIC FORCES

We have seen in Section 2.1 that the major contributions to rotor noise are made by the fluctuating lift and drag forces which act on the rotor blades and are constantly in motion. The basic equation of sound generation by an aerodynamic force in motion is (Equation 20)

$$\rho = \frac{1}{4\pi a_0^2}\left[\frac{x_i - y_i}{a_0\, r(1-M_r)^2}\left\{\frac{\partial F_i}{\partial t} + \frac{F_i}{1-M_r}\cdot\frac{\partial M_r}{\partial r}\right\}\right]$$

where the space integral has been removed, since the F_i represent a point force. Thus, the sound pressure (or density) fluctuation at any point due to the force is a function of its position relative to the observer $(x_i - y_i)/r$, its rate of change $(\partial F_i/\partial t)$, and its velocity and acceleration toward the observer $(M_r, \partial M_r/\partial t)$. The F_i are of course the three orthogonal components of the resultant force acting at the point y_i. In reality, the forces acting on a rotor are distributed pressures, and it is only for mathematical convenience that we perform an integration of these pressures to arrive at equivalent point forces. It is also for convenience that the net aerodynamic load on a rotor blade section is conventionally broken down into the two components known as lift and drag. It will be seen that these components are not particularly useful for the numerical acoustic calculations, and further resolution, into a coordinate system which is fixed in space, is preferable.

However, Equation (20) shows the information required for a sound calculation based on a single source. A helicopter rotor represents a complex distribution of aerodynamic pressures in space, and it is necessary to make use of a distribution of sources which lie on the rotor blade axes. The sketch shows how the distributed lift and drag loads acting on the blades are simulated by a series of point forces. What this diagram does not show are the variations and motions of these forces as the blade rotates.

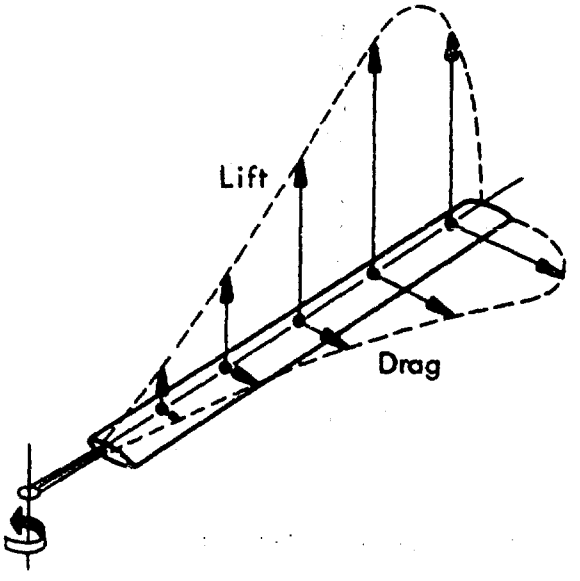

The hovering rotor is relatively straightforward aerodynamically since the forces acting on the blades are effectively steady. Provided the rotor is operating in undisturbed free space, the flow is completely axisymmetrical, and there are, in principle, no perturbations to change the steady forces as the blade rotates. In forward flight, however, when the rotor is essentially sideslipping, providing both lift and propulsive force for the helicopter, the flow over the blades is asymmetric, due to a velocity differential over the advancing and retreating blades. Rotor control is obtained by "cyclic pitch" change, which is the name given to the first harmonic variation applied to the blade pitch angle as it rotates. Since the relative air velocity over the blade also has a first harmonic variation and since aerodynamic forces are proportional to the square of the relative velocity, we may expect to find at least three harmonics in the force fluctuations acting on the blades. This would be true if the flow through the rotor were uniform. However, due to the proximity of the rotor to its own vortex wake, which is swept backwards under the rotor disc, the flow is far from uniform, and velocity fluctuations are induced which give rise to very many harmonics of blade loading. The calculation of these higher harmonic blade loads is an extremely complex problem which, to date, has been performed numerically only by digital computers (for example, References 29, 30, and 31) and then with only limited success. Such calculations were beyond the scope of this study and, as will be shown, would not be justified in any case.

As a first step, a simplified analysis is followed which helps to clarify the general problem.

4.2 ESTIMATION OF BLADE LOADS AND MOTIONS AS A FUNCTION OF FLIGHT CONFIGURATIONS

One of the main prerequisites to performing the noise calculation is to compute the lifting rotor attitude in space, together with the coning angle which dominates the blade flapping motion terms. A procedure by which this information can be accurately derived follows.

Force Balance

The starting point in these calculations is the flight configuration defined by:

W = aircraft gross weight, lb

V = forward velocity, ft/sec

C_{D_p} = fuselage parasite drag coefficient

δ_0 = blade section profile drag coefficient.

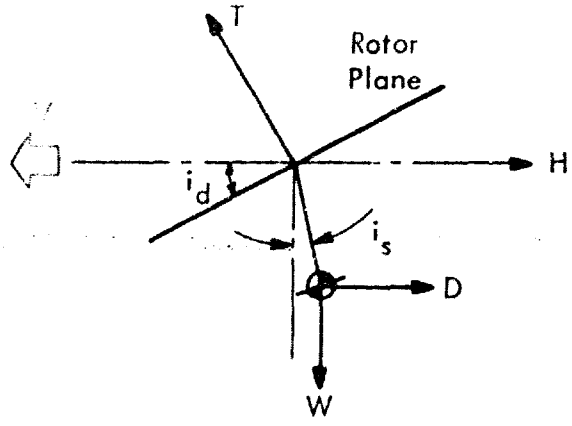

When the rotor thrust vector is assumed to be normal to the tip path plane (and experiment has shown this to be true to within 1° according to Reference 27) and when the rotor weight with respect to the total is ignored, the shaft inclination is

$$i_s = \tan^{-1}\left(\frac{D}{W}\right) \simeq \frac{D}{W}$$

and the disc incidence is

$$i_d = \tan^{-1}\left(\frac{H + D}{W}\right) \simeq \frac{H + D}{W} \tag{39}$$

where D = fuselage drag and H = rotor drag.

Defining a rotor thrust coefficient $C_T = T/0.5\,\rho\,A\,\overline{\Omega R^2}$, a fuselage parasite drag coefficient $C_{D_p} = H/0.5\,\rho A V^2$, a rotor drag coefficient $C_{H_o} = H/0.5\,\rho A V^2$, Equation (39) can be rewritten

$$i_d \simeq \mu^2 \left[\frac{C_{D_p} + C_{H_o}}{C_T}\right] \tag{40}$$

Payne[28] (p. 202) gives

$$C_{H_o} \simeq \mu\, t_2 \frac{\delta}{a} + \frac{1.7\ \mu^2\, t_1\, \delta_0}{a} + \frac{3\,\mu^3\,\delta}{a}$$

where $$\delta = \delta_0 \left[1 + \frac{a^2\, C_{T_b}^{\ 2}}{\left\{t_3^2 + \mu^2\,(2\,t_2^{\ 2} + t_1\,t_3)\right\}}\right]$$

Induced Flow

When the disc angle of attack is known, actuator disc theory is used to calculate the induced flow through the rotor. The momentum relationship is

$$T = 2\rho A v_0 \sqrt{V^2 + v_0^2}$$

A refinement is obtained by introducing the concept of effective area which uses aerodynamic blade root and tip stations to account for tip losses and the blade's ending distance from the rotor hub, $e = s_2^2 - s_1^2$. Using this, the above equation can be written

$$\lambda_{i_0} [\lambda_{i_0}^2 + \mu^2]^{\frac{1}{2}} = C_T/4e \tag{41}$$

A more realistic induced flow distribution is one that is not uniform but increases linearly from the front to the rear of the rotor according to Glauert's classical equation

$$\lambda_i (x, \psi) = \lambda_{i_0} (1 + K x \cos \psi) \tag{42}$$

where K is given by,[28]

$$K = \frac{(4/3)(\mu/\lambda)}{1.2 + (\mu/\lambda)}$$

and λ is the total mean inflow, $\mu \sin i_d + \lambda_{i_0}$.

Rotor Control Settings

Conventional blade element theory is used to establish blade section loadings (see Figure 15),

$$\vartheta = \vartheta_R - \vartheta \cdot - A_1 \cos\psi - B_1 \sin\psi$$

where ϑ_R is the collective pitch setting, and A_1 and B_1 are cyclic pitch coefficients. The normal and tangential velocity components are, putting $s = r/R$;

$$U_p = \lambda \Omega R$$

$$U_T = \Omega R (s + \mu \sin\psi)$$

The lift increment dL on the blade element of width dr is

$$dL = \frac{1}{2}\rho (U_p^2 + U_T^2) C_L c\, dr$$

$$\simeq \frac{1}{2}\rho U_T^2 a \alpha c\, dr \qquad (\text{since } U_p << U_T) \tag{43}$$

where $$\alpha = \vartheta - \phi \simeq \vartheta - \frac{U_P}{U_T}$$

Substitution for U_T and α in this equation eventually yields

$$\frac{dL}{dz} = \frac{1}{2} \rho \overline{\Omega R^2} a c R \left[\left\{ \left(s^2 + \mu^2 \right) \left(\vartheta_R - \vartheta_T s \right) - \mu \times B_1 - \times \lambda_0 \right\} \right.$$

$$- \left\{ \left(s^2 + \frac{1}{4} \mu^2 \right) A_1 + \lambda_{i_0} K s^2 \right\} \cos \psi$$

$$+ \left\{ 2 \mu s \left(\vartheta_R - \vartheta_T s \right) - \left(s^2 + \frac{3}{4} \mu^2 \right) B_1 - \mu \lambda_0 \right\} \sin \psi$$

$$+ \left\{ \mu s B_1 - \frac{1}{2} \mu^2 \left(\vartheta_R - \vartheta_T s \right) \right\} \cos 2\psi - \left\{ \mu s A_1 + \frac{1}{2} \mu K s \lambda_{i_0} \right\} \sin 2\psi$$

$$\left. + \left\{ \frac{1}{4} \mu^2 A_1 \right\} \cos 3\psi + \left\{ \frac{1}{4} \mu^2 B_1 \right\} \sin 3\psi \right] \qquad (44)$$

This analysis assumed zero coning angle. If the coning angle is a_0, then the inflow λ is increased by a factor $\mu a_0 \cos \psi$. Thus, the coefficient $\lambda_{i_0} K s$ is increased to $(\lambda_{i_0} K s + \mu a_0)$. This introduces the additional terms $+ \mu s a_0$ in the $\cos \psi$ bracket and $+ 1/2 \mu^2 a_0$ in the $\sin 2\psi$ bracket.

The blades adopt a "coning" angle to balance lift and centrifugal forces (in the case of the conventional hinged rotor); and when moments about the flapping hinge are equated, it is found by the spanwise integration of the steady term of Equation (44) that

$$a_0 = \frac{- k_4 + \vartheta_R \left(t_4 + \frac{1}{2} \mu^2 t_2 \right) - \frac{1}{2} \mu^2 k_2 - (\mu B_1 + \lambda) t_3}{\gamma} \qquad (45)$$

Since this analysis is conducted with respect to the rotor disc plane, i.e., the "plane of no flapping", the first harmonic section loadings must integrate, over the length of the blade, to zero. This yields two further relationships

$$A_1 = - \frac{(\mu t_3 a + \lambda_{i_0} K t_4)}{\left(t_4 + \frac{1}{4} \mu^2 t_2 \right)} \qquad (46)$$

and $$B_1 = \frac{\left(t_2 + \frac{1}{2}\mu^2 t_1\right)\vartheta_R - \left(C_{T_b} + k_3 + \frac{1}{2}\mu^2 k_1 + \lambda t_2\right)}{\mu^3 t_2} \qquad (47)$$

Finally, the steady term of Equation (44) is integrated to yield the total rotor thrust, which, after substitution of the blade thrust coefficient C_{T_b} gives the following expression for the collective pitch:

$$\vartheta_R = \frac{\left(t_4 + \frac{3}{4}\mu^2 t_2\right)\left(C_{T_b} + k_3 + \frac{1}{2}\mu^2 k_1 + \lambda t_2\right) - \mu^2 t_2 \left(2k_3 + \lambda t_2\right)}{\left(t_3 + \frac{1}{2}\mu^2 t_1\right)\left(t_4 + \frac{3}{4}\mu^2 t_2\right) - 2\mu^2 t_2 t_3} \qquad (48)$$

Equations (48), (47), (45), and (46) are solved sequentially, in that order, for ϑ_R, B_1, a_0 and A_1.

As noted previously, these quantities are derived with respect to disc axes. If the cyclic pitch coefficients are required with respect to the shaft axes (which is more physically meaningful), the following transformations must be applied.

$$A_{1_s} = A_1 + b_{1_s} \qquad \text{and} \qquad B_{1_s} = B_1 - a_{1_s}$$

where b_{1_s} and a_{1_s} are flapping coefficients measured relative to the shaft axes. In this case,

$$a_{1_s} = i_d - i_s \qquad \text{and} \qquad b_{1_s} = 0$$

4.3 LIMITATIONS OF SIMPLE THEORY

The simplified analysis of the preceding section has been used to calculate the control settings and blade loads for the H-34 helicopter in a variety of flight conditions. The computed results have been compared with the experimental data from Reference 21, and some of the comparisons are shown in Figures 16 through 18. Figures 16(a) through 16(d) are the variations of disc angle of attack i_d, collective pitch ϑ_c and cyclic pitch coefficients A_{1_s} and B_{1_s} with advance ratio μ. The most noticeable feature of these plots is the apparently large scatter of the experimental data. However, it should be noted that these points correspond to a large number of flights of the same helicopter under different atmospheric and loading conditions and slightly different rotor speeds. No attempt has been made to normalize these results, although such a step would probably reduce the scatter somewhat. The main reason for not doing so is that insufficient information is available in Reference 21 to perform an adequate normalization. However, in spite of this scatter, it can be seen that the agreement between theory and experiment is fair.

Figures 17 and 18 show the sine and cosine components of the first ten blade section airload harmonics for the two advance ratios $\mu = 0.15$ and $\mu = 0.30$. The experimental points were obtained by the integration of a chordwise distribution of differential pressure measurements and therefore represent the normal blade section loading. The theoretical curves represent section lift loadings which are not exactly aligned with the normal force, although of course the numerical differences in these two forces are very small.

In both velocity cases, the agreement between theory and experiment is good for the steady loading, fair for the first harmonic components, and poor for the second harmonics. Little can be said about the third harmonic comparisons, since there is very little correlation. The simple theory of course predicts no harmonics greater than the third. This is quite clearly unrealistic, since the amplitudes of the harmonics up to the tenth are seen to be significant experimentally. The main conclusion to be drawn from this comparison is that the simple theory based on momentum concepts is adequate for the calculation of rotor performance parameters such as thrust, disc angle of attack, coning angle, and control settings, but it is quite inadequate for the prediction of the harmonic airloads which are so vital to the noise problem.

The deficiencies in the method are fairly obvious. It is important to remember that the momentum theory is simply a crude analogy for the induced flow through the rotor and that the main justification for it is that it gives good agreement with experiment in performance calculations. To obtain a more realistic picture of the induced flow, we must turn to a consideration of the rotor wake and of the vortex sheet theories. Again, in a somewhat crude fashion, it may be considered that if the circulation about a certain length of blade changes instantaneously, then an elemental vortex, of equal but opposite strength to the increment in the bound vortex, will be shed from the blade with its axis parallel to that of the blade. Further, if there is a difference in the circulation about two adjacent segments of the blade, then a vortex will be trailed from that intersection, with its axis parallel to the flow, and with a strength equal to the difference between the two bound vortex strengths. Now, in practice, the lift varies continuously along the blade radius as the blade rotates with a corresponding variation in circulation. Thus, the wake behind each blade may be thought of as a lattice structure of shed and trailing vortex elements. In fact, such a model has been included in a digital computer program for the numerical calculation of vortex wake effects,[30] and the sketch on the following page illustrates the concept.

If this wake structure could be accurately and realistically defined, then the induced flow in the vicinity of each rotor blade could be calculated by summing the velocity components induced by each vortex eleme. Although this method represents an order of magnitude of improvement over earlier attempts to account for the wake flow (which were necessarily oversimplified in the absence of powerful computing equipment), it has been frustrated by further factors which are difficult to include. One of the fundamental difficulties is that changes in the bound vortex strength do not, in practice, occur

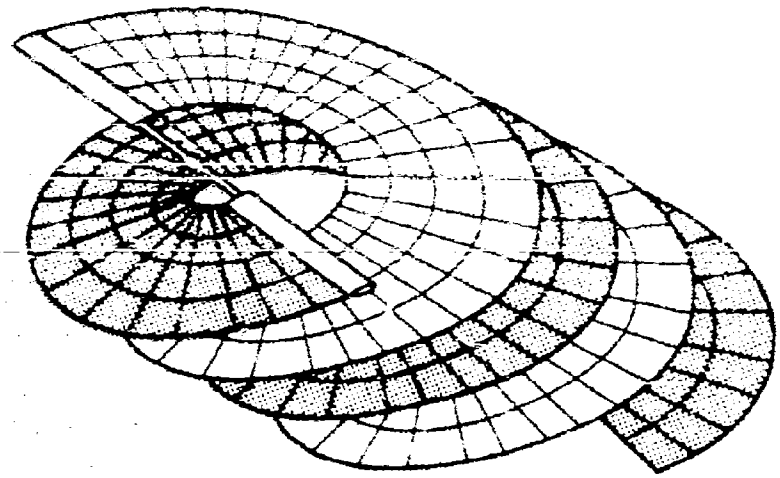

in discrete steps. All changes are continuous and the real wake behind the blade is a vortex sheet, a continuous surface of vorticity. However, this sheet is unstable and as is well known, rolls up into at least one vortex tube, and possibly more. Each tube moves away from the rotor in the form of a helix, which, because of interactions between different vortices, rapidly becomes distorted. Although in principle it is possible to calculate these distortions[32], the overall problem becomes immensely complex. Furthermore, the basic helical vortex shape, even in hover, is unstable for pitches below 0.3 (Reference 33).

The above discussion illustrates just one of the problems. Further difficulties include compressibility effects near the advancing blade tips, reverse flow over the inboard end of the retreating blade, blade stall near the retreating blade tips, and interference effects between the rotor and the fuselage and between rotors.

A factor which has a profound effect upon the wake calculations described above, and which also has a direct influence on the radiated noise, is the dynamic response of the rotor blades. Blade mountin mechanisms take a variety of forms, the most complex of which is the flap-lag hinge system. In this system, the blade has freedom of rotation about its root both in and out of the rotor plane. Further, the blade is flexible, and thus bends in normal and transverse directions and twists about its pitching axis. The fluctuating airload environment causes oscillatory motions in all these degrees of freedom. Aerodynamically, these motions modify the applied airloads and subsequent vortex shedding actions, so that the entire blade loading/response/wake system forms a closed-loop problem. Acoustically, the blade response generates sound directly through the motions of the aerodynamic noise sources, in addition to the indirect consequences of the modified airloads.

4.4 AERODYNAMIC LOADING TERMS FOR INPUT TO NOISE CALCULATIONS

During the present study, considerable effort has been devoted to the development of simplified methods for the estimation of realistic airload and blade motion input terms for the acoustic calculations. The basic aim of this work was to devise semiempirical techniques to extend the simplified analytical approach of Section 4.2 to cover the higher loading harmonics. The analyses were programmed for digital computer solution, using normal mode structural response theory to calculate realistic blade motions in all degrees of freedom from the estimated loading distributions.

For two reasons this approach had to be abandoned. First, a thorough study of available experimental airload data[21,34] revealed no accurately predictable trends. Second, as the acoustic study progressed, it became increasingly clear that (1) a very large number of loading harmonics are required for the calculation of a moderate number of sound harmonics, and (2) the loading fluctuations must become increasingly random as frequency increases. This is to be expected from a consideration of the turbulent flow processes which generate these higher frequencies.

It is clear that new information is required before firm conclusions can be drawn regarding the acoustically important characteristics of the blade loadings. Continuous recordings of blade section pressure differentials should be acquired by a system having an audio frequency range, and be subjected to a power spectral density analysis, rather than a Fourier analysis, to determine not only the load harmonic amplitudes but also their bandwidths. This subject is discussed further in Section 5.2 and Appendix II. Nevertheless, it has been possible to draw tentative conclusions from an examination of the first ten harmonic amplitudes experimentally measured and reported in References 21 and 34.

Data from these references are presented in figures 19 and 20 which show a selection of 85-percent-radius section loading harmonic amplitudes, plotted against harmonic number, on logarithmic scales. These plots suggest that the harmonic decay follows a power law of the form

$$F_\lambda = F_0 \lambda^{-k} \tag{49}$$

where λ is the harmonic number and $F_\lambda = \sqrt{L_n^2 + M_n^2}$ is the section harmonic loading amplitude. F_0 is the steady component of the section loading. Consequently, straight lines have been fitted to all plots for the available forward speed cases (steady, level flight), enabling the loading law exponent k to be calculated in each case. Figure 21(a) shows the exponent values plotted against advance ratio μ. A line has been sketched through these points, but in view of the scatter, there seems to be little point in assuming any departure from the value k = 2 for all speeds. The most surprising feature of these results is the relative constancy of this loading law. Despite expectations of an increase in the higher harmonic amplitudes with forward speed, no

such trend is noted. The harmonic amplitudes are practically as great in the hover as they are at the limiting advance ratio of 0.3. To study this phenomenon in more detail, a second set of straight lines was fitted to the harmonic amplitude plots, constraining the lines to pass through the second harmonic point, which, even by the simple theory, is predicted to rise rapidly with forward speed. The alternative loading law exponents derived in this manner are plotted against advance ratio in Figure 21(b). More variation is observed this time, and the sketched curve bears a remarkable resemblance to the rotor "power required" curve (compare with Figure 16(a)). The significance of this has not been established and, because the scatter about the fitted straight lines was somewhat increased by this procedure, the point was not pursued. It should be noted that although the bulk of the results were derived from the H-34 data of Reference 21, four cases were available in the UH-1B data of Reference 34. The close agreement between the two sets of data is of considerable interest, since the two rotor systems are very different. The H-34 has a four-blade articulated rotor of 56-ft diameter, and the UH-1A has a two-blade teetering rotor of 44-ft diameter.

Figures 19 and 20 give results for a single position on the blade at 0.85 span. It is of interest to look at the loading variation along the span of the blade which is shown in Figure 22. Local sectional force coefficients in the various harmonics are plotted. The immediately obvious effect in Figure 22 is that the higher harmonic loading coefficients rise toward the tip of the blade. In terms of power laws, the results vary from an inverse square law based on second harmonic near the root to an inverse first power law at the 0.95 span location. Based on the steady loading coefficient, the three inboard stations correspond to about an inverse cube power law, while the three outboard stations correspond to an inverse square. Since the outboard stations are much more effective as producers of sound, this effect provides additional justification for the use of an inverse square law based on steady loading in the final calculation.

The fairly wide variation in harmonic levels should again be noted. For instance, all sections have second harmonic levels close to 0.003, except one at the 0.85 station which shows an increase by a factor 3. This increase in second harmonic level is not observable at the 0.75 or the 0.9 station, and it is further evidence of the highly localized nature of the loading forces even for the low harmonics. Similarly, the 0.9 station shows an exceptionally high level of the fifth harmonic. While it is possible that part of these effects may be explained by experimental error, it seems probable that most of the observed effects are real. For instance, the very high level of second harmonic is observed at the 0.85 station for all the low forward velocity cases given by Scheiman;[21] this suggests that some repeatable vortex pattern is the cause.

It is also of interest to look at the measured loading effects for some rough running cases shown in Figure 23 in comparison with the hover case in Figure 22. Note that the rough running cases have higher levels of the higher harmonics. The

rough running cases also generally have much lower second harmonic loadings, which results in power laws based on the second harmonics always being at inverse first power law or higher. The power laws based on the steady loading show less effect, but it is thought that for these rough running cases it will be overconservative to use laws based on the steady loading. On physical grounds, it is clear that for cases where the shed vortex passes very close to the blade, there will be an impulsive loading applied, which will tend to produce all harmonic loadings with roughly equal magnitude. It is tentatively suggested that an inverse first power loading law be used for the rough running cases which would include blade slap.

The power laws discussed above appear to give the amplitude of the loading harmonics with reasonable accuracy. However, as will be discussed in Section 5.2, the phase of the loading is equally, or perhaps even more, important in determining the sound radiation characreristics. During initial work on this project, attempts were made to predict the phase of the various loading harmonics as a function of span. This was found to be impossible; no coherent picture emerged, as is shown by typical plots, again from Scheiman's data,[21] in Figure 24. Clearly, the best assumption is of random phase, particularly at the higher loading frequencies. This introduces some mathematical complexity, and the approach which has been used is described in Section 5.2.

Effect of Blade Vortex Interactions

It was noted in the Introduction that a primary source of fluctuating airloads on the blades is their passage over, or even through, a concentrated vortex trailing from another blade. It is worthwhile at this point to consider the form of the rotor wake geometry, since it does have such an important influence on the noise problem. As discussed in Section 4.3, the vortex sheet shed by a blade is unstable and rapidly rolls up into at least one concentrated vortex having an apparent origin near the blade tip. In fact, its precise origin varies as the blade rotates, and it does lie a little inboard of the blade tip. However, for the present purposes it is satisfactory to assume that each blade trails a single vortex from its tip. Furthermore, it will be assumed that each element of the vortex remains at the precise point in space where it was shed. The plan view of a single vortex therefore will look something like the accompanying sketch. The radial station s of the nth following blade which intersects the vortex is given by the simultaneous equations.[31]

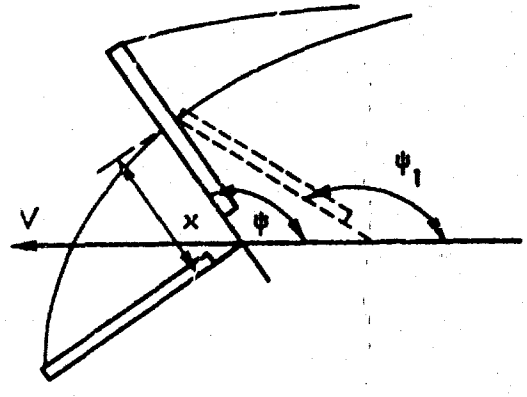

$$\left.\begin{aligned} \mu\Psi \sin\psi &= \sin\left(\frac{2\pi n}{B} - \Psi\right) \\ x &= \cos\left(\frac{2\pi n}{B}\right) + \mu\Psi\cos\psi \end{aligned}\right\} \qquad (50)$$

where $\Psi = 2\pi n/B + \psi - \psi_1$,

and $\frac{2\pi n}{B}$ = the angle between the two blades, where the symbols are defined in the sketch. These equations were solved numerically on a computer for a variety of rotor configurations and advance ratios, and the results are shown in Figure 25. The curves in each case represent the loci of blade/vortex intersection points on a single blade as it rotates. The number on each locus corresponds to the sequency of preceding blades. For example, in the top left-hand diagram for $b = 4$, $\mu = 0.1$, the number 1 corresponds to the intersection point of the vortex shed by the blade which leads the reference blade by 90 degrees; 2 is the blade leading by 180 degrees, and so on. Only the first B vortices are shown for clarity, so that the last curve in each case represents the intersection of the blade with its own vortex shed earlier. Also, the vertical displacement of the vortex from the blade, which of course is not shown, will generally increase as the number increases, so that the higher numbered intersections will have a decreasing influence on the blade loads.

Results are shown for rotors having 4, 5, and 6 blades moving at advance ratios of 0.1 through 0.5. However, the results for 2 and 3 blades can be seen in the plots for 4 and 6 blades as alternate curves. This is the reason for the alternate broken lines in those cases.

The most obvious feature of these results is the general movement of the intersection points to the region of the disc corresponding to low values of ψ as forward velocity increases. More important than this from the standpoint of loading fluctuations, however, is the decrease in the angles between the blade and the intersection loci. Since it can be assumed that, near any intersection, local section loadings will be strongly influenced by the presence of the vortex, these loci indicate the motion of loading peaks (or troughs) along the blade. As shown by the general acoustic Equation (21), aerodynamic forces in motion generate sound which increases rapidly with velocity and acceleration. At low advance ratios, the curves show that the motion of these forces is relatively low, of the order of half a radius in half a revolution. This corresponds to a convection Mach number along the blade of the order of 0.2. It is clear that as advance ratio increases, this convection speed increases. Typically, at $\mu = 0.5$, the intersections move half a radius in 10 degrees of rotation, corresponding to a convection Mach number of the order 2.0.

Thus, this fairly crude consideration shows through Figure 25 that even at moderate advance ratios, blade vortex intersections can travel along the blade at supersonic trace speeds. Such supersonically moving forces are efficient generators of sound, and it is interesting to consider that blade slap, for example, could be generated by this kind of mechanism. Although such an approach has not been taken in this study, it would be possible to perform an analysis of the sound generated by a blade/vortex intersection in arbitrary motion.

Physically, of course, a rapidly moving intersection corresponds to a loading fluctuation which is practically in phase along the entire blade, effectively a distributed impulsive sound source. Viewed in either manner, it is important to note that such a source will be highly directional with a marked lobe pointing near to the direction of the blade axis. Thus, blade slap generated by this mechanism may be expected to peak in azimuth directions within the first quadrant of rotation.

Figure 26 shows a contour plot of an airload distribution measured by Scheiman[21] for a four-blade rotor at an advance ratio of 0.29. This was plotted by computer using Scheiman's data directly. Superimposed on this plot are the blade/vortex intersection loci for $B = 4$, $\mu = 0.29$. The effects of the vortices are reflected in the loading gradients, remembering that increased angle of attack is to be expected outboard of a vortex location.

5.0 COMPUTATIONAL METHODS AND ACCURACY

5.1 SUMMARY OF COMPUTATIONAL METHODS

Two digital computer programs have been prepared during the course of this study for the CDC 3300 Computer to calculate the sound field of a helicopter rotor. The development of the first of these, code named HERON 1, was in fact one of the primary objectives of the investigation. This program is completely comprehensive in that it calculates the sound field generated simultaneously by an arbitrary number of rotors of any dimensions. For each of these rotors, the program accounts for the aerodynamic lift and drag section loadings, articulated and flexible blade motions in all degrees of freedom, rotor geometry including number of blades and rotor diameter, and the attitude and motion of the rotor in space. From this information, the program computes and outputs the amplitudes and frequencies of the fundamental rotational noise component and its harmonics at any specific point in space. Both geometric and acoustic near-field effects are included so that the result is accurate at any point.

Program HERON 2, on the other hand, was written specifically for the direct numerical evaluation of Equation (37), which, as discussed in Section 3.4, is a closed-form solution for the far-field sound of a rigid-rotor system whose only admissible blade motion is steady coning. However, as will be shown in Section 6, this solution is satisfactory for practical application in the study of helicopter noise, and this second program has proved to be useful in aiding a general understanding of an extremely complex problem. Unlike HERON 1, this program was written entirely as a special-purpose mathematical tool and has been revised and refined to perform a wide variety of computations based on Equation (37). Consequently, no general-purpose version was developed.

Program HERON 1 is described in detail in the companion report.[40] A complete specification including operating instructions is included. The discussion in this section is limited to some of the pertinent features of the computational method together with some notes regarding accuracy.

The acoustic Equation (20) is defined in a coordinate system which is fixed in space with a distributed acoustic source in arbitrary motion relative to a stationary medium.

$$p = \frac{1}{4\pi a_0^2} \int \left[\frac{x_i - y_i}{a_0 r (1 - M_r)} \frac{\partial}{\partial t} \left(\frac{F_i}{r (1 - M_r)} \right) \right] d\underset{\sim}{\eta}$$

where $\underset{\sim}{\eta}$ is the position vector of the aerodynamic force having components F_i.

The sound generated by a rotor blade in motion is the result of that motion and the distributed aerodynamic pressure acting over its entire surface. For numerical purposes, however, it is necessary to simulate the actual distributions by a radially distributed set

of point loads, as is common in rotor aerodynamics. Further, it is convenient to specify these point loads as having orthogonal lift and drag components normal to the blade axis, and acting at the same point. When one knows the orientation of the blade in space, as a function of time, it then becomes a relatively straightforward matter to resolve the lift and drag into the three components F_i defined in Equation (20). Strictly then, Equation (20) should be written

$$\rho = \frac{1}{4\pi} \sum \left[\frac{x_i - y_i}{a_0 r (1 - M_r)} \frac{\partial}{\partial t} \left(\frac{F_i}{r (1 - M_r)} \right) \right] \tag{51}$$

where the tensor subscript applies to the three fixed coordinate directions, and the summation is carried out over all assumed radial loading points (and over all blades). In addition, the near-field pressure fluctuations are calculated according to Equation 18 of Reference 8, which is

$$\rho' = \frac{1}{4\pi} \sum \left[\frac{1}{(1 - M_r)^2 r^2} \left\{ \frac{F_i (x_i - y_i)}{r} \frac{(1 - M^2)}{(1 - M_r)} - F_i M_i \right\} \right] \tag{52}$$

To evaluate Equations (51) and (52), the summations have to be performed at the appropriate retarded times (which the brackets denote). This is simply saying that we have to calculate the sound pressure at the observer position x_i, due to all the the aerodynamic forces F_i acting at the point Y_i on the rotor system when they generated the acoustic disturbances, which all reach the observer at the same instant. The accompanying sketch shows clearly that the sound generated by a number of points on a rotor at the same instant does not necessarily reach an observer at the same time. The arrows denote the distance travelled by the sound originating from each point when the first sound reaches the observer. Figure 27 shows the computed positions of the blade axes of a four-blade rotor corresponding to the appropriate retarded time of each blade element. The sound generated by each element, when it was in the position denoted, arrived at the specified observer position at the same instant.

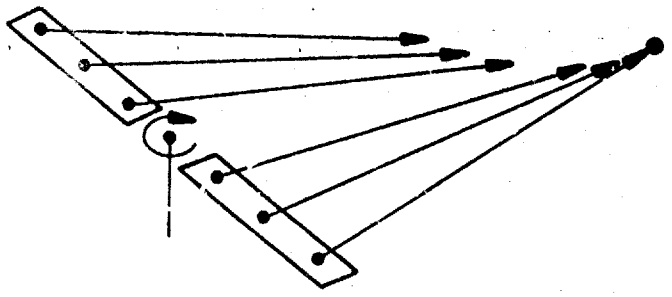

The observer positions and the rigid body motions of the helicopter (in terms of its position, and linear and angular velocities) are defined with respect to a set of "ground axes"

which are fixed in space. For convenience, all blade loadings and motions are specified with respect to a set of rotor axes which are parallel and normal to the rotor plane of rotation and whose origin is coincident with and moves with the rotor hub. The azimuthal variations of all section airloads and motions are input to the program either as time histories or as sets of Fourier coefficients. By performing the appropriate axis transformations, the coordinates of each blade element and the force components acting upon it can be defined with reference to the ground axes in a form suitable for direct input to Equations (51) and (52) as a function of time. All that is required to perform the summations involved in those equations is the correct retarded time for each blade element.

This is calculated by an iterative procedure. For uniform linear motion of the rotor, the retarded time for the hub itself can be obtained from the equation

$$t - t' = \frac{(x_i - y_i)\,\dot{y}_i + \sqrt{\{(x_i - y_i)\,\dot{y}_i\}^2 + r^2\,(a_0^2 - \dot{y}_i^2)}}{a_0^2 - \dot{y}_i^2} \qquad (53)$$

where the y_i are the coordinates of the rotor hub at time t. This gives a good approximation to the retarded time for the most inboard blade station, which is then found by iteration. The converged value is used as a starting value for the next blade station, and so on, until all have been determined.

The sound pressure at each observer position is calculated as a time history at a series of equal time intervals over a total period equal to the rotor rotational period divided by the number of blades. This is the period of the fundamental sound harmonic. Starting at time $t = 0$, the retarded times are calculated for all blade loading stations on all blades, and Equations (51) and (52) are evaluated to give the sound pressure $p(0)$. The process is then repeated for $t = \Delta t, 2\Delta t \ldots$, and so on, until the complete time history is obtained. This is then Fourier analyzed to give the amplitudes of each sound harmonic.

Numerical Accuracy

The implications of simulating the distributed aerodynamic loadings by a set of discrete point forces are fully discussed in Section 5.2. From that point on, the computed results are exact within the numerical accuracy of the computer. For sound level calculations, this is somewhat limiting due to the very large dynamic range of the hearing mechanism of around 140 dB in sound intensity. Due to the limitations of the computer word length in the machine used, the useful dynamic range is only around 90 dB. However, for most practical purposes, this is more than adequate.

Another question of accuracy arises in the specification of the airload data. The number of sound harmonics computed by the program is approximately $m/2B$ where m is

the number of azimuth stations used to define the azimuth variation of loading and motion and B is the number of blades in the rotor. Since m values are sufficient to accommodate approximately m/2 loading harmonics, the program effectively calculates 1/B times as many sound harmonics as loading harmonics. It will be seen in Section 6 that a certain number of loading harmonics can lead to the accurate computation of somewhat less than 1/B times as many sound harmonics; therefore, the possibility of error in the highest harmonics must always be borne in mind.

Although the program contains provisions for helicopter pitch and roll angular velocities, it is assumed that these do not result in any change of flight direction during the entire range of retarded time, which is approximately equal to 1/B times a rotor rotational period. This assumption avoids very considerable computational complexity and is believed to involve very small errors.

5.2 ACCURACY CONSIDERATIONS - EFFECTS OF RANDOM LOADINGS

One of the principal requirements in any numerical study is, of course, that accuracy be obtained in the answers. In the present approach, the availability of two independent methods for calculating the noise has acted as a powerful check against computational errors, but several extremely important and rather subtle points affect either method equally. In fact, it will be shown that the lack of detailed experimental knowledge of the higher harmonics of helicopter noise can easily lead to the introduction of errors. These errors result from the nature of the assumptions made to cover the lack of experimental data and are by no means obvious.

It was shown in the previous section how actual blade lift and drag loading distributions are represented, for the purpose of numerical calculation of the sound field, by a finite number of discrete point forces. At this point the question arises: how, precisely, is this simulation performed in terms of numbers and distributions of the point loads?

If we knew the actual pressure distributions on the blade surfaces as a function of time or blade position, with sufficient accuracy, it is clear that the most accurate solution would be to use a very large number of loading points, both radially and around the azimuth (or in the case of harmonic representation, the maximum number of Fourier coefficients for each radial position). It is equally clear, however, that (a) we cannot define the actual blade loadings with sufficient accuracy to justify more than a certain number of radial and azimuthal intervals (note that the use of 1-degree and 2-degree azimuth intervals in previous investigations cannot improve the accuracy over the 15-degree intervals for which the loadings were originally specified; the higher harmonics yielded by this technique are in error), and (b) it is necessary to minimize the number of points for computational expediency. In the present program the azimuthal interval defines how many sound harmonics we can calculate, whereas the radial intervals govern the accuracy with which they are calculated. Therefore, for a given number of sound harmonics, the required azimuth interval (or number

of loading harmonics) is fixed, and it only remains to optimize the number and distribution of radial loading points in order to obtain adequate answers. Let us consider, then, some of the relationships between the loading distributions and the sound which they generate.

Taking one pair of results from Equations (37) (specifically for $n - \lambda$ even), and dividing the cosine harmonic by the sine harmonic we obtain the following result

$$\frac{a_{n\lambda}}{b_{n\lambda}} = \frac{\frac{x}{r} b_{\lambda T}(J_1') - \frac{b_{\lambda D}}{nM}(J_2') - \frac{y}{2r} a_{\lambda C}(J_3')}{\frac{x}{r} a_{\lambda T}(J_1') - \frac{a_{\lambda D}}{nM}(J_2') - \frac{y}{2r} b_{\lambda C}(J_3')} \qquad (54)$$

where

$$J_1' = J_{n-\lambda}\left(\frac{nMy}{r}\right) - (-1)^{\lambda} J_{n+\lambda}\left(\frac{nMy}{r}\right)$$

$$J_2' = (n-\lambda) J_{n-\lambda}\left(\frac{nMy}{r}\right) - (-1)^{\lambda}(n+1) J_{n+\lambda}\left(\frac{nMy}{r}\right)$$

$$J_3' = J_{n-\lambda+1}\left(\frac{nMy}{r}\right) - J_{n-\lambda-1}\left(\frac{nMy}{r}\right) + (-1)^{\lambda} J_{n+\lambda+1}\left(\frac{nMy}{r}\right) - J_{n+\lambda-1}\left(\frac{nMy}{r}\right)$$

n is the sound harmonic number and λ is the loading harmonic number (where the rotational frequency is the fundamental). The coefficients $a_{n\lambda}$ and $b_{n\lambda}$ are the in-phase and quadrature amplitudes of the nth sound harmonic that are attributable to the λth loading harmonic. The λth loading harmonic is represented by the coefficients $a_{\lambda T}$, $b_{\lambda T}$, etc., which correspond to the harmonics of a point force acting somewhere on the blade. The radial location of this force affects only the value of M, the rotational Mach number, which is directly proportional to radius. Equation (54) gives the phasing of the sound harmonic since $\tan \phi_{n\lambda R} = (a_{n\lambda}/b_{n\lambda})_R$, where the suffix R applies to the force acting at radius R.

We see from this equation that if only one force is acting (having thrust, drag and radial components), the phase of the sound harmonic is essentially independent of the point of action of the load, apart from a minor variation due to the effect of M on the drag term. Similarly, if many loads, acting on the blade at different points, are in phase with each other (i.e., a_λ/b_λ = constant), then their contributions to any

sound harmonic are also in phase, and we have simply

$$a_{n\lambda\,TOTAL} = a_{n\lambda R_1} + a_{n\lambda R_2} + a_{n\lambda R_3} + \cdots$$

$$b_{n\lambda\,TOTAL} = b_{n\lambda R_1} + b_{n\lambda R_2} + b_{n\lambda R_3} + \cdots \qquad (55)$$

where R_i are the loading points, and the ratio $\dfrac{a_{n\lambda\,TOTAL}}{b_{n\lambda\,TOTAL}} = \dfrac{\sum a_{n\lambda R_i}}{\sum b_{n\lambda R_i}}$ for all i.

However, if the various loads are not in phase with each other, or if the ratios $a_{\lambda T} : a_{\lambda D} : a_{\lambda C}$ and $b_{\lambda T} : b_{\lambda D} : b_{\lambda C}$ are not constant, then the phases $\tan^{-1}(a_{n\lambda}/b_{n\lambda})_{R_i}$ vary with i.

The consequence of this is that if the harmonic loading is in phase along the blade, it can be quite accurately represented by a single loading point if the correct forces (for example, the integrated blade thrust, drag, and outward component harmonics) are applied at the correct point. This is precisely what has been done in accepted propeller noise theory,[15,16] and it allows considerable simplification of the computations. It is important to note, though, that the effective loading point is a function of λ and n, and thus it takes on many different values in a complete calculation for all λ and n. However, if the loading is not in phase, then an effective single load would have to be specified in terms of position and phase for each field point, which is obviously impractical.

Unfortunately, as we have seen in the case of the helicopter, it is only the steady loading which remains in phase along the blade (by definition), the phase of the harmonics showing increasingly greater variations as frequency increases. As a general rule, it seems safe to say that the higher the loading harmonic, the more radially distributed the point loads must be for accurate sound calculation. It is equally certain that, under the present state of the art, we cannot define the loading harmonics with sufficient resolution to satisfy the requirements of the acoustic theory, since the final results are extremely sensitive to loading phase, as will be seen in Section 6.

Fortunately, due to the nature of rotor aerodynamic loads, we are able to simplify the problem in a manner which enables us to make reasonable estimates of the sound field up to very high harmonics of the blade passage frequency. The basis for this simplification is that the flow processes which cause the fluctuating airloads become increasingly random as frequency increases. This is apparent from experimental data on the first ten loading harmonics (Section 4.4) and is clearly true at frequencies of

the wake turbulence. Experimentally, this randomness shows itself as a lack of repetition of results, either in successive experiments or in successive blade revolutions. For example, if an electrical signal, which is proportional to the blade section loading at any station, were passed through a very narrow filter to extract some particular harmonic level, the output would be seen to fluctuate in amplitude and phase. To understand the implications of a random loading variation along the blade, consider the integration of the curves shown in the sketch below which can be thought of as representing the acoustic contributions from each element of the rotor blade.

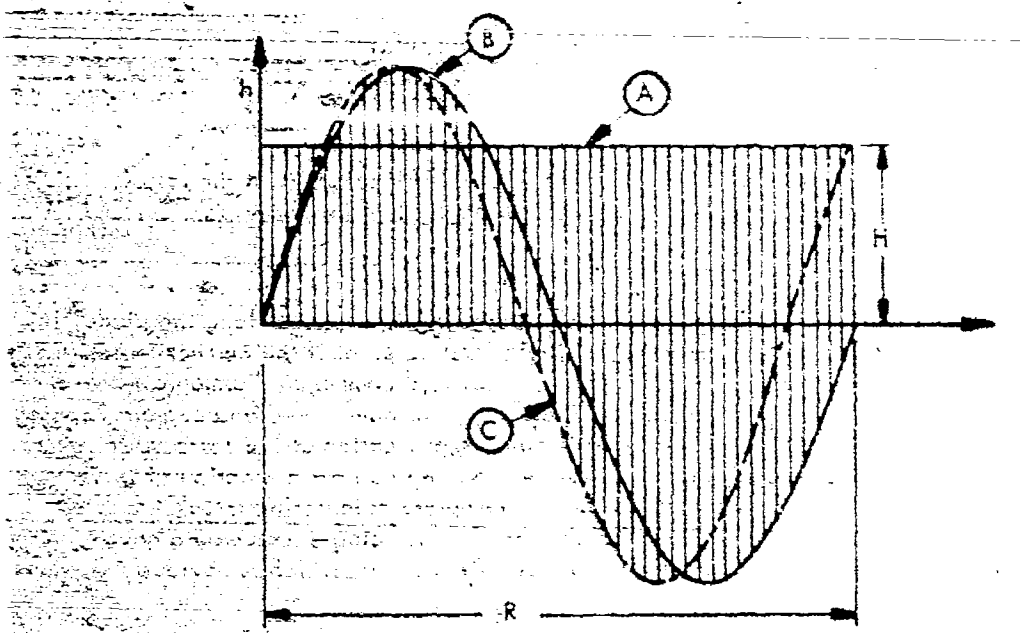

All have the same root mean square value (H) over the range of interest. Consider first the simple straight-line case (A). Suppose that this is divided into (say) 100 parts each of length R/100. Then each part will contribute one 100th of the total integral. Now in sound calculations, we must take the square of the result. If we add each contribution and then square, the result will be $R^2 H^2$; but if we square each contribution and then add, the result will be $R^2 H^2/100$. In other words, the value of the sum of the squares can be made as small as we like by taking more and more elements.

Next consider the curve B, which is a perfect sine wave. Divide this into 100 pieces, and add. The result is identically zero; but if we square each contribution and then add, the result is again $R^2 H^2/100$. Thus in this case, the result of taking the sum of the squares is always greater than taking the square of the sum. The difference lies in the relative phasing along the length of the curve. The straight line was all in phase, so each segment added to its neighbor. For the sine wave, all contributions cancelled exactly. Curve C shows a further case where the sine wave

is incomplete. Clearly, the sum of the squares will again be closely equal to $R^2 H^2/100$, while for a direct summation, the whole contribution of curve C will cancel except for the last uncancelled part angle.

These simple considerations clearly indicate the acoustics problem. Suppose a load harmonic is taken to be in phase over the whole blade span. Because of the retarded time effects, radiation from different parts of the span will reach the observer at different times. Thus, the in-phase loading input becomes an out-of-phase acoustic result. In other words, curves like A are transformed into curves like B or C via the acoustic retarded time effects. Fortunately, however, in the integrated result Equation (54), there is no phasing dependence on radius due to the acoustics. But the loading phase effects are still of extreme importance. It is well known (see Section 2.1) that these blade loadings can be very localized, being the result of vortex interaction effects, so that it is extremely unlikely that they are in phase over the span. The most convenient assumption is that the higher harmonic loads are random in phase along the blade, as was discussed above. In this case, the sum of the squares calculation applies. However, here another problem arises. It can be seen that the sum of the squares can be made as small as desired, simply by choosing a sufficiently large number of divisions along the span. Again, this is obviously incorrect. The fallacy behind this limit is that, as the divisions get smaller and smaller, it becomes less and less accurate to assume that the phases of successive divisions are random. The phases of nearby divisions are approximately equal, so that they must be calculated via the square of the sum rather than the sum of the squares. The key question is: how many successive divisions can be regarded as being in phase?

The answer to this question lies in the space correlation of the fluctuating loads along the blade. Consider the in-phase and out-of-phase combinations to the nth sound harmonic $a_{n_1}, a_{n_2}, a_{n_3}, \ldots a_{n_K}$ and $b_{n_1}, b_{n_2}, b_{n_3}, \ldots b_{n_K}$ due to K loading points chosen to act at various blade stations and representing the distribution of the λth loading harmonic. If these K loads are constant in both amplitude and phase, so are the a_{ni}, b_{ni} (i = 1, 2, 3, ... K), and we can write that sound pressure level of the nth sound harmonic as

$$c_n^2 = \left(\sum_i^K a_{n_i}\right)^2 + \left(\sum_i^K b_{n_i}\right)^2 = \sum_i^K \sum_j^K \left(a_{n_i} a_{n_j} + b_{n_i} b_{n_j}\right) \quad (56)$$

Now if the K loads are random, i.e., not constant in amplitude and phase, the above result is not true, and we must write

$$c_n^2 = \sum_{i}^{K} \sum_{j}^{K} \left(\bar{r}_{ij}\, a_{n_i}\, a_{n_j} + \bar{s}_{ij}\, b_{n_i}\, b_{n_j} \right) \tag{57}$$

where $\bar{r}_{ij}$ and $\bar{s}_{ij}$ are the space correlation coefficients which define the degree of randomness between a_{n_i} and a_{n_j} or b_{n_i} and b_{n_j}. These coefficients have values ranging between zero and unity, where the former implies complete randomness and the latter, as follows from equating Equations (56) and (57), implies complete correlation. If the K loads are completely random, $r_{ij} = 0$ (except when $i = j$, since r_{ii} is always unity) and then

$$c_n^2 = \sum_{i}^{K} \left(a_{n_i}^2 + b_{n_i}^2 \right) \tag{58}$$

In general, the coefficients will lie somewhere between the two extremes and will decrease as $|i - j|$ increases. In order to make use of Equation (57), it is necessary to define the $\bar{r}_{ij}$ and $\bar{s}_{ij}$. In doing so we make the following assumptions:

1) That $\bar{r}_{ij} = \bar{s}_{ij}$

2) That $\bar{r}_{ij}$ decreases exponentially with the separation ξ (expressed as a fraction of the radius) between the ith and jth loading stations.

3) That the "correlation length", defined here as the distance over which the correlation coefficient falls to some fixed value, is inversely proportional to harmonic number λ.

Using these assumptions, we arrive at the result

$$\bar{r}_{ij} = \bar{s}_{ij} = e^{-a\lambda\xi} \tag{59}$$

where a is a constant to be determined. The variation of $\bar{r}_{ij}$ with ξ and λ is sketched on the following page.

In order to use Equations (57) and (59) in a numerical procedure, a further calculation is required. If the correlation coefficient does not differ substantially between

successive loading points, then Equation (57) probably gives sufficient accuracy. If the coefficient does change significantly, however, the random changes that occur over a single loading segment may be expected to affect the results, since the effective load is somewhat lower than the assumed value. This is clarified below.

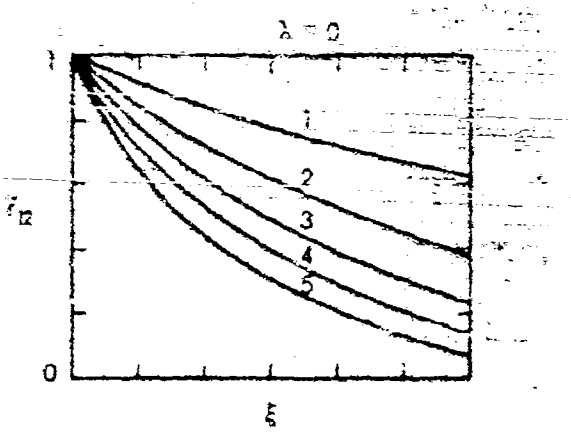

Consider a single radial segment of the rotor blade between the stations S_1 and S_2. If the section loading is well correlated along its length then the harmonic amplitude of the total force acting upon it is simply

$$\Delta F_\lambda = \int_{S_1}^{S_2} F'_\lambda(s)\, ds \qquad (60)$$

where $F'_\lambda(s)$ is dF_λ/ds, the amplitude of the λ th harmonic section loading. If $F'_\lambda(s)$ is not well correlated, then we must resort to the method illustrated by Equation (57) to determine a value of an "effective" load increment F_{E_λ} acting on the segment. In fact, we can write

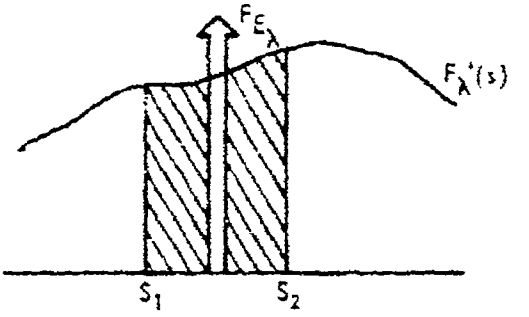

$$F^2_{E_\lambda} = \int_{S_1}^{S_2}\int_{S_1}^{S_2} r_{12}\, F'_\lambda(s)\, F'_\lambda(\bar{s})\, ds\, d\bar{s} \qquad (61)$$

Now assuming the same form for the correlation coefficient

$$r_{12} = e^{-a\lambda\xi}, \quad \text{where } \xi = s - \bar{s}$$

and assuming a "triangular loading" pattern (i.e., the local loading is proportional to radial distance) for the λth harmonic amplitude so that

$$F'_\lambda(s) = 2F_\lambda \cdot s$$

we can express the following relationship for the effective load F_{E_λ}.

$$F^2_{E_\lambda} = 4F^2_\lambda \int_{S_1}^{S_2} \left[\int_{S_1}^{\bar{s}} \bar{s} \cdot s \cdot e^{-a\lambda(\bar{s}-s)}\, ds + \int_{\bar{s}}^{S_2} \bar{s} \cdot s \cdot e^{-a\lambda(s-\bar{s})}\, ds \right] d\bar{s} \tag{62}$$

Evaluation of this integral gives

$$F^2_{E_\lambda} = \frac{4F^2_\lambda}{a\lambda} \left[\frac{2}{3}(S_2^3 - S_1^3) + \frac{2e^{-a\lambda(S_2 - S_1)}}{a\lambda} \left(S_1 - \frac{1}{a\lambda}\right) \left(S_2 + \frac{1}{a\lambda}\right) - \frac{1}{a\lambda}\left\{ S_1^2 + S_2^2 - \frac{2}{a^2\lambda^2} \right\} \right] \tag{63}$$

It is of interest to put $S_1 = 0$ and $S_2 = 1$, for then we obtain the effective loading for the entire blade

$$F^2_{E_\lambda} = \frac{4F^2_\lambda}{a\lambda} \left[\frac{2}{3} - \frac{1}{a\lambda} + \frac{2}{a^3\lambda^3} \left(1 - e^{-a\lambda}\right) \right] \tag{64}$$

Note that for $a\lambda >> 1$

$$F^2_E = \frac{3F^2}{3a\lambda} \tag{65}$$

Combining Equation (65) with Equation (49) and using the recommended value of 2 for k, we have the approximate result

$$F_{E_\lambda} \sim T_B \lambda^{-2.5} \qquad (60)$$

(where T_B = total blade thrust).

That is, if the loads are actually falling in magnitude as λ^{-n}, then the effective power law due to random effects is $\lambda^{-2.5}$, and this can be used in the computations.

Equations (63) and (66) have been used to study the effects of blade loading distributions, and the results are discussed in Section 6.

A second equivalent error problem occurs in the calculation of the sound from the summation of all the loading harmonics. Reference to Equation (36) or (37) shows that the contributions to any sound harmonic of every second loading harmonic will have a sign change. Now, by the time the loadings reach the twentieth or so, their magnitude changes little with change in harmonic number. Thus, all the sound from the loading harmonic would be cancelled out by the sound from the next if they both had the same phase angle. Clearly, it is extremely unlikely that such harmonics would have the same phase, but, as shown in Section 4, beyond about the second harmonic we have no real idea of what the phase is. Again, the only logical choice is to assume that the harmonics have random phase, so that the sum of the squares of successive harmonics must be taken rather than the square of the sum, if realistic answers are to be expected. On the other hand, if the phase is well known (as for instance on the first harmonic airload), then it can be included, and the second expression can be used. It may be noted that the definition of the loading harmonics via a root mean square value automatically takes care of these problems in the azimuthal integration. These points were not considered by previous investigators,[10,12] and this is another source of the low levels they find in the higher noise harmonics. All the points made above via physical argument can be duplicated mathematically. A mathematical analysis is given in Appendix II.

As a final point, it is worthwhile to consider the chordwise integration. The general conclusions above about correlation functions for the high harmonics do apply in a modified form, but the object here is to study the direct effects of a chordwise distribution of loading. Schlegel et al,[12] followed Gutin[15] in using a rectangular distribution, and Loewy and Sutton[10,11] used a straight-line approximation which gave a complex algebraic result. In fact, these modifications are both unnecessary and inaccurate. Figure 28, taken from Reference 35, shows the Fourier coefficients of various chordwise loading shapes, a typical real distribution (from Reference 36), and assumed rectangular and sinusoidal shapes. Several points may be observed. First, the lack of certain harmonics is peculiar to the artificial shapes and does not occur

for the real case. Second, the real loading gives higher levels of harmonics than do the artificial shapes. This is basically due to the strong first peak of the real loading. Third, solidities typical of a helicopter have much higher harmonic content than equivalent propeller cases. Fourth, the delta function approximation (equal harmonic content) is very acceptable for helicopter loadings and is certainly more accurate than rectangular distributions. (The results shown in Figure 35 are not, of course, noise harmonics. The effective values must be taken through the full computation of Equation (36) to give the final noise radiation.) It is clear that details of the mean chordwise loadings distribution are unlikely to be important. This result was found in the computations of Loewy and Sutton.[10,11] Thus, it is suggested that point chordwise loadings (delta functions) be used in helicopter noise calculations, and this has been followed throughout the present work.

It is quite probable that the use of the point loading approximation is conservative, in that it will generally give higher harmonic noise levels than any other chordwise loading distribution. The overall sectional lift coefficients used in the present work are derived from Scheiman's[21] data, as discussed in Section 4.4.. The data are the result of averaged pressure readings over the blade. Examination of raw pressure data (as, for instance, sketched in Cox and Lynn's report[3]), inevitably shows many local fluctuating pressure peaks. These pressure peaks will radiate noise efficiently at the high frequencies. Alternatively, the peaks would be reflected in an increase of the Fourier amplitude coefficients with an increase in frequency in Figure 28. Watkins and Durling[37] showed a similar effect, in that any part of the blade with a small loading pattern will also possess high levels of the high Fourier coefficients. It might also be noted that the smoothing operations used by Scheiman[21] could be a source of considerable error in estimating the levels of the harmonic airloads. This point certainly justifies further study.

6.0 RESULTS AND DISCUSSION

6.1 PARAMETER STUDY

The initial requirement in the analysis of the results is to determine the general features of the noise radiation from the helicopter. This has been achieved by a thorough study of the results using Equation (37) of this report (Computer Program HERON 2). The more detailed study of near field and blade motion effects was accomplished by using the exact computer program (HERON 1) via Equation (20) of this report.

Acoustic Effectiveness of Individual Loading Harmonics

First of all, the effectiveness of the various loading harmonics as sound sources will be evaluated. Figures 29 and 30 give the sound radiated in various harmonics of a four-blade rotor by various loading harmonics. The magnitude of each loading harmonic (including the steady) has been assumed to be the same, and in each case the load has been reduced to a single point fluctuation force acting at 0.8 of the blade span. The rotational Mach number of this point is 0.5, so that the graph corresponds to a tip Mach number of 0.625. The magnitude of the thrust component has been assumed to be equal to 10 times that of both the drag and outward components of force, which are assumed to be equal. This proportionality is typical of a helicopter rotor. Figure 29 gives curves corresponding to a field point 10 degrees below the rotor disc, and Figure 30 gives curves for a field point 10 degrees from the rotor axis. The same general features may be observed in each of the harmonics plotted. Only a limited range of loading harmonics contributes to each noise harmonic. Take, for instance, the fourth sound harmonic ($n_1 = 4$) in Figure 29. Loading harmonics below the eighth can be seen to produce little noise. Between the eighth and twenty-fourth, the sound produced varies but is of roughly the same order of magnitude, while beyond the twenty-fourth loading harmonic the sound radiation falls away rapidly. Thus, it may be concluded that on a real helicopter rotor, when all loading harmonics can contribute to the observed noise, loading harmonics between the eighth and twenty-fourth must be included to obtain an accurate calculation of the fourth harmonic. This conclusion explains why Schlegel et al. calculate such low levels for the fourth harmonic in their report[12] (see also Figure 12), since they include only loading harmonics up to the tenth.

This effect may be understood by reference to Equation (36). There are two basic terms in this equation, the $J_{n-\lambda}$ and the $J_{n+\lambda}$. For the values of the argument of the Bessel function typical of the helicopter problem, the $J_{n+\lambda}$ terms will be quite insignificant compared to the $J_{n-\lambda}$ terms and can be ignored (except perhaps for the low harmonic noise). Now $n = mB$ where m is the harmonic order and B is the number of blades. Thus, as the loading harmonic λ increases, the order of the Bessel function $n-\lambda$ will decrease, eventually going negative. For example, for $m = 1$, $B = 4$; $n-\lambda = 6$ for $\lambda = 10$ (the tenth loading harmonic); and $n-\lambda = -6$ for $\lambda = 22$. The absolute value of a

Bessel function with a negative order is equal to the value of the Bessel function with a positive order. Thus, we expect the results for the $\lambda = 10$ and 22 cases to be the same for the fourth harmonic case. Inspection of Figure 29 will show this to be so. Indeed it will be observed that each curve in Figure 29 is symmetrical about $\lambda = mB$, which corresponds to $\lambda = 16$ for the fourth harmonic.

Figure 29 showed the sound pressure levels calculated for an elevation of 10 degrees below the rotor disc plane. Figure 31 illustrates the variation of the sound level at other elevations and shows how, as the point of observation is moved away from the disc plane toward the rotor axis, the number of loading harmonics contributing to a specific acoustic harmonic is reduced. Indeed, in the limit, immediately under the rotor disc, only the single loading harmonic, $\lambda = mB$ contributes. The effect may again be understood by reference to Equation (36). The argument of the Bessel function terms includes the factor y/r. Thus, moving away from the rotor disc reduces the magnitude of the argument and, hence, the range of effectiveness of the loading harmonics. In the limit when $y/r = 0$, then only the J_0 term has a finite value, equal to unity. The increase in amplitude of the loading harmonics on moving toward the rotor axis may also be understood by reference to Equation (36). The thrust term, which dominates the results, is multiplied by x/r. Moving toward the rotor axis gives increasing values of x/r and accounts for about a 15-dB increase between the 10-degree and 80-degree cases. The remaining increment comes from the increasing peak magnitude of the lower order Bessel functions. The fact that sound radiation immediately under the helicopter rotor is dependent on a very limited range of loading harmonics may be of some potential significance in naval applications. However, it should also be noted that, immediately under the helicopter, the refractive effects of the downwash can also be important.

The key requirement now is to be able to predict which loading harmonics are necessary for the acoustic calculation of any given sound harmonic. From considerations of the basic features of Bessel functions, it is possible to show[18] that the range of interest of loading harmonics is roughly

$$mB\,(1 - M) < \lambda < mB\,(1 + M) \qquad (67)$$

where M is the rotational Mach number. The accuracy of this equation may be checked in Figure 29 where $M = 0.5$. The equation will be found to be conservative when applied to Figures 30 and 31 for points removed from the rotor disc. In fact, here the formula $mB\,(1 - My/r) < \lambda < mB\,(1 + My/r)$ can be used if desired. However, for general-purpose calculations, Equation (67) is appropriate. Figure 32 shows the effect of rotational Mach number on the noise radiation. It will be observed that the range of loading harmonics which contributes to the noise is substantially increased as Mach number increases. Again the effects are as given by Equation (67). Figure 33 gives a plot of Equation (67) and may be used to determine the range of loading harmonics necessary for accurate calculation of any given noise harmonic.

Figure 34 shows the contribution of the three force components to the overall sound pressure. The proportions of components used in this and all the other calculations of the parameter study are thrust:drag:outward component = 10:1:1. It will be observed that in the inefficient region of radiation (well down the shoulders of Figure 29), the effects of all three components are about equal. However, over the efficient radiation range, the thrust term dominates. The substantial movement of the plots between successive harmonic levels corresponds to moving past lobes in the sound patterns, as will be discussed in more detail later. Note how the thrust and drag terms show similar fluctuations, but in "antiphase" to the outward component term. Thus, the curve for overall level which combines the three components shows smaller fluctuations. The drag term is very inefficient in the central region. This is the effect of the $(n-\lambda)$ multiplier in Equation (36). For most practical purposes, it would appear to be a good approximation to consider the thrust term only. The other terms contribute significantly only directly in the plane of the rotor disc and in the inefficient radiation region; for instance, the steady loading contributions at low rotational Mach numbers.

Combination of Loading Harmonics

All the data presented so far apply to the effects of a single loading harmonic. In reality, the observed noise at any point results from the sum of the effects of all harmonics. As was discussed in Section 5.2, the sums of the squares of the contributions of the individual loading harmonics must be taken for a realistic result. The key effect in this summation is the comparative magnitude of the loading harmonics. This problem was discussed in Section 4, and it was shown how a harmonic inverse power law approximation seemed to be the most accurate. In order to study the effects of various harmonic loading laws, Figure 35 has been prepared. The figure corresponds to a summation of the results like those presented in Figure 29 with an appropriate weighting according to the harmonic loading inverse power law applied. The first 60 loading harmonics are summed for each point. The results apply 10 degrees below the disc of a four-blade rotor.

Figure 35a gives the results of the zeroth power law case, which corresponds to the direct summation of all the harmonic levels with equal weighting. Note how the noise is predicted to go up with harmonic order, actually rising at 6 dB per doubling of order. This may be compared with Loewy and Sutton's results,[10,11] where their input of what was essentially a zeroth harmonic power loading law gave rapidly decreasing sound harmonics. Although this must be partially due to the limited range of input harmonics (0-20), it is thought that their results also strongly suggest an undetected computational error. Note that, because of the limited number (60) of loading harmonics used, the present calculation loses accuracy above a sufficiently high sound harmonic. Referring to Figure 33, it may be predicted that accuracy will be lost beyond about the eighth, ninth and tenth harmonics for M = 1.0, 0.75, and 0.5, respectively. Figure 35a shows how this is indeed true. The effect of Mach number is also shown in Figure 35a. It will be observed that the effect of Mach number is small for this zeroth power case. This is consistent with the effects noted in Figure 32, where increase in Mach number gave an

increased range of loading harmonics, but not a significantly increased amplitude of the typical sound radiated by a single harmonic.

Figure 35a also gives the results of assuming only a steady loading. This corresponds to the classic propeller noise calculation.[15] Note how the increase in Mach number has a very pronounced effect on the noise radiation by the steady loading. The same effect may be observed by studying the intercepts of the various curves in Figure 32 with the vertical axis. In fact, Figure 35a also shows how the steady loading is particularly high for the M = 1.0 case. This effect may be understood by reference to Equations (37). Both a $J_{n-\lambda}$ and a $J_{n+\lambda}$ term are present. In general, as was mentioned above, the $J_{n-\lambda}$ term is much larger than the $J_{n+\lambda}$ term. However, for the $\lambda=0$ case, the terms are identically equal and are thus additive. The lower first harmonic loading points in Figure 32 result from the particular phasing used in the calculations and are not a general result.

Figures 35b to 35d give the results of assuming other loading harmonic power laws. In each case the loading harmonics have been derived from the zeroth by using the appropriate inverse power law, as shown. (The first and zeroth loading harmonics always have equal magnitude.) In each figure, the result for steady loading only is also shown. This may be considered as the result for the minus infinity power law for loading harmonics. The inverse first power law case is shown in Figure 35b. For M = 0.5 and 0.75, the result is very closely a constant sound level for all harmonics. This would correspond to a very impulsive banging type of noise. For M = 1.0, the sound rises with frequency. However it will be observed that the effect of the steady loading alone gives virtually all the observed effects. Thus, it appears that the observed levels in Figure 35b at M = 1.0 are basically due to steady loading effects, with fluctuating forces playing a minor role. Figure 35c shows the inverse square law loading results. Here the curves drop off more rapidly with increase in sound harmonic. It may be observed that change of rotational Mach number is starting to have a more significant effect. Also, it can be seen that the M = 0.75 case is governed by the steady loading for the first five harmonics, and only above this is there any significant effect of the fluctuating loads. It may be noted that, because of the markedly reduced effect of the higher loading harmonics in this inverse square loading law, the inaccuracies introduced by the limitation to 60 loading harmonics disappear, and Figure 35b is probably accurate out to the sixteenth sound harmonic. The inverse third power law results given in Figure 35d show all these effects to an even greater degree, with the steady loading dominating the M = 0.75 case out to about the twelfth harmonic and the M = 0.5 case out to the fourth.

All these results applied to the case 10 degrees below the rotor disc, which is one of the principal directions of interest from the detectability point of view. The same general effects occur in all directions under the helicopter, but naturally detail changes do occur. Figure 36 shows the effects 10 degrees from the rotor axis. In this position, the effect of the steady loading is extremely small at all Mach numbers. Indeed, the

second and higher harmonics are too small to be plotted on the graph. Thus, all the effects in this position are due to the fluctuating forces alone. It will be seen that the effect of Mach number is small in all cases and that the sound harmonic curves correspond closely to a straight line on the log-log plot. Figure 36 may be regarded to some extent as giving the basic effects of the fluctuating forces, uncomplicated by the effects of the steady loading which had to be included in Figure 35.

The sound power laws observed in Figure 36 may be predicted by an approximate theoretical argument. Reference to Figure 29 shows that, over the range of maximum noise production, higher sound harmonics produce more noise than lower ones. In Reference 18 it was shown how the acoustic efficiency was actually proportional to mBM. The peak noise levels for the various harmonics in Figures 29 through 32 will be found to follow this law closely. However, there is no basic trend due to loading harmonic on any given frequency observable in Figure 29, apart from the limit in the number that contribute. As suggested by Equation (67), the loading harmonics contribute over the range $mB(1-M) < \lambda < mB(1+M)$. Furthermore, sound intensity is proportional to loading squared, and, thus, if the loading harmonics follow an inverse k^{th} power law, the arguments above suggest that the acoustic intensity follows the law given by

$$p^2 \sim mBM \int_{mB(1-M)}^{mB(1+M)} \lambda^{-2k} \, d\lambda$$

That is,

$$p^2 \sim (mB)^{2-2k} \frac{M}{1-2k} \left\{ (1+M)^{1-2k} - (1-M)^{1-2k} \right\} \qquad (68)$$

Thus, the predicted sound power law variation with harmonic number is +2, 0, -2, -4 for loading power laws of 0, 1, 2, 3, respectively. These laws agree virtually exactly with the results shown in Figure 36. The expression for dependence on Mach number shown above is not universal and essentially applies only in the plane of the disc. The law reduces to an M^2 law for the zeroth power loading, and this can also be shown to hold near the rotor axis for all loading laws. This M^2 law can be observed in Figure 36. (Note that this is based on constant thrust.) The results shown in Figure 35 also show the same trends. At a sufficiently high sound harmonic number the curves follow the harmonic law stated above. At a lower sound harmonic dependent on the loading law and rotational Mach number, the effects of these laws are overcome by the contribution of the steady loading. The effect of rotational Mach number in Figure 35 can also seem to follow broadly the law given in Equation (68), beyond the range where the steady loading effects are significant. Thus, the equation does give an approximate indication of the effects of rotational Mach number on the higher harmonics of the noise.

However, the most important use of these laws given in Equation (68) is in prediction of the higher sound harmonics, which cannot be readily calculated on a computer.

Using Equation (68), predicted sound levels can be extrapolated with confidence to the highest harmonics. Furthermore, this suggests that it will be quite accurate to determine the basic blade loading power laws from the acoustic spectrum. In either case, the correlation length discussed in Section 5 must be included. Nevertheless, from these considerations it does appear feasible to predict the amplitude of the higher harmonic blade loadings from a measurement of the radiated sound signal.

It is of particular interest to compare the predictions made above with experimental data trends. Figures 5 through 7 gave results from Stuckey and Goddard's work,[5] and were discussed in Section 2.1. It was shown how at low tip Mach numbers the first harmonic levels were lower than the fluctuating loads, while for high tip Mach numbers the contribution at the lower sound harmonics was greatly increased. Essentially the same effects are shown here. Figure 35 clearly shows the increased significance of the steady loading as tip Mach number increases. Because of this, the first few harmonics can be seen to rise at a far faster rate with Mach number than the high harmonics. As mentioned in Section 2.1, theory suggests that the first harmonic levels rise according to a M^{2B} law, and this was shown to be broadly consistent with the data trends of Figure 6. Equation (68) suggests an M^2 law for the high harmonics, since Goddard and Stuckey's data correspond to a fairly rough running case. Again this M^2 law was observed in the data of Figure 7. Thus, the basic trends established by the parameter study are reflected in the experimental data.

The effect of blade number B may also be studied via Equation (68). As the loading inverse power law varies through $k = 0, 1, 2, 3$, the suggested overall acoustic power trend is through B^2, B^0, B^{-2}, B^{-4}. Thus, the equation suggests that during blade slap conditions when $k \sim 0$ or 1, the sound power will go up with an increase in blade number, while under more normal flight conditions, where $k \sim 2$, the sound power will go down with blade number. Although these arguments do not apply to the first few harmonics of the sound, these harmonics are not too important subjectively. Thus it appears that an increase in blade number will reduce the noise radiation under normal flight conditions. This is consistent with the considerably lower "vortex" noise levels predicted by Schlegel for a five- and six-blade rotor, compared to Davidson and Hargest's results[4] for a three-blade rotor. However, the equations also suggest that if a multiblade rotor gets into blade slap or rough running conditions, much more noise will be radiated. This, in turn, suggests that multiblade rotors will not be advantageous on tandem helicopters. Little data on this point are available.

Forward Speed Effects

The effect of forward velocity was discussed in Section 3.5. It is clearly of considerable interest to study the effects of this velocity on the radiated sound, and Figures 37 through 39 give some computed results. The calculations were made using the basic transformation discussed in Section 3.5. Those transformations were based on the retarded time position of the helicopter; that is, the position of the helicopter when it emitted the sound. The results shown in Figures 37 through 39 are based on the actual

position of the helicopter when the sound is observed. This requires an additional transformation, which essentially is that followed by Garrick and Watkins[16] and Loewy and Sutton.[10,11]

Figures 37 through 39 again apply to the basic case of a single point loading with rotational Mach number M, for a four-blade helicopter rotor, with the observer 10 degrees below the rotor disc. For zero forward speed, the sound field is completely symmetrical around the rotor (at least under the random phase assumptions made here.) However, for the case of forward speed, more sound is radiated forward than aft. Thus the results include both the forward and aft radiation cases. The key factor in the theory is $(1 - M_{or})$ where M_{or} is the component of the hub convection Mach number in the direction of the observer. Thus, when the helicopter is flying toward or away from the observer, the maximum effect is observed; when the helicopter is flying at right angles to the observers' line of sight, the convection Mach number component is negligible. In Figures 37 through 39, both forward and aft radiation cases are given, together with the zero velocity condition which, thus, also corresponds to the sideways radiation. As before, the effect of steady loading only is given in each case as a reference.

In each case, the forward radiation is higher than the aft. For the zeroth loading law (Figures 37a through 39a), little change is noticeable, but for the steady loading alone, the forward velocity has a substantial effect. For the 0.125 forward Mach number in Figure 37, the sound due to the steady loading alone is increased by around 20 dB in the forward direction compared to the aft. Plots of the other loading law cases in Figure 37 show that in each the sound is increased in the forward and reduced in the aft directions. Plots for other rotational and forward Mach number cases in Figures 37 through 39 show the same general effects. The higher harmonics due to steady loading alone are increased by over 50 dB forward compared to aft in Figure 38. Figures 37 through 39 are the results for the integrated loadings under various power laws. It is of interest to study the individual harmonic effects, and a typical plot is shown in Figure 40. It can be seen that for the forward cases a larger range of harmonics contributes than for the aft radiation cases. Figure 40 also shows how the effect of velocity on the first order (steady) loading harmonic is considerably greater than on, say the sixteenth.

The effects of forward velocity noted on both Figures 37 through 39 and on Figure 40 are very similar to the effects observed simply due to change in rotational Mach number (compare with Figures 35 and 32). This suggests that it may be possible to estimate the effects of forward velocity simply by choosing an effective rotational Mach number for the forward speed case. That this is so can be seen from a study of the basic Equation (36) as modified by the $(1 - M_{or})$ term suggested in Section 3.5. The argument of the Bessel function terms is $nMy/r(1 - M_{or})$. Now $n = mB$ is the sound harmonic number and is unaffected by forward speed. Near the plane of the disc, both y and r are increased, by a roughly equal amount, due to the effects of the retarded position of

the helicopter. Their effects therefore cancel. Thus, if an effective rotational Mach number M_e is taken such that $M_e = M/1 - M_{or}$, then the effects of forward speed on the Bessel function term are simulated. This Bessel function term is the most important single term in the results. It governs the overall harmonic efficiencies which are shown graphically in Figures 29 and 40. This effective Mach number approximation takes care of this term. Further study of the equations shows that both the drag and the outward force component terms are correctly approximated by this method. However, the thrust term is in error by a factor $(1 - M_{or})$ and will be too high by this amount in the effective Mach number approximation. Unfortunately, as has already been shown, the thrust term dominates the sound field. However, the error is quite small for typical helicopter cases, of the order of 1 dB near the plane of the disc for a forward Mach number of 0.125, and about 2 dB for 0.25. It may be concluded that this effective rotational Mach number approximation is a useful tool for the study of forward velocity effects.

Figure 41 shows the effectiveness of the approximation. A forward Mach number case of 0.25 on top of an actual rotational Mach number of 0.75 is compared to the case of rotational Mach number of 1.0. Since the field point is near the plane of the disc, $M_e \approx 0.75/1-0.25 \approx 1.0$. Figure 41 shows good agreement between the more exact and the approximated solution.

It should be noted that the M_{or} is the component of the convection Mach number M_o in the direction of the observer. It is thus positive in the forward direction, having a maximum in the plane of the disc equal to $+M_o$. Moving the observation point around the helicopter will reduce M_{or}, and it is zero at the side of, or immediately beneath, the rotor. In the aft direction, M_{or} becomes negative, reading a minimum of $-M_o$ in the plane of the disc. Thus, the present results for forward velocity, and the approximate rule, explain one of the frequently observed effects in helicopter noise - that the helicopter has a harsh popping sound on approach, but a very moderate thumping sound as it recedes. This can be attributed directly to the increased effectiveness of the higher harmonics in front of the helicopter compared to behind. It will be observed that Figure 38 predicts a 10-dB difference if an inverse square loading law is assumed. Unfortunately, no published data for direct comparison with this prediction are available.

Directionality Patterns

The next major point to be discussed is directionality. Clearly, the direction in which the sound radiates is of key importance in determining its significance. Some of the effects have already been noted, for instance in Figure 31, but the problem justifies a closer study. Note, first of all, that, under the randomizing approximations used in this report, no variation in sound pressure around the azimuth occurs. Little variation is actually observed in practice. The small differences in sound pressure measured

could easily be due to experimental error or the effect of the rail rotor, to mention just two possible effects. Azimuthal variations would be predicted if a definite phase for the various loading harmonics were introduced into the calculation, and Equations (37) could be used here. But under the random phase condition assumed in the present case, such variations are not possible, and the sound field is circularly symmetric.

On the other hand, distinct variations in sound level are predicted on passing above or below the helicopter disc. Figure 42 shows the directionality patterns due to various individual force components. All plots are based on a single point loading, with the observer a constant radius from the hub, and have been nondimensionalized so that rotational Mach number effects enter only through the frequency parameter mBM. The zero-dB line on all plots corresponds to the average sound power radiated, so that the plotted curves give the correction factor (directivity index) to be added to the spherical spreading law to give the sound in any direction. The dotted lines on the plots correspond to contours of equal ground noise. As the helicopter flies over the ground, the sound radiated fore or aft has to travel much further before striking the ground than the sound radiated immediately downward. Over this additional distance, the sound will attenuate according to the inverse square law (see Equation (2)). The dotted lines on Figure 42 allow for this spherical spreading, assuming that the rotor disc is parallel to the ground. Thus, sound levels lying on the same dotted lines will be observed as the same level at the ground. The plots in Figure 42 are given in the first quadrant but are entirely symmetrical, so that sound radiated up equals sound radiated down in magnitude.

In each of the plots, the same general effects can be observed. For large values of $mB - \lambda$ and low frequencies (mBM), the sound radiation pattern is substantially outward, in the plane of the disc. This is, of course, particularly disadvantageous, but it should be noted that the overall sound efficiency in these cases is poor, with sound levels well down the shoulders of the curves in Figure 29. On the other hand, these cases essentially correspond to the effect of low harmonics of the loading, which are generally of greater magnitude. As frequency is increased, or as $mB - \lambda$ is decreased, the peak of the directionality pattern moves around toward the axis of rotation, and the patterns have a stronger and stronger lobe structure. All the cases with a lobed structure correspond to efficient acoustic radiation, with levels across the top of the curves in Figure 29. It may be noted that an increase in rotational Mach number M corresponds to a movement from left to right in each pattern matrix given. However, an increase in harmonic order m or blade number B corresponds to a movement both across and down (at least for the lower loading harmonics λ), since mB occurs as a parameter on both axes.

Individual comparison of the plots in Figure 42 shows that all the thrust terms go to zero in the plane of rotor disc. This is the effect of the x/r term on the thrust in Equation (36), and = 0 at the rotor disc. Note also that all harmonics of all force components go to zero at the rotor axis except for one case. That is the thrust component for $mB - \lambda = 0$, which has a maximum there. Thus only the single loading mode $\lambda = mB$ contributes

immediately under the helicopter. This was also observed in Figure 31. The drag terms shown in Figure 42 have the opposite effect. All $mB - \lambda = 0$ cases are virtually zero. This can also be seen in Figure 34. This occurs because of the $mB - \lambda$ multiplication factor in the drag term of Equation (36). Note that there is also an $mB + \lambda$ term which does not go to zero, but this is so small as to be negligible in virtually all cases. Also, its relative magnitude is a function of mB and λ separately rather than the single term $mB - \lambda$. Thus, no case corresponding to $mB - \lambda = 0$ has been plotted on Figure 42 for the drag component. The $mB - \lambda$ multiplication factor has another effect. When λ is greater than mB, it goes negative. The amplitude of the negative cases is the same as the equivalent positive case, but the phase has been shifted 180 degrees with respect to the thrust. Hence, the drag terms add to the thrust terms below the rotor for positive $mB - \lambda$ and subtract for negative. Since the thrust is dominant, the effect is of little practical importance, but this does explain the small asymmetries near the plane of the rotor disc in Figure 43, to be discussed later. The same general effects can be observed on the outward components of force terms. These terms become significant slightly nearer the rotor axis than the thrust and drag terms for any given harmonic. Note that all the zeros in the thrust and drag terms are matched by maxima in the outward terms, and vice versa. This is due to the outward terms containing the differential of the Bessel function term used in the thrust and drag expressions.

Figure 43 gives the result of the summation of the three terms for each loading harmonic on the assumption that the thrust to drag to outward components are in the ratio 10:1:1, consistent with the previous results. Figure 43 must be plotted in two quadrants because of the asymmetry in the final result. As discussed above, thrust and drag add in the downward and subtract in the upward quadrant for $mB - \lambda > 1$. For $mB - \lambda < 1$, the position is reversed. The figures should be inverted for this case. The thrust dominates the results for the total case, as can be seen by comparison of Figures 42 and 43. The drag and outward component terms are only significant in the immediate vicinity of the plane of the disc. Figure 34 shows that even 10 degrees from the plane of the disc the thrust was dominant. An additional effect is that the overall plots do not go to zero between lobes as in the case of the individual components. Since the outward components are out of phase they do contribute there. These valleys of the lobes are shown only approximately in Figure 43.

The lobed sound patterns given in Figures 42 and 43 are basically idealizations and are unlikely to occur in practice for two reasons. First, the random effects discussed before will rarely allow such an ordered pattern to occur. Second, and far more important, the observed sound level is, of course, the sum of the contributions from all loading harmonics. The effects of any one harmonic will usually be lost in the overall pattern. Figure 44 gives a typical overall pattern for various sound harmonics. It is based on an assumed 2.5 inverse power law for the loading harmonics, with realistic inputs which will be discussed in more detail later.

Figure 44a gives a polar plot of the sound radiation field in hover. As expected the detailed lobe structures of Figures 42 and 43 do not appear in Figure 44 at any harmonic. However, a gross directionality pattern is evident. The sound field is symmetric on both sides of the rotor axis, with a maximum at about 20 degrees below the rotor disc. A minimum occurs above the rotor disc which is at about 10 degrees for the first harmonic and moves toward the rotor disc for the higher harmonics. The minimum is basically due to the correlation between the thrust-and-drag terms above the disc noted previously. Below the rotor disc, away from the minimum, the sound field is fairly uniform, and in the higher harmonics it only varies a few dB from a spherical distribution. The results shown in Figure 44 are, of course, very dependent on the randomization and harmonic loading laws assumed. On a real helicopter rotor it must be expected that particular combinations of loading harmonics will occur depending on the flight condition. This will be reflected in a much stronger lobe structure, more like Figures 42 and 43. Furthermore, particular phasings of these loading combinations can give azimuthal variations in sound level. However Figure 44a should reflect the basic trends.

Figures 44b and 44c give results for forward flight cases. Sound is given relative to the position of the helicopter when the sound is heard, as before. Both figures show how forward flight causes a general swelling forward of the sound field. Details of the minimum also vary somewhat with forward speed, but this is of comparatively little significance. In both forward flight cases the maximum effect is observed in the plane of the disc, and also for the second and third harmonics plotted. For a forward Mach number of 0.125 (Figure 44b), the difference between the forward and aft radiation amounts to about 5 dB for both the first harmonic and for the higher harmonics but up to 10 dB for the second and third. At a forward Mach number of 0.25 (Figure 44c) the corresponding figures are 10 dB and 20 dB, respectively. For harmonics higher than the tenth (not shown here), the differences are slightly less.

Near-Field Effects

A limited number of cases have been investigated in order to estimate the order of magnitude of near-field effects. Figure 45 shows the polar distribution of the first harmonic sound radiated by a hovering four-blade rotor represented by single lift and drag forces acting at the 80-percent-radius point. The radiation is in a plane normal to the rotor disc. The actual levels have been normalized to an arbitrary reference since the two cases were computed at distances of 1 diameter and 25 diameters from the rotor. Spherical spreading corrections have been applied in order to illustrate the direct effects of the near-field terms. In fact, the far-field results (25 diameters) agreed with those calculated using Gutin's equation to within a fraction of a dB at all points, which verifies the accuracy of the program. At 1 diameter it can be seen that the biggest influence of the near-field effects occurs above the rotor, although the absolute levels are still slightly less than those which occur below the rotor. It seems that in addition to smoothing out the lobes the near-field pressures are more evenly distributed about

the rotor plane than is the radiated sound. In this case, the maximum amplification in the near field occurs 10 degrees above the disc and is equal to 27 dB. This corresponds to the position where the thrust and drag components cancel in the radiation field. However, below the disc the maximum difference is approximately 4 dB. This smoothing out of the dips in the radiated sound by near-field effects was also shown by Loewy and Sutton.[10, 11] However, it should be noted that the far-field lobe structure will theoretically occur sufficiently far from the rotor. In practice, the lobes may not be observed because of atmospheric effects, but any observed smoothing in the far-field will not be due to near-field effects.

Possibly of more interest than these particular results for a distance of 1 diameter are those presented in Figure 46, which illustrate the decay of the near-field effects with increasing distance for the first three harmonics. Three curves are shown in each case. The first is the radiation field, which can be seen to decay at 6 dB per distance doubling. The second includes geometric near-field effects; i.e., the effects caused by the special distribution of the source at distances of the order of the extent of the source. The third includes both geometric and acoustic near-field effects, where the latter are given by Equation (52). It should be noted that the acoustic near field effects actually mitigate some of the effects of source geometry for the first two harmonics, reducing the amplitude of the first by some 3 dB at a distance of 1 diameter. The most significant finding is that the near-field is of little importance at distances greater than 2 diameters from the rotor. This is in disagreement with the suggestions of Loewy and Sutton,[10, 11] that the near-field may be significant at distances as great as 100 diameters.

Blade Motion Effects

The direct effects of blade vibration on the noise field were examined by computing the sound field of a rotor with steady loading but with 20 realistic harmonics of flapping. The analysis presented in Appendix I indicates that the maximum influence of blade motion will be found in the close vicinity of the rotor, so the sound was calculated at a distance of 1 diameter at 10-degree intervals from directly above to directly below the rotor. The only noticeable effect of the blade excitations was found within 10 degrees of the rotor axis where the amplitude of the first and second sound harmonics was increased by approximately 2 dB. However, since the absolute level was close to zero dB (re: 0.0002 dyne/cm^2), this is of no practical significance. Elsewhere, the effect of the flapping motion was negligible, of the order of 0.1 dB in all harmonics up to the fourth. Consequently, it is concluded that blade motion has no acoustic effect of practical importance, and no further studies of motion effects were made.

Accuracy of Computation Methods

Some of the precautions necessary to ensure accuracy were discussed in Section 5.0.

In addition, the accuracy of the computer programs has been verified by comparison with previous work and with each other. The numerical method (HERON 1) and the analytical method (HERON 2) agreed with each other and with Gutin's equation for the case of steady blade loading. The actual comparisons are shown in Figure 45. The slight differences between the computed figures and the Gutin curve can probably be attributed to errors in the latter which was hand calculated, using tables of Bessel functions. The two programs agreed with each other in all cases where valid comparison could be made, namely, in the far-field.

The problems of simulating a continuous aerodynamic pressure distribution by a number of point loads for the purposes of acoustic calculations were discussed in Section 5.2. In order to examine the magnitudes of possible errors, a series of cases were computed which clearly illustrated the importance of the phase relationships between the various loading harmonics. Using realistic harmonic load data, with definite phase relationships between the harmonics, the distributed loads were represented by 1, 2, 5, 10 and 20 radial loading points. It was found, as may be expected, that the results varied somewhat and that the differences increased with acoustic harmonic number. In general, there was little difference in the results for 10 or 20 load points (less than a dB or so for frequencies up to the 10th sound harmonic); a slight difference between 10 and 5 (typically up to 2 dB); but very great differences among 5, 2, and 1. At the higher frequencies, for example, differences of more than 20 dB were found.

In Section 5.2 it was shown that the large differences are to be expected for definite load phasing patterns, but that these differences are illusory. It was also suggested that the assumption of randomized phasing of the spanwise loads removed the phase sensitivity of the acoustic field. Accordingly, a computer program was modified to calculate the effective load distributions defined by Equation (55) and to use the space correlation concepts reflected in Equations (57) and (59) to calculate the sound generated by a variety of loading points. A thrust of 10,000 lbs was assumed with a ratio thrust:drag:outward component of 10:1:1, as before. The value chosen for the correlation parameter a was 3/3, so that the asymptotic form for the overall effective loading (see Equation (55)) was $F_{E_\lambda} = F_\lambda/\sqrt{\lambda}$, where F_λ is the total λ-harmonic force amplitude acting on the blade. The particular value of the correlation parameter chosen above was somewhat arbitrary, although an examination of the blade loading distributions shown in Figures 17 and 18 suggests a number of this order. A more realistic value could only be obtained through experimental measurement of correlation patterns over a blade in flight or through a comprehensive comparison of theoretical and experimental sound measurements. A second inverse power law was chosen for the harmonic loading amplitude, in accordance with Equations (50) and (53). The results of this test are summarized in Figure 47, where the sound harmonics calculated for 1, 5, and 10 loading points are compared. Although the first harmonic levels for the 10 loading point case were not obtained, it is clear that the differences

are small, the maximum discrepancy being less than 2 dB. However, the most striking feature of these results is that the errors now occur at low frequencies, as opposed to the high frequencies encountered previously. At the higher frequencies all three distributions lead to the same results. All the present calculations have used this random phase assumption with a single point loading. Figure 47 shows that errors introduced by this are small.

6.2 THE THEORY IN PRACTICE

The above parameter study has given a considerable amount of information on the basic trends which can be observed in the results. It was also shown that the general trends predicted by the theory were in agreement with the trends observed in available experimental data. It is thus worthwhile to compare theory and experiment more closely and to attempt to develop a prediction technique for helicopter rotor noise calculation.

Comparison of Theory and Experiment

As was noted in Section 2.1, very little reliable experimental data on helicopter noise are available. Consequently it has not been possible to perform a detailed comparison of the theoretical and experimental results. Results of a comparison in a hover case are shown in Figure 12a, which gives data (and also theory) from Schlegel et al.[12] It can be seen that fairly good agreement is achieved, at least for the first three harmonics. The fourth harmonic is a little low. The theoretical results shown in Figure 12a are the result of the 60 loading harmonics, randomized inverse 2.5 law discussed in Section 6.1. It will be observed that these levels are significantly higher than Schlegel's theory. This is due simply to the inclusion of a higher number of loading harmonics in the present calculations. Figure 33 shows that for the present case ($mB = 16$, $M = 0.5$) to up to 24 loading harmonics are required for accurate calculations. Schlegel et al used Scheiman's data[21] which are limited to the first 10 loading harmonics.

A further comparison of the present calculations and Schlegel's results is given in Figure 48. This applies to the same S-58 (H-34) helicopter in level flight at a velocity of 40 kts. This case was chosen to correspond to a flight condition reported by Scheiman[21] for which loading data were available. For this comparison, Scheiman's data were also used in the present program. For this reason, accuracy cannot be expected in the fourth harmonic case. Agreement between theory and experiment is fair for the first and second harmonic, but it falls off rapidly at the third and fourth as expected. It will be observed that only fair agreement with Schlegel's theoretical results is obtained. The maximum differences occur at maximum helicopter range, that is, near the plane of the rotor disc, and reach above 10 dB for the fourth harmonic. These differences are due to slight differences in theory. The present program included both the radial force components which arise through the coning angle and forward speed effects. These corrections are expected to cause differences near the disc

plane. It may be noted that other check calculations run during the present study for simple cases showed good agreement between Schlegel's theory and the present one. Figure 48 also shows the differences in the sound radiated to port and starboard of the helicopter. This difference is a function of the phasing of the blade loads only and again shows the sensitivity of the acoustic field to the loading phase. Differences of over 20 dB may be observed. Whether such differences would be measured in practice is debatable. Better definition of the harmonic loads would undoubtedly remove most of the bigger differences from the results.

It was shown in Section 5.2 that harmonic blade loads may be assumed to vary inversely as the 2.5th power of harmonic number. Using this approximation and a single loading point (as justified by the findings reported in this Section 6.1), the rotational noise spectrum for the Bell UH-1 helicopter has been calculated for comparison with available measurements.[3,7] The randomized phase assumption was used (Section 5.2), and 60 loading harmonics were included. The comparison is shown in Figure 49. The experimental data were obtained on three separate occasions under very different conditions and show remarkable consistency. Because of uncertainties regarding the overall levels, they have been normalized on the basis of power in the third and higher harmonics. This step reduces the probability of error due to the low-frequency response of the microphones and tape recorders which is certainly poor at the fundamental frequency (around 12 Hz). Although for this reason nothing can be said about overall levels; the agreement, insofar as spectral shape is concerned, is good up to the thirtieth harmonic.

Figures 50 and 51 show some further experimental data obtained by Wyle Laboratories[7] for a twin-rotor helicopter, the CH-47B Chinook. No harmonic blade loading data are available for this aircraft, so that no computations could be made for comparison. However, in both figures, the slope of the fitted line is approximately -20 dB per decade at an inverse second power law. When the simplified relationship between the loading and acoustic power laws given in Section 6.1 is used, namely

$$p^2 \simeq mB^{(2-2k)}$$

it can be assumed that for the Chinook the loading power exponent is 1.5, as opposed to 2.0 for the UH-1 and H-34 (ignoring the correlation effect which adds a further 0.5). This rise in higher harmonic loading levels is almost certainly due to the overlap of the two rotors which causes one to pass through the wake of the other. The undesirability of overlapping rotors from the standpoint of noise is thus fairly clear.

Two further points regarding Figures 50 and 51 should be mentioned. The first is that Figure 50 compares internal and external noise, and, although detail differences are significant, the trends are obviously similar. The second is that one case plotted in Figure 51 is the analysis of a recording of moderate blade slap. The main difference between these points and the second set of data (which was recorded a few seconds

later when no blade slap was observed) is in the region of the tenth harmonic, or 100 Hz, where the levels are some 6 dB higher in the presence of slap.

Although the comparisons of theory and experiment are somewhat limited they do tend to support the basic theoretical results. More importantly, they show that the lack of good experimental data is a serious handicap to the advancement of rotor noise control methods.

Prediction Methods for Rotor Noise

This study, like previous work on the subject, has shown that methods for the calculation of helicopter rotor noise require extensive numerical calculations which can be performed only on a digital computer. Furthermore, the accuracy which can be achieved is limited.

In the light of the comparisons of theory and experiment described above, it is concluded that the most realistic approach at the present time is to make use of the assumption of random blade loading phase. This gives results which are at least as accurate as methods which make use of known phase relationships, if not more so. It also offers the advantage that, in conjunction with the power law assumption for estimation of harmonic loading levels, it can be used to calculate high sound harmonics. In addition, it has been shown that although the forward velocity of the helicopter has an important effect on the radiated rotor noise, it can be accounted for with reasonable accuracy by using the concept of an "effective Mach number".

Consequently, a set of tentative design charts has been prepared which enables the sound field of a rotor to be calculated for any conditions of steady flight. These charts are presented as part of Appendix III, where the detailed instructions for their use may also be found. A review of the underlying theory is included. With careful use of these charts, a few simple hand calculations will yield any reasonable number of rotational noise harmonics, at any point in the far field of the rotor, to within 2dB of the accuracy obtained by computer. The experimental comparison discussed above suggests that, although the design charts may be in error for the overall levels, they should give the parameter trends quite accurately. The charts should, therefore, be useful tools for design trade-off studies.

6.3 METHODS FOR REDUCING THE NOISE OUTPUT

The results of the last section show fair agreement between the present theory and available data. It is therefore of interest to suggest methods for reducing the sound output of the helicopter rotor. By no means have all the points made in the theory been verified, but it is thought that the basic trends should be correct.

The most useful data from the noise control viewpoint were presented in Figures 2 and 3. It was shown how the sound radiated by the helicopter rose substantially at both high and low values of collective pitch, due to still and wake interactions, respectively. It therefore appears worthwhile to attempt to define optimum collective pitch settings for minimum noise. As far as is known, little work has been accomplished on this. Note particularly that some of the results shown on Figures 6 and 7 are as much as 10 dB lower than expected. It seems quite possible that this is a real effect due to collective pitch variations.

The basic mechanism underlying the effect of collective pitch is, the displacement of the shed vortex wake as far as possible beneath the oncoming blade, so that harmonic airloads are substantially reduced. Any effect which achieves greater wake displacement, less vortex strength, or less blade load response to the fluctuating aerodynamic input will reduce the noise. Work on increasing the size of the vortex and thus reducing its peak velocity was reported by Sternfeld et al.,[38] and this has considerable potential for noise reduction purposes.

It should be noted that collective pitch is the important parameter for optimization based on the operation of a particular rotor. For a given rotor producing a given amount of thrust, the downward velocity of the wakes is essentially constant, so that the vertical distance between a blade and the vortex trailing from the tip of the previous blade is increased by reducing the tip speed. To do this, of course, collective pitch must be increased. Beyond a certain limit the blade stalls, causing the increase in noise which has been noted. The tip speed thus affects noise in two ways: through the direct effects of Mach numbers and through the blade/wake spacing.

Another step which would appear to be beneficial is to increase the number of blades. The trailing vortex from each blade would be of less strength; but, more importantly, if the blades were sufficiently close together, the wake would not have had time to roll up. Results on wings[39] suggest that a distance of the order of one-half the span is required for vortex rollup to occur. It appears that if each blade was close enough to the preceding one, rollup effects would be averted. Indeed it can be seen that for very closely spaced blades, the wakes would be affected more by their neighbors than by themselves, and rollup might be substantially delayed. Possibly this is a partial explanation of Schlegel et al's results,[12] (Equation (4)), which implied 7.5 dB less "vortex" noise radiation from five- and six-blade rotors than Davidson and Hargest's

results[4] for a three-blade rotor (Equation (3)). Furthermore, as noted in Section 2.1, Cox and Lynn's results[3] suggest that a three-blade rotor produces 3 dB less noise than a two-blade one. The trends for blade number suggested in the theory in Section 6.1 were typically a B^{-2} law, and this is certainly consistent with the above results. The increase in frequency which would accompany the use of more blades would have a double effect. At short distances from the rotor the effect would be undesirable in that the harmonics would be shifted to frequencies where the hearing is more sensitive. On the other hand, atmospheric attenuation of sound increases with frequency, so that the frequency increase could result in a further decrease in detectability.

One obviously undesirable feature from the wake interaction point of view is the use of multiple-rotor helicopters. Here, one rotor can interact with the wake of the other, and Figure 51 (discussed on page 72) shows how the higher harmonics are increased in a tandem rotor case. From a general viewpoint, it might be possible to design a quieter tandem rotor helicopter if the vortex interactions, which are the major noise producers, could be minimized, while at the same time allowing sufficient rotor separation to permit the wake to diffuse. However, this seems to pose a difficult design problem. It may also be noted that interactions of the main rotor with the fuselage and the tail rotor can also be undesirable acoustically because of the local blade loading increments they produce. Indeed, it should be possible also to reduce the noise radiated by the tail rotor by minimizing interaction effects due to the main rotor. It is fairly straightforward to minimize these interactions by design if desired.

An alternative way of minimizing wake interactions is to use high-lift airfoil sections on the blades. Such rotors will tend to direct the wake well away from succeeding blades, thus reducing higher harmonic airloads and sound output. This will generally result in higher disc loadings and increased frequencies, so that sound output at the fundamental frequency becomes more important. Reduction of tip speed when using such devices is therefore indicated.

The theory also indicates that noise output is proportional to the product of thrust and disc loading. Since the thrust is not a design variable, the rotor diameters should be as great as possible for minimum noise.

It has also been shown that the sound radiation theoretically rises as the square of the tip speed. Unfortunately, even a reduction from 700 to 500 fps in tip speed will give only a reduction of about 3 dB according to this trend. On the other hand, it has been demonstrated that the sound output at the lowest frequency is proportional to a high power of the tip velocity. Although this first harmonic sound output is only of limited significance in the far-field, it can be more important in the internal noise field, because of potential increases in subjective response at high levels due to various forms of coupling through structural vibrations. Particularly for high blade numbers it is probably well worthwhile to adopt a minimal tip speed for noise control.

A further possible method for reducing the noise is to increase the blade chord. Results derived in Reference 18 showed that, for a fixed-frequency input, the integrated aerodynamic load was proportional to the inverse square root of the chord length. Thus, sound output would be predicted as inversely proportional to chord. Also, an increase of chord at fixed thrust and collective pitch causes a decrease in tip speed with its associated acoustic benefits. Perhaps any increase in rotor blade area would be more efficiently employed as an extra blade. Nevertheless, it is thought that a more detailed study of blade chord effects would be valuable.

One last feature of potential use is the directionality characteristics. A quite definite minimum just above the plane of the disc is predicted. It may be possible to design or fly a helicopter so that this minimum occurs at the field position where minimum noise is desired. It should be particularly noted however that this minimum has not been confirmed experimentally.

It would seem well worthwhile to perform detailed (possibly scale model) experiments to study some of these noise control methods. The experiments should be deliberately designed to cover cases outside normal operating ranges so that the trends can be well defined. Such experiments could be of considerable value in reducing helicopter rotor noise radiation.

The major design requirements for minimum noise can be summarized as follows:

- Low tip speed
- Large number of blades
- Low disc loading
- Large blade chord
- Minimum interference with rotor flow
- Any features which will reduce the high frequency airload fluctuations.

7.0 CONCLUSIONS

The present work has uncovered many new factors of importance in the study of helicopter rotor noise. In order to categorize the results, the conclusions will be grouped under several subheadings.

I. BASIC MECHANISMS

a) Farfield noise radiation from the helicopter is dominated by main rotor noise.

b) Main rotor noise, especially at the higher frequencies, is due to the high harmonics of the fluctuating airloads imposed upon it.

c) Blade slap should not be regarded as essentially different from other forms of rotor noise.

d) Discrete frequency peaks due to main rotor rotational noise are observable to 400 Hz.

e) "Vortex" noise as previously defined includes a substantial contribution from rotational noise.

II. EXPERIMENTAL DATA REVIEW

a) The most striking feature of available data is its wide scatter, perhaps ± 10 dB.

b) Very little experimental data on helicopter noise are yet published.

c) High harmonics of rotational noise obey a tip velocity squared law for constant thrust.

d) Low harmonics of rotational noise obey a tip velocity to the sixth or eighth power law (constant thrust).

e) Spectral content of helicopter noise is strongly dependent on tip speed.

f) Noise output in all harmonics obeys a thrust power law between 1 and 2.

g) Noise levels increase as the rotor approaches stalled operation (high collective pitch).

h) Noise levels increase at low collective pitch due to wake interaction effects.

i) An optimum collective pitch for minimum noise exists.

III. ACOUSTIC THEORY

Excellent agreement has been obtained between analytical and numerical solutions to the fundamental acoustic equation in regions where the analytical approximations are valid.

IV. AERODYNAMIC LOADS STUDIES

a) Simple rotor theory is adequate for predicting performance data only since predictions of second and higher harmonic loading levels are badly in error.

b) Available data show a negligible effect of forward flight on higher harmonic aerodynamic loads. Substantial levels occur even in hover.

c) Higher harmonic loads are extremely localized on the blade span, but they are generally more intense toward the blade tips.

d) It is impossible to predict the phase of the higher harmonic loads.

e) The airloads follow an approximate loading harmonic power law, which is very approximately an inverse square, based on the steady loading for two- and four-blade single rotors.

f) In rough running cases, higher levels of the higher harmonics occur, suggesting an inverse first power law.

V. COMPUTATION AND ACCURACY

a) The present results are substantially self-checking due to the use of two independent computer programs.

b) Results obtained agree with previous results obtained for steady loading input. Spanwise loading introduces small errors.

c) For limited loading harmonic inputs, computation time has been substantially reduced, to the order of 10 seconds a field point for the general-purpose program based on Equation (20), and to about one-tenth of a second a field point for a special program based on Equation (37).

d) The phase of the loading is equally as, or more, important than the amplitude. Lack of knowledge of the phase of the aerodynamic loads can be reflected in substantial underestimation of the sound produced.

e) A random phase assumption has been used in the present computations, both over the span of the blade and between loading harmonics. This introduces the necessity for definition of a correlation length not given by available data, but suggested theoretically to be inversely proportional to loading

harmonic numbers. Using this assumption the sound field can be computed with reasonable accuracy using a single spanwise loading point.

f) The assumption of a point chordwise loading is probably conservative.

VI. RESULTS OF PARAMETER STUDY

a) A limited range of loading harmonics contributes to any one sound harmonic.

b) The range is centered on the loading harmonic $\lambda = mB$, where m is the sound harmonic and B is the number of blades.

c) The harmonic $\lambda = mB$ is the only harmonic contributing to noise directly on the rotor axis.

d) In the plane of the rotor disc, loading harmonics up to $mB(1 + M)$ contribute. For instance, for the tenth sound harmonic of a four-blade rotor with $M = 0.5$, loading harmonics up to the sixtieth contribute.

e) Neither theory nor experiment gives data on these high loading harmonics.

f) For typical helicopters, the thrust fluctuations dominate the noise field except close to the plane of the disc.

g) For the loading power law typical of helicopter rough running, an acoustic spectrum identical with blade slap is produced.

h) For the loading power law typical of normal operation, the acoustic spectrum closely resembling normal helicopter noise is found.

i) The steady loading dominates the levels of the first few harmonics.

j) Typical variation of the higher harmonics is as tip velocity squared.

k) Typical variation of the first harmonic is as tip velocity to the 2B power, where B is the number of blades.

l) Typical variation of all harmonic levels is as thrust times disc loading.

m) Higher levels of sound are predicted in the forward direction compared to aft for forward flight cases.

n) Forward flight cases are well predicted applying an effective velocity rule to the hover results.

o) The overall sound radiation pattern has a maximum at a small angle below the rotor disc and a minimum slightly above.

p) Near-field effects are negligible more than 2 diameters from the rotor.

q) Blade motion does not produce a significant sound field.

VII. EXPERIMENTAL PREDICTION

a) Computed and measured levels of the first four harmonics agree fairly well in a hover case.

b) Calculated higher harmonic levels are lower than data for a forward flight case.

c) Spectral shapes are predicted well for a hover case out to the thirtieth harmonic.

d) Prediction methods based on the theory should be accurate for predicting trends but may be in error in overall levels.

e) Design charts for general use in helicopter rotor noise prediction are presented in Appendix III.

VIII. NOISE CONTROL

a) An optimum collective pitch exists for minimum noise, which requires detailed experimental study.

b) Minimum rotor noise output requires that the rotor interaction effects be minimized.

c) Configuration changes should ensure minimum interactions due to the fuselage and tail rotor.

d) Multiple-rotor systems are unfavorable acoustically.

e) Increase of blade number seems to offer the best possibility of noise reduction.

f) Use of high-lift blade sections should reduce high harmonic noise.

g) Reduction of tip velocity will have significant effects only on the fundamental, but this may be important, particularly in conjunction with (e) and (f) above.

8.0 RECOMMENDATIONS

On the basis of the results of this investigation, it is recommended that:

a) A systematic experimental study be performed to provide accurate and detailed acoustic data on helicopters of all types.

b) Measurements be made of model and/or full scale rotor airloads using audio-frequency range instrumentation, possibly in conjunction with acoustic measurements. The data should be analyzed into power and cross-power spectra.

c) The noise control measures suggested in Section 6.3 be evaluated through a model or full scale study.

d) Further theoretical work be performed to specify helicopter noise output in terms of the cross-power spectrum of the loading inputs (see Appendix II)

e) A theoretical study be made of the noise generated by the motion of blade/vortex interaction points along the blade span.

f) The theoretical prediction methods presented be subjected to detailed experimental verification, both to establish confidence in their utility and, possibly, to suggest empirical correction factors which may be applied.

LITERATURE CITED

1. Hubbard, H.H., and Maglieri, D.J., NOISE CHARACTERISTICS OF HELICOPTER ROTORS AT TIP SPEED UP TO 900 FEET PER SECOND, Journal of the Acoustical Society of America, Vol. 32, No. 9, September 1960, pp. 1105-1107.

2. Sternfield, H., Jr., Spencer, R.H., and Schaeffer, E.G., STUDY TO ESTABLISH REALISTIC ACOUSTIC DESIGN CRITERIA FOR FUTURE ARMY AIRCRAFT, Vertol Division, The Boeing Company, TREC Technical Report 61-72, U.S. Army Transportation Command, Fort Eustis, Virginia, June 1961.

3. Cox, C.R., and Lynn, R.R., A STUDY OF THE ORIGIN AND MEANS OF REDUCING HELICOPTER NOISE, Bell Helicopter Company, TCREC Technical Report 62-73, U.S. Army Transportation Research Command, Fort Eustis, Virginia, November 1962.

4. Davidson, I.M., and Hargest, T.J., HELICOPTER NOISE, Journal of the Royal Aeronautical Society, Vol. 69, No. 653, May 1965, pp. 325-336.

5. Stuckey, T.J., and Goddard, J.O., INVESTIGATION AND PREDICTION OF HELICOPTER ROTOR NOISE: 1 WESSEX WHIRL TOWER RESULTS, Journal of Sound and Vibration, Vol. 5, No. 1, January 1967, pp. 50-80.

6. Leverton, J.W., and Taylor, F.W., HELICOPTER BLADE SLAP, Journal of Sound and Vibration, Vol. 4, No. 3, November 1966, pp. 345-357.

7. Ollerhead, J.B., SOME ANALYSES OF HELICOPTER NOISE, Wyle Laboratories, WR 68-8, Wyle Laboratories Research Staff, Huntsville, Alabama (To be published).

8. Lowson, M.V., THE SOUND FIELD FOR SINGULARITIES IN MOTION, Proceedings of the Royal Society of London A, Vol. 286, August 1965, pp. 559-572.

9. Lowson, M.V., BASIC MECHANISMS OF NOISE GENERATION BY HELICOPTERS, V/STOL AIRCRAFT, AND GROUND EFFECT MACHINES, Journal of Sound and Vibration, Vol. 3, Pt. 3, 1966, pp. 454-466.

10. Loewy, R.G., and Sutton, L.R., A THEORY FOR PREDICTING THE ROTATIONAL NOISE OF LIFTING ROTORS IN FORWARD FLIGHT, INCLUDING A COMPARISON WITH EXPERIMENT, Rochester Applied Science Labs. Inc. USAAVLABS Technical Report 65-85, U.S. Army Aviation Materiel Laboratories, Fort Eustis, Virginia, January 1966.

11. Loewy, R.G., and Sutton, L.R., A THEORY FOR PREDICTING THE ROTATIONAL NOISE OF LIFTING ROTORS IN FORWARD FLIGHT INCLUDING A COMPARISON WITH EXPERIMENT, Journal of Sound and Vibration, Vol. 4, No. 3, November 1966, pp. 305-349.

12. Schlegel, R.G., King, R.J., and Mull, H.R., HELICOPTER ROTOR NOISE GENERATION AND PROPAGATION, Sikorsky Aircraft, USAAVLABS Technical Report 66-4, U.S. Army Aviation Materiel Laboratories, Fort Eustis, Virginia, October 1966, AD 645 884.

13. Loewy, R.G., AURAL DETECTABILITY OF HELICOPTERS IN TACTICAL SITUATIONS, Journal of the American Helicopter Society, October 1963, pp. 36-53.

14. Kryter, K.D., and Pearsons, K.S., SOME EFFECTS OF SPECTRAL CONTENT AND DURATION ON PERCEIVED NOISE LEVEL, Journal of the Acoustical Society of America, Vol. 35, No. 6, June 1963, pp. 866-883.

15. Gutin, L.Ya., ON THE SOUND FIELD OF A ROTATING PROPELLER, from Physiks Zeitschrift der Sowjetunion, Band A Heft 1, (1936), pp. 57-71, Translated as NACA TM-1195, National Advisory Committee for Aeronautics, October 1948.

16. Garrick, J.E., and Watkins, C.E., A THEORETICAL STUDY OF THE EFFECT OF FORWARD SPEED ON THE FREE SPACE SOUND PRESSURE FIELD AROUND PROPELLERS, NACA Report 1198. National Advisory Committee for Aeronautics, 1954.

17. Deming, A.F., NOISE FROM PROPELLERS WITH SYMMETRICAL SECTIONS AT ZERO BLADE ANGLE II, NACA TN-679, National Advisory Committee for Aeronautics, 1938.

18. Lowson, M.V., THEORETICAL STUDIES OF COMPRESSOR NOISE, Wyle Laboratories WR 68-5, Wyle Laboratories Research Staff, Huntsville, Alabama, February 1968.

19. Hubbard, H.H., and Maglieri, D.J., AN INVESTIGATION OF SOME PHENOMENA RELATING TO THE AURAL DETECTION OF AIRPLANES, NACA TN-4337, National Advisory Committee for Aeronautics, December 1958.

20. Sutherland, L.C. (Ed.), SONIC LOADING ON AEROSPACE GROUND FACILITIES - A DESIGN MANUAL, Wyle Laboratories WR 68-2, Wyle Laboratories Research Staff, Huntsville, Alabama, March 1968.

21. Scheiman, J., A TABULATION OF HELICOPTER ROTOR-BLADE DIFFERENTIAL PRESSURES, STRESSES, AND MOTIONS, AS MEASURED IN FLIGHT NASA TM-X-952, National Aeronautics and Space Administration, Washington, D.C., March 1964.

22. Bendat, J.S., PRINCIPLES AND APPLICATIONS OF RANDOM NOISE THEORY, New York, John Wiley and Sons, 1958.

23. Morse, P.M., and Ingard, K.U., THEORETICAL ACOUSTICS, New York, McGraw-Hill Book Company, 1968.

24. Arnold, I., Lane, F., and Slutsky, S., PROPELLER SINGING ANALYSIS, GASL TR-221, General Applied Science Laboratories, Westbury, New York, 1961.

25. Lighthill, M.J., ON SOUND GENERATED AERODYNAMICALLY I GENERAL THEORY, Proceedings of the Royal Society of London A, Vol. 211, 1952, pp. 564-587.

26. McLachlan, N.W., BESSEL FUNCTIONS FOR ENGINEERS, 2nd EDITION, Oxford, Oxford University Press, 1961.

27. Gressow, A., and Myers, G.C., Jr., AERODYNAMICS OF THE HELICOPTER, New York, Frederick Ungar Publishing Company, 1967.

28. Payne, P.R., HELICOPTER DYNAMICS AND AERODYNAMICS, London, Sir Isaac Pitman and Sons, 1959.

29. Miller, R.H., UNSTEADY AIRLOADS ON HELICOPTER ROTOR BLADES, Journal of the Royal Aeronautical Society, April 1964, pp. 217-229.

30. Piziali, R.A., METHOD FOR THE SOLUTION OF THE AEROELASTIC RESPONSE PROBLEM FOR ROTATING WINGS, Journal of Sound and Vibration, Vol. 4, No. 3, November 1966, pp. 445-489.

31. Harrison, J.M., and Ollerhead, J.B., THE NATURE OF LIMITATIONS IMPOSED ON THE PERFORMANCE OF A HELICOPTER ROTOR, Journal of Sound and Vibration, Vol. 4, No.3, May 1966, pp. 422-454.

32. White, R.P., VTOL PERIODIC AERODYNAMIC LOADINGS: THE PROBLEMS, WHAT IS BEING DONE AND WHAT NEEDS TO BE DONE, Journal of Sound and Vibration, Vol. 4, No. 3, November 1966, pp. 305-344.

33. Levi, H., and Forsdyke, A.G., STEADY MOTION AND STABILITY OF A HELICAL VORTEX, Proceedings of the Royal Society of London A, Vol. 120, 1928, pp. 670-690.

34. Burpo, F.B., and Lynn, R.R., MEASUREMENT OF DYNAMIC AIRLOADS ON A FULL SCALE SEMI-RIGID ROTOR, Bell Helicopter Company, TCREC Technical Report 62-42, U.S. Army Transportation Research Command, Fort Eustis, Virginia, December 1962.

35. Lowson, M.V., SOME OBSERVATIONS ON THE NOISE FROM HELICOPTERS, Southampton, Institute of Sound and Vibration Research, April 1964.

36. Meyer, J.R., and Falabella, G., AN INVESTIGATION OF THE EXPERIMENTAL AERODYNAMIC LOADING ON A MODEL HELICOPTER BLADE, NACA TN-2953, National Advisory Committee for Aeronautics, 1953.

37. Watkins, C.E., and Durling, B.J., A METHOD FOR THE CALCULATION OF FREE SPACE SOUND PRESSURES NEAR A PROPELLER IN FLIGHT INCLUDING CONSIDERATIONS OF CHORDWISE BLADE LOADING, NACA TN-3809, National Advisory Committee for Aeronautics, 1955.

38. Spencer, R.H., et al., TIP VORTEX THICKENING FOR APPLICATION TO HELICOPTER NOISE REDUCTION, Vertol Division, The Boeing Company, USAAVLABS Technical Report 66-1, September 1966.

39. Spreiter, J.R., and Sacks, A.H., THE ROLLING UP OF THE TRAILING VORTEX SHEET AND ITS EFFECT ON THE DOWNWASH BEHIND WINGS, Journal of the Aeronautical Sciences, Vol. 18, 1951, pp. 21-32.

40. Ollerhead, J.B., and Taylor, R.B., DESCRIPTION OF A HELICOPTER ROTOR NOISE COMPUTER PROGRAM, Wyle Laboratories Research Staff, USAAVLABS Technical Report 68-61, 1968.

41. Ffowcs Williams, J.E., and Hawkings, D.L., THEORY RELATING TO THE NOISE OF ROTATING MACHINERY, Department of Mathematics, Imperial College, London, ARC 29,821, Aeronautical Research Council, London, England, January 1968.

APPENDIX I
ANALYTIC EXPRESSION FOR BLADE MOTION EFFECTS

It would clearly be of interest to attempt to describe analytically the sound field while the rotor is flapping. Let us attempt to do this following the methods of Section 3.4. The key change is in the value of r used in the retarded time integral. For the blade motion case, suppose the motion is given by

$$r = x_1 - y_1 = x - \xi\ ,\ y + \eta\ \sin\theta - R\cos\theta,\ -\eta\ \cos\theta - R\sin\theta$$

ξ and η are functions of θ. ξ represents the out-of-plane flapping motion, and η represents the in-plane motion. Radial motions could be included if desired.

Thus,
$$r^2 = (x - \xi)^2 + (y + \eta\cos\theta)^2 - 2(y + \eta\sin\theta)\,R\cos\theta + \eta^2\cos^2\theta + 2\eta\ R\cos\theta\sin\theta + R^2 \quad (69)$$

Following through the same approximation as before, ignoring squares and products of ξ, η, and R in comparison with x and y, gives

$$r \approx r_1 \left\{1 - \frac{yR\cos\theta + x\xi - y\eta\ \sin\theta}{r_1^2}\right\} \quad (70)$$

Substituting in the expression for the sound radiation gives then (identifying y with Y and θ with $\theta - \phi$)

$$C_n = \frac{1}{4\pi a_o^2}\int_0^{2\pi}\sum_{\lambda=-\infty}^{\infty}\frac{A_\lambda}{r_1}\ \exp i\left\{(n-\lambda)\theta + \frac{n\Omega r_1}{a_0} - \frac{n\Omega YR}{a_0 r_1}\cos(\theta-\phi) - \frac{n\Omega x\,\xi}{a_0 r_1} + \frac{n\Omega Y\eta\ \sin(\theta-\phi)}{a_0 r_1}\right\} d\theta \quad (71)$$

If ξ and η are arbitrary functions of θ, then evaluation of this integral is possible only on the computer. For some special cases an analytic solution is possible, and

one case of some interest is when $\xi = \xi_1 \cos(\theta - \phi)$, $\eta = 0$. This corresponds to a first harmonic flapping motion. The ξ and Y terms in the exponential then combine. The result is then simply that given by Equation (33), except that the argument of the Bessel function is

$$\frac{n\Omega R}{a_0}\left(Y + \frac{x\,\xi_1}{R}\right)$$

Since ξ_1/R can be safely assumed to be small, it can be seen that the slight distortion of the sound field produced in this case is of little practical consequence (except close to the x - axis).

Unfortunately, use of a Fourier series to describe to flapping motion does not lead to any simpler result in the present case, since the various components cannot be separated. It is probable that a solution can be obtained in terms of hypergeometric functions, but this approach was not taken in the present work. Thus, analysis of flapping and the blade motion effects has been limited to the computation using the general program.

APPENDIX II
NOISE RADIATION BY RANDOM LOADS

The basic objective of the present report has been to calculate the noise radiated by the fluctuating loads on the rotor. The assumption in Section 3.4 that the loads could be expanded as a Fourier series limited the analysis to the loadings which occurred at some harmonic of the rotational speed. However, it is clear that random loads can also act on the blades at any frequency, so that it is important to be able to calculate the noise radiation from such sources. Furthermore, it was shown in Section 5 how that even the harmonic airloads had to be assumed to be random in phase to obtain meaningful results. It is clear that a more detailed analysis of the random case is necessary. This appendix presents a preliminary study of the problem. It should be noted that the analysis presented is not rigorous and several assumptions which could possibly be of importance have been made; but, although only an outline proof is given, the results are of fairly clear physical significance, and can be used directly in calculation of noise radiation from experimental data.

First of all, since random loads can occur at any frequency it is necessary to obtain an expression for the spectrum function of the sound radiation at any frequency. The analysis follows that of Reference 18, and the results of Reference 24 may also be studied for comparison. Ffowcs Williams and Hawkings [41] have recently presented arguments essentially similar to those given here.

We wish first of all to evaluate

$$G(\omega) = \int p \exp i\omega t \, dt \tag{72}$$

where G is a spectrum function. The limits on the time integral are left undefined at present. p is the sound pressure observed at a point $\underset{\sim}{x}$ and time t, and is given by Equation (20) as

$$p(\underset{\sim}{x}, t) = \left[\frac{x_i - y_i}{(1 - M_r)\, a_0\, r} \frac{\partial}{\partial t} \left\{ \frac{F_i}{4\pi r (1 - M_r)} \right\} \right] \tag{73}$$

Equation (72) applies for a single point input on the blade. When the variables are changed back to source time $\tau = t - r/a_0$, Equations (72) and (73) give

$$G(\omega) = \int \frac{x_i - y_i}{a_0 r} \frac{\partial}{\partial \tau} \left\{ \frac{F_i}{4\pi r (1 - M_r)} \right\} \exp i\omega(\tau + r/a_0) \, d\tau$$

and integrating by parts, ignoring the near field, gives (see also Reference 18)

$$G(\omega) = \int \frac{-i\omega(x_i - y_i)F_i}{4\pi a_0 r^2} \exp i\omega(\tau + r/a_0)\, d\tau \qquad (74)$$

For the rotor case, we can apply the usual formulas for the force components and retarded time approximation[15, 18] to give

$$G(\omega) = \int \frac{i\omega}{4\pi a_0 r_1}\left\{\frac{xT}{r_1} + \frac{y\Omega}{r_1}\sin\Omega\tau - \frac{yC}{r_1}\cos\Omega\tau\right\} + \exp\left\{i\omega\left(\tau + \frac{r_1}{a_0} - \frac{yR}{a_0 r_1}\cos\Omega\tau\right)\right\} d\tau \qquad (75)$$

Notation is the same as that used in Section 3.4.

Now put $T = T_\nu \exp(-i\nu\tau)$ and similarly for the other force components, that is we assume that the forces are varying at a circular frequency ν not necessarily equal to a multiple of the rotational frequency. Also from formula 44 in McLachlan's book,[26]

$$\exp i z\cos\theta = \sum_{n=-\infty}^{+\infty} i^n J_n(z)\cos n\theta$$

Thus, (75) becomes

$$G(\omega) = \int \frac{i\omega}{4\pi a_0 r_1}\left\{\frac{xT_\nu}{r_1} + \frac{yD_\nu}{r_1}\sin\Omega\tau - \frac{yC_\nu}{r_1}\cos\Omega\tau\right\}\exp i(\omega-\nu)\tau + \sum_{n=-\infty}^{+\infty}(-i)^n J_n\left(\frac{\omega y R}{a_0 r_1}\right)\cos n\Omega\tau\; d\tau$$

Now put $\sin \Omega \tau = \frac{1}{2i}\left\{\exp(i\Omega\tau) - \exp(-i\Omega\tau)\right\}$

and $\cos \Omega = \frac{1}{2}\left\{\exp(i\Omega\tau) + \exp(-i\Omega\tau)\right\}$

and use orthogonality relations on the integration. For the thrust term, for instance, only the frequencies $(\omega - \nu) = \pm n\Omega$ can contribute. We obtain

$$G(\omega) = \frac{i\omega}{4\pi a_0 r_1}\left\{\frac{xT_v}{r_1}(-i)^n J_n + \frac{yD_v}{2ir_1}\left((-i)^{n+1}J_{n+1} - (-i)^{n-1}J_{n-1}\right) + \right.$$

$$\left. + \frac{yC_v}{2r_1}\left((-i)^{n+1}J_{n+1} + (-i)^{n-1}J_{n-1}\right)\right\} \qquad (76)$$

where the argument of all the Bessel functions is $\omega y \bar{R}/a_0 r_1$

Now[26] $J_{n-1}(z) + J_{n+1}(z) = 2n J_n(z)/z$

and $J_{n-1}(z) - J_{n+1}(z) = 2J_n'(z)$

Thus, Equation (76) can be written as

$$G(\omega) = \frac{(-i)^{n-1}\omega}{4\pi a_0 r_1}\left\{\left(\frac{xT_v}{r_1} - \frac{n\Omega}{\omega}\frac{D_v}{M}\right)J_n\left(\frac{\omega y R}{a_0 r_1}\right) + \frac{iyC_v}{r_1}J_n'\left(\frac{\omega y R}{a_0 r_1}\right)\right\} \qquad (77)$$

where $G(\omega)$ exists only at $\omega = \nu \pm n\Omega$

Thus, input of an arbitrary frequency ν on the blade gives rise to many frequencies in the sound field, displaced an integral number of rotational frequencies from the input frequency. The effect is the same as is observed in frequency modulated radio signals. It occurs here because of the frequency modulation due to the varying Doppler frequency shift as the blade rotates toward and away from the observer. Equation (77) is consistent with Equation (36) derived for the integer loading harmonic case.

If we now suppose that a complete frequency spectrum $F(\nu)$, the same for each component, is present, then clearly all loading frequencies ν removed $n\Omega$ from the acoustic frequency of interest that ω will contribute. Thus, if the overall contribution at ω is $S(\omega)$, we may write

$$S(\omega) = \sum_{n=-\infty}^{+\infty} F(\omega - n\Omega)\, G(\omega) \tag{78}$$

where the T, D and C terms in G now contain only magnitude and direction, and not frequency.

It now remains to extend the result to the complete blade. The observed pressure from the total blade p_T is given by

$$p_T(\underset{\sim}{x}, t) = \int_{\eta} p(\underset{\sim}{x}, \underset{\sim}{\eta}, t)\, d\underset{\sim}{\eta}$$

where p is the single point pressure previously determined and $\underset{\sim}{\eta}$ is a coordinate fixed in the moving blade. Thus also the overall spectrum function is given by

$$S_T(\underset{\sim}{x}, \omega) = \int_{\eta} S(\underset{\sim}{x}, \underset{\sim}{\eta}, \omega)\, d\eta$$

By the usual rules for establishing power spectra from spectral functions (for example Reference 22), the power spectral density of the sound is given by

$$P(\underset{\sim}{x}, \omega) = \lim_{T \to \infty} \frac{1}{T} \int_{\eta} \int_{\eta'} S^*(\underset{\sim}{x}, \underset{\sim}{\eta}, \omega)\, S(\underset{\sim}{x}, \underset{\sim}{\eta}', \omega)\, d\underset{\sim}{\eta}\, d\underset{\sim}{\eta}' \tag{79}$$

If we write $\underset{\sim}{\eta}' = \underset{\sim}{\eta} + \underset{\sim}{\xi}$ so that $\underset{\sim}{\xi}$ is a vector separation, then Equations (78) and (79) may be combined to give

$$P(\underset{\sim}{x},\omega) = \lim_{T\to\infty} \frac{1}{T} \int_{\eta} \int_{\xi} \sum_{n=-\infty}^{+\infty} \sum_{m=-\infty}^{+\infty} F(\underset{\sim}{\eta},\omega - n\Omega)\, F^{*}(\underset{\sim}{\eta}+\underset{\sim}{\xi},\omega - m\Omega)$$

$$G_n(\underset{\sim}{x},\underset{\sim}{\eta})\, G_n^{*}(\underset{\sim}{x},\underset{\sim}{\eta}+\underset{\sim}{\xi})\, d\underset{\sim}{\xi}\, d\underset{\sim}{\eta} \qquad (80)$$

If we now assume that the cross terms in the summation cancel, and that G and F vary little over the typical dimension $\underset{\sim}{\xi}$, then Equation (80) becomes

$$P(\underset{\sim}{x},\omega) = \int_{\eta} \int_{\xi} \sum_{n=-\infty}^{+\infty} P_B(\underset{\sim}{\eta},\underset{\sim}{\xi},\omega - m\Omega) \left|G_n(\underset{\sim}{x},\underset{\sim}{\eta})\right|^2 d\xi\, d\eta \qquad (81)$$

Here $|G|^2$ is the absolute value of the acoustic transfer function given by (77) and can be a function of observer position $\underset{\sim}{x}$, point on the blade $\underset{\sim}{\eta}$, and input frequency. P_B is the cross-power spectral density on the blade at frequency $\omega - n\Omega$ and spacing ξ. P_B has been permitted to vary with $\underset{\sim}{\eta}$, allowing for inhomogeneity. P_B can be measured experimentally using a transducer array. In fact, the $\underset{\sim}{\xi}$ integration can be performed to give

$$P(x,\omega) = \int_{\eta} \sum_{n=-\infty}^{+\infty} A_{\omega - n\Omega}(\eta)\, P_B(\eta,\omega - m\Omega) \left|G_n(x,\eta)\right|^2 d\eta \qquad (82)$$

where P_B is now the spectral density, and $A_{\omega - n\Omega}$ is the correlation area which can be a function of frequency and blade position.

Note again that the observed sound at any given frequency is the result of random loading contributions at a wide range of frequencies, each removed $n\Omega$ from the acoustic frequency of interest. In fact the transfer function $|G|^2$ is virtually identical to that used for the harmonic loadings in the text of the report, and it will thus possess all the features discussed in Section 6.1. In particular, it will act as an efficient acoustic transfer mechanism over the range $-\omega M/\Omega < n < \omega M/\Omega$; i.e., over the range of loading spectrum spaced over ωM on either side of ω. Thus, for a typical rotational Mach number, $M = 0.5$, the broad-band contribution at any given

frequency will come from all loading spectral densities within an octave band centered on that frequency.

The method of accounting for the random loads actually used in the present report (Section 5.1) essentially corresponds to Equation (82). Note that the overall level is given by the sum of the squares of the contributing harmonic loads, and that the force input spectrum P_{rs} is multiplied by a correlation area. Each of these features occurs in the present work. It is of interest to note that for the harmonic input case, a definite phase relation will exist between the force input on each blade, so that the harmonics cancel out for frequencies that are not multiples of the blade passage frequency (see Section 3.5). However, no such definite phase relation will occur for the random loads, so that all values of n must be taken in (82), and the effect of B blades will simply be to multiply all output by B. It should also be noted that the effective neglect of retarded time in Equations (81) and (82) could be of significance in some circumstances.

APPENDIX III
DESIGN CHARTS FOR THE ESTIMATION OF HELICOPTER ROTATIONAL NOISE*

Background

The equation for the magnitude of the mth sound harmonic of a B-bladed rotor in the hover (Equation 36) can be written in the form

$$C_n = \sum_{\lambda=0}^{\infty} K \frac{1}{r} \left\{ \frac{nM}{R} \sin\theta\, c_{\lambda T} J_1' - \frac{c_{\lambda D}}{R} J_2' + \frac{nM}{R} \cos\theta\, c_{\lambda C} J_3' \right\} \qquad (83)$$

where K is a constant

r is the distance from the rotor center
θ is the angle from the rotor disc plane
} defining the field point

R is the radius of action of the blade forces

$c_{\lambda T}$, $c_{\lambda D}$, and $c_{\lambda C}$ are the thrust, drag, and radial force harmonic coefficients

$n = mB$ = harmonic number x number of blades

M is the rotational Mach number = $\Omega R/a_0$

J_1', J_2', and J_3' are complex collections of Bessel functions of argument $nM\cos\theta$

C_n is the amplitude of the nth sound harmonic observed at the field point 0 when the helicopter is hovering at point x (see sketch) a distance r away.

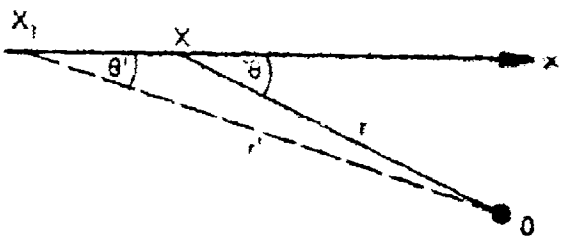

Now if the helicopter is moving along the x-axis at a Mach number M_F, the sound that reaches the observer at 0 when the rotor is at x was actually generated at some previous instant. At this time the rotor was at x_1 so that the sound actually traveled a distance r'.

When the necessary transformations are applied to account for the forward speed, Equation (83) is written

---

*The rotation in this section differs from that in the main body of the report.

$$C_n = \sum_{\lambda=0}^{\infty} K \frac{1}{r'(1-M_r')} \left\{ \frac{nM}{R} \frac{\sin\theta'}{1-M_r'} c_{\lambda T} J_1' - \frac{c_{\lambda D}}{R} J_2' + \frac{nM}{R} \frac{\cos\theta}{(1-M_r')} c_{\lambda C} J_3' \right\} \tag{84}$$

where the Bessel functions involved now have the argument $nM \cos\theta'/(1-M_r')$, and M_r' is the component of M_F along the line r', but $r'(1-M_r') \simeq r$ so that

$$\frac{\sin\theta'}{1-M_r'} \simeq \sin\theta \qquad \text{and} \qquad \frac{\cos\theta'}{1-M_r'} \simeq \frac{\cos\theta}{1-M_r}$$

and Equation (84) simplifies to

$$C_n = \sum_{\lambda=0}^{\infty} K \frac{1}{r} \left\{ \frac{nM}{R} \sin\theta\, c_{\lambda T} J_1' - \frac{c_{\lambda D}}{R} J_2' + \frac{nM}{r} \frac{\cos\theta}{(1-M_r)} c_{\lambda C} J_3' \right\} \tag{85}$$

Now suppose instead of performing the correct velocity transformations, we merely substitute $M_F = M/(1-M_r)$ into Equation (83) to give the correct forward speed value of the Bessel functions. We obtain

$$C_n = \sum_{\lambda=0}^{\infty} K \frac{1}{r} \left\{ \frac{nM \sin\theta}{R(1-M_r)} c_{\lambda T} J_1' - \frac{c_{\lambda D}}{R} J_2' + \frac{nM \cos\theta}{r(1-M_r)} c_{\lambda C} J_3' \right\} \tag{86}$$

Note that Equation (86) is identical to Equation (85) with the exception of the additional $(1-M_r)$ in the denominator of the thrust term.

Now since $M_r = M_F \cos\theta$, the $(1-M_r)$ factor is most significant as $\theta \to 0$, i.e., as $\sin\theta \to 0$. As θ increases and the thrust term becomes important, M_r decreases. Consequently, it may be expected that the error in the thrust term may not be too significant. To illustrate this point, two cases were computed. The first was computed using the correct forward speed transformations, and the second was computed merely using a modified Mach number ($= M/1 - M_F \cos\theta$). The results are shown in Figure 52 for $M = 0.5$, $M_F = 0.125$, for the first, second, fourth, and eighth harmonics of a typical four-blade rotor. The random phase assumption discussed in Section 5.2 of the report was used for the additionally extreme case of random phase among the thrust, drag, and radial force components. (Note that this leads to an acoustic symmetry about the rotor plane, since the phase difference between the thrust and drag components is eliminated.)

It can be seen in Figure 52 that the maximum error in the equivalent Mach Number case is less than 2 dB. In the plane of the rotor there is no error since the thrust term is zero. The average error is considerably less than 1 dB. Thus, it is concluded that the concept of an "Effective Mach Number" takes adequate account of forward speed effects, at least for typical helicopter velocities.

It has been shown in Sections 4.5 and 6 of the report that, using a randomized phase assumption, and based on experimental airload data, the thrust loading harmonic amplitude can be represented for the purpose of sound calculation by the relationship

$$c_{\lambda T} \propto \frac{T}{\lambda^{2.5}}$$

Furthermore, using these assumptions, a single loading point gives accurate results. If we assume that the ratio thrust : drag : radial component = 10:1:1, which is typical of helicopter rotors, we can write Equation (84) in the form

$$C_n \propto \sum_{\lambda=0}^{\infty} \frac{T}{R r \lambda^{2.5}} \left\{ (10\, nM \sin\theta)\, J_1' - J_2' + (nM \cos\theta)\, J_3' \right\} \qquad (87)$$

Finally, the sound intensity of the nth harmonic can be represented by a relationship of the form

$$C_n^2 \propto \frac{T^2}{r^2 A} f(mB, M, \theta) \qquad (88)$$

where A is the rotor disc area (πR^2), and the function f can be inferred from Equation (87).

The sound pressure level corresponding to C_n^2 has been computed for a wide range of mB, M, and θ for a rotor having nominal dimensions (T = 10,000 lb, radius = 20 ft, r = 1000 ft, and with the loads acting at the 80-percent radius point). The results are presented in polar chart form in Figure 53. The charts thus effectively give the form of the function f in Equation (88) above, and they allow straightforward calculation of C_n^2 for any specified condition.

Parameters Required

The following parameters are required for use in the noise calculations using the design charts.

x, y, z	Field point coordinates relative to helicopter measured in feet with x measured positive in the direction of motion (parallel to ground in hover), y measured sideways in the plane of the disc, z measured downwards from helicopter. (Results for +y equal results for - y.)
A	Disc area, ft^2 (or T/A = disc loading in lb/ft^2)
Ω	Rotor angular velocity, rads/sec (Ω = rpm x $2\pi/60$)
V	Flight velocity, ft/sec
a_0	Speed of sound in free air, ft/sec
i_d	Disc incidence (angle between disc and x-axis), deg
m	Sound harmonic (equals 1 for fundamental, 2 for second harmonic, etc.)
B	Number of blades
T	Thrust, lb
R	Rotor radius, ft

Instructions for Use of Design Charts

To calculate the rotational noise spectrum occurring instantaneously at any point r, θ relative to the rotor center and its direction of motion

1) Calculate range $r = \sqrt{x^2 + y^2 + z^2}$

2) Calculate the rotational Mach Number M

$$M = 0.8 \frac{\Omega R}{a_0}$$

3) Calculate the flight Mach number

$$M_F = V/a_0$$

4) Calculate the angle θ' between the flight direction and the line joining the rotor and the field point

$$\theta' = \cos^{-1}(x/r)$$

5) Calculate the Effective Rotational Mach Number

$$M_E = \frac{M}{1 - M_F \cos \theta'}$$

6) Calculate the angle θ between the rotor plane and the line r. If the disc incidence is i_d, this is given by

$$\theta = \tan^{-1} \left(\frac{z}{\sqrt{x^2 + y^2}}\right) - i_d \left(\frac{x}{\sqrt{x^2 + y^2}}\right)$$

7) Using the values of M_E and θ, look up each chart to obtain values of the harmonic sound pressure level I_n for n = 2, 3, 4, 6, 8, 10, 12, 16, 20, 30, 40, and 60.

8) Correct the values obtained for thrust, disc, loading, and distance according to

$$SPL_n = \left[I_n + 11 + 10 \log_{10} \frac{T}{r^2} \left(\frac{T}{A}\right)\right] \quad \text{dB re: } 0.0002 \text{ dyne/cm}^2$$

9) Plot SPL_n against n and fit smooth curve.

10) The sound pressure levels from this curve for n = B, 2B, 3B, ... give the required harmonic level at the point x,y,z.

11) The fundamental frequency is $\Omega B / \left(2\pi (1 - M_F \cos \theta)\right)$ Hz.

Example -- Calculate the rotational noise spectrum 1000 ft from a three-blade rotor at an angle of 20 deg below the flight path for the following parameters: T = 10,000 lb, $T/A = 7$ lb/ft^2, V = 200 ft/sec, $i_d = 5$ deg, $\Omega R = 600$ ft/sec, and $a_0 = 1117$ ft/sec

1) r = 1000 ft

2) $M = 0.8 \times 600/1117 = 0.429$

3) $M_F = 200/1117 = 0.179$

4) $\theta' = 20$ deg

5) $M_E = \frac{0.429}{1 - .179 \times .938} = 0.516$

6) $\theta = 20^\circ - 5^\circ = 15^\circ$

7) From charts

n	2	3	4	6	8	10	12	16	20	30	40	60
I_n	84.5	82.5	81.5	77.5	72	67	63	57	54	48	44.5	38.5

8) Correction = $10 \log_{10}\left(\frac{10,000}{1000^2} \cdot 7\right) + 11 = +8.5$ dB

n	2	3	4	6	8	10	12	16	20	30	40	60
SPL_n	85	82	81	77	71.5	66.5	63.5	56.5	53.5	47.5	44	38

The results of Steps 9 and 10 can be seen in the sketch below where the harmonic levels corresponding to m = 1, 2, 3, ... are drawn as vertical lines.

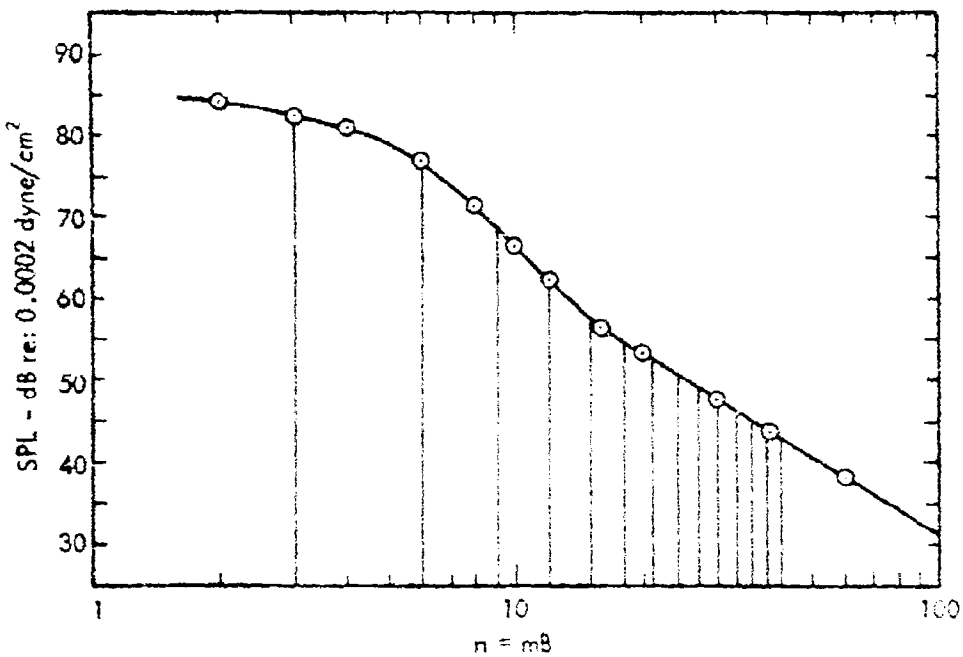

11) The fundamental frequency in this case is

$$\frac{\Omega B}{2\pi\ (1 - M_r)} = \frac{\Omega R}{2\pi \sqrt{\frac{A}{\pi}}\ (1 - M_r)} = \frac{600}{2\pi \sqrt{\frac{10,000}{7\pi}}\ (.832)} = 16.1 \text{ Hz}$$

Comparison with Experiment

To demonstrate the usefulness and accuracy of this simplified method some case have been calculated to compare with the measured data from Reference 12. Figures 54 and 55 show the results. For comparison, the theoretical results obtained by Schlegel et al[12] using a computer program are also included. It can be seen that the simple technique produces results which on the average are more accurate than the computed results.

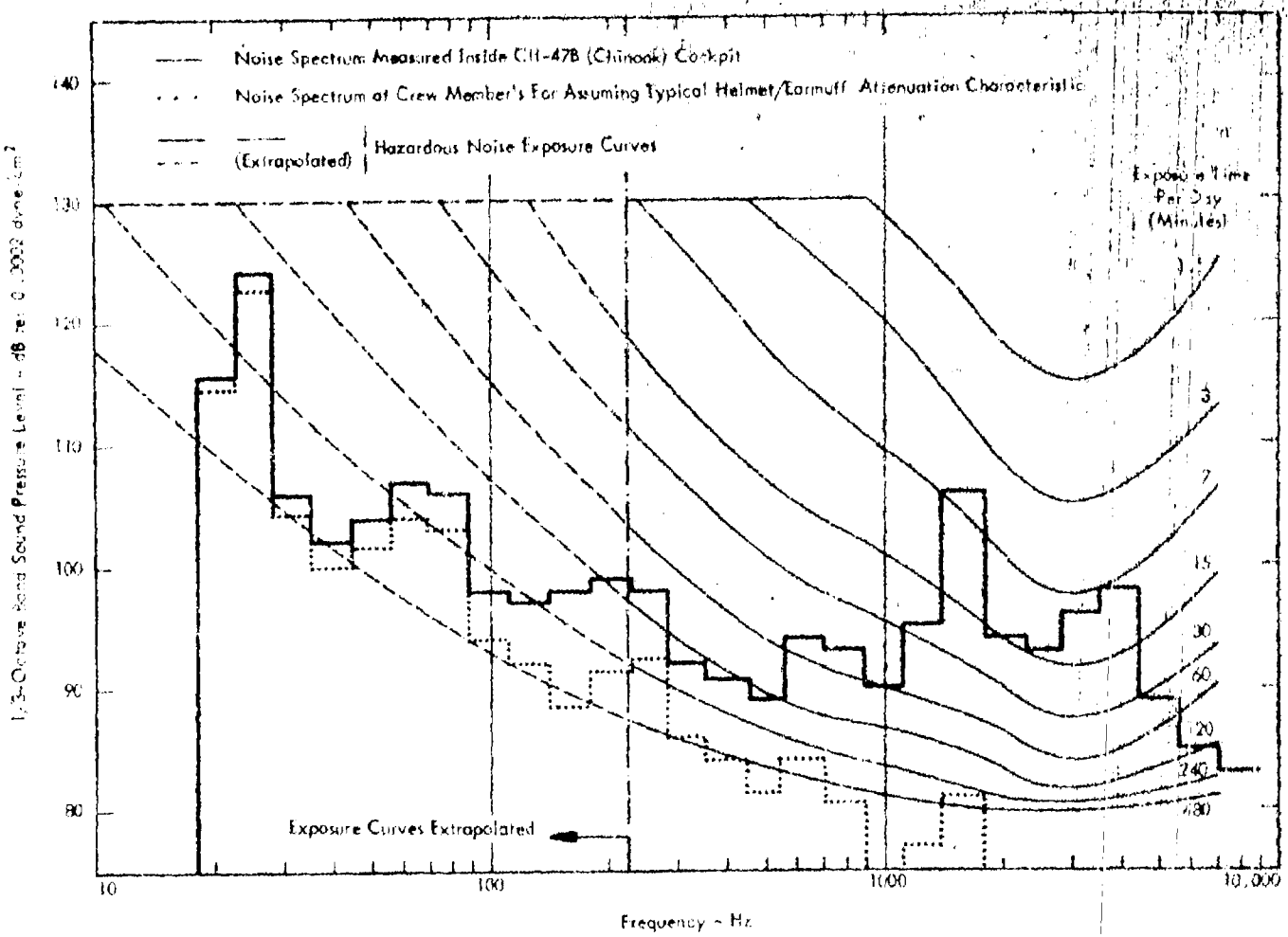

Figure 1. Measured Internal Noise Compared With Hazardous Exposure Times - With and Without Ear Protection.[7]

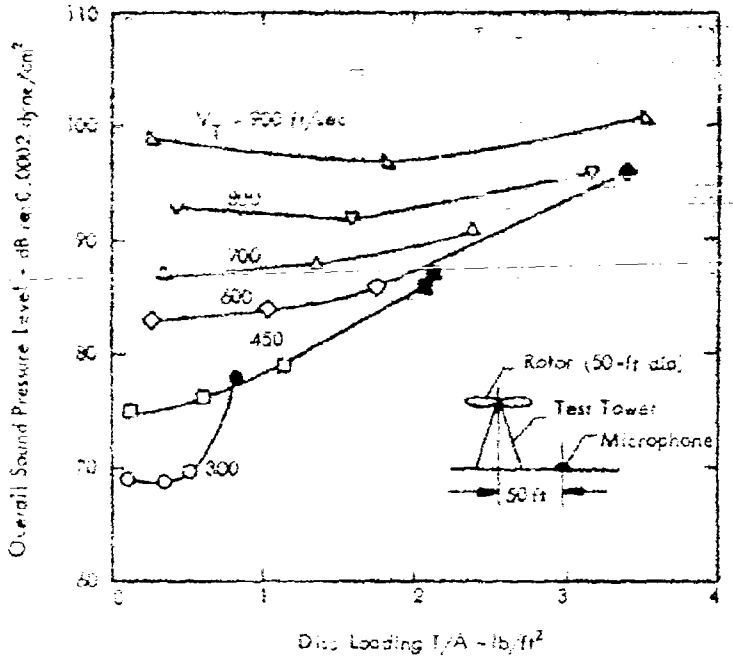

Figure 2. Rotor Noise Overall Levels From Hubbard and Maglieri.[1]

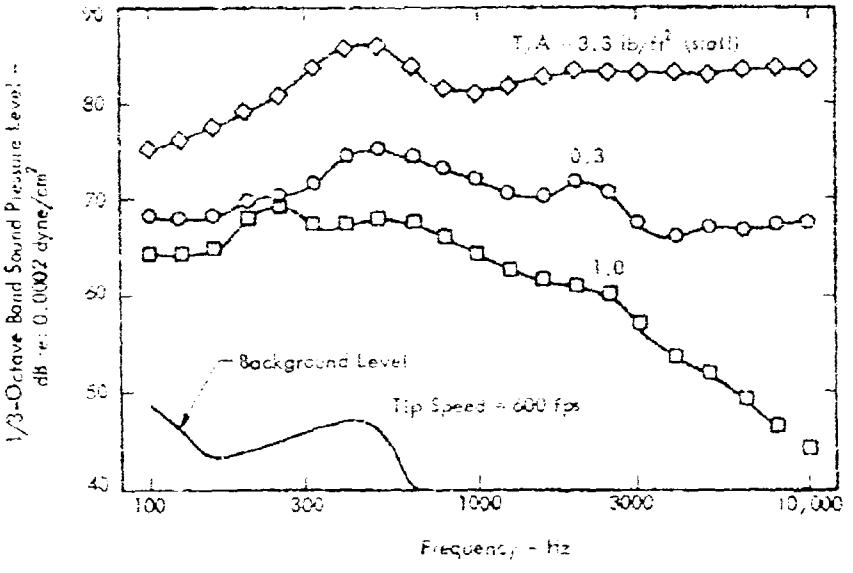

Figure 3. One-Third Octave Band Spectra of Rotor Noise for Various Disc Loadings, From Hubbard and Maglieri.[1]

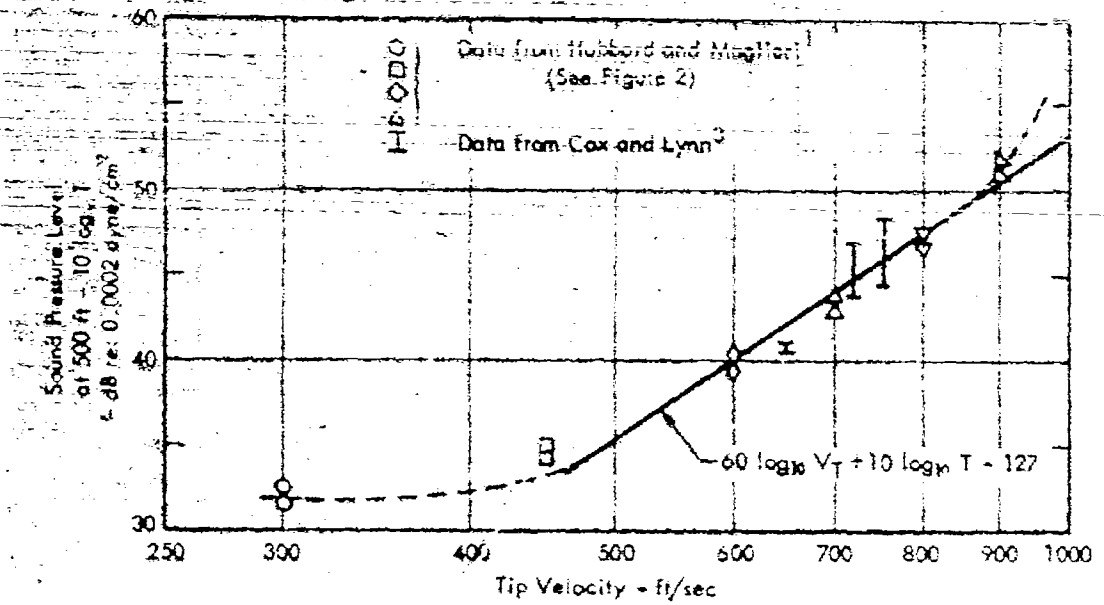

Figure 4. Helicopter Noise Overall Levels.

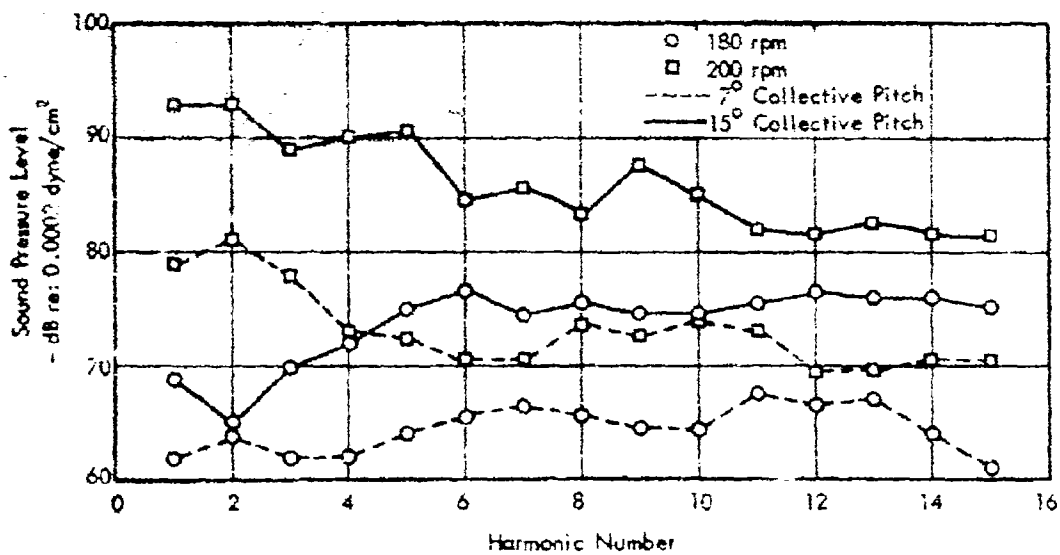

Figure 5. Rotor Noise Harmonic Levels From Stuckey and Goddard.[5]

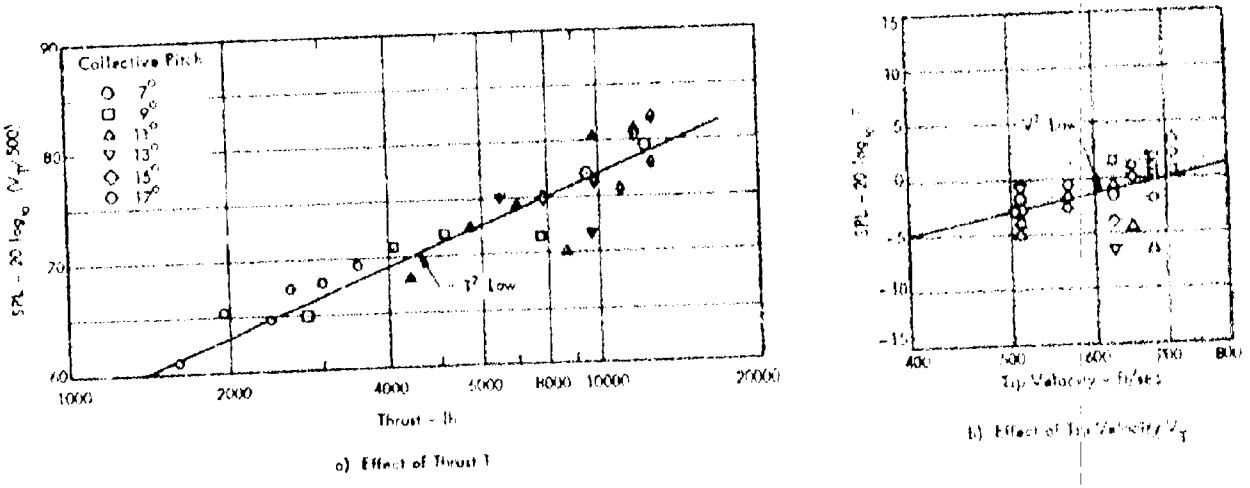

Figure 6. Fifteenth Harmonic Levels, Results from Stuckey and Goddard.[5]

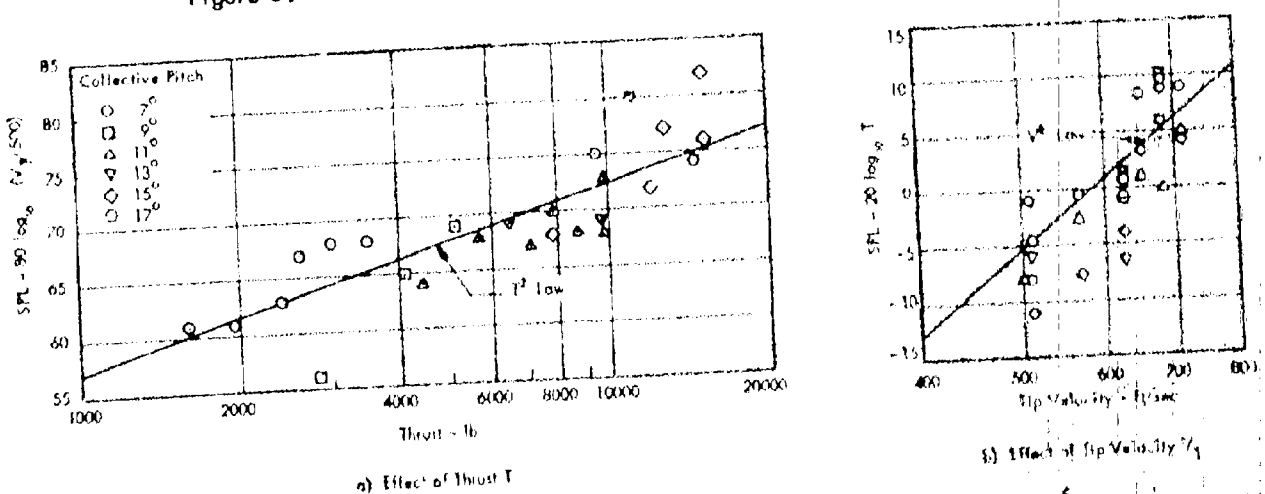

Figure 7. First Harmonic Levels, Results From Stuckey and Goddard.[5]

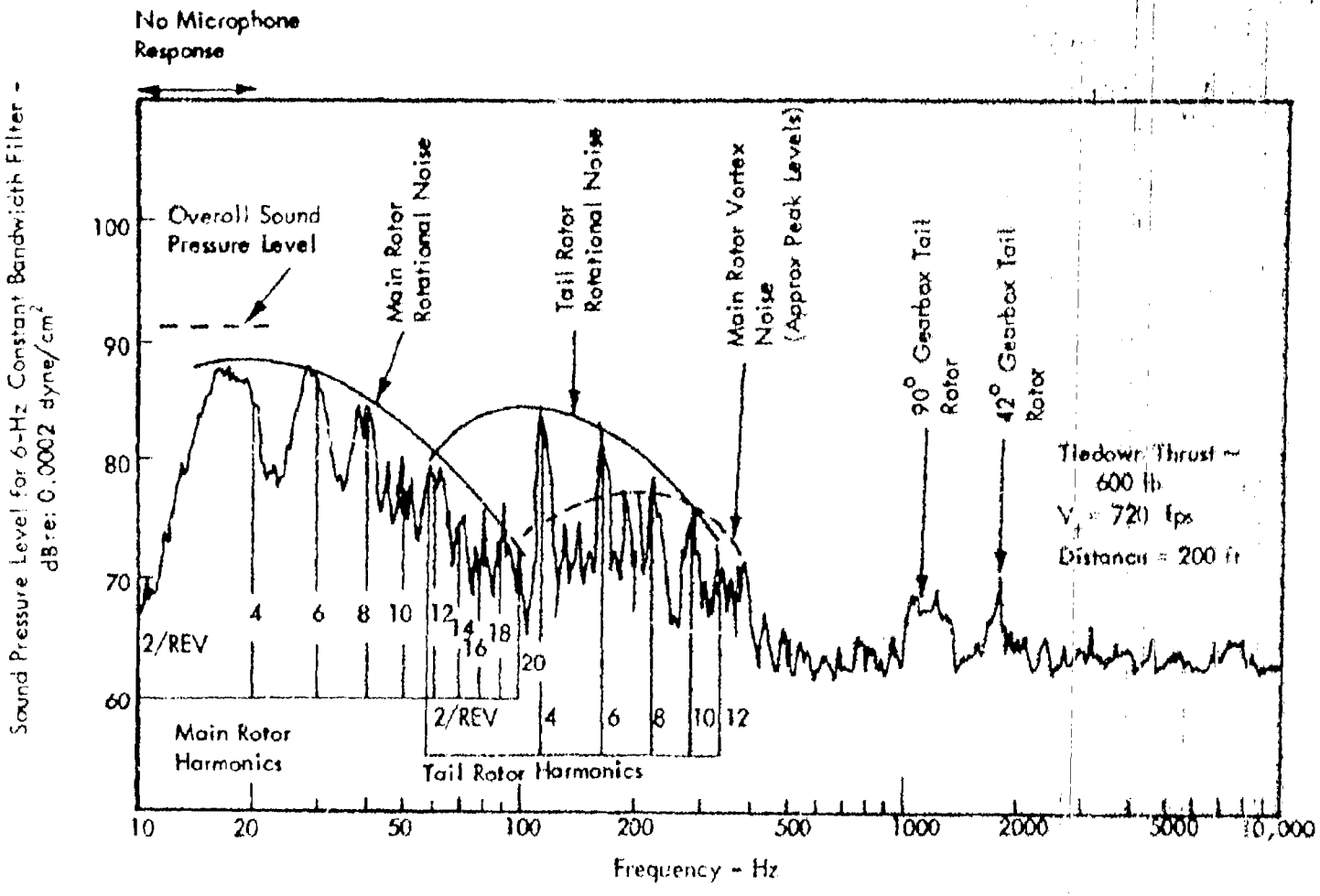

Figure 8. UH-1A External Noise Spectrum. Derived From Reference 5.

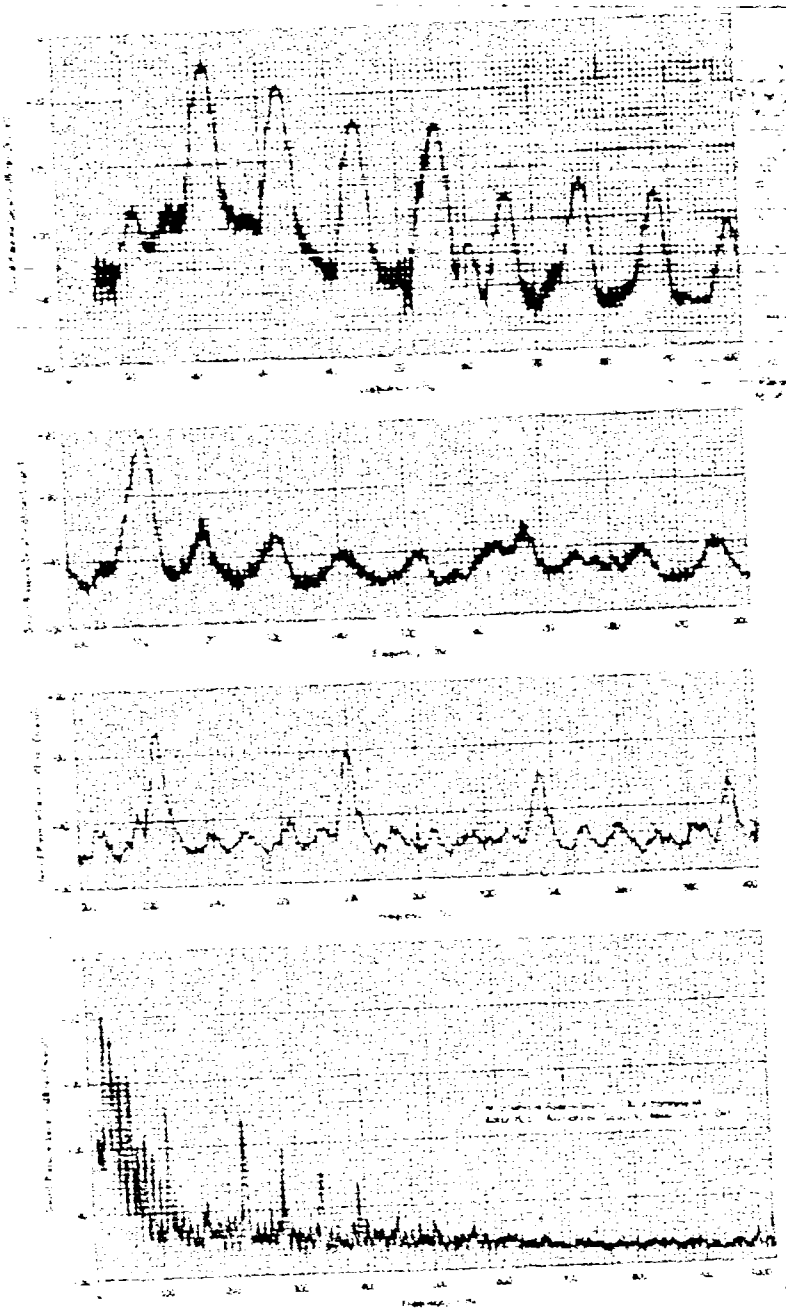

Figure 9. Two-Hz Bandwidth Analysis of UH-1B Noise Spectrum.

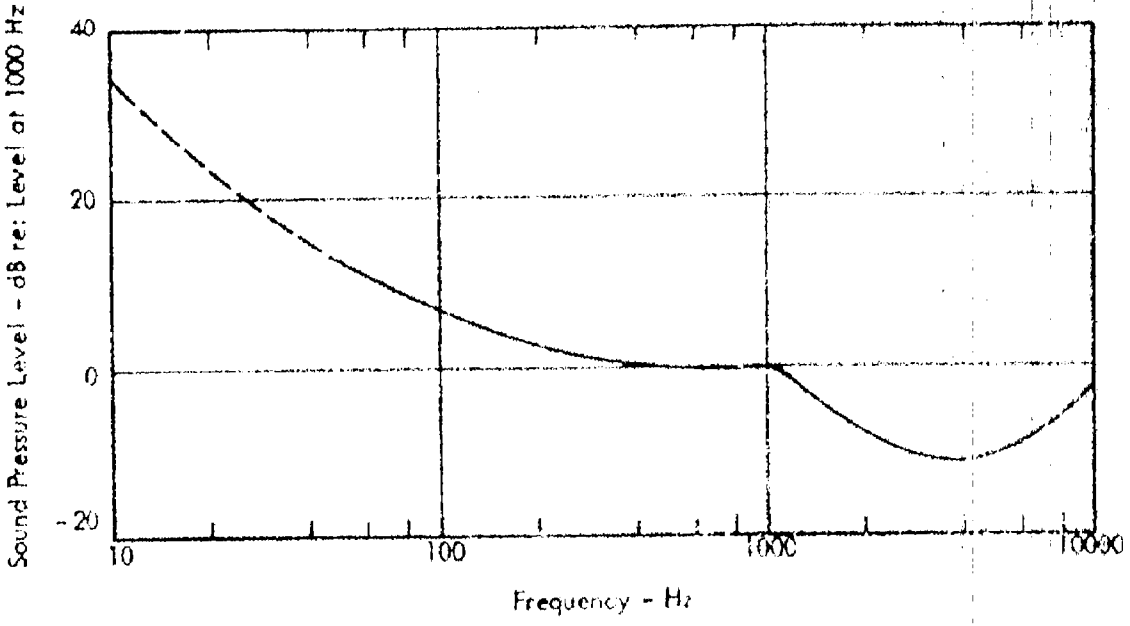

Figure 10. Typical Equal Subjective Response. Extrapolated N Weighting (32 Noy) Curve.[14]

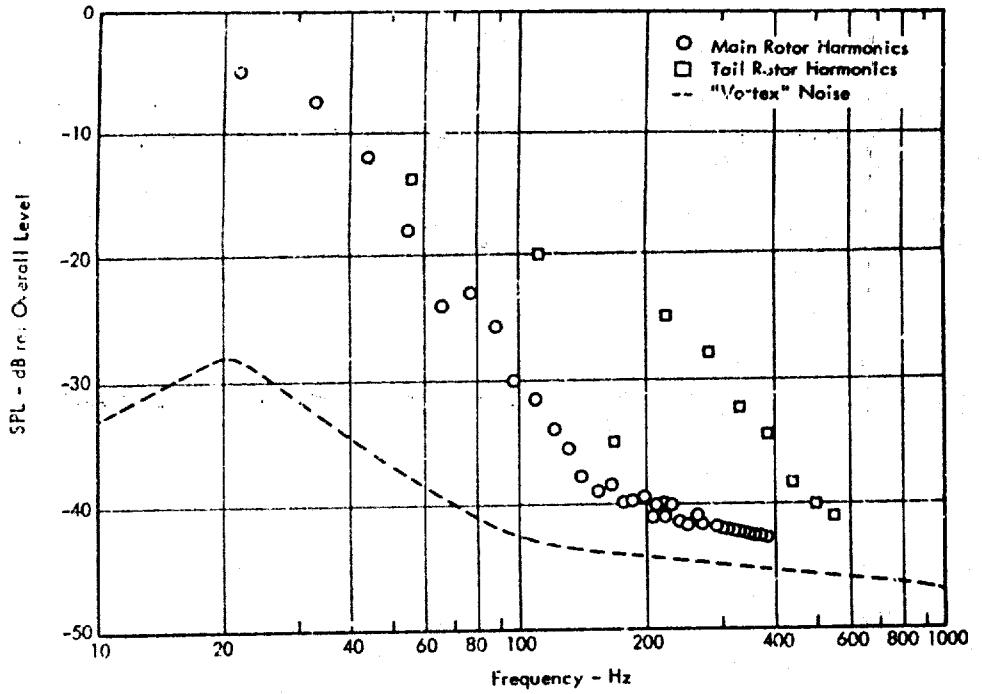

a) Measured Levels in 2-Hz Bandwidth (Replot of Figure 9).

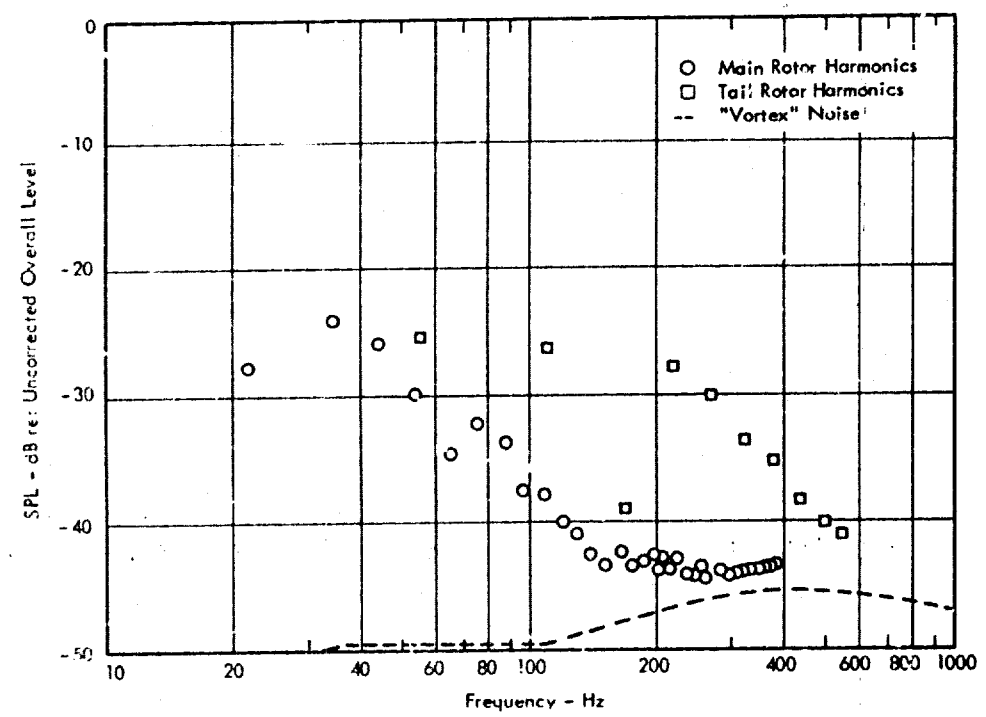

b) Subjectively Corrected Measured Levels.

Figure 11. Contribution of Helicopter Noise Components Via Various Methods of Data Presentation.

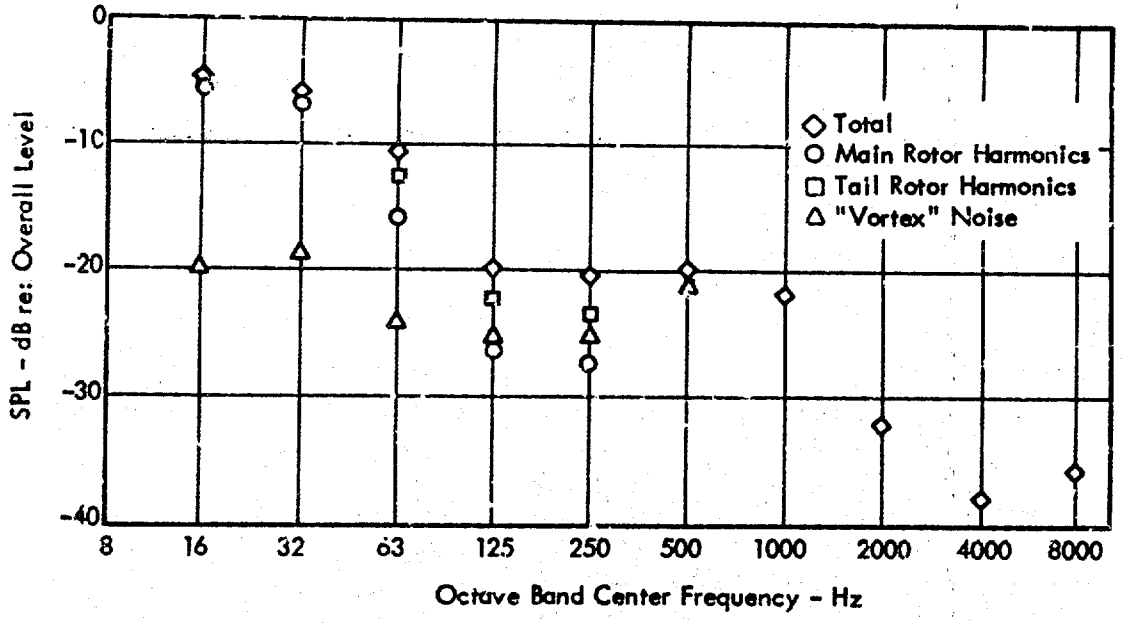

c) Octave Band Levels.

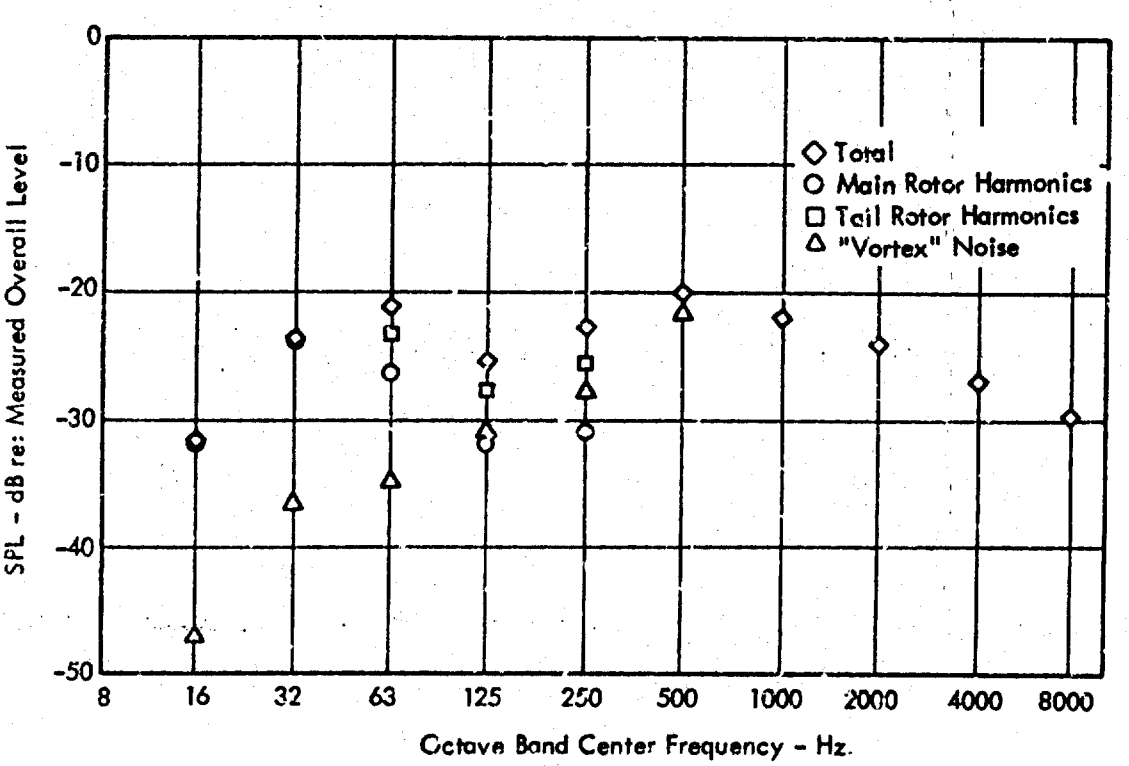

d) Subjectively Corrected Octave Band Levels.

Figure 11. (Continued).

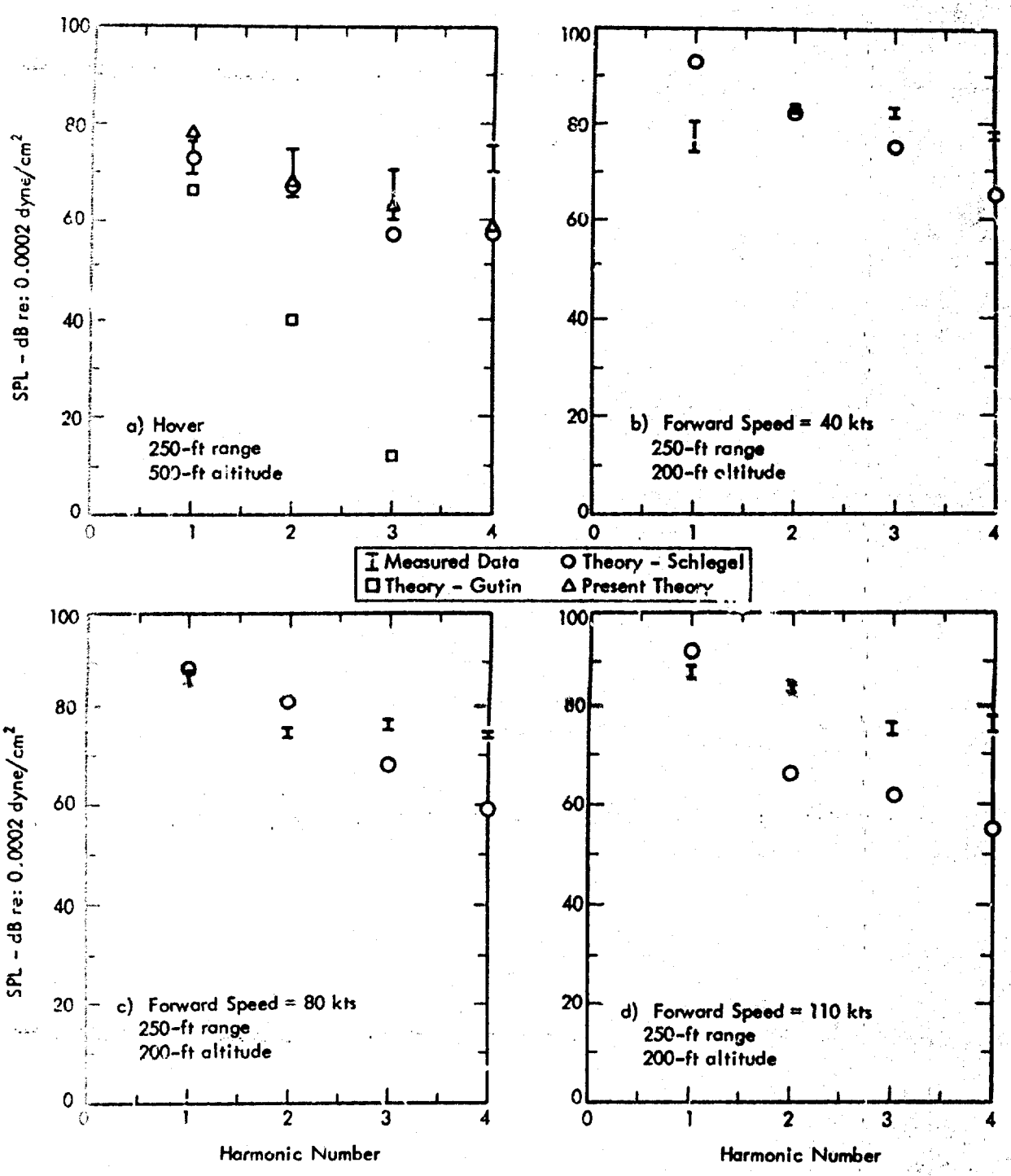

Figure 12. Experimental and Theoretical Results at Side of Helicopter From Schlegel et al.[12]

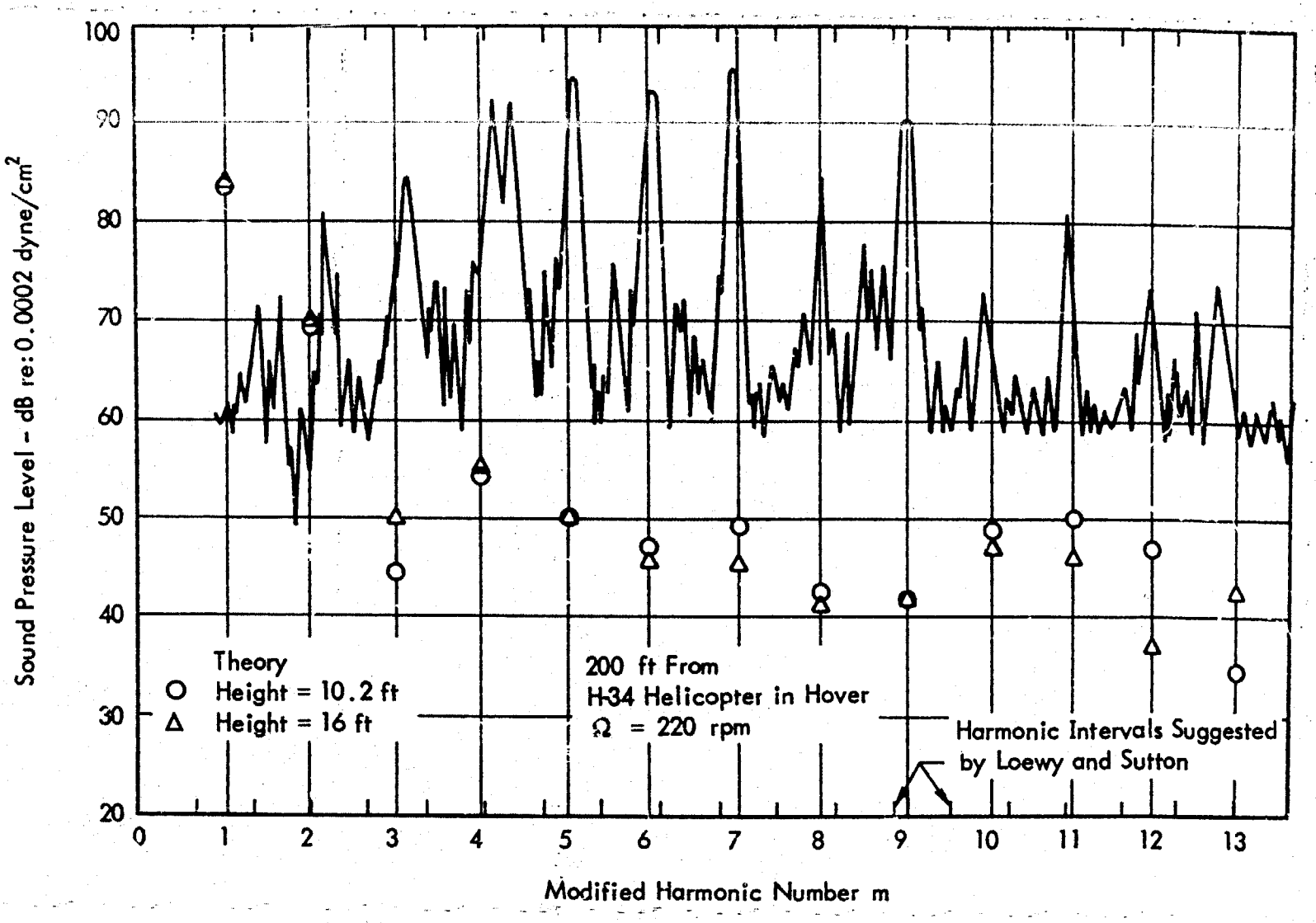

Figure 13. Loewy and Sutton,[10,11] Comparison of Theory and Experiment.

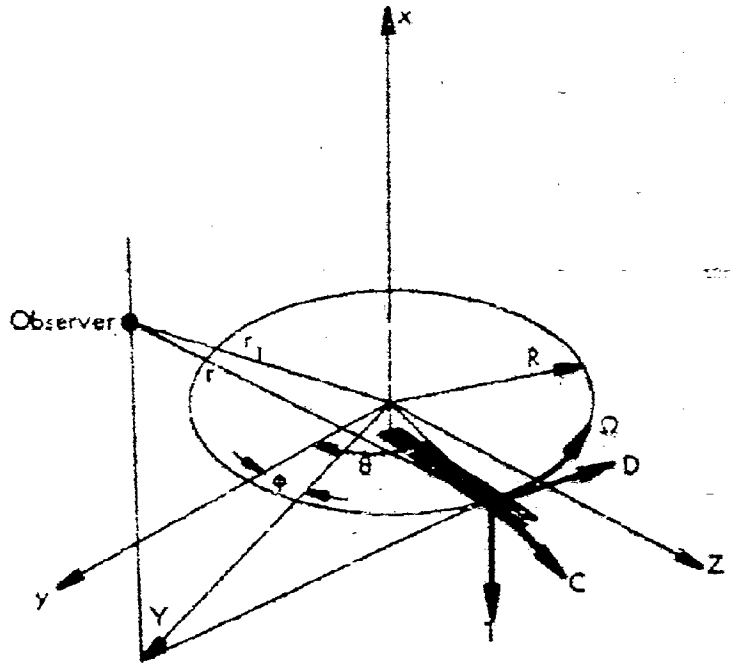

Figure 14. Coordinate System for Helicopter Acoustic Calculations.

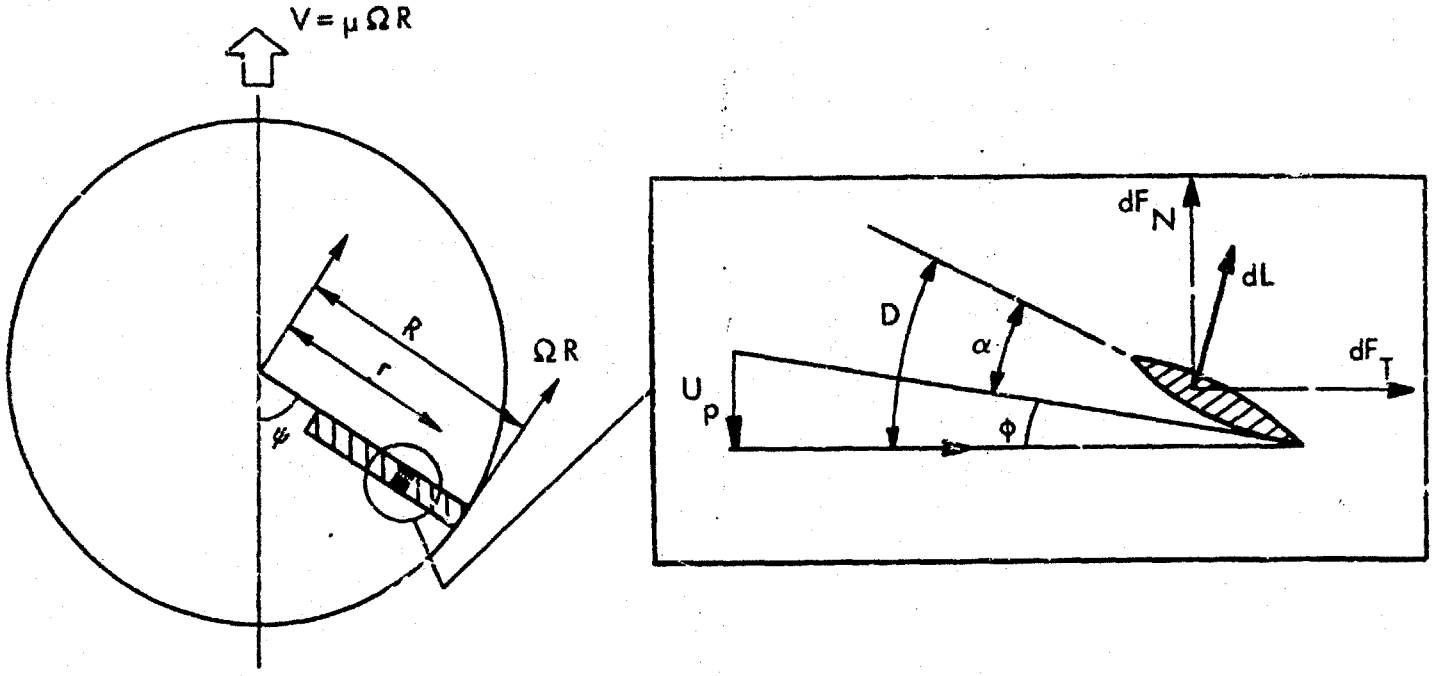

Figure 15. Blade Section Aerodynamics.

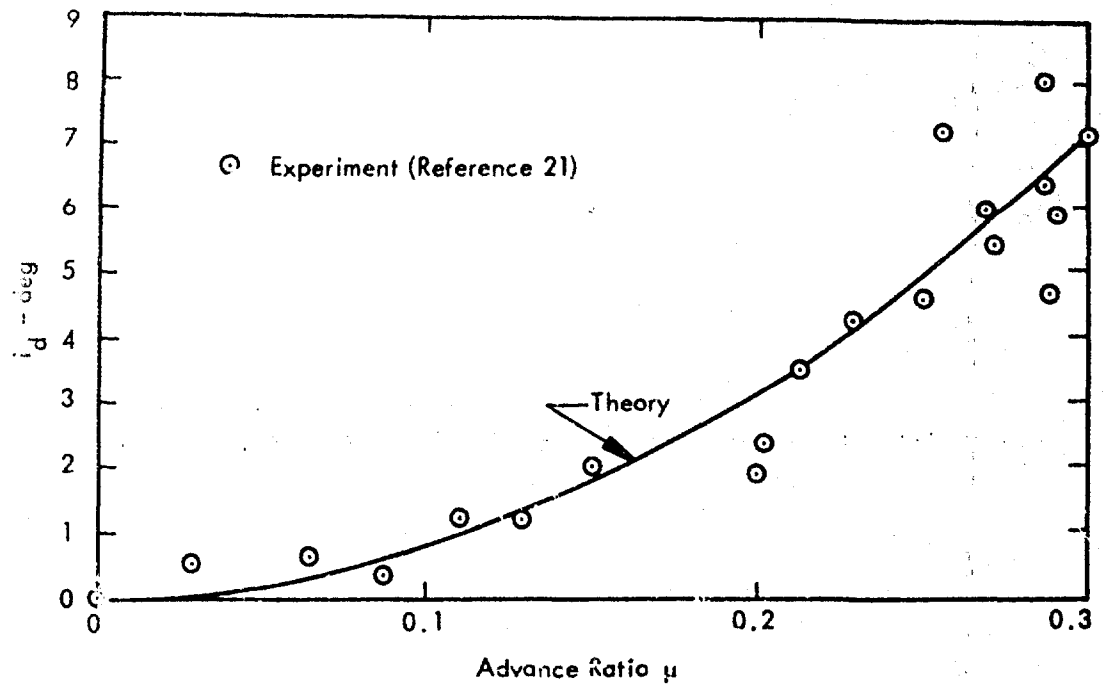

a) Disc Incidence

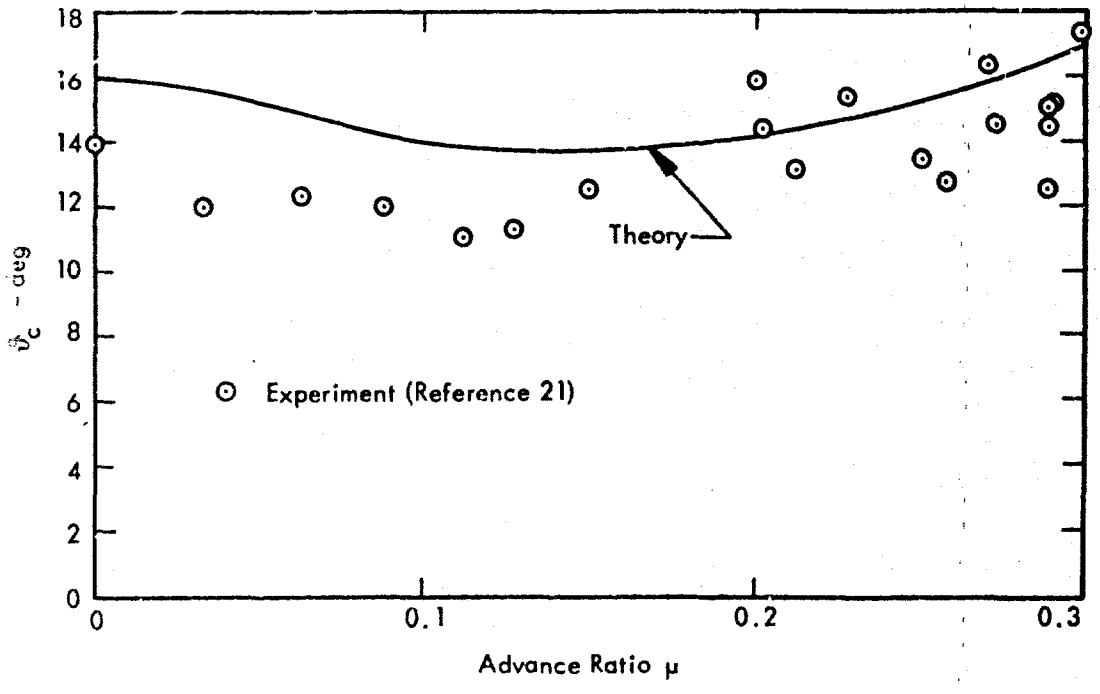

b) Collective Pitch Angle

Figure 16. Comparison of Theoretical and Experimental Values of Various Rotor Control Parameters for H-34 Helicopter.

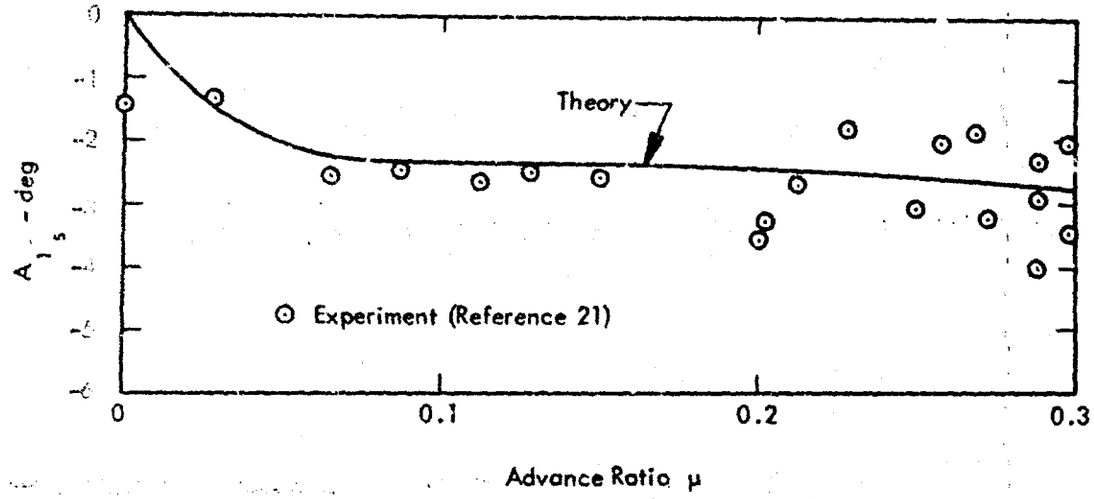

c) Longitudinal Cyclic Pitch

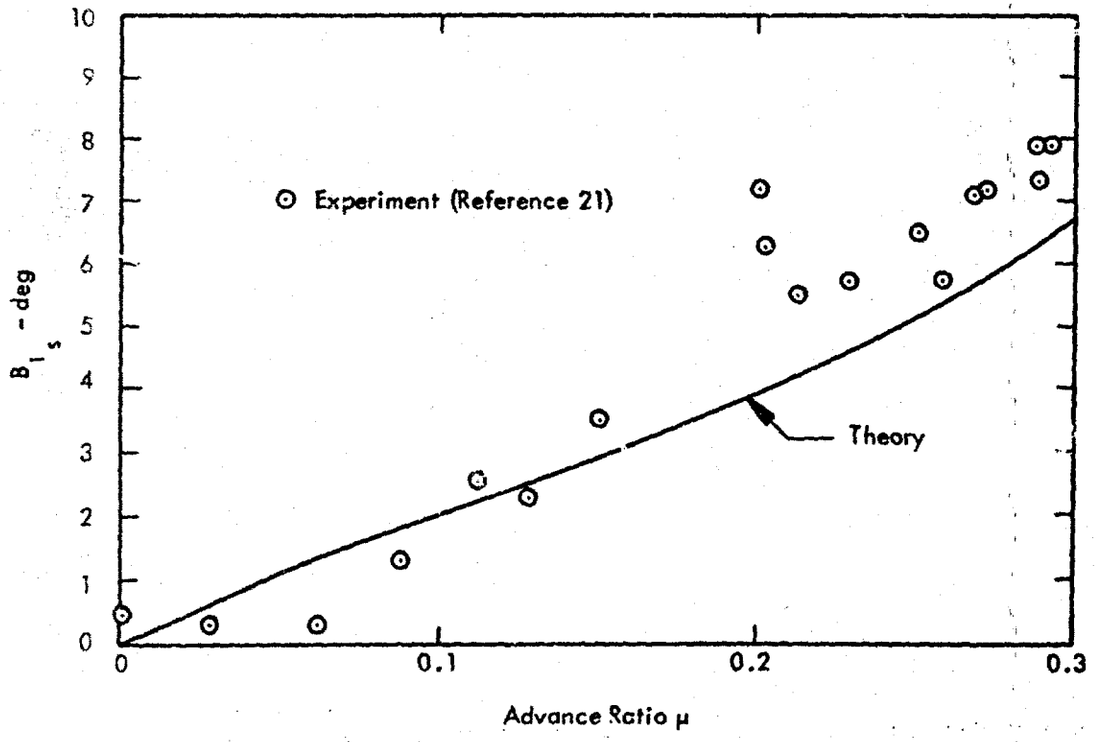

d) Lateral Cyclic Pitch

Figure 16. (Continued).

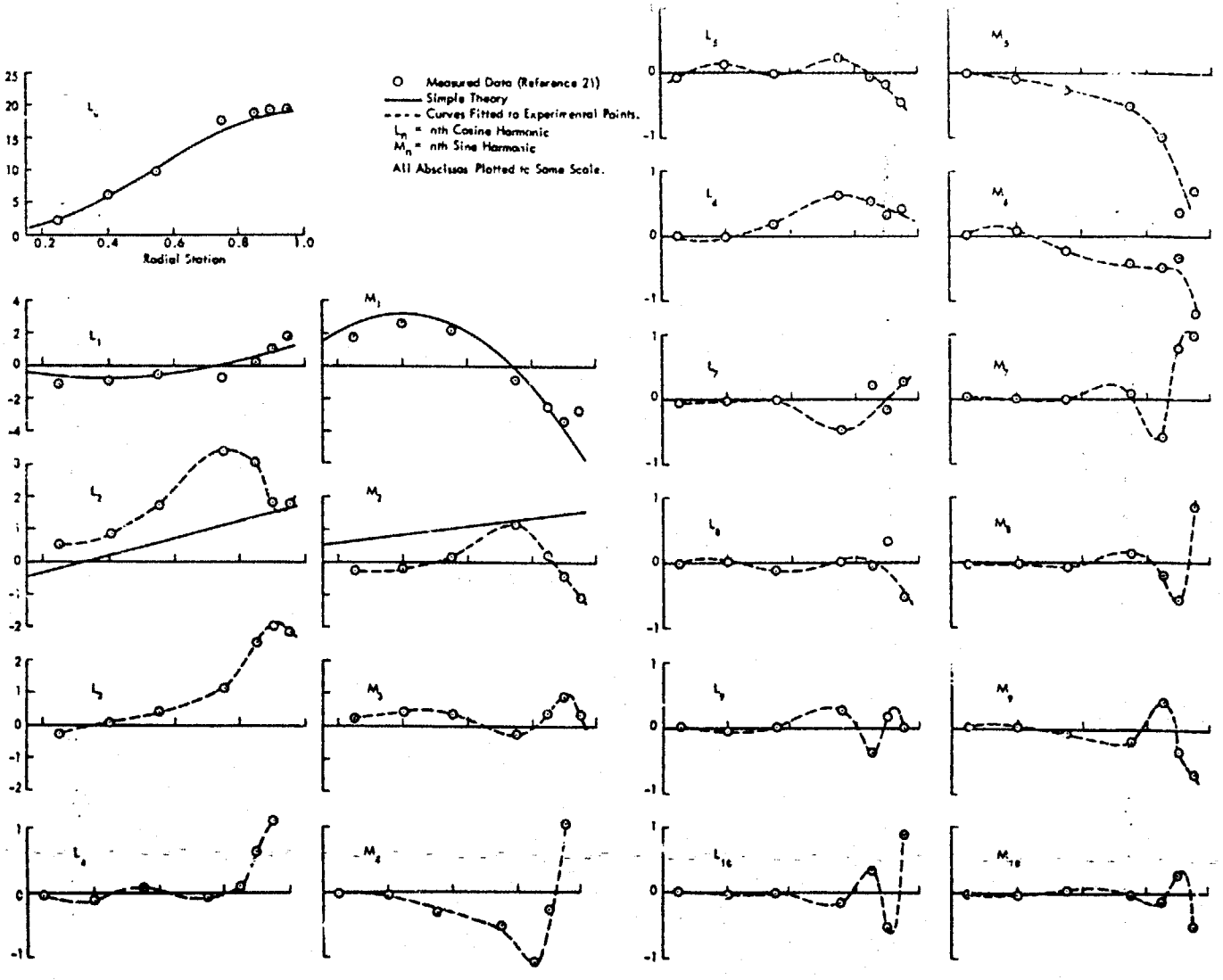

Figure 17. Blade Section Airload Harmonics for H-34 Helicopter - lb/in. Advance Ratio $\mu = 0.15$.

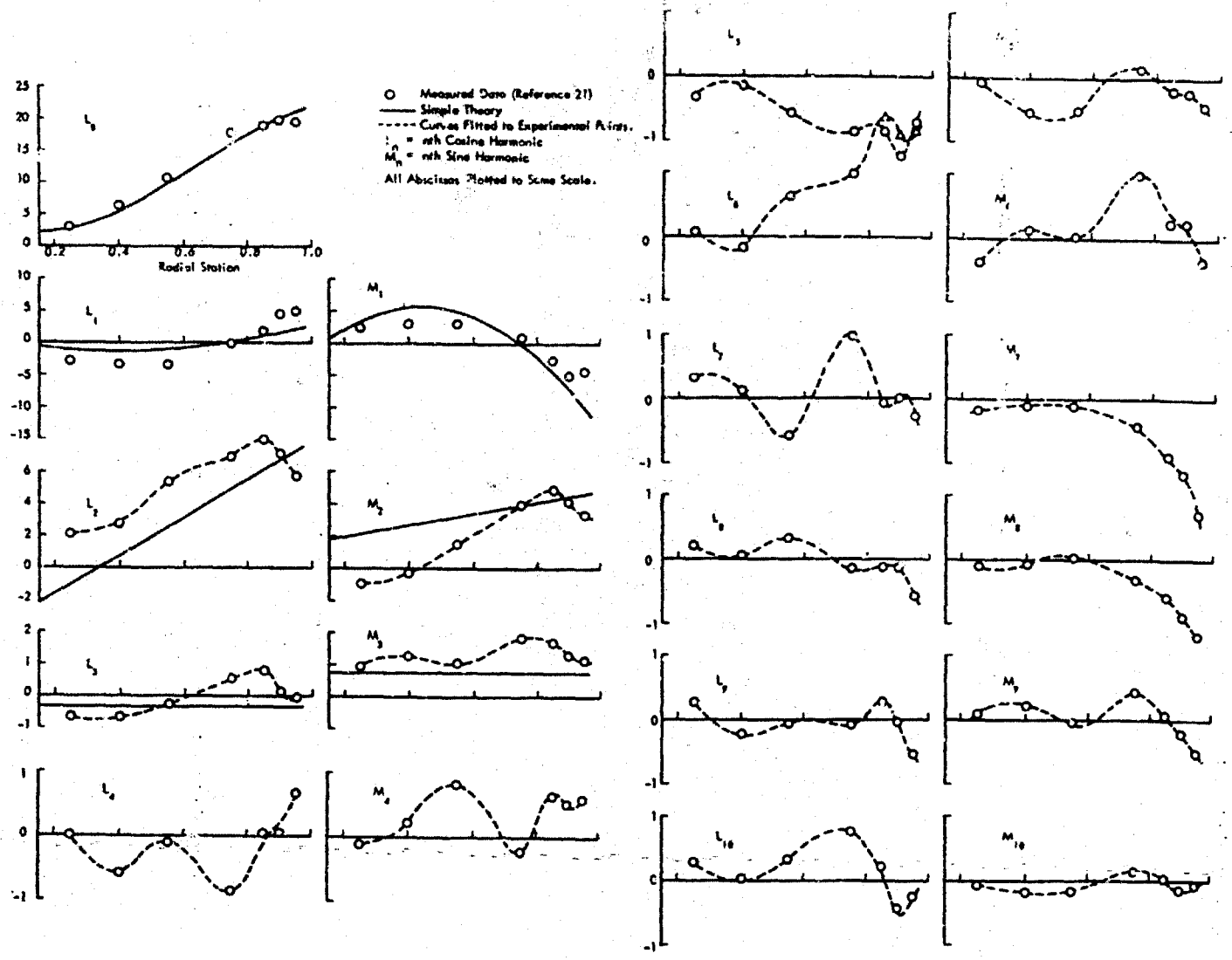

Figure 18. Blade Section Airload Harmonics for H-34 - lb/in.
Advance Ratio $\mu = 0.30$.

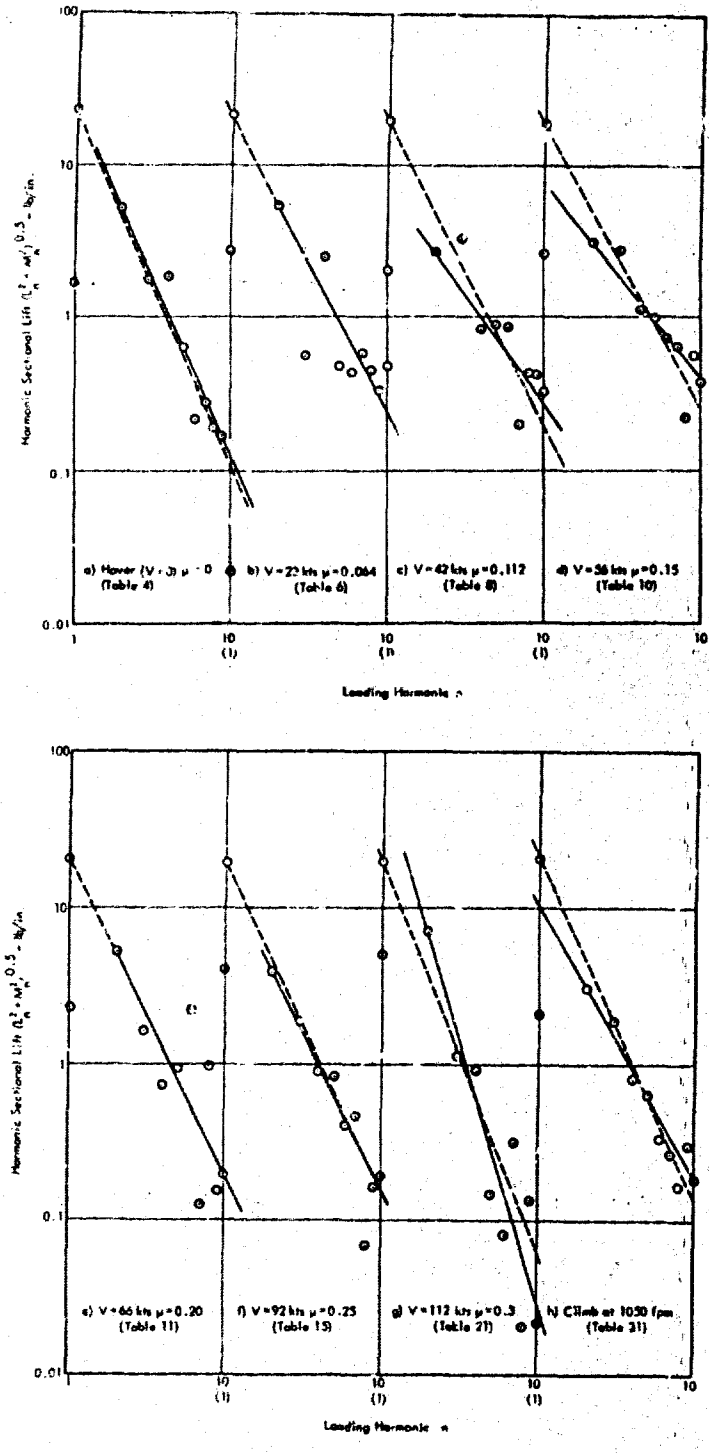

Figure 19. Rotor Harmonic Loadings at 0.85 Span for Various Advance Ratios. Data From Scheiman[21] for H-34 Helicopter.

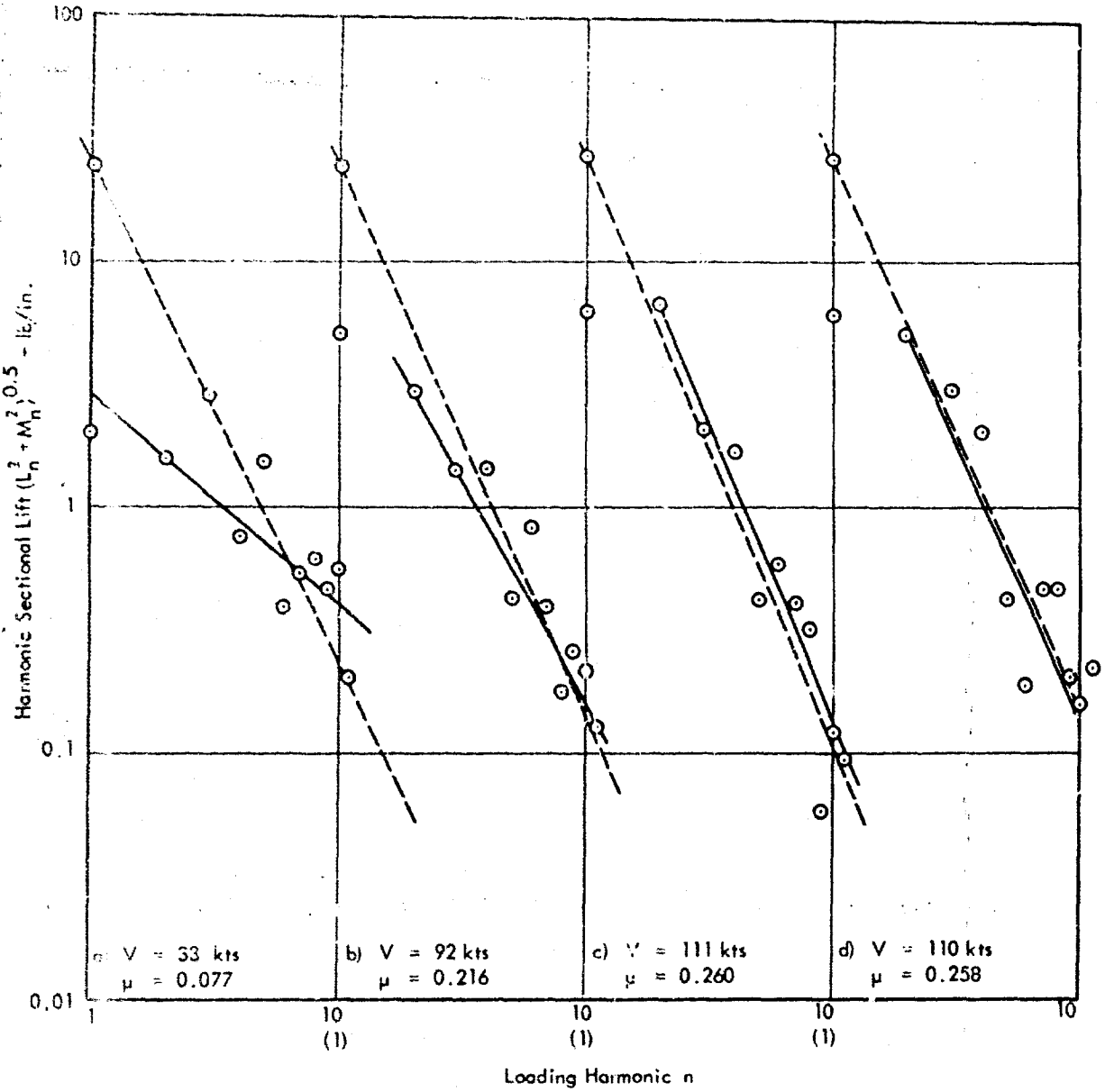

Figure 29. Rotor Harmonic Loadings at 0.85 Span. Data From Burpo and Lynn[34] for UH-1 Helicopter.

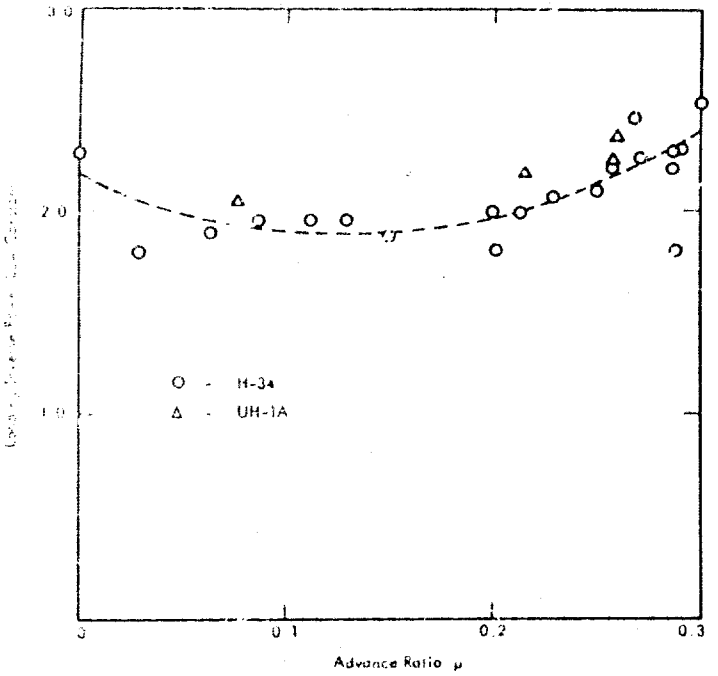

a) Law Based on Steady Loading

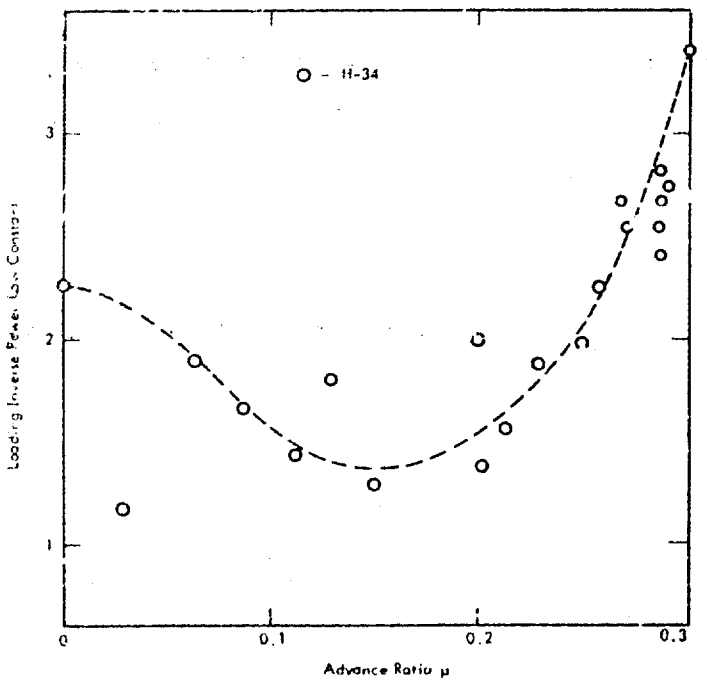

b) Law Based on Second Harmonic Loading

Figure 21. Variation of Loading Power Law Constant With Advance Ratio.

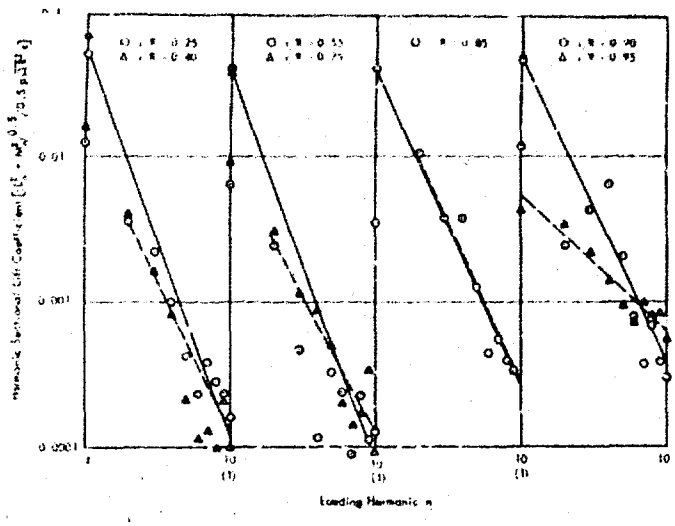

Figure 22. Rotor Harmonic Loadings as a Function of Spanwise Station. Data From Scheiman.[21]

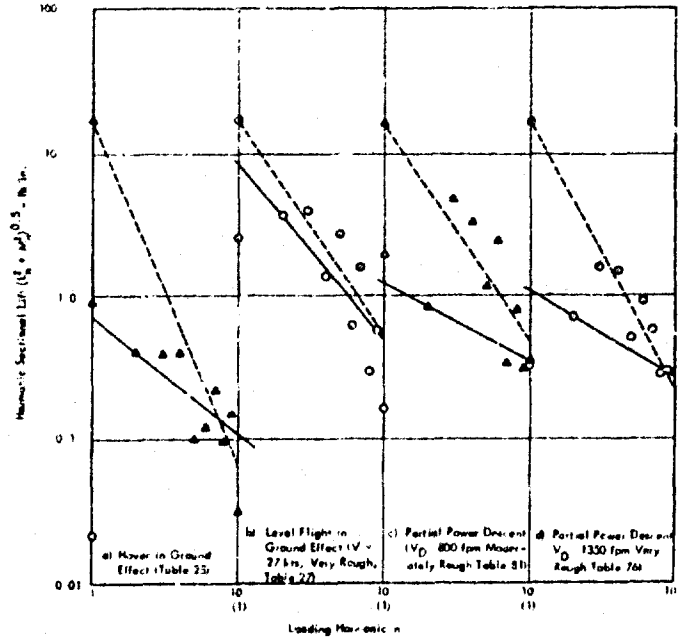

Figure 23. Rotor Harmonic Loadings at 0.85 Span in Several Rough Running Cases for H-34 Helicopter. Data From Scheiman.[21]

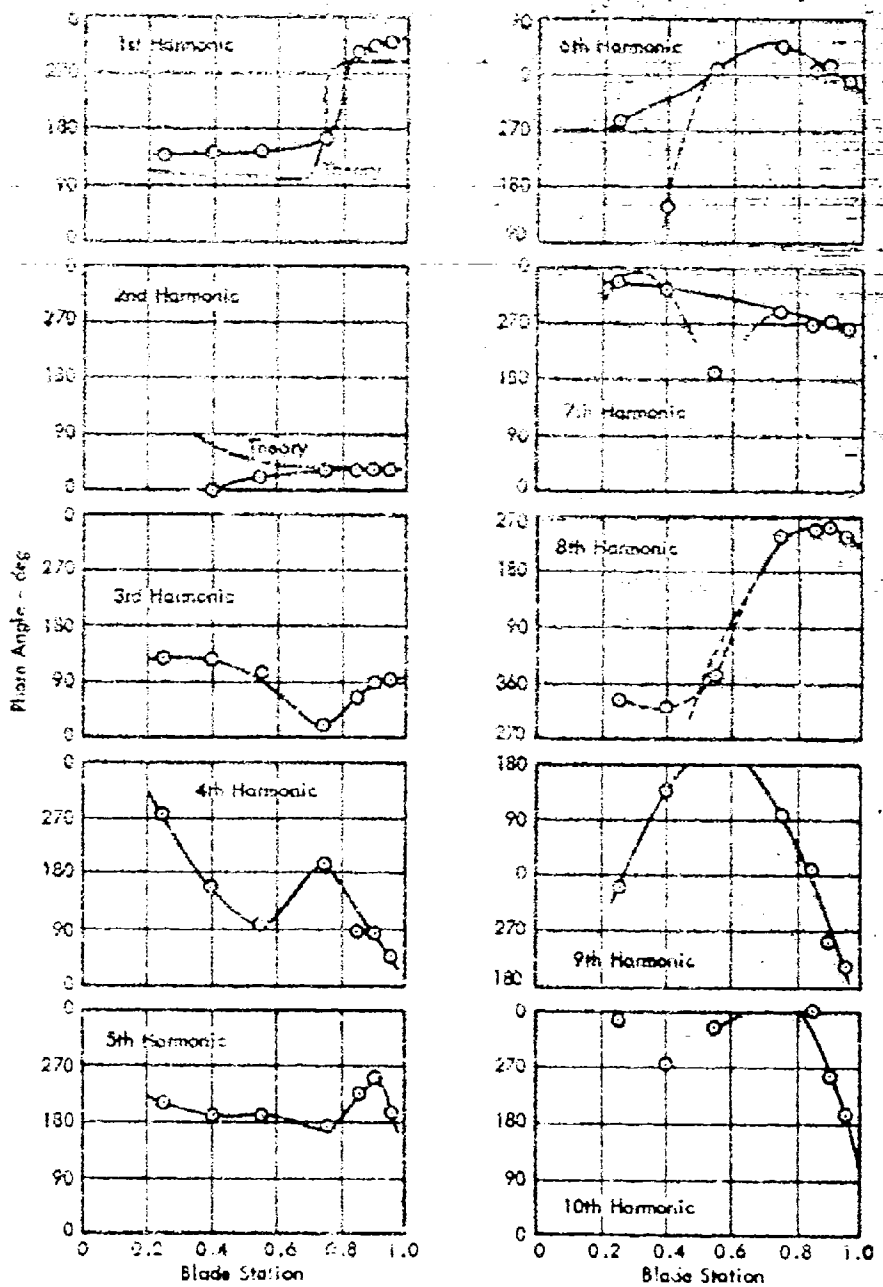

Figure 24. Radial Distribution of Phase of Harmonic Airloads. Data From Scheiman.[21]

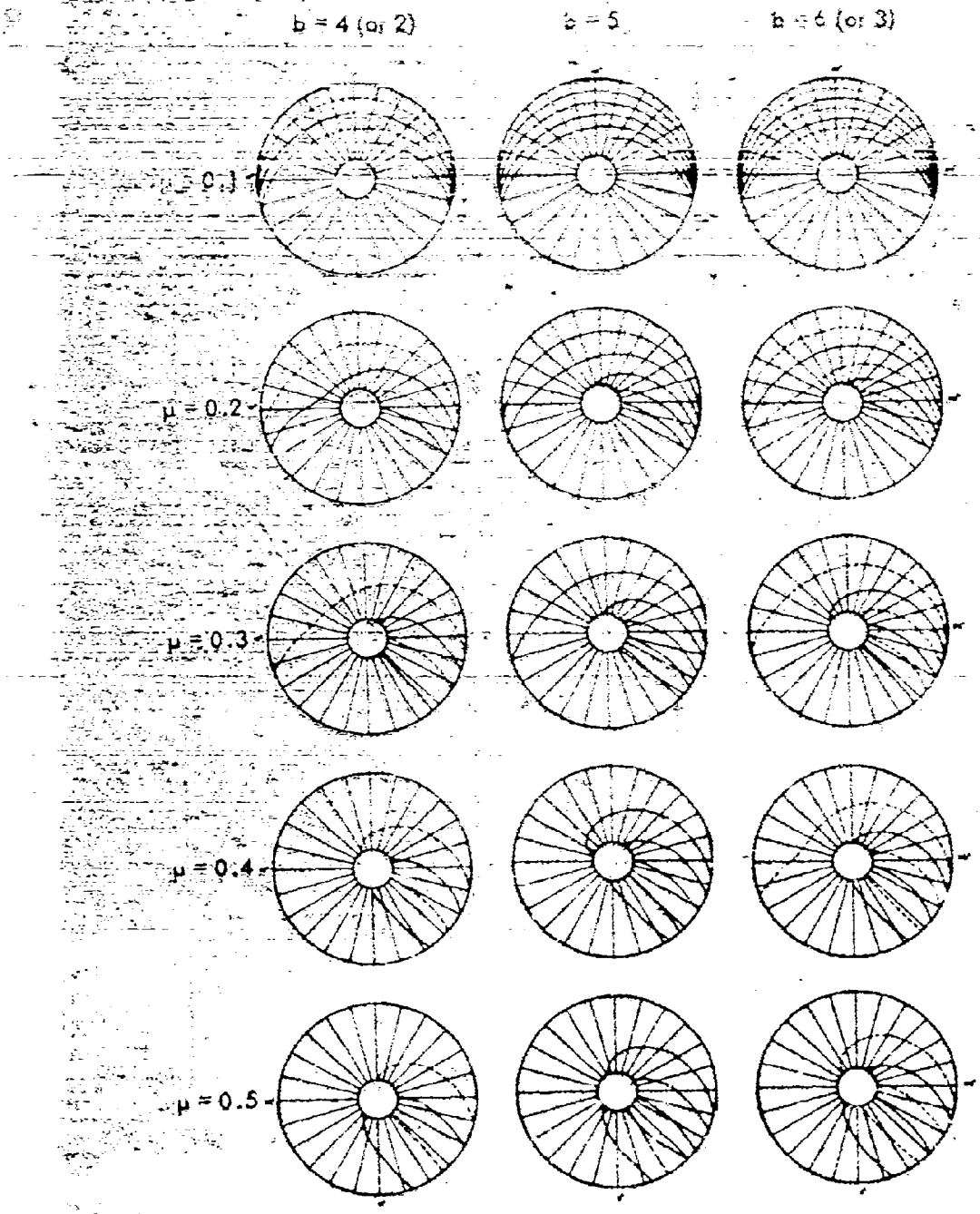

Figure 25. Loci of Blade/Vortex Intersection Points as a Function of Advance Ratio and Number of Blades

Alternate fringes represent 2-lb/in. increments of blade section loading. Boundaries between light and dark fringes correspond to lines of constant loading which are identified in lb/in. H-34 helicopter in steady level flight. Rotor speed = 210 rpm, V = 105 kts, $\mu = 0.29$. Blade/vortex intersection loci are superimposed.

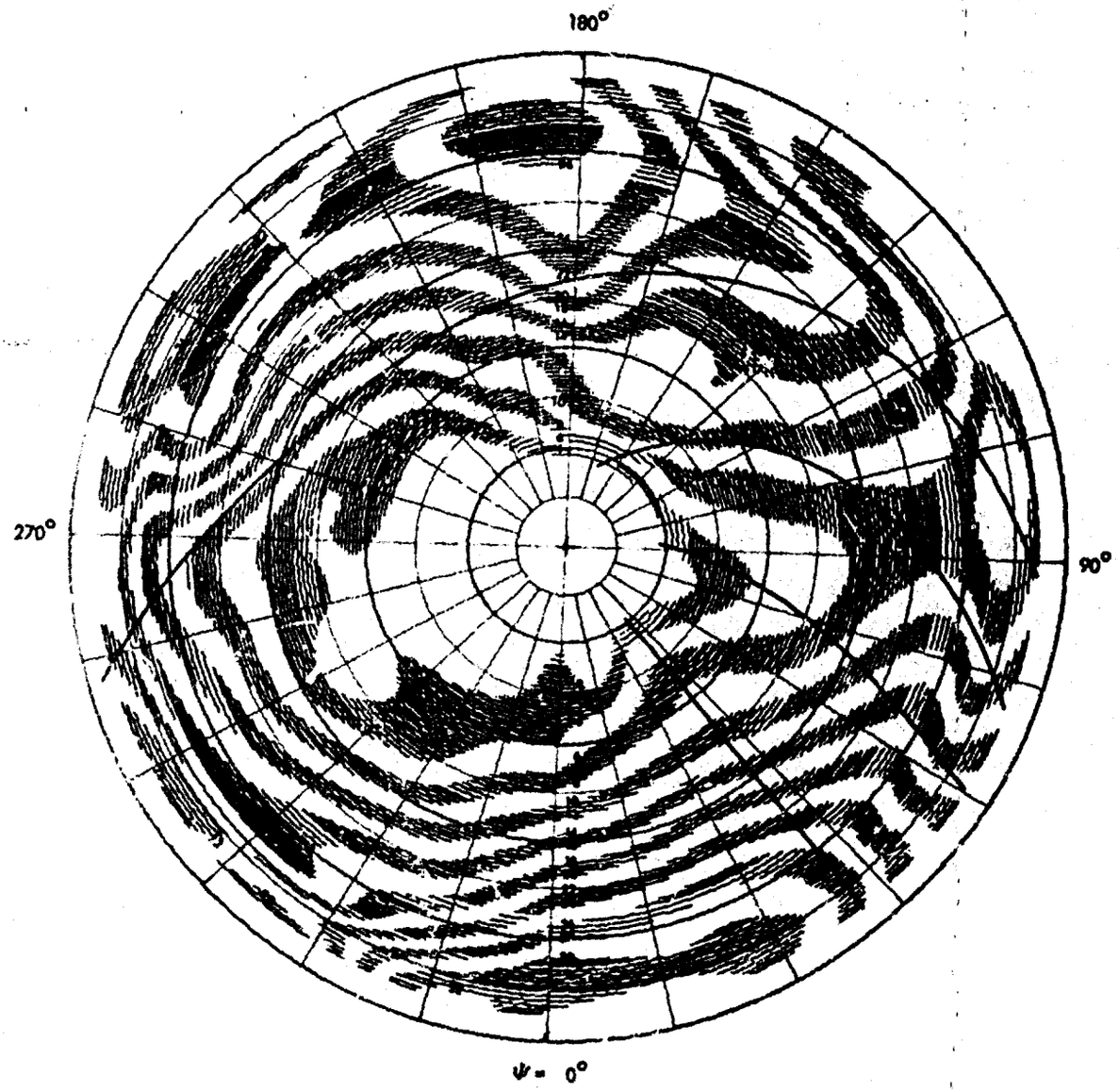

Figure 26. Computer-Drawn Contour Plot of Blade Airload Data From Scheiman.

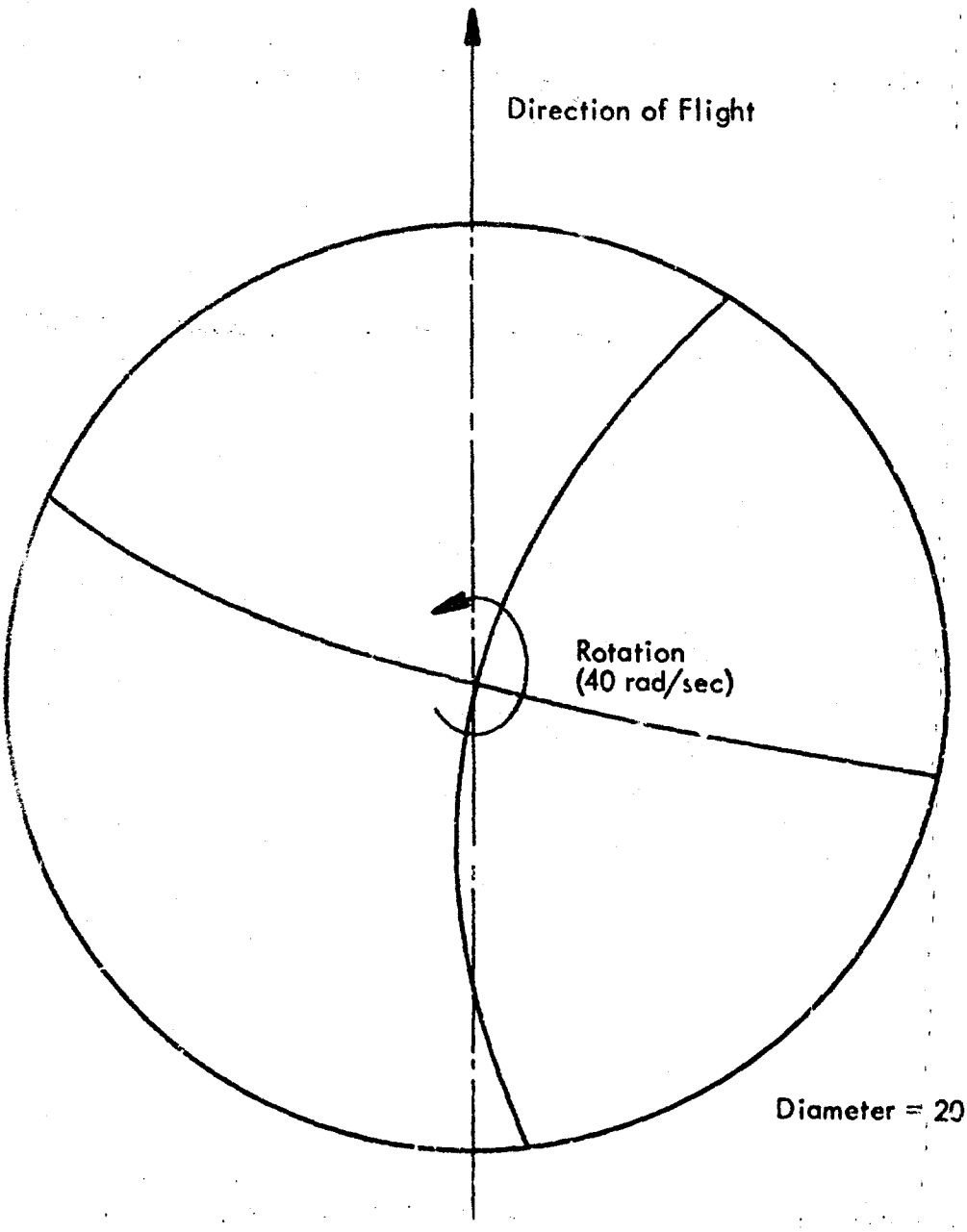

Figure 27. "Retarded Position" of Four-Blade Rigid Rotor Showing Blade Element Location at Retarded Times for Sound at Point 50 Feet in Front of Rotor.

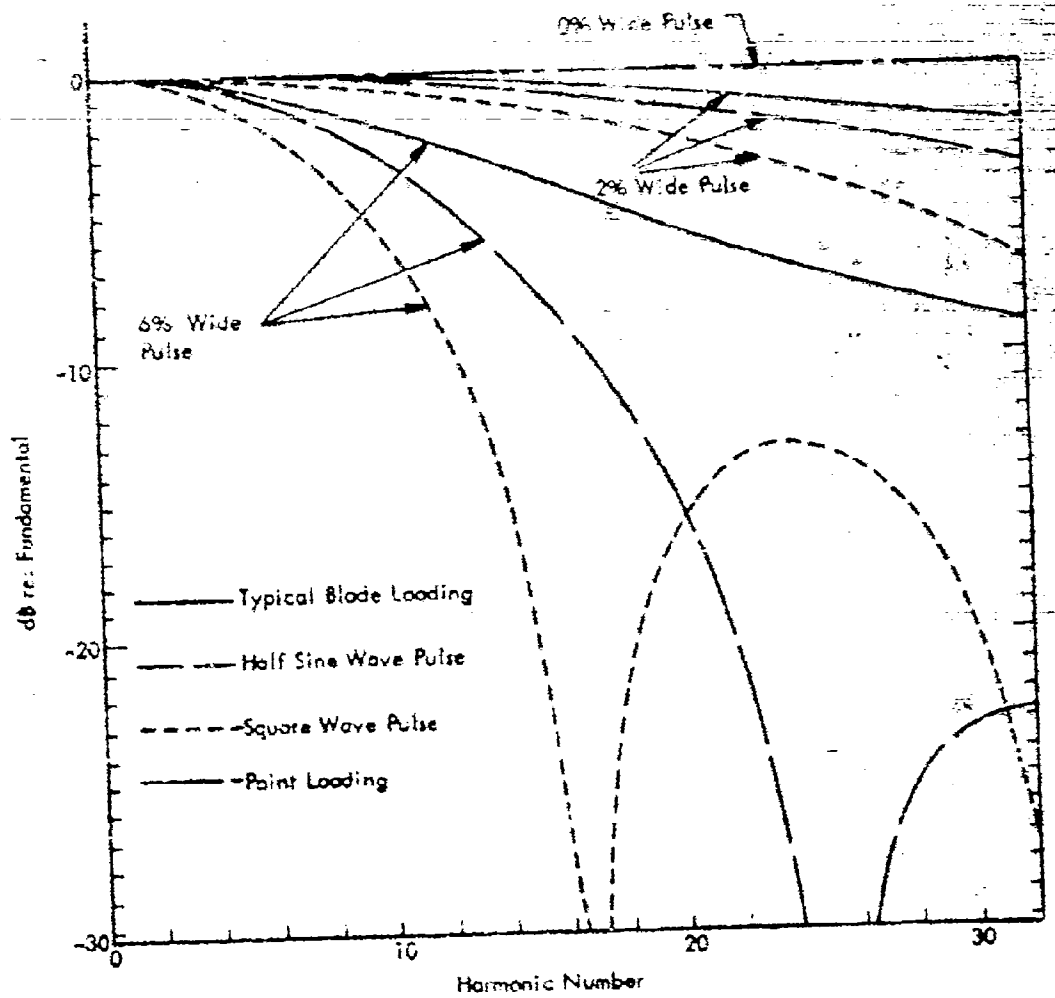

Figure 28. Fourier Coefficients of Various Pulse Shapes.

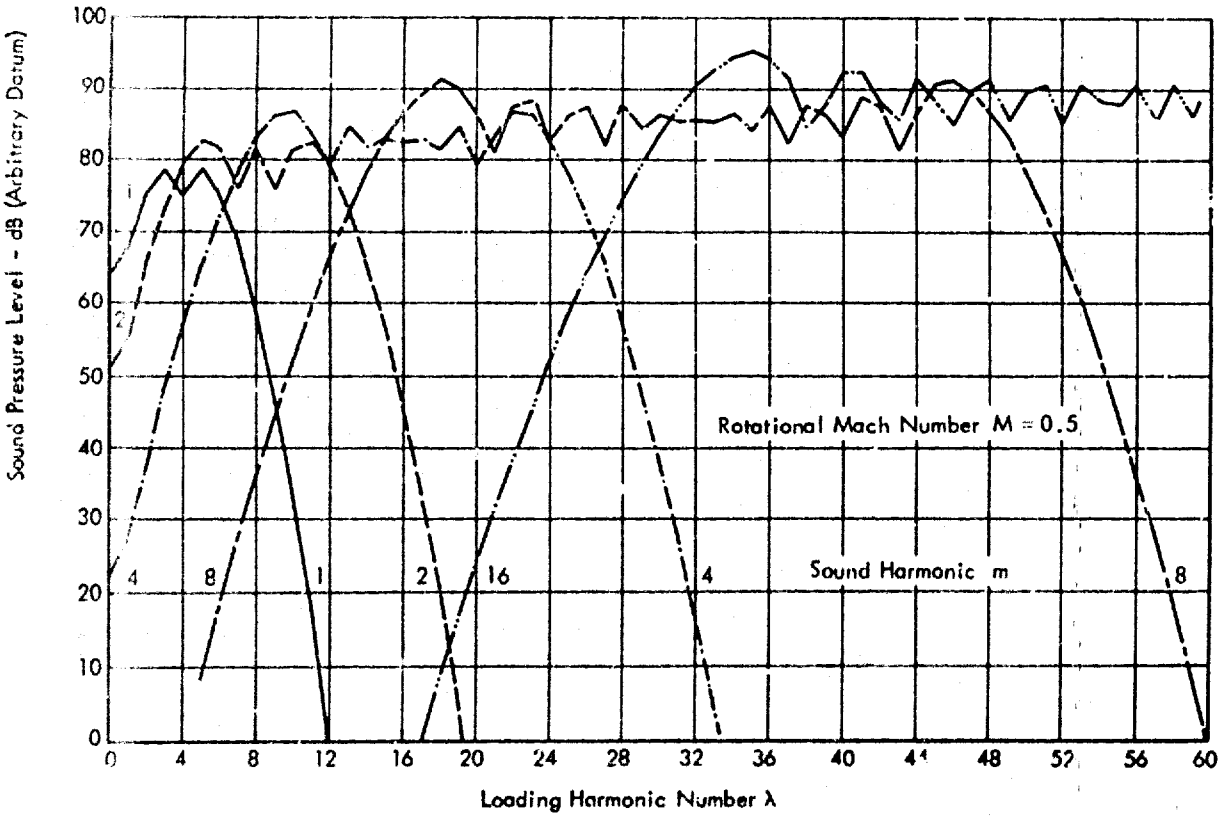

Figure 29. Acoustic Contribution of Loading Harmonics 10° Below Rotor Disc.

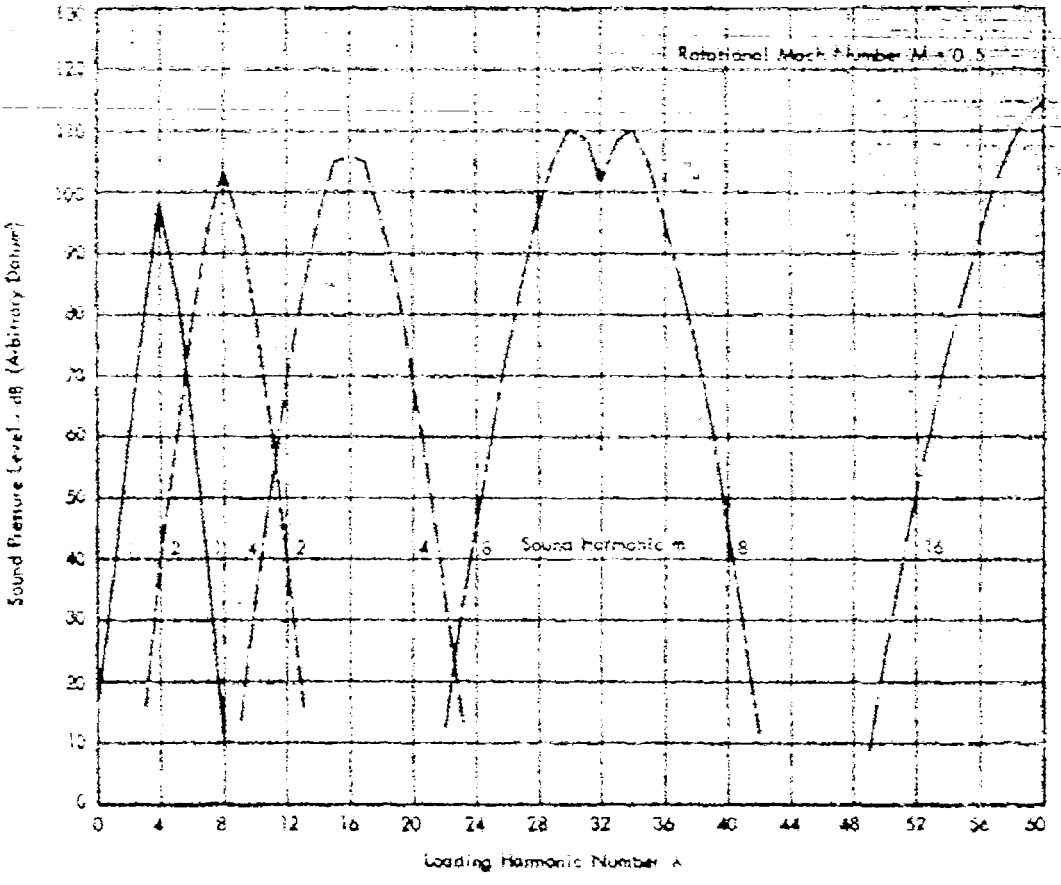

Figure 30. Acoustic Contribution of Loading Harmonics 10° From Rotor Axis.

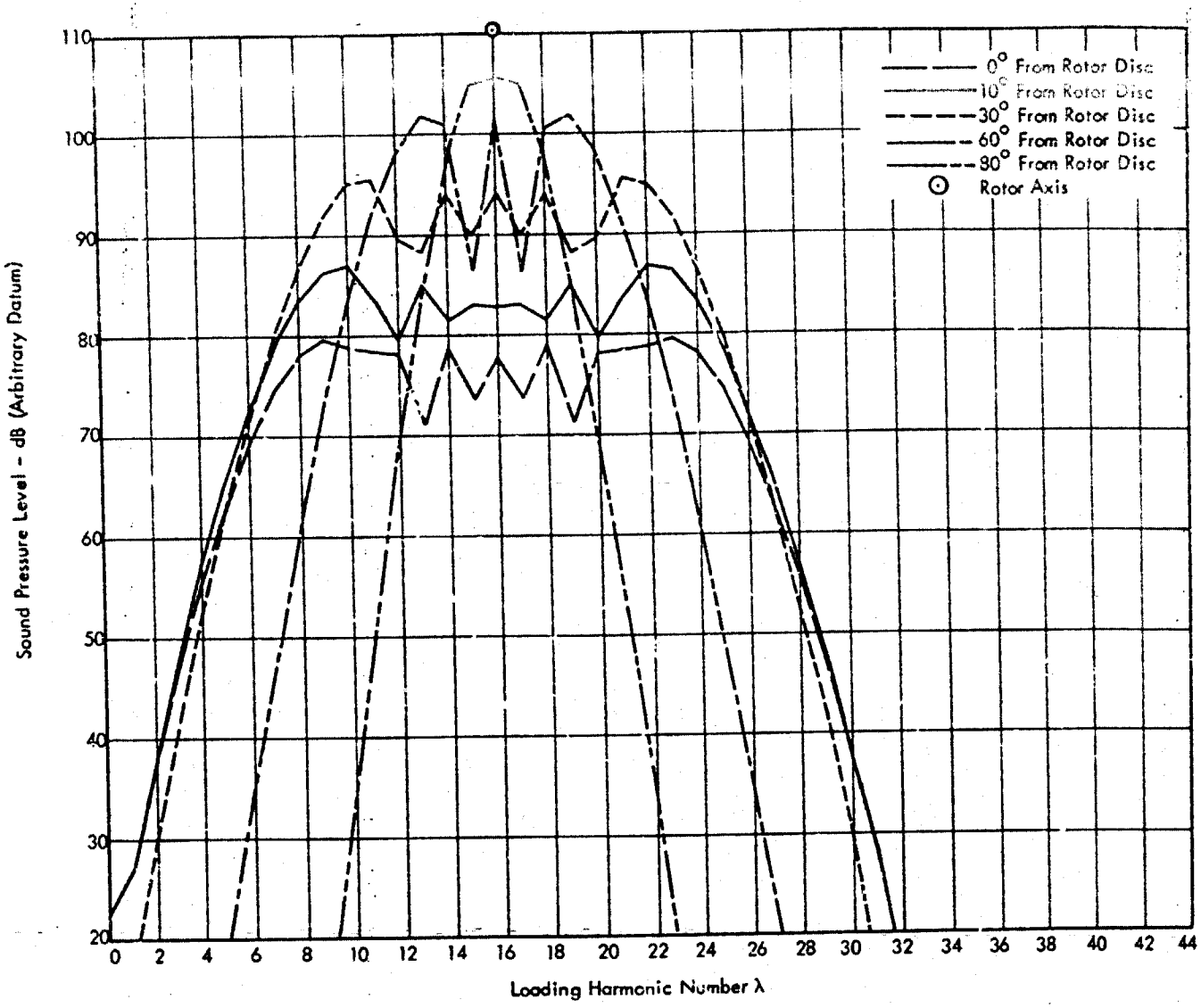

Figure 31. Effect of Field Position on Contribution of Loading Harmonics to Fourth Harmonic Sound.

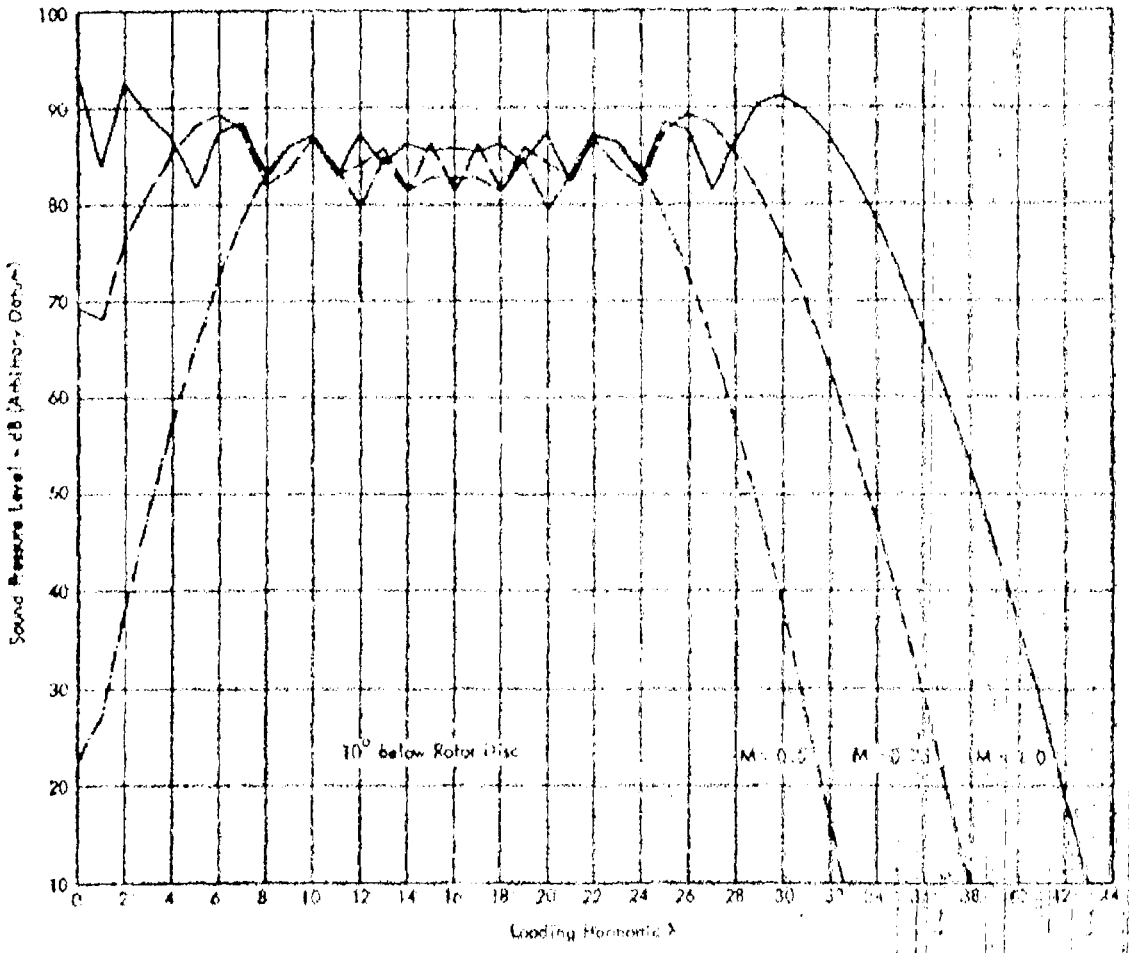

Figure 32. Effect of Mach Number on Contribution of Loading Harmonics to Fourth Harmonic Sound.

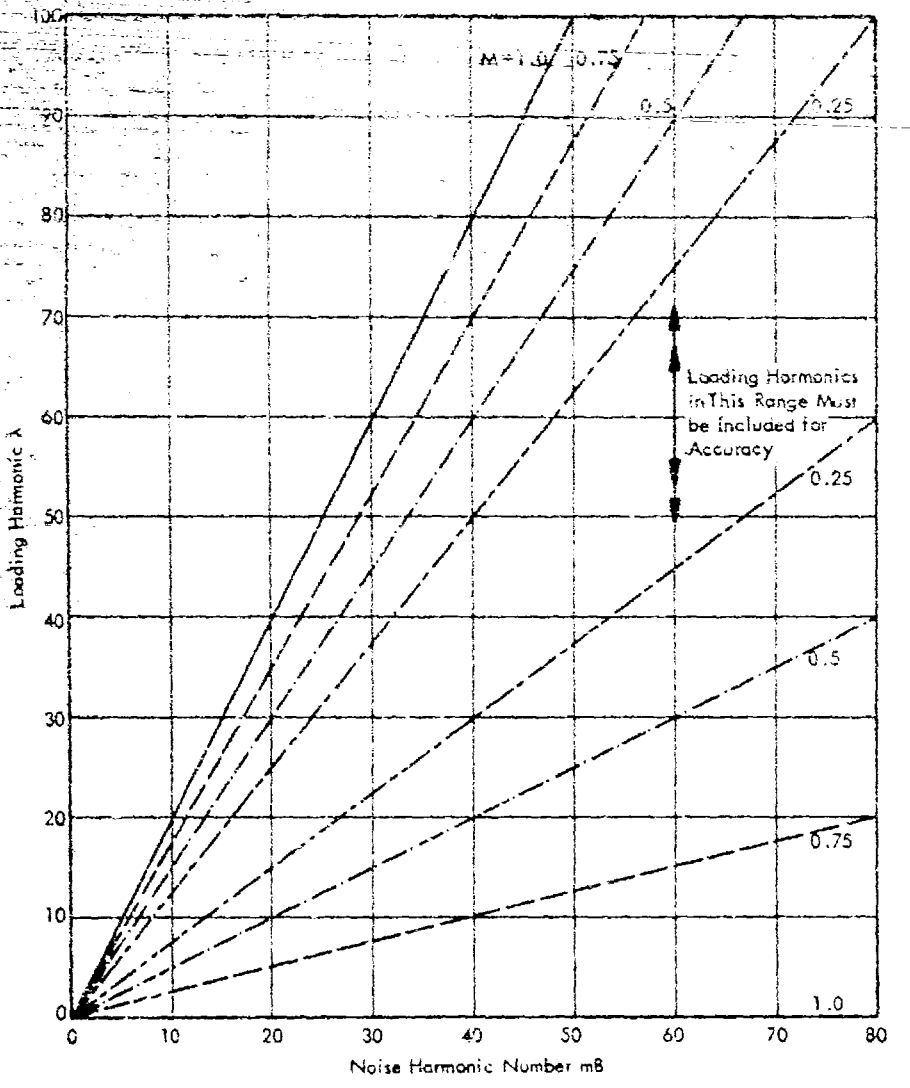

Figure 33. Range of Effective Contribution of Loading Harmonics to Sound Radiation.

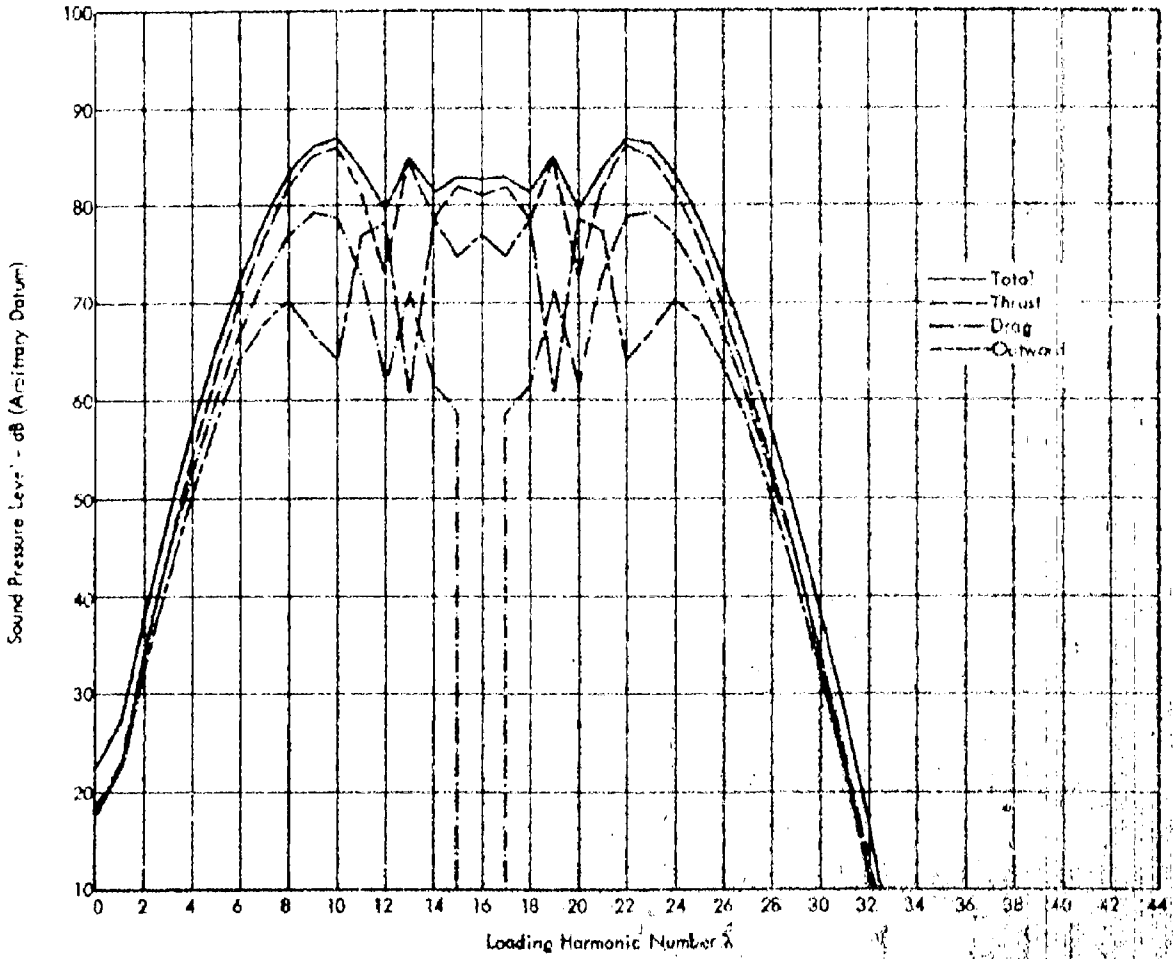

a) At Rotational Mach Number M = 0.5,

Figure 34. Contribution of Force Components to Fourth Harmonic Noise 10° Below Rotor Disc.

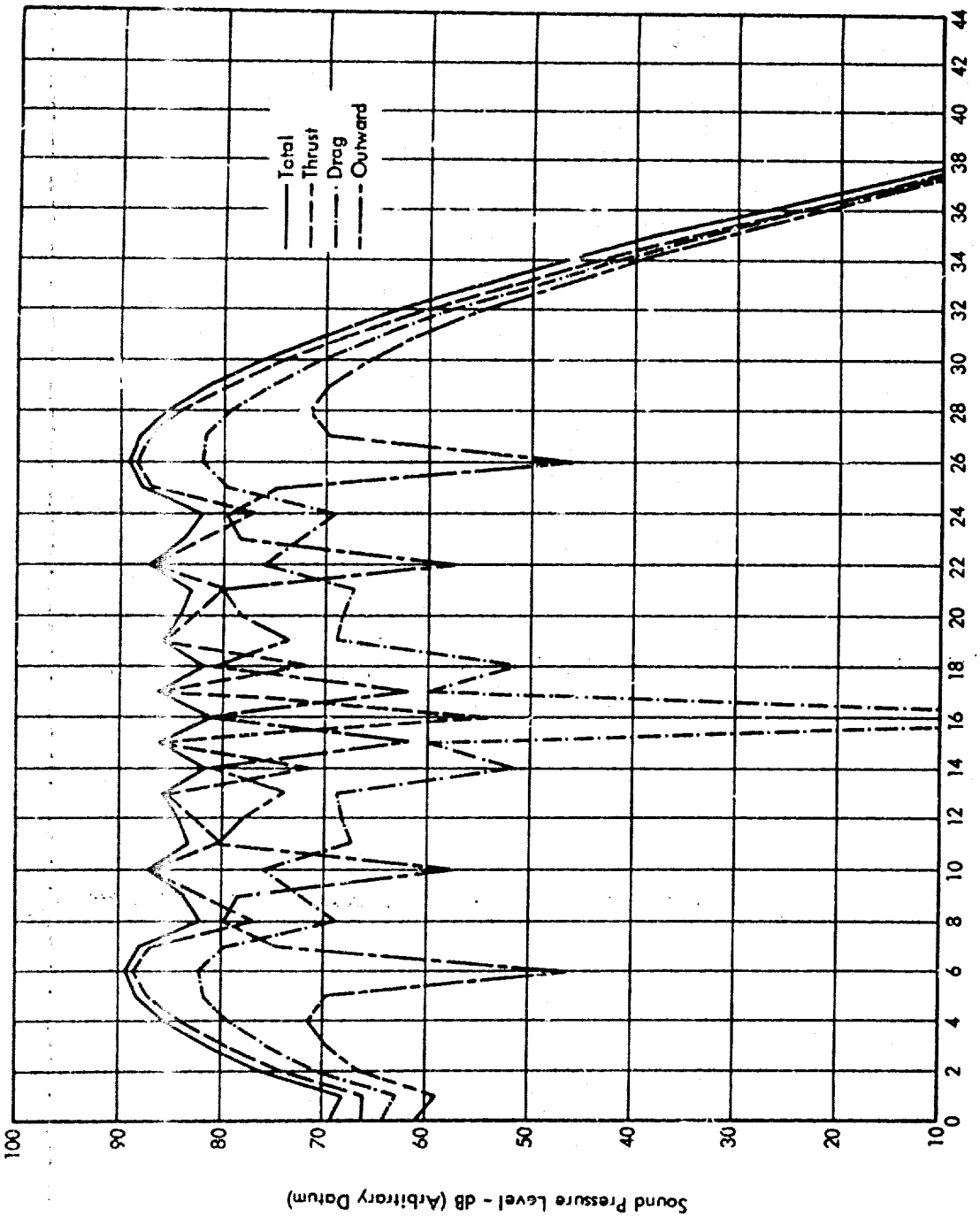

b) At Rotational Mach Number M = 0.75.

Figure 34. (Continued)

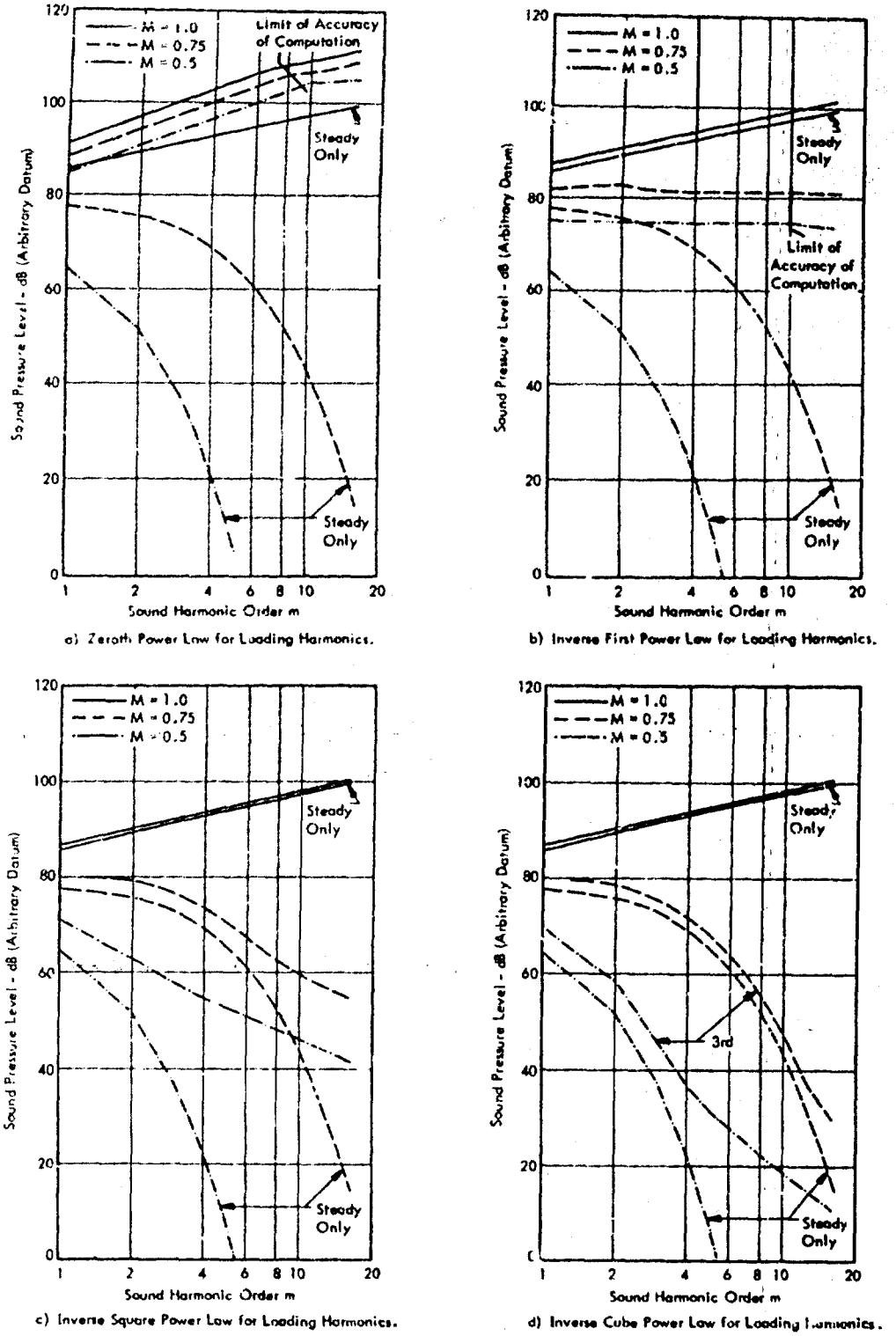

a) Zeroth Power Law for Loading Harmonics.

b) Inverse First Power Law for Loading Harmonics.

c) Inverse Square Power Law for Loading Harmonics.

d) Inverse Cube Power Law for Loading Harmonics.

Figure 35. Effect of Loading Power Law at Various Rotational Mach Numbers M, Sound Radiation 10° Below Rotor Disc in Hover.

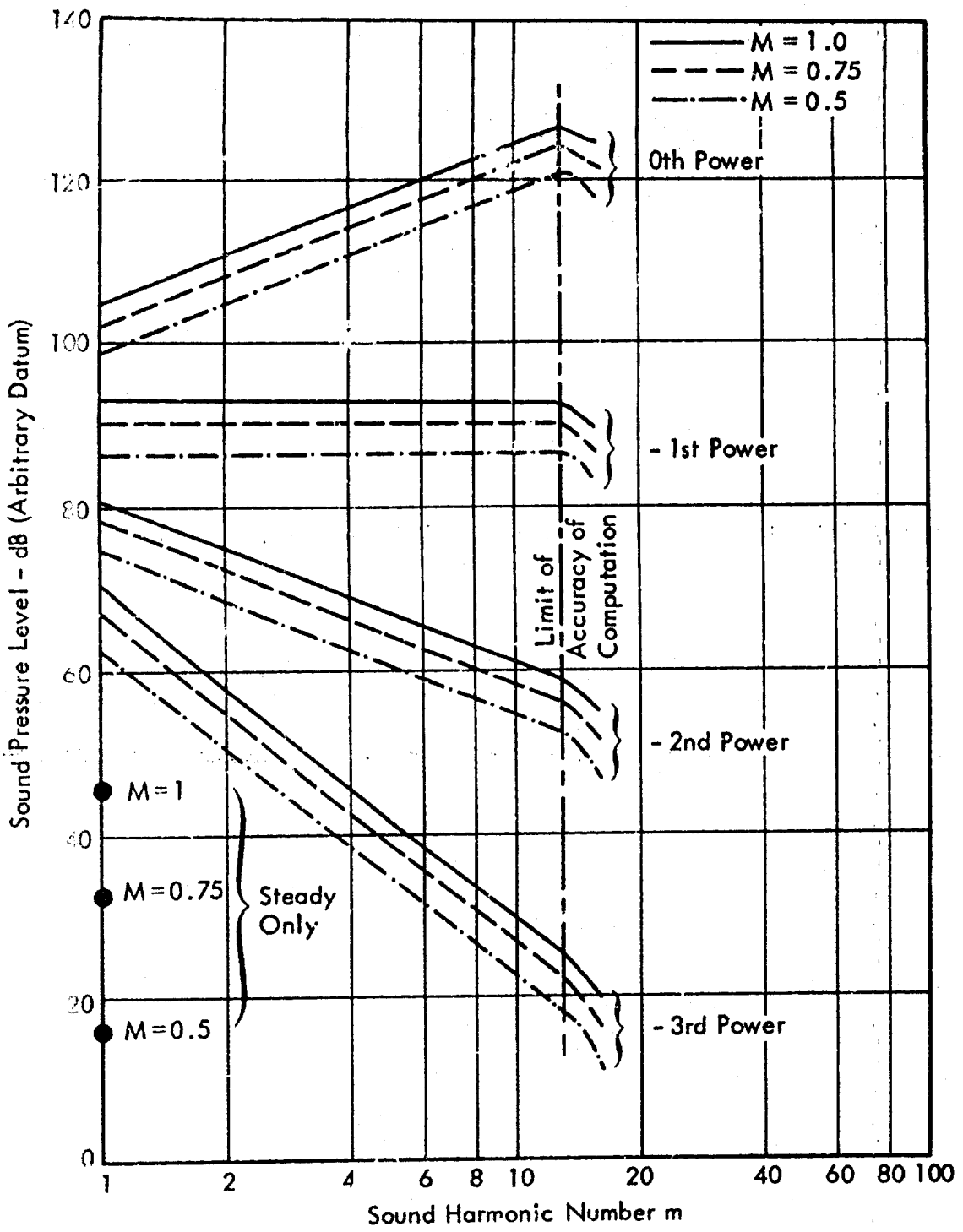

Figure 36. Effect of Rotational Mach Number M on Sound Radiation 10° From Rotor Axis in Hover.

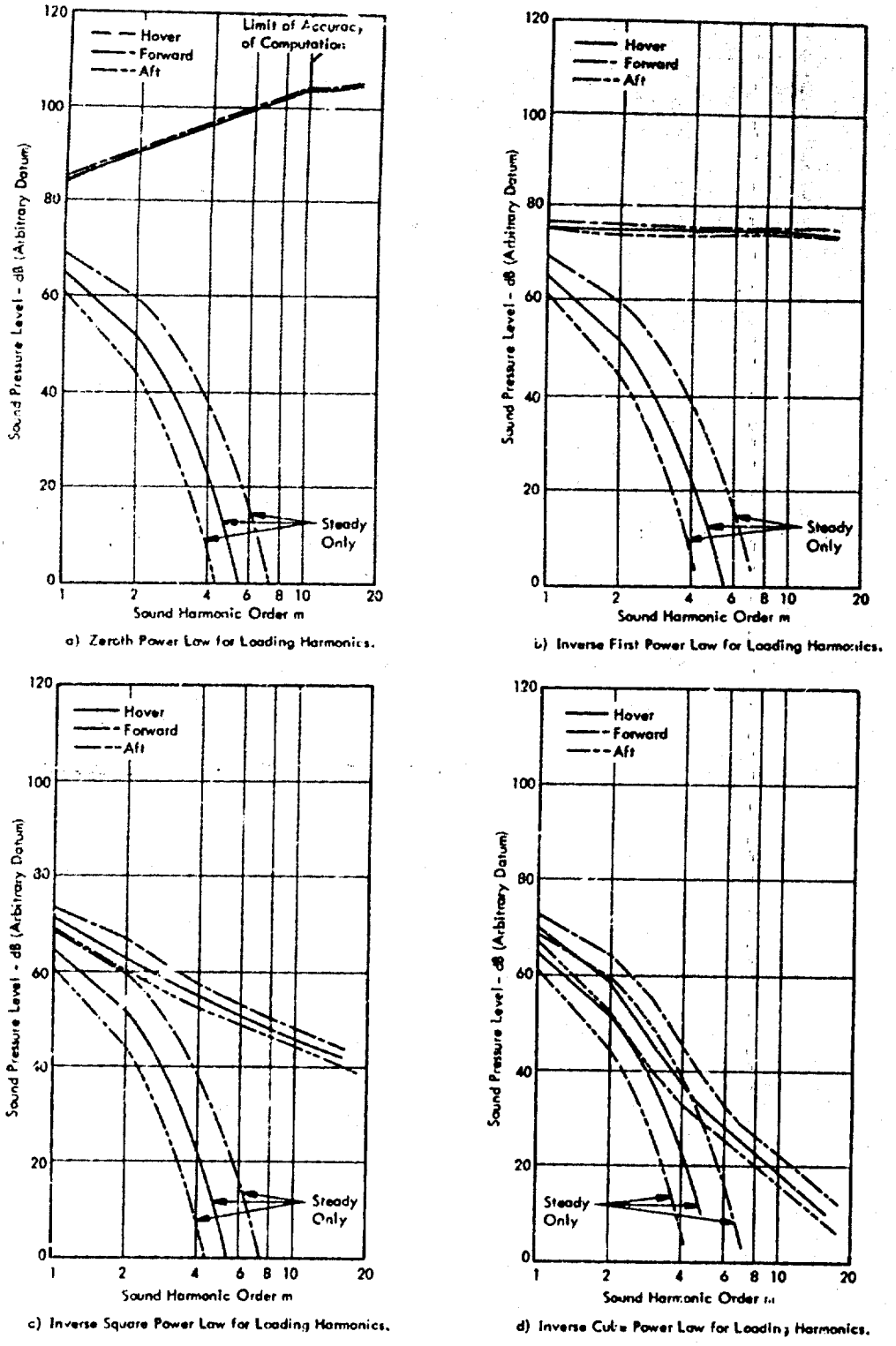

Figure 37. Effect of Forward Velocity ($M_F = 0.125$) on Sound Radiation 10° Below Rotor Disc. Rotational Mach Number M = 0.5.

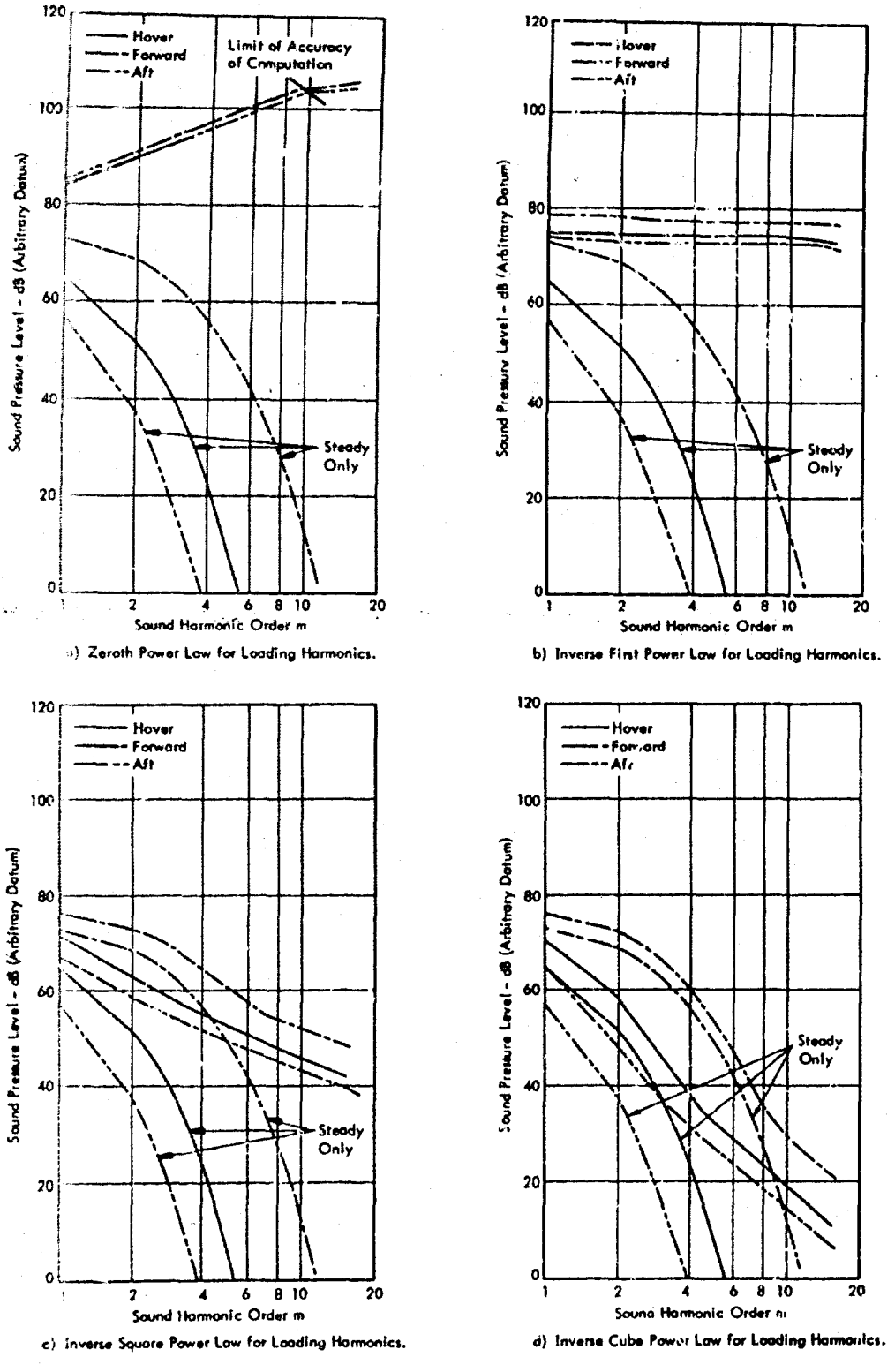

Figure 38. Effect of Forward Velocity (M_F = 0.25) on Sound Radiation 10° Below Rotor Disc. Rotational Mach Number M = 0.5.

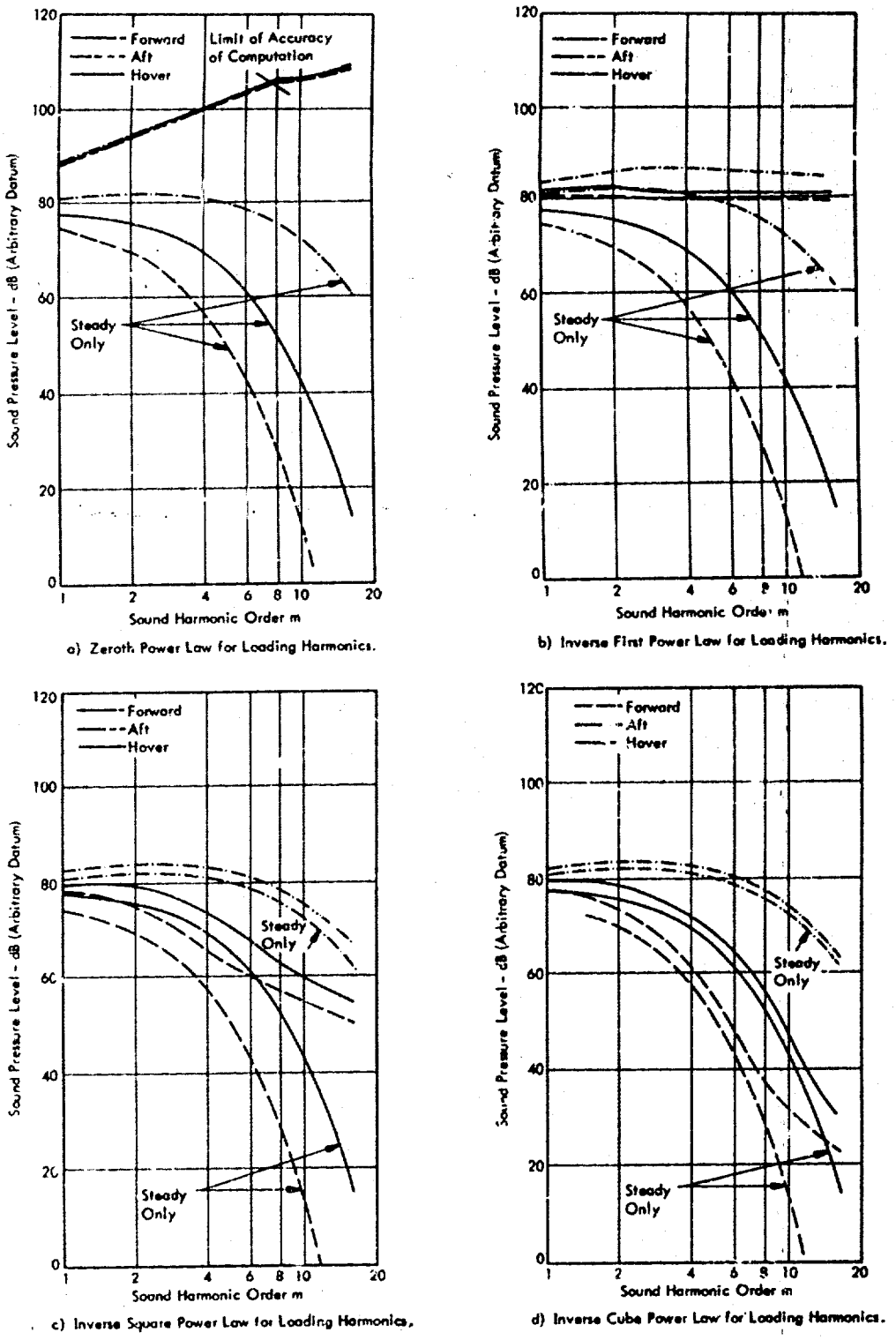

Figure 39. Effect of Forward Velocity ($M_F = 0.125$) on Sound Radiation 10° Below Rotor Disc. Rotational Mach Number $M = 0.75$.

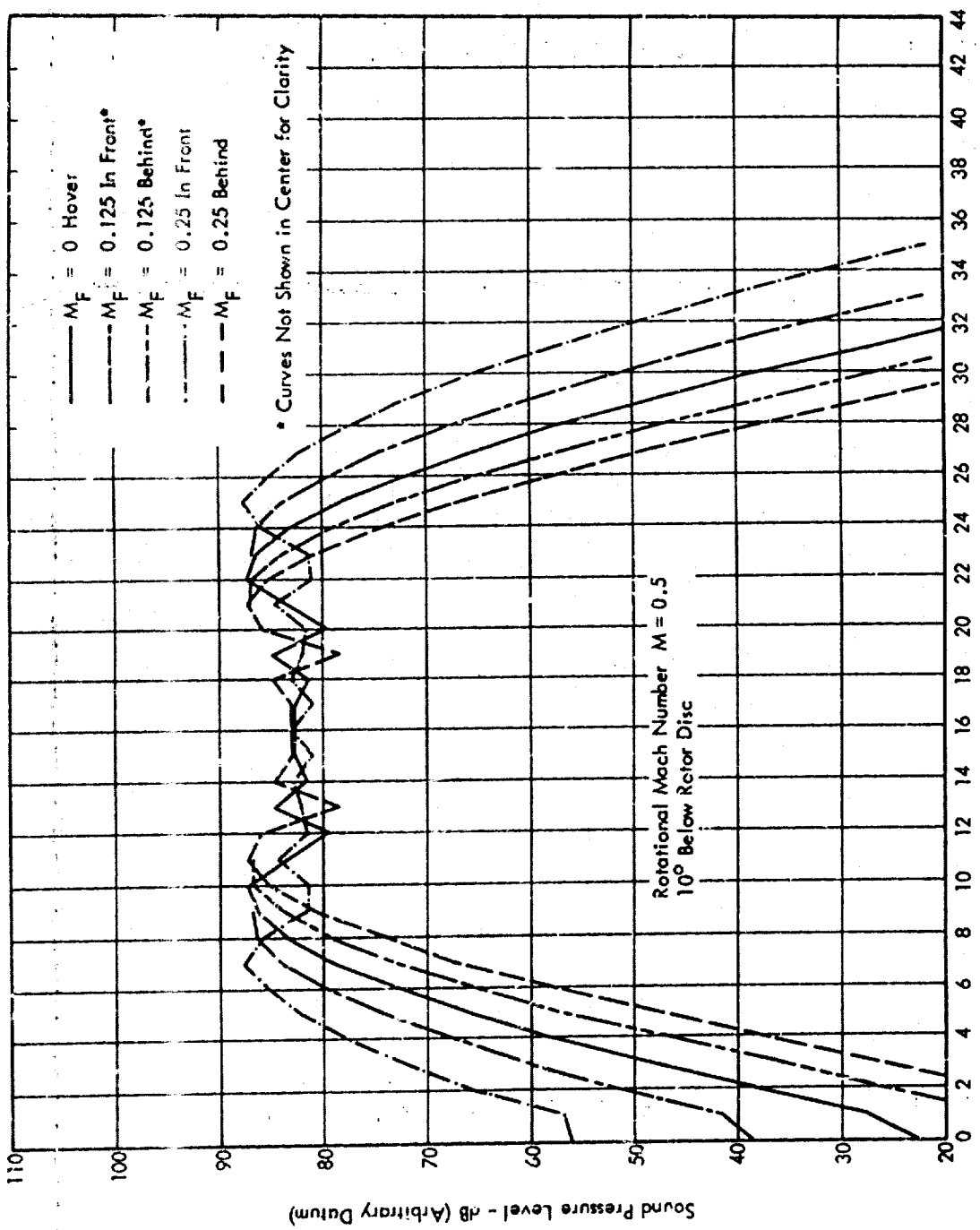

Figure 40. Effect of Forward Speed on Contribution of Loading Harmonics to Fourth Harmonic Sound.

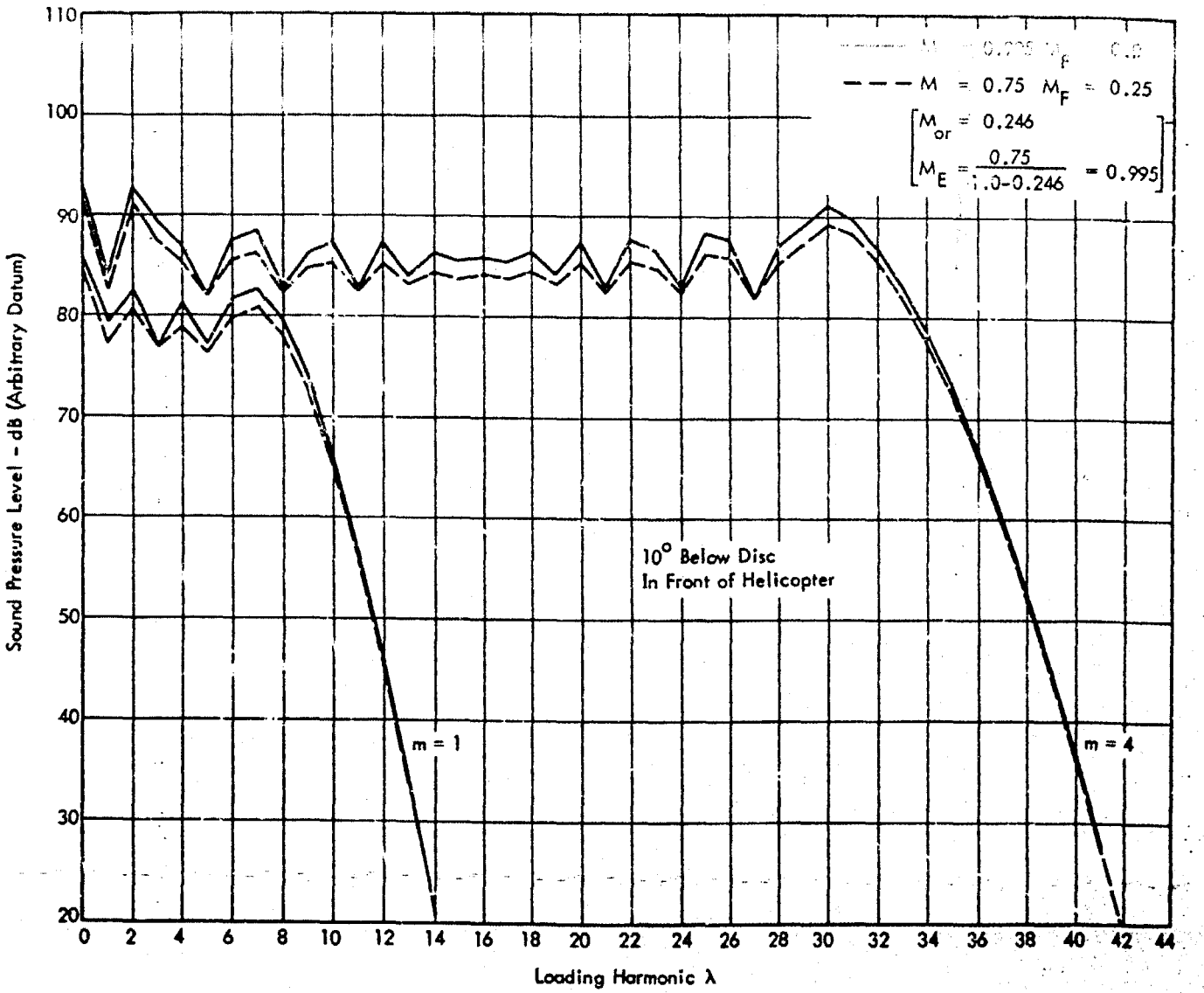

Figure 41. Accuracy of Effective Velocity Approximation.

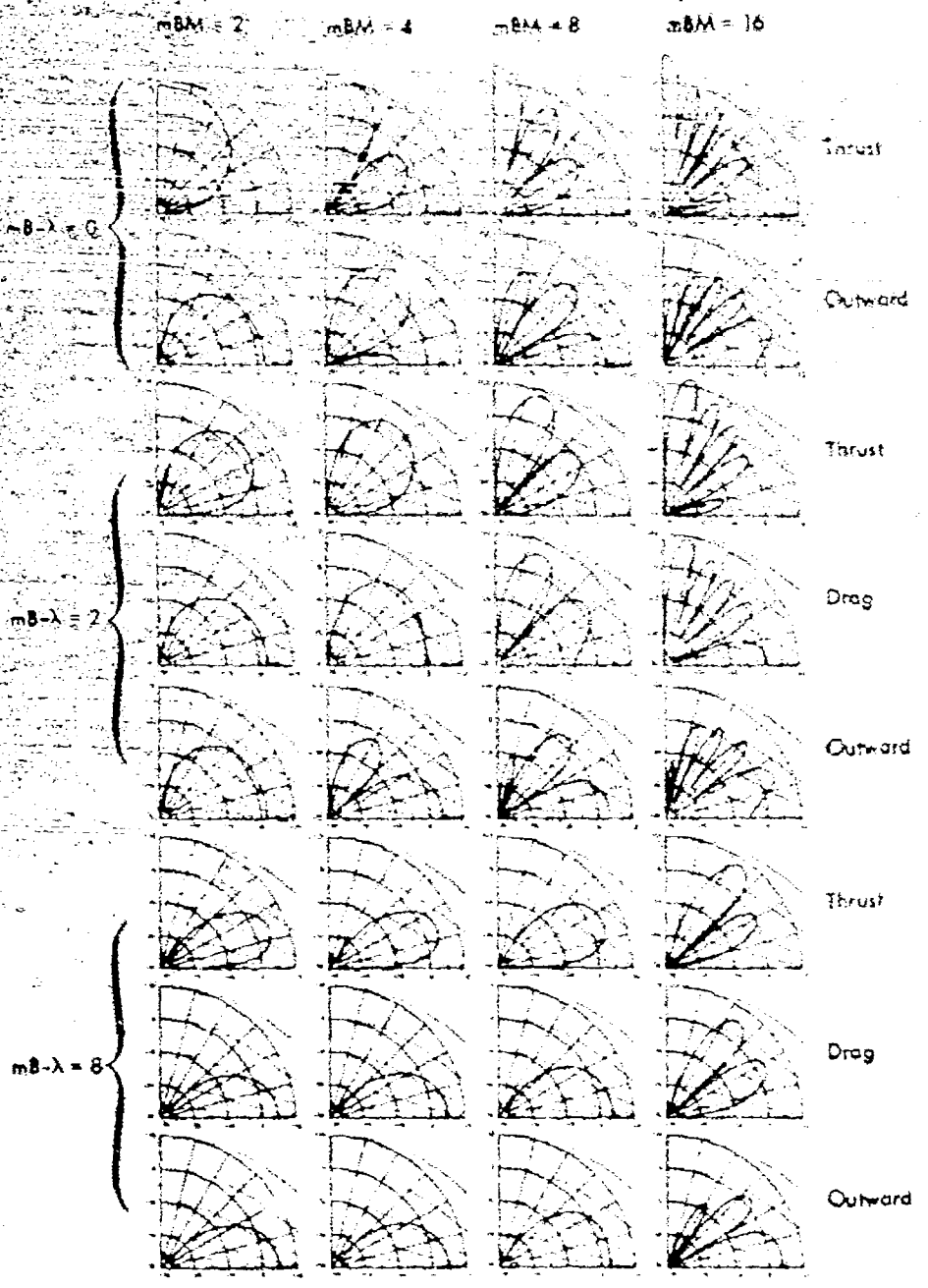

Figure 42. Directionality Patterns of Various Loading Components.

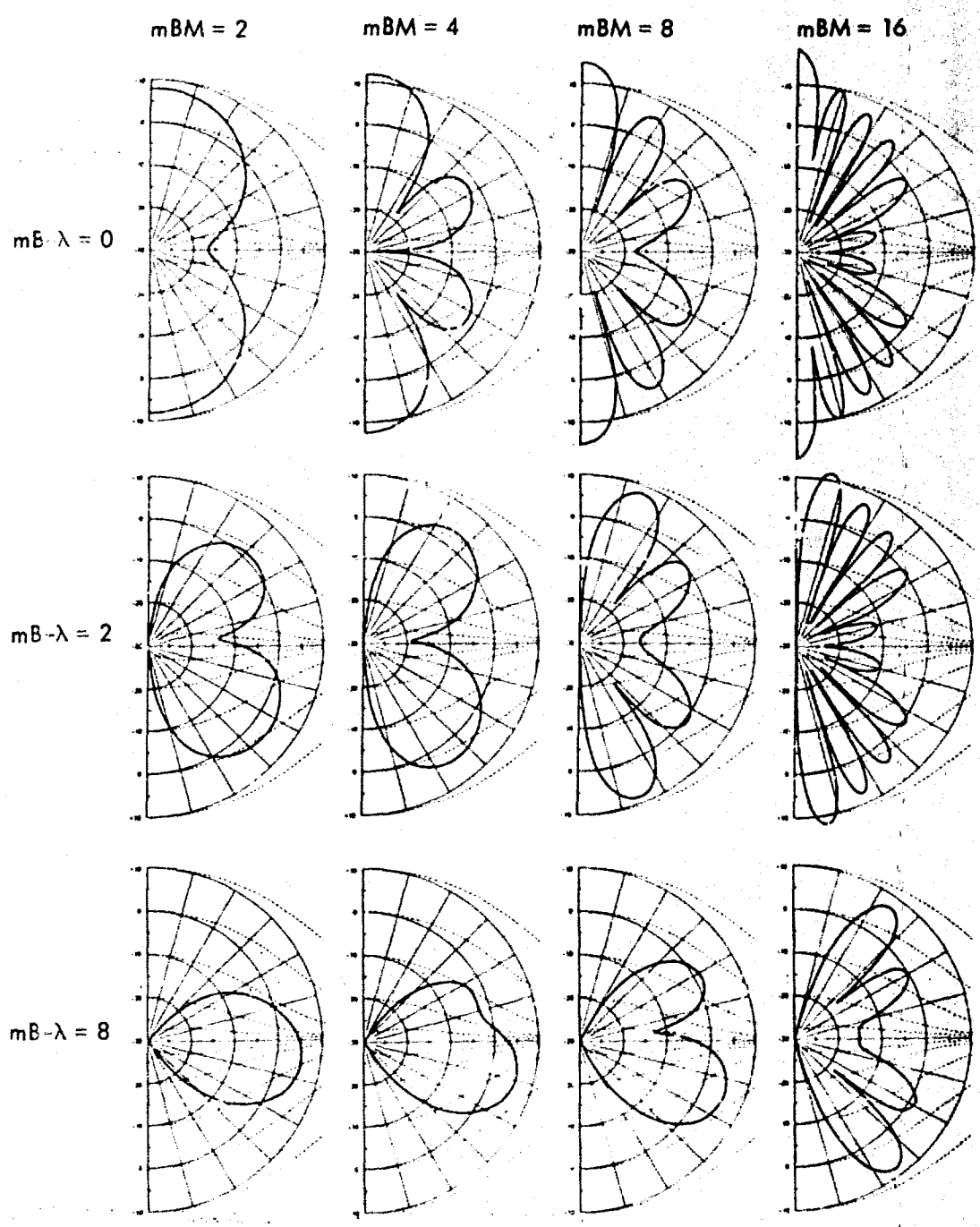

Figure 43. Directionality Patterns for Combined Load in Any One Harmonic.

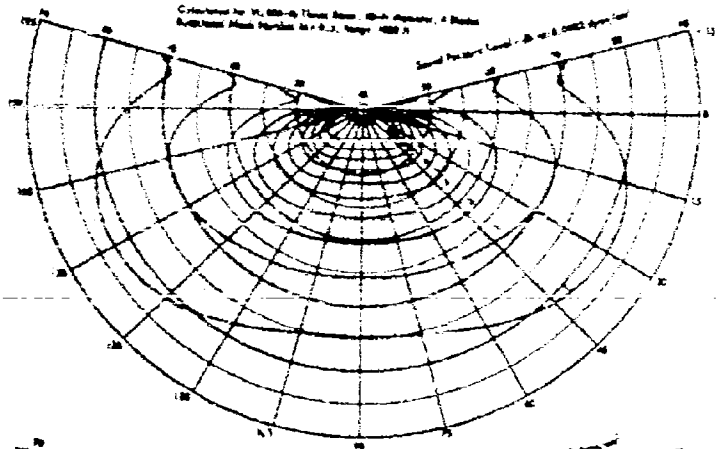

c) Hover

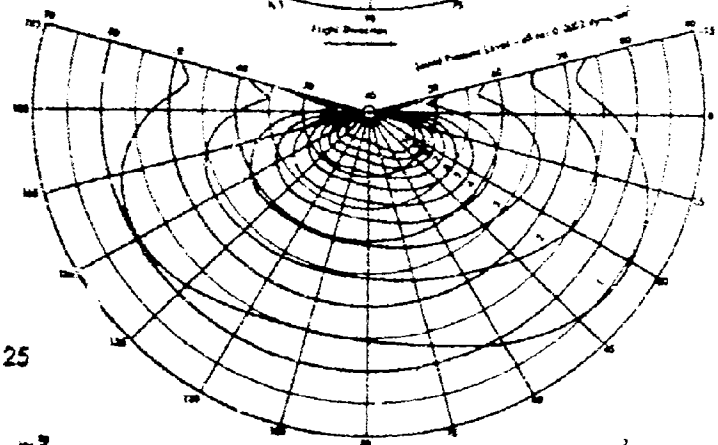

b) Forward Speed
Mach Number = 0.125

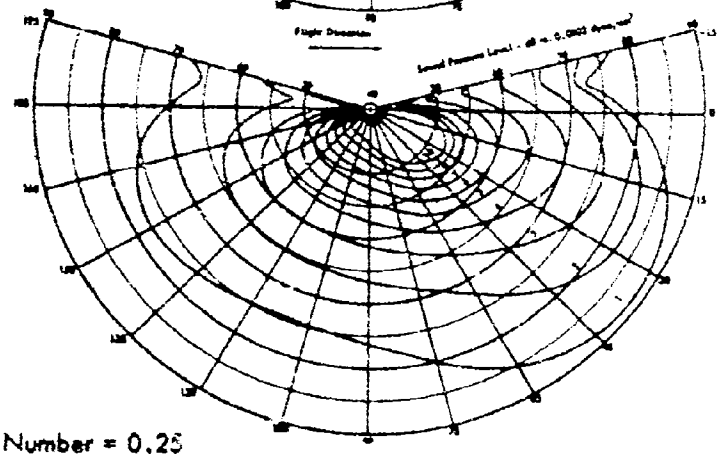

c) Forward Speed Mach Number = 0.25

Figure 44. Overall Sound Patterns Beneath Rotor for Various Harmonics.

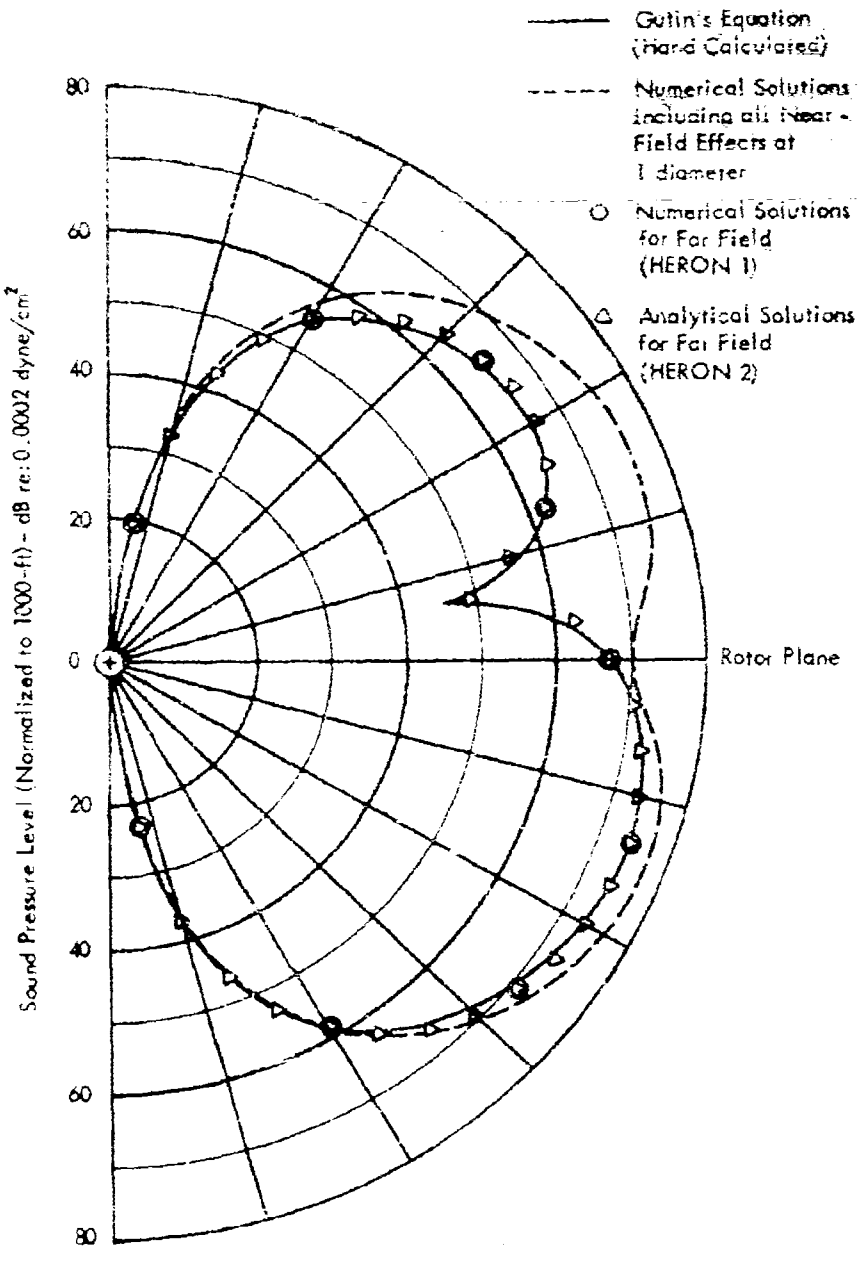

Figure 45. Near-Field Effects on First Sound Harmonic. Four-Blade Rotor - Steady Thrust and Drag Only.

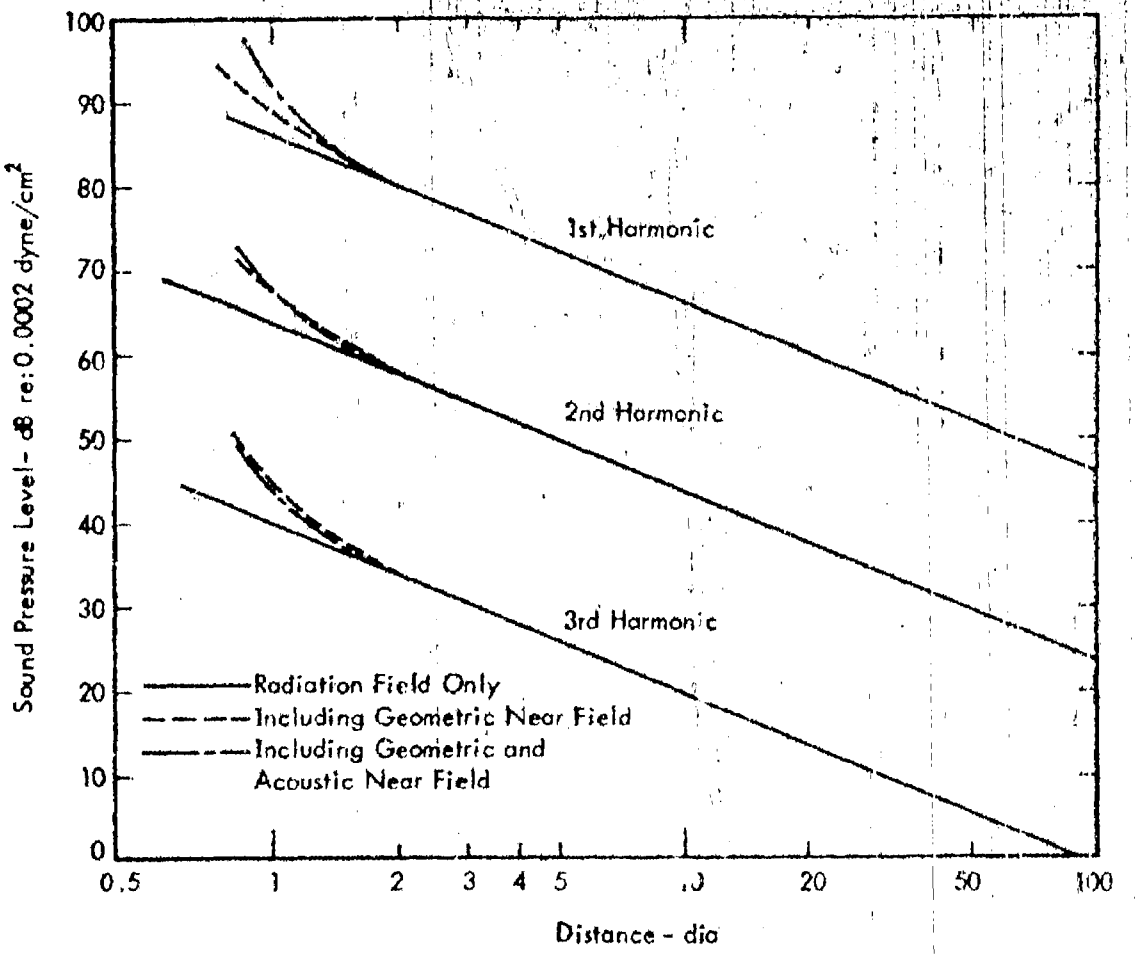

Figure 46. Near-Field Effects 10 Degrees Below Rotor Disc.

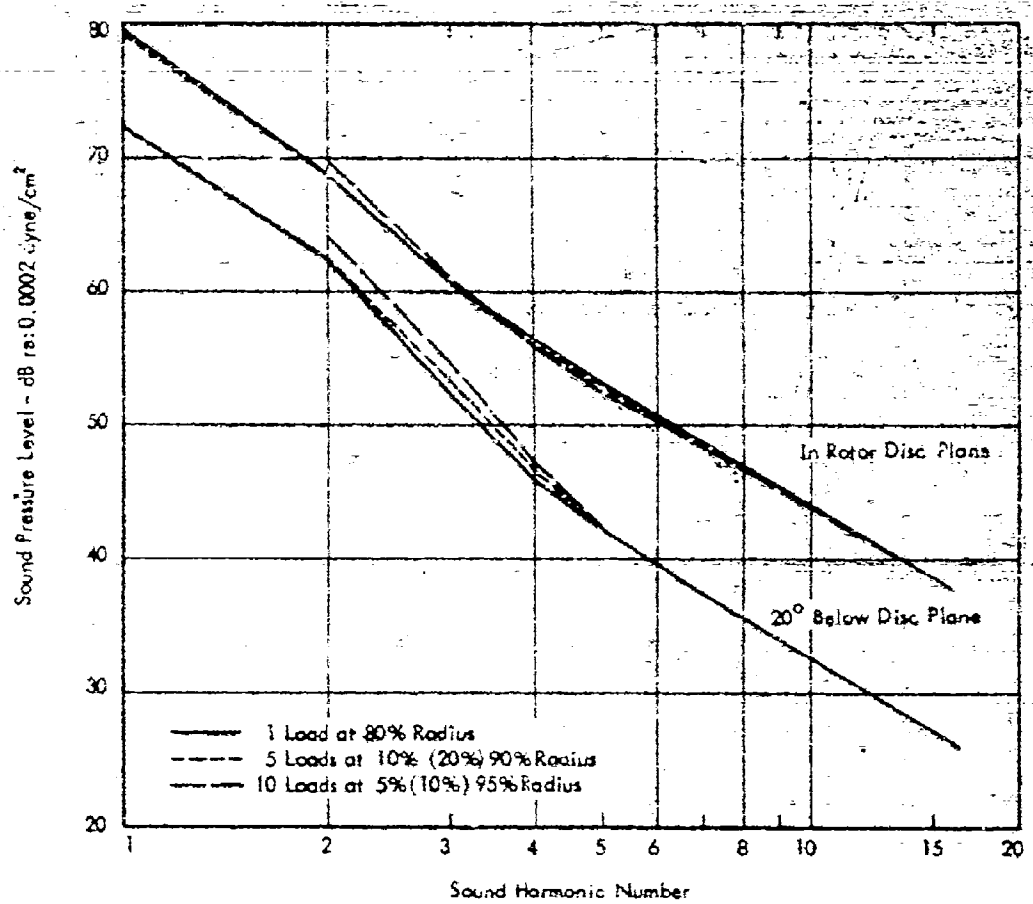

Figure 47. Effect of Loading Distribution on Sound Field for Randomized Loads.

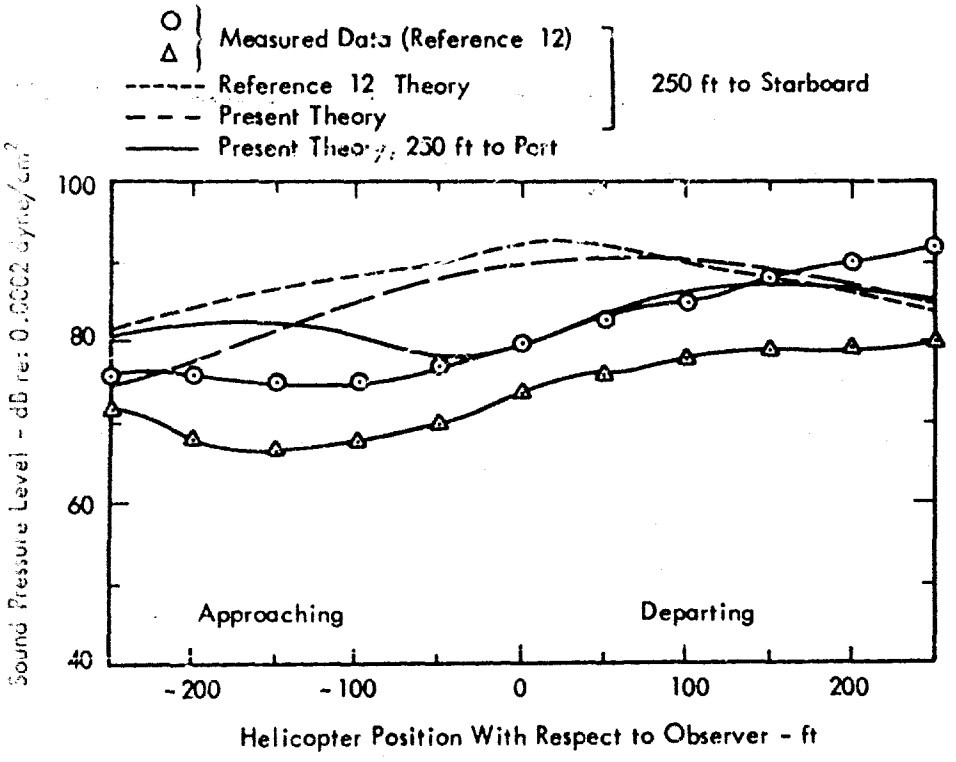

a) First Harmonic

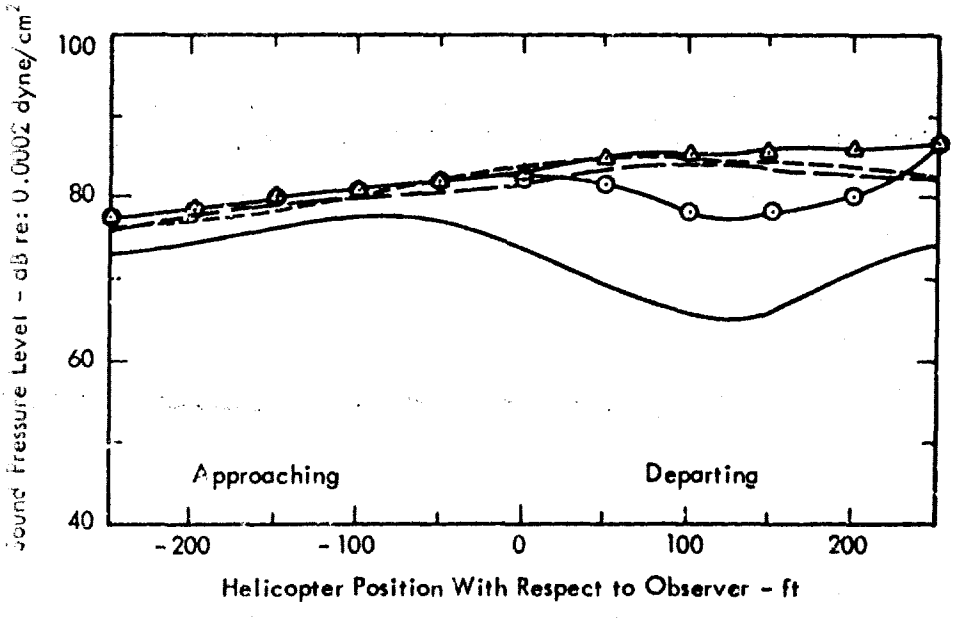

b) Second Harmonic

Figure 48. Comparison of Theoretical and Measured Harmonic Sound Pressure Levels for H-34 Main Rotor. Aircraft Altitude 200 ft. Data From Reference 12.

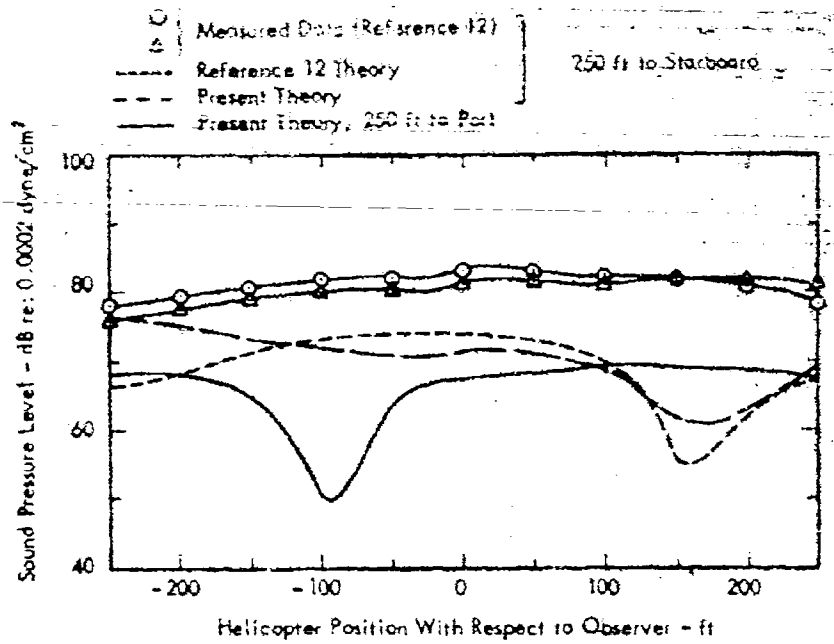

c) Third Harmonic

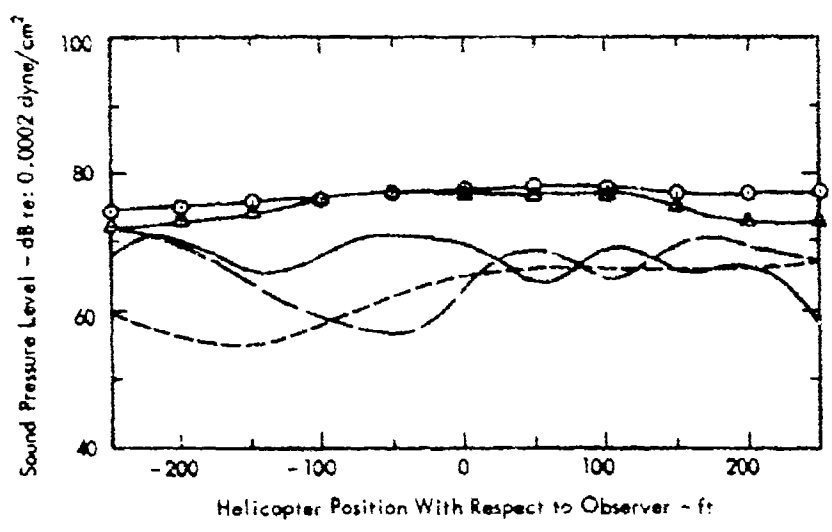

d) Fourth Harmonic

Figure 48. (Continued).

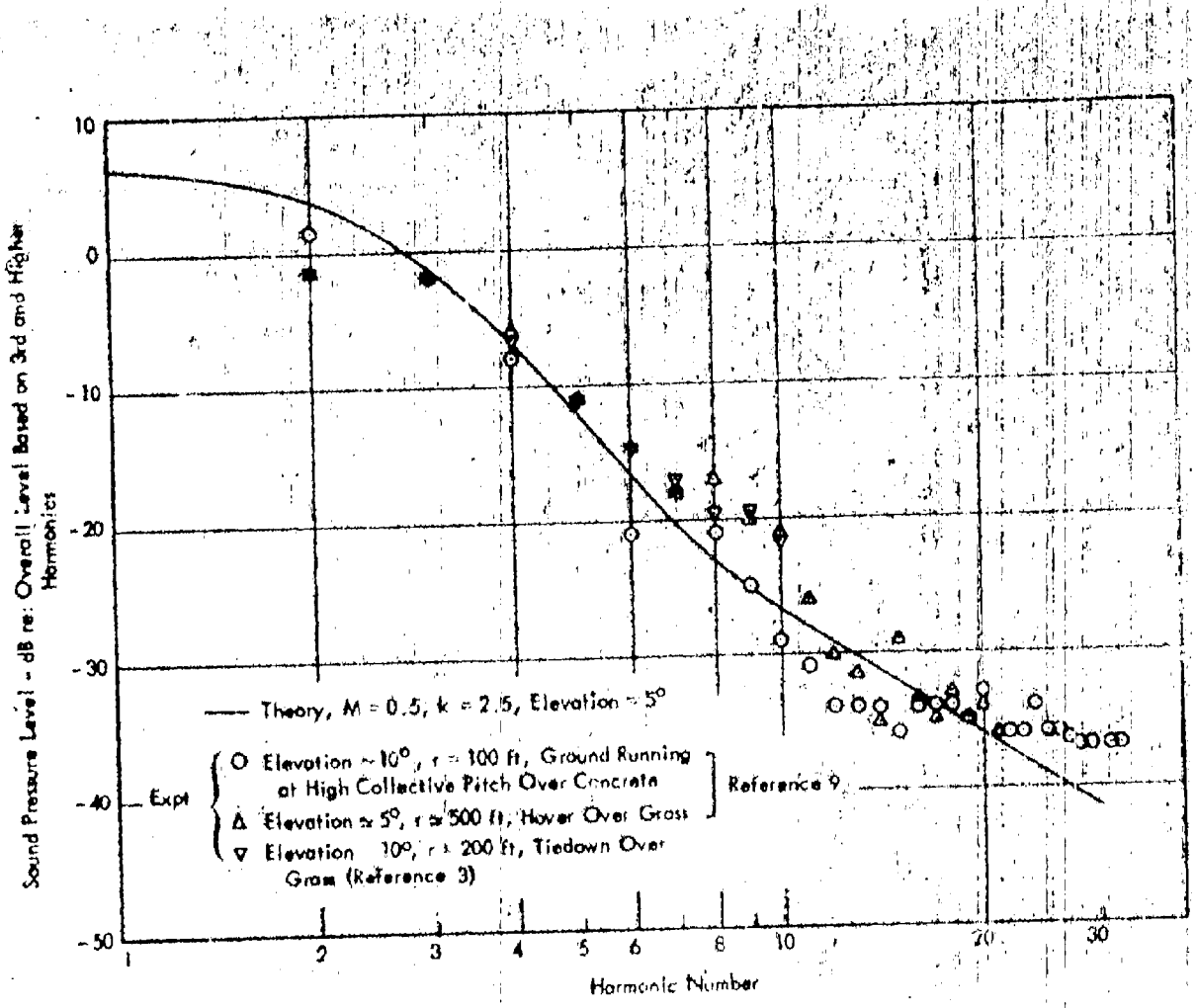

Figure 49. Noise Spectrum - Comparison of Theory and Experiment for Two-Blade Rotor (UH-1A and UH-1B).

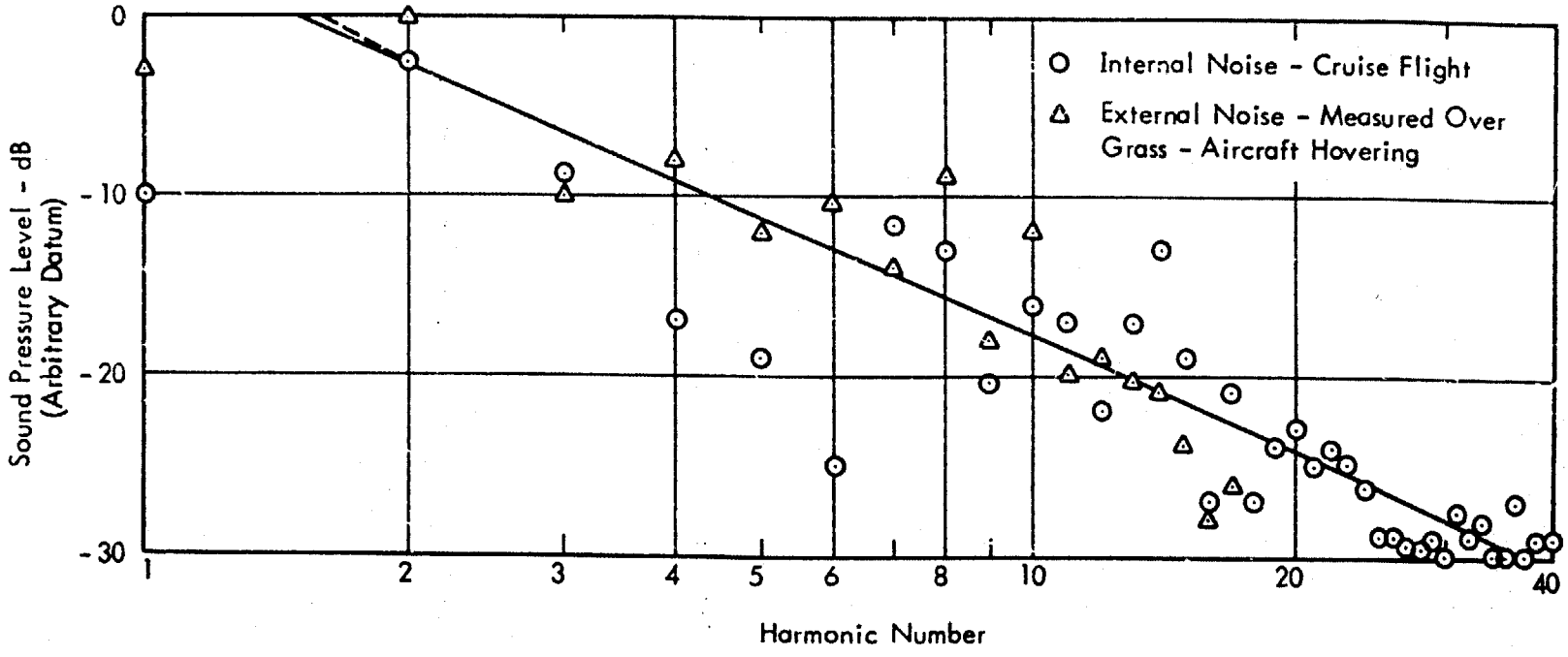

Figure 50. Comparison of Measured Internal and External Harmonic Sound Levels for CH-47B Chinook. Data From Reference 7.

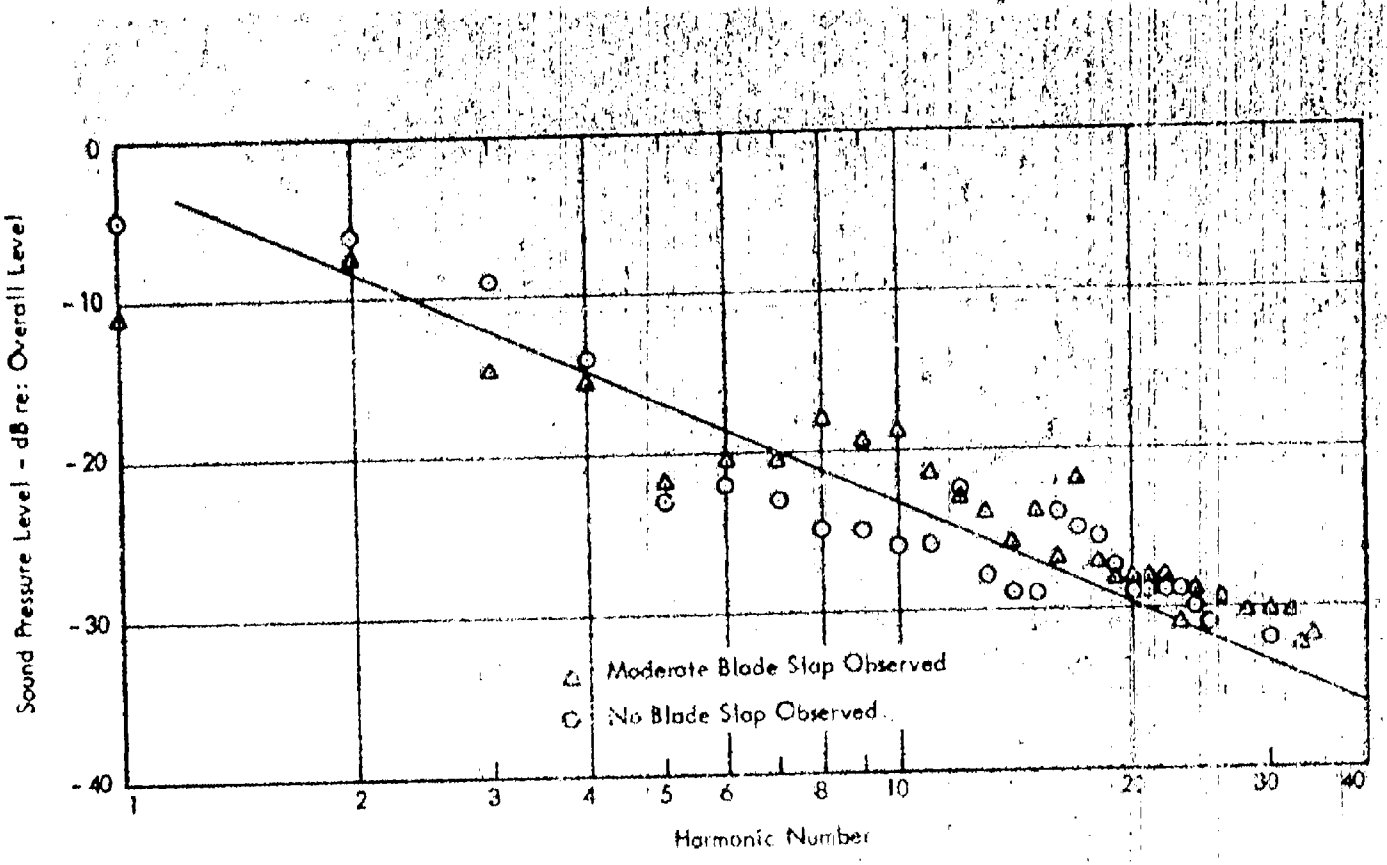

Figure 51. Measured Harmonic Sound Levels for CH-47B Chinook Helicopter Hovering at Approximately 10-ft Altitude, 200 ft From Microphone. Recorded Over Grass. Data From Reference 7.

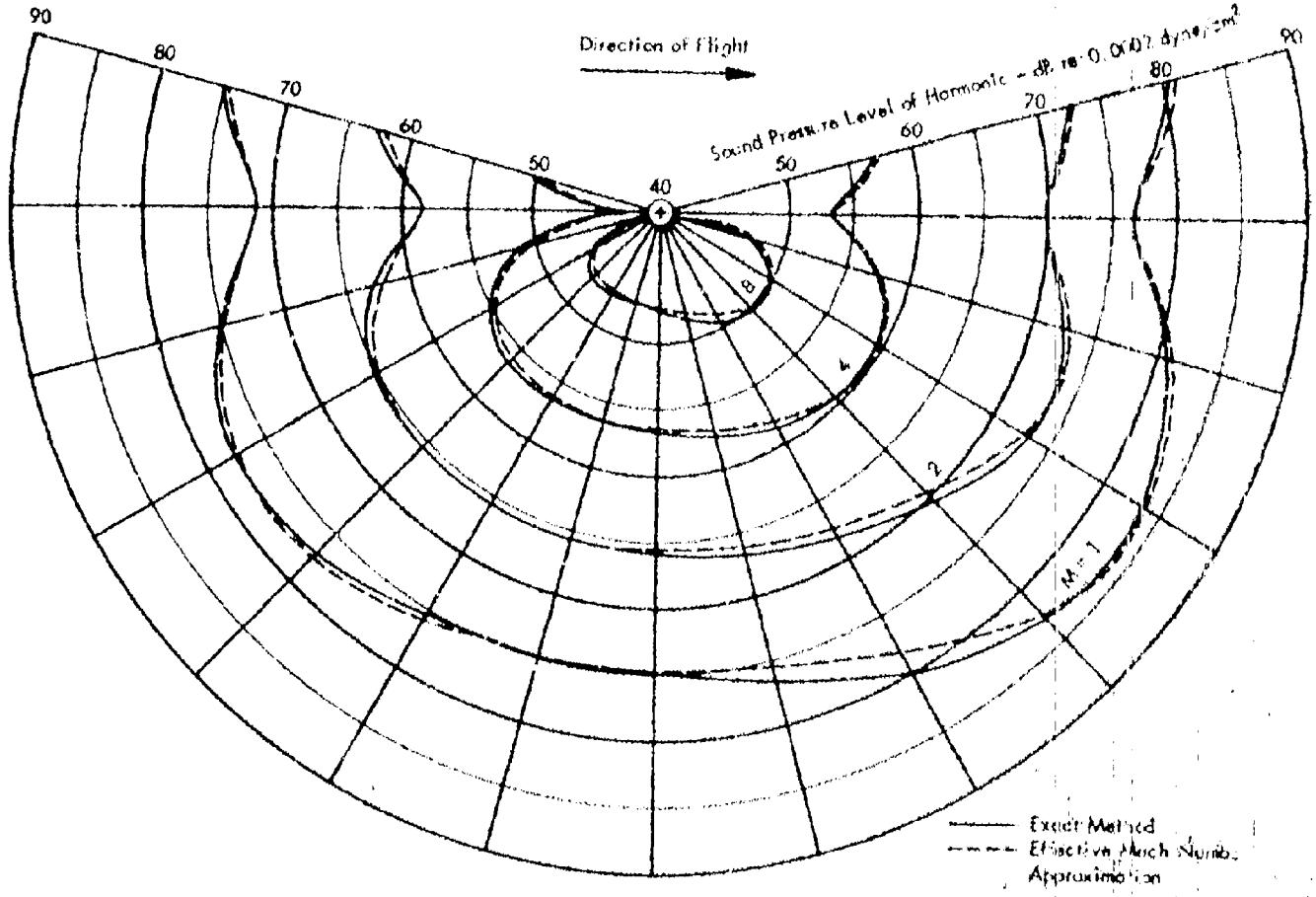

Figure 52. Comparison of Exact Method and "Effective Mach Number" Approximation for Rotor in Forward Flight. $M = 0.5$, $M_F = 0.125$.

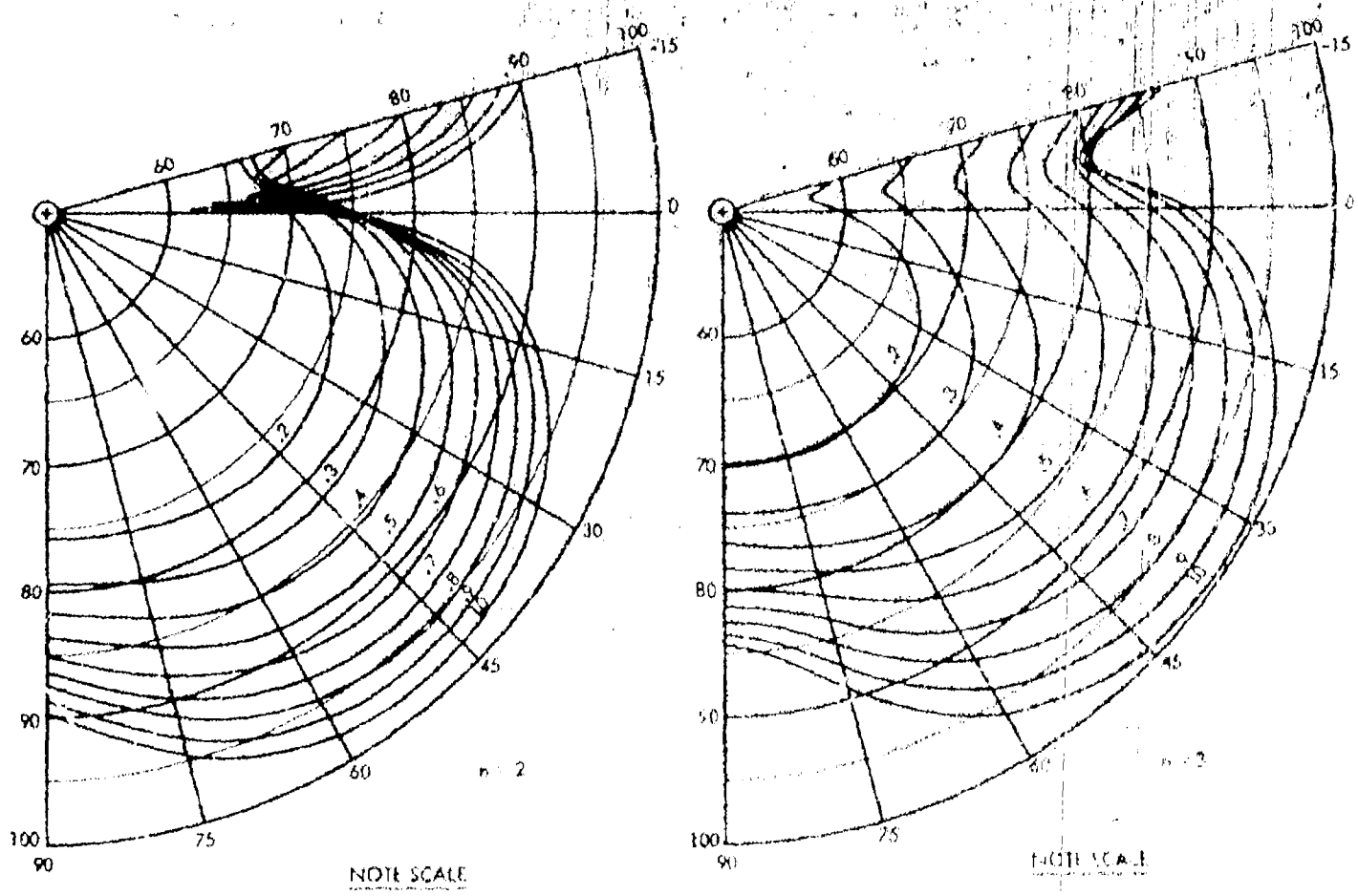

Figure 53. Rotor Noise Harmonic Sound Pressure Levels L_n as Functions of Harmonic Number, Rotational Mach Number, and Angle From Disc Plane.

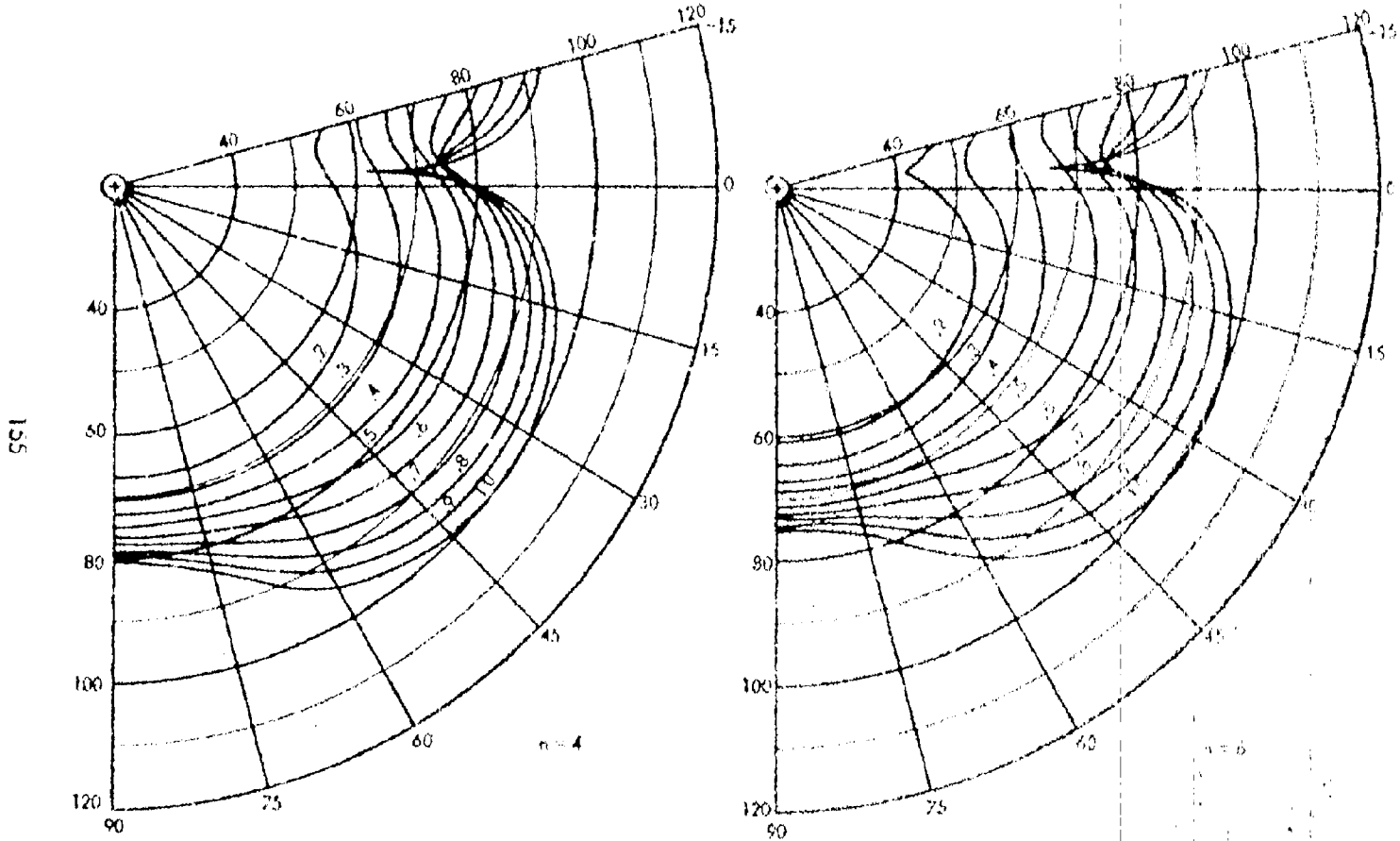

Figure 53. (Continued).

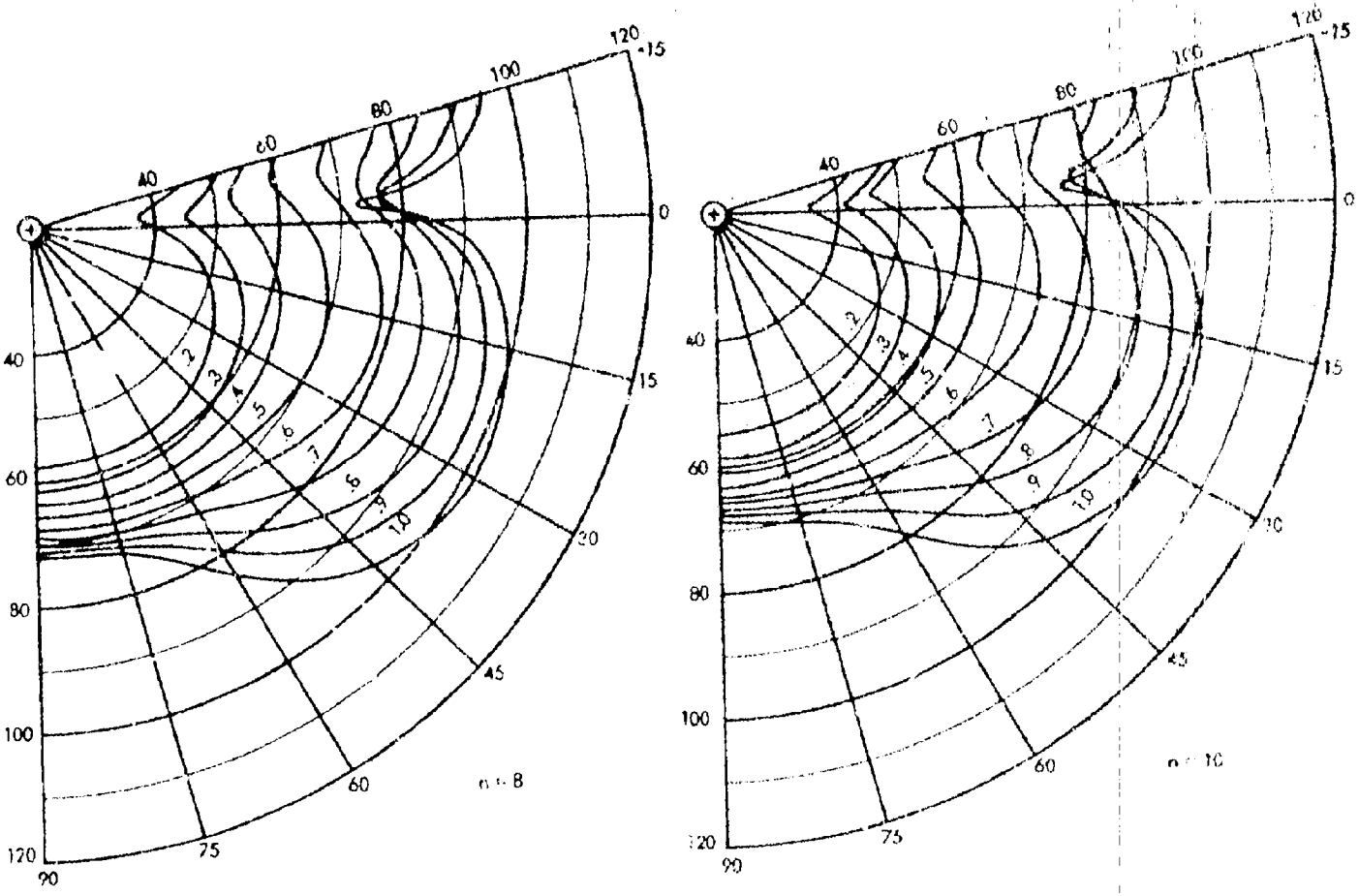

Figure 53. (Continued).

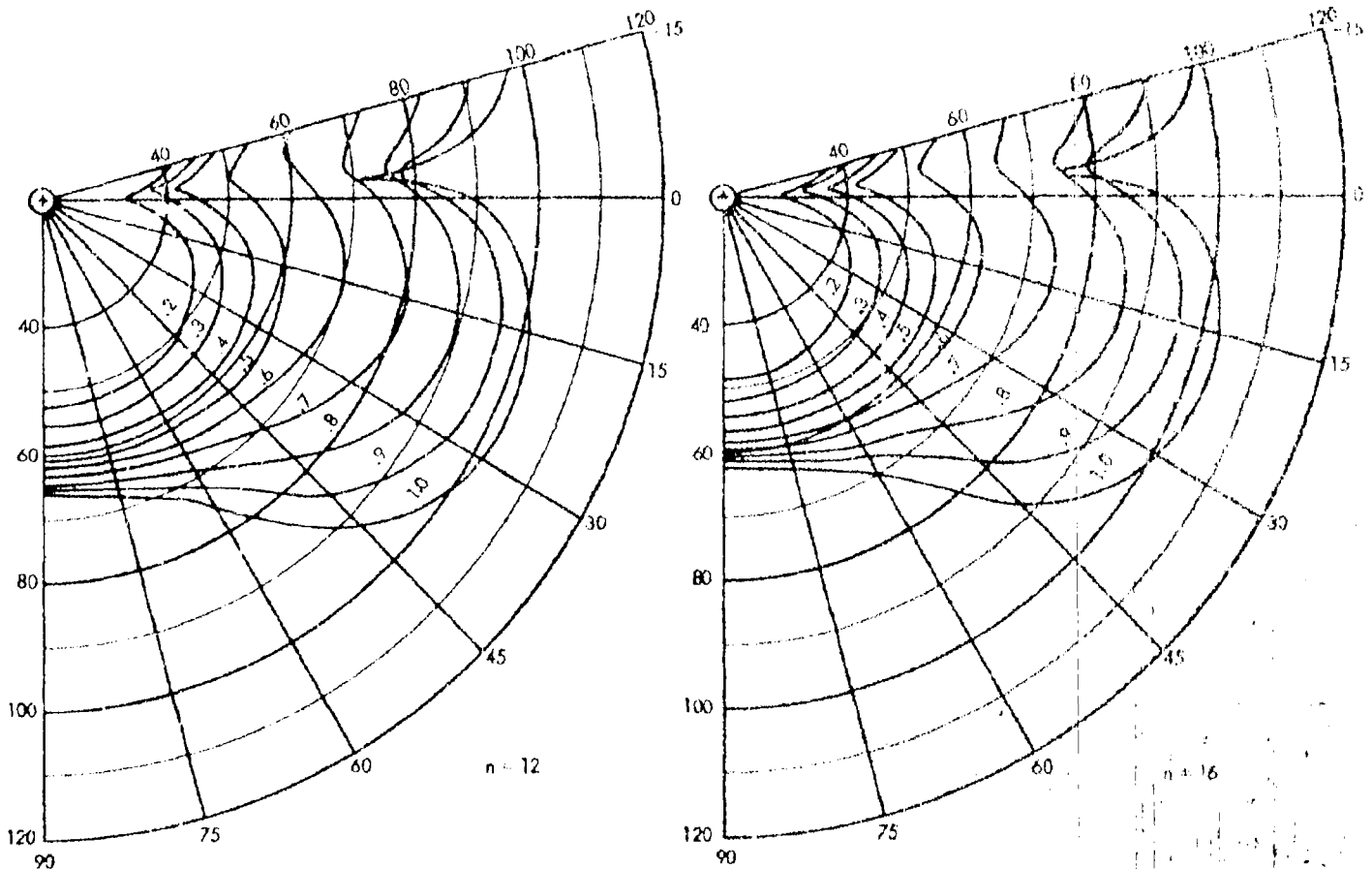

Figure 53. (Continued).

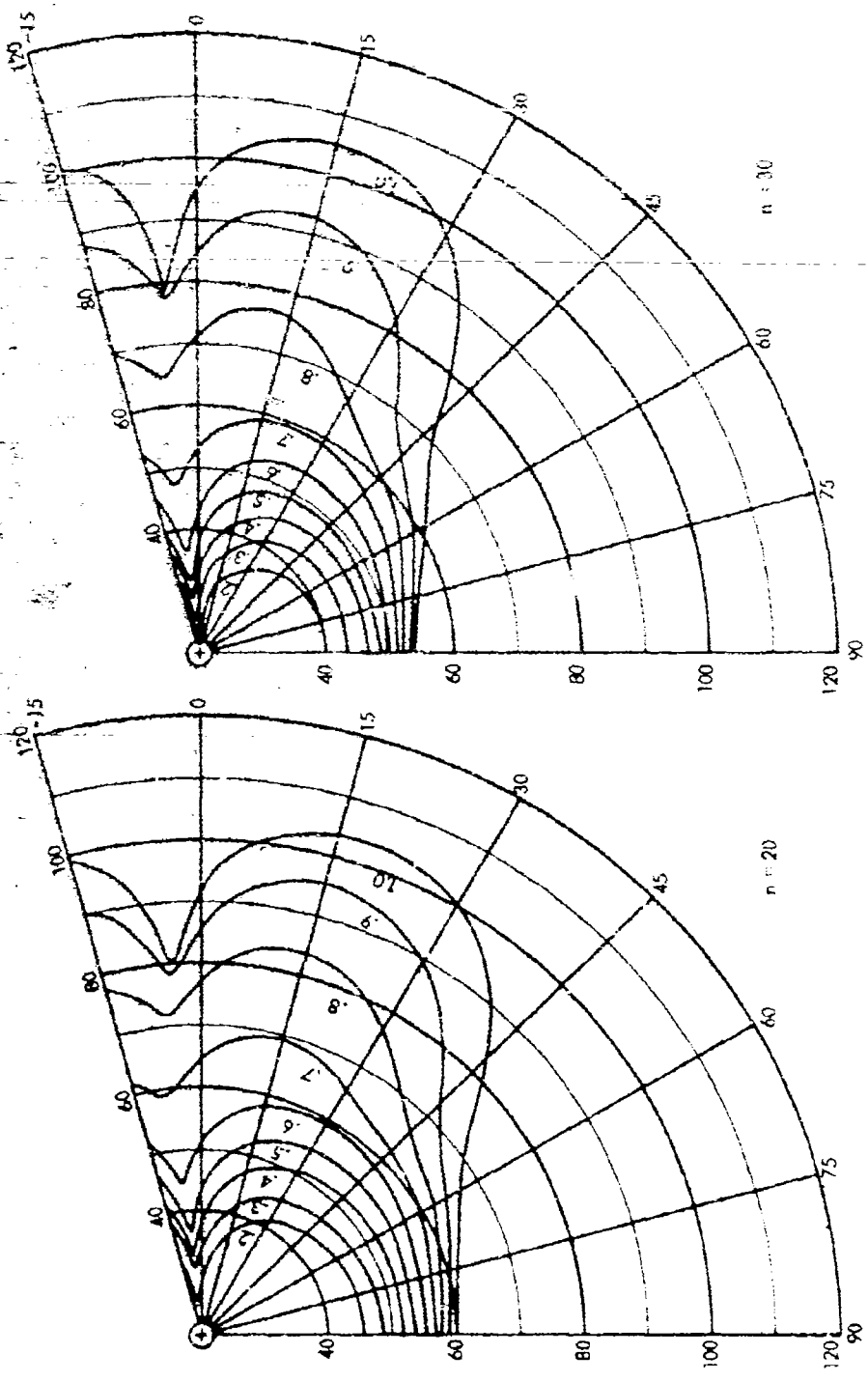

Figure 53. (Continued).

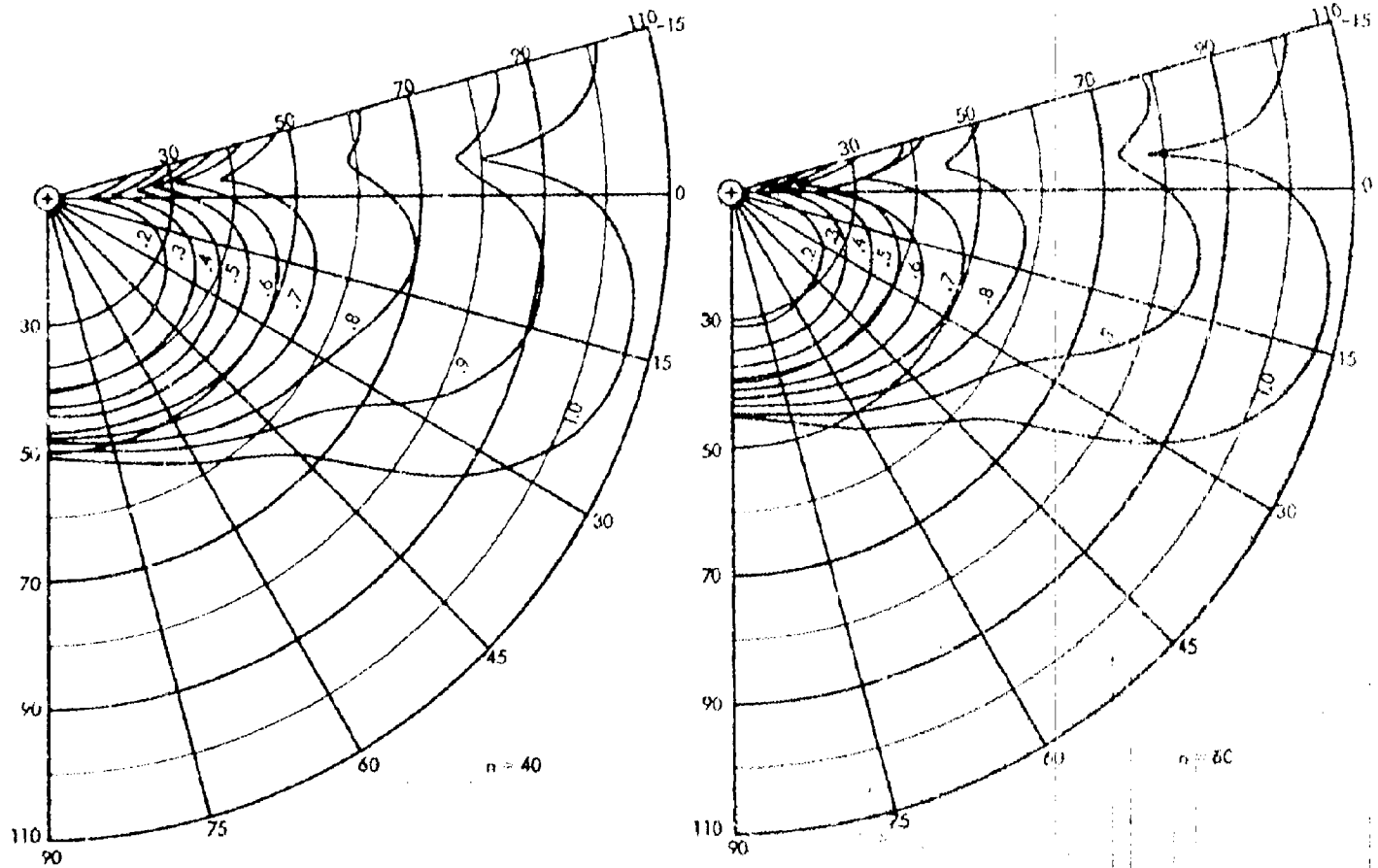

Figure 53. (Continued).

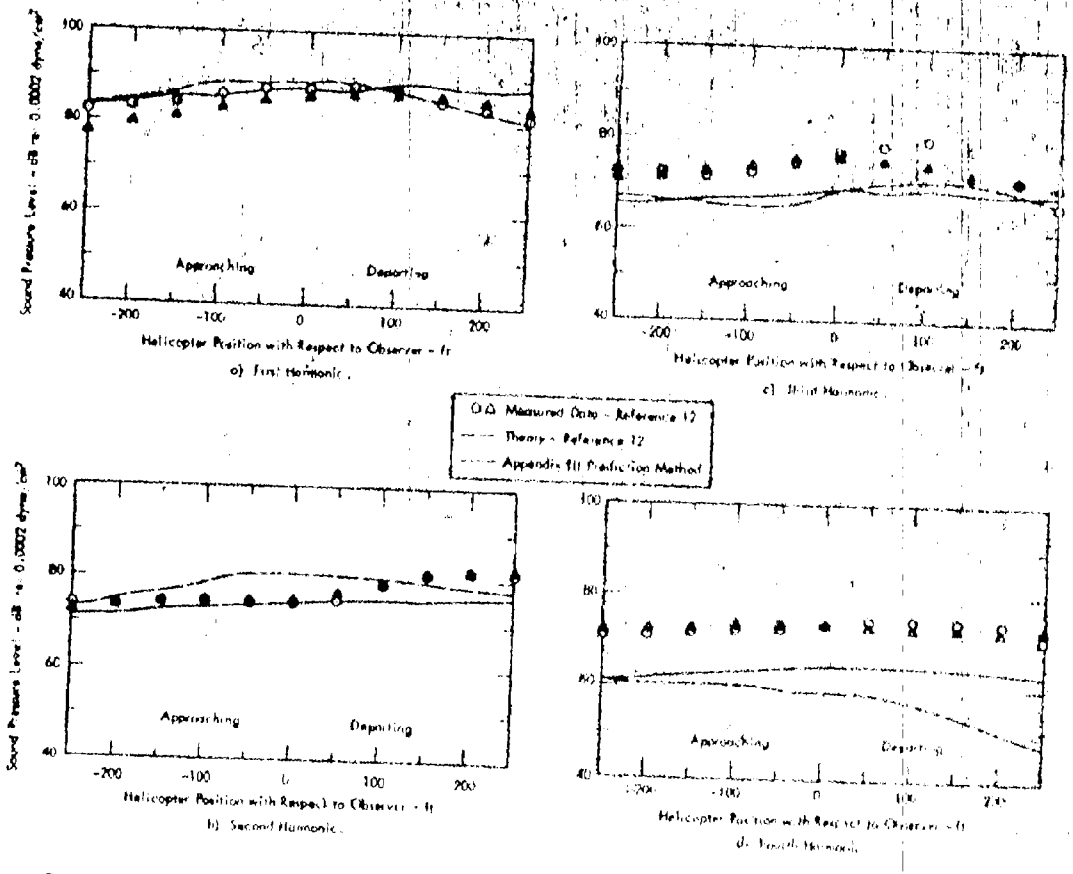

Figure 54. Comparison of Theoretical and Measured Harmonic Sound Pressure Levels for H-34 Main Rotor. Aircraft Altitude 200 Ft. Velocity = 80 Kts.

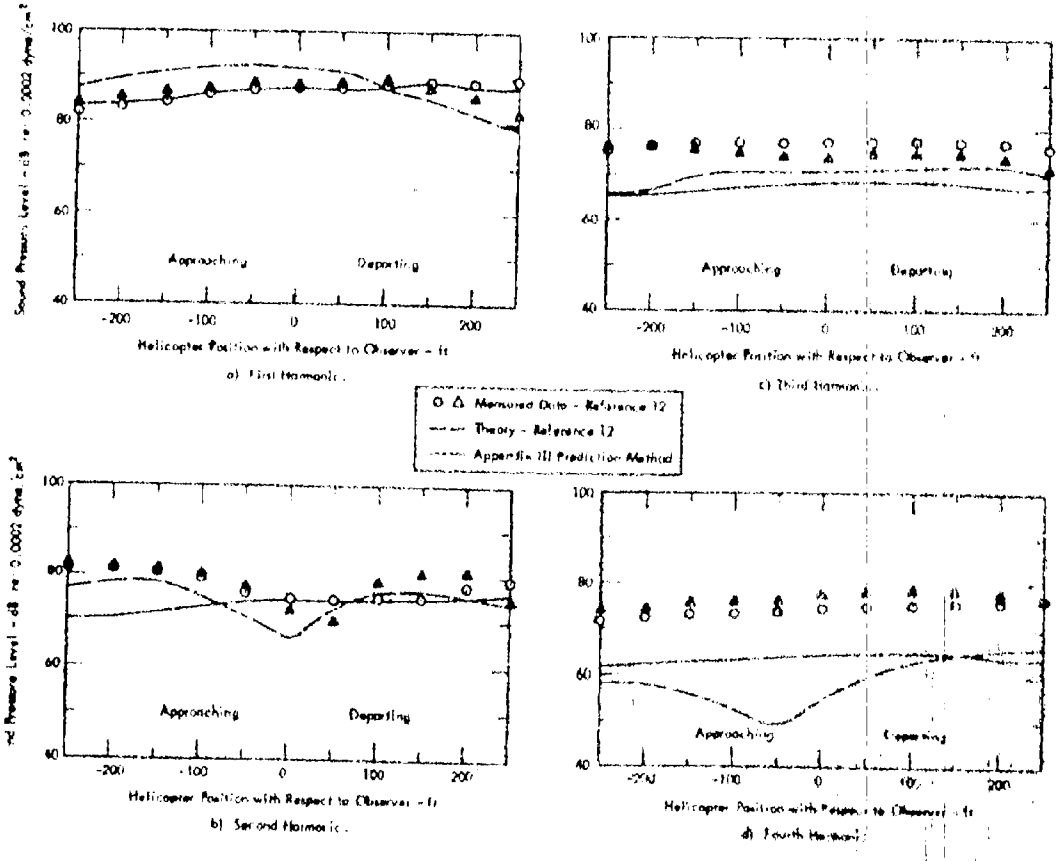

Figure 55. Comparison of Theoretical and Measured Harmonic Sound Pressure Levels for H-34 Main Rotor. Aircraft Altitude 200 Ft. Velocity = 110 Kts.

UNCLASSIFIED
Security Classification

DOCUMENT CONTROL DATA - R & D

(Security classification of title, body of abstract and indexing annotation must be entered when the overall report is classified)

1. ORIGINATING ACTIVITY (Corporate author)
Wyle Laboratories
Huntsville, Alabama

2a. REPORT SECURITY CLASSIFICATION
Unclassified

2b. GROUP

3. REPORT TITLE
Studies of Helicopter Rotor Noise

4. DESCRIPTIVE NOTES (Type of report and inclusive dates)
Final Report, March 1967 - October 1968

5. AUTHOR(S) (First name, middle initial, last name)
Lowson, Martin V., and Ollerhead, John B.

6. REPORT DATE	7a. TOTAL NO. OF PAGES	7b. NO. OF REFS
January 1969	179	41

8a. CONTRACT OR GRANT NO.	9a. ORIGINATOR'S REPORT NUMBER(S)
DA J02-67-C-0023	USAAVLABS Technical Report 68-60
b. PROJECT NO. Task 1F121401A14801	
c.	9b. OTHER REPORT NO(S) (Any other numbers that may be assigned this report)
d.	WR 68-9

10. DISTRIBUTION STATEMENT
This document has been approved for public release and sale; its distribution is unlimited.

11. SUPPLEMENTARY NOTES	12. SPONSORING MILITARY ACTIVITY
	U.S. Army Aviation Materiel Laboratories Fort Eustis, Virginia

13. ABSTRACT

A comprehensive study of the problem of helicopter noise radiation is presented. After a review of the basic features of the noise, the limited experimental data are reviewed in some detail, and empirical laws are proposed. An exact theoretical expression for the noise is derived. This expression has been used as the basis for the development of a comprehensive computer program to calculate helicopter noise at any field point, including all effects of fluctuating airloads and all possible rigid and flexible blade motions. Under very reasonable approximations, an analytic expression has been found for the sound field far from the helicopter, and computations based on this expression have been made. The results show all the higher harmonics of the loading, at least up to the sixtieth, to be significant for noise generation. A study of the harmonic airloads is presented. Comprehensive acoustic results from the theory include the effect of various loading inputs, thrust, tip velocity, number of blades, blade motion, and forward speed. Fair agreement with experiment is found for overall levels, and good agreement is found with experimental trends. Design charts are presented which enable routine calculation to be made of noise radiated from any helicopter in hover or forward flight.

DD FORM 1 NOV 68 1473 REPLACES DD FORM 1473, 1 JAN 64, WHICH IS OBSOLETE FOR ARMY USE.

UNCLASSIFIED
Security Classification

14. KEY WORDS	LINK A		LINK B		LINK C	
	ROLE	WT	ROLE	WT	ROLE	WT
Noise						
Helicopter Noise						
Helicopter Rotors						
Aerodynamic Loading						